Epigenetic modification of the Wnt pathway mediated by Brg1

Aliaksei Holik

Cardiff University

Ph.D.

$2007 - 2011$

Acknowledgements

Abbreviations and definitions

Symbols

°C	Degrees Celsius
μg	Micrograms
μl	Microlitres
μm	Micrometre
μM	Micromolar

A

ABC	Avidin Biotin Complex
AhCreERT	Aryl Hydrocarbon Cre recombinase Estrogen Receptor transgene
Ascl2	Achaete Scutelike 2
APC	Adenomatous Polyposis Coli
AXIN	Axis Inhibitor

B

BCA	Bicinchoninic Acid
Bmi1	polycomb ring finger oncogene
BMP	Bone Morphogenic Protein
BMPRII	Bone Morphogenic Receptor type II
bp	Base Pair
BrdU	5-Bromo-2-deoxyuridine
Brg1	Brahma related gene 1
Brm	Brahma
BSA	Bovine Serum Albumin

C

CRC	Colorectal Cancer
CBC cells	Crypt-Base-Columnar cells
cm	Centimetre
CSL	CBF1/RBP-Jκ/Suppressor of Hairless/LAG-1
CreERT	Cre recombinase-Estrogen receptor fusion transgene
CT	Cycle Time

D

DAB	3,3-diaminobenzidine
dATP	Deoxyadenosine Triphosphate
DCAMKL1	Doublecortin and Calcium/Calmodulin-dependent protein Kinase-Like-1
DCC	Deleted in Colorectal Cancer
ddH$_2$O	double distilled water
dGTP	Deoxyguanosine Triphosphate
Dhh	Desert Hedgehog
dH$_2$O	deionised water
DNA	Deoxyribonucleic Acid
DNase	Deoxyribonuclease
dNTP	Deoxynucleotide Triphosphate
DSH	Dishevelled
DTT	Dithiothreitol
dTTP	Deoxythymidine Triphosphate

E

E-cadherin	Epithelial Cadherin
ECL	Electrochemiluminescence
EDTA	Ethylenediamine Tetra-acetic Acid
EGFP	Enhanced Green Fluorescent Protein
EpCAM	Epithelial Cell Adhesion Molecule
ER	Estrogen Receptor
Erk	Extracellular regulated MAP kinase
ES cells	Embryonic Stem cells

F

FAP	Familial Adenomatous Polyposis
FLP	flippase
FRT	FLP Recognition Target

G

GEF	Guanine Nucleotide Exchange Factor
GSK-3	Glycogen Synthase Kinase-3
GTP	Guanosine Triphosphate
GTPase	Guanosine Triphosphatase
Gy	Gray

H

H&E	Haematoxylin and Eosin
HNPCC	Hereditary Nonpolyposis Colorectal Cancer
h	Hour
HRP	Horse Radish Peroxidase

I

IGF-1	Insulin-Like Growth Factor-1
IHC	Immunohistochemistry
Ihh	Indian Hedgehog
IP	Intraperitoneal

J

JPS	Juvenile Polyposis Syndrome

K

KDa	Kilodaltons
kg	Kilograms
KRAS	Kirsten Rat Sarcoma viral oncogene homolog

L

l	Litre
Lgr5	Leucine-rich repeat-containing Gprotein coupled receptor 5
LN$_2$	Liquid Nitrogen
LOH	loss of heterozygosity
loxP	Locus of crossover of Bacteriophage P1

M

MAPK	Mitogen Activated Protein Kinase
MEK	Mitogen Activated Erk Kinase1/2
mg	Milligrams
MIN	Multiple Intestinal Neoplasia
min	minutes

MLH1	MutL homolog 1	TBS/T	Tris Buffered Saline with Tween 20
mm	Millimetre		
MMR	Mismatch Repair	Tcf/Lef	T-cell factor and Lymphoid enhancer factor
MSH2	MutS E.Coli homolog of 2		
mTERT	mouse telomerase reverse transcriptase	TEMED	N,N,N,N-teramethylethylenediamine
mTOR	mammalian target of rapamycin	tetO	Tet Operon
M/W	Microwave	TGF-β	Transforming Growth Factor-β
N		tTA	Tetracycline-controlled Transactivator
NCID	Notch Receptor Intracellular Domain		
NGS	Normal Goat Serum	**V**	
NRS	Normal Rabbit Serum	V	Volts
O		VillinCreERT	Villin Cre recombinase ER transgene
Olfm4	Olfactomedin 4		
O/N	Overnight	v/v	Volume per Volume
P		**W**	
pAkt	phospho-Akt	W/B	Waterbath
PBS	Phosphate Buffered Saline	w/v	Weight per Volume
P/C	Pressure Cooker	WT	Wild Type
PCR	Polymerase Chain Reaction	Wnt	Wingless-type murine mammary tumour virus Integration site family
pErk	phospho-Erk		
PKA	Protein Kinase A		
PLL	Poly-L-Lysine		
pMEK	phospho-MEK	**X**	
pmTOR	phospho-mTOR	x g	times gravity
PTEN	Phosphatase and tensin homolog deleted on chromosome ten	**123**	
		3HTdR	Tritiated Thymidine
PI	Post induction		
PI3K	Phosphatidylinositol-3-Kinase		
Q			
qRT-PCR	Quantitative Reverse-transcription PCR		
R			
RNA	Ribonucleic Acid		
RNase	Ribonuclease		
RPM	Revolutions Per Minute		
RT	Room Temperature		
rtTA	reverse Tetracycline-controlled Transactivator		
RTK	Receptor Tyrosine Kinase		
S			
SDS	Sodium Dodecyl Sulphate		
SDS-PAGE	Sodium Dodecyl Sulphate-Polyacrylamide Gel Electrophoresis		
sec	Seconds		
Shh	Sonic Hedgehog		
T			
TA	Transit-Amplifying		
TACE	Tumour Necrosis Factor Converting Enzyme		
Taq	DNA polymerase from Thermus aquaticus		
TBE	Tris Borate EDTA		

Abstract

Colorectal cancer is one of the most clinically significant types of cancer due to both high incidence and mortality. Despite the well-established role of aberrant Wnt signalling in initiation and progression of colorectal cancer, therapies that specifically target the Wnt pathway are exceptionally limited. The development of such therapies is, in part, restricted by the toxicity of Wnt signalling inhibition for adult tissue homeostasis. Given this limitation, therapies that target downstream components and target genes of the Wnt pathway are required to minimise potential toxicity.

The chromatin remodelling ATPase subunit Brg1 has been found to interact with β-catenin and facilitate transcriptional program driven by the Wnt pathway. In this thesis I aimed to explore Brg1's potential as a therapeutic target in Wnt driven intestinal tumourigenesis. To achieve this, I conditionally deleted Brg1 in the murine small intestinal epithelium under normal physiological conditions and in the context of aberrant Wnt signalling using a range of transgenic mouse models. Additionally, I investigated the potential toxicity of Brg1 inhibition by analysing the effects of Brg1 loss in a range of epithelial tissues from the gastrointestinal tract and bladder.

The results presented in this thesis demonstrate that Brg1 deficiency impedes Wnt-driven tumourigenesis in the murine small intestinal epithelium via attenuation of Wnt signalling and the elimination of stem cell derived tumours, which have a higher tumourigenic potential. Additionally, Brg1 was found to play a major role in the maintenance of normal small intestinal stem cell homeostasis, as loss of Brg1 in the small intestinal epithelium resulted in ablation of the stem cell population. The impact of Brg1 deficiency on homeostasis of other tissues of the gastrointestinal tract and bladder exhibited a remarkable diversity, from induction of epithelial hyperplasia to very subtle alterations in cell differentiation.

Overall, the results presented in this thesis portray Brg1 as a promising potential therapeutic target in Wnt-driven neoplasia and suggest that specific targeting of the Brg1/β-catenin interaction rather than the catalytic activity of Brg1 may help to avoid any Wnt-independent toxicity of Brg1 inhibition.

Contents

List of Figures

List of Tables

Chapter 1

General introduction

1.1 The Mammalian Small Intestine

1.1.1 General anatomy and functions of the gastrointestinal tract

The digestive tract in mammals forms a central part of the digestive system with specific functions assigned to its different parts. The major function of the digestive tract is to enable the passage of consumed food, while it is being processed, digested and absorbed in the form of the elementary nutrients. The largest part of the digestive tract is represented by the gastrointestinal tract that consists of the stomach and the intestines. The stomach serves as a temporary storage compartment for consumed food, where the latter is mixed and subjected to the initial stages of digestion and undergoes limited absorption. Glands embedded in the stomach epithelium secrete hydrochloric acid, a number of digestive enzymes and mucus that protects the mucosa from damage by the hydrochloric acid and digestive enzymes. Finally, the muscular layers embedding the stomach enable mixing of its contents and facilitate propulsion of the partially digested food into the intestine (Seeley *et al.*, 2002).

The mammalian intestine is divided into two major parts - the small and large intestines. The small intestine, in turn, is divided into three regions: the duodenum, jejunum and ileum. With the exception of two papillae that serve as entry points for the bile and pancreatic ducts and the presence of Brunner's glands in the submucosa of the duodenum, all three regions of the small intestine share a similar organisation (Figure 1.1). The outermost layer of the intestine is represented by the connective tissue of the serosa. Underneath the serosa, two layers of muscle (longitudinal and circular) surround the submucosa composed of connective tissue containing blood vasculature and nerves. Finally, the small intestinal mucosa is composed of a muscularis mucosae, a lamina propria and the simple columnar epithelium. The useful surface area of the human small intestinal epithelium is increased about 600 fold via a number of modifications. Firstly, both mucosa and submucosa are formed into circular folds perpendicular to the intestinal axis. Secondly, the mucosa is organised in finger-like projections extending into the in-

testinal lumen, termed villi. At the bottom of the villi, the epithelium forms pocket-like invaginations into the lamina propria termed the crypts of Lieberkühn. Finally, the apical membrane of the absorptive columnar epithelium covering the surface of the villi forms multiple cytoplasmic protrusions called microvilli further increasing the epithelial surface area. Progressing from the duodenum towards the ileum, the number of the circular folds decreases as does the density and the size of the villi. The mucosa and submucosa of the small intestine also contain numerous lymph nodes termed Peyer's patches protecting the intestine from microorganisms (Seeley *et al.*, 2002).

In addition to the digestive enzymes produced by the pancreas, the small intestinal epithelium secretes a number of enzymes that remain associated with the epithelial surface, which aid the final stages of digestion. The majority of the water, electrolytes and nutrients present in the contents of the intestine are absorbed in the small intestine (primarily in the duodenum and jejunum) while the rest is absorbed in the large intestine. The large intestine is organised into four compartments: caecum, colon, rectum and anal canal, the colon forming the major part of the large intestine. The colonic epithelium differs from the small intestinal mucosa in the absence of circular folds and villi. The mucosa of the colon is organised into crypts similar to those found in the small intestine. There is, however, a shift in the cell type abundance. While absorptive cells form the major population of the small intestinal epithelium, the mucus secreting cells predominate in the colon (Seeley *et al.*, 2002).

1.1.2   Micro-architecture of the small intestinal epithelium

As mentioned in the previous section, the intestine is lined with a single sheet of columnar epithelial cells. This sheet is organised into folds termed villi, which protrude into the gut lumen; and crypts, pocket-like invaginations that extend into the underlying stromal tissue (Figure 1.1). The crypts are occupied by dividing cells that originate from the stem cells positioned at the crypt base. These actively proliferating cells form a transit amplifying (TA) zone, where they undergo several rounds of cell division and the initial stages of differentiation. Partially differentiated progenitor cells migrate towards the crypt-villus junction, where they lose their proliferative capacity and terminally differentiate into one of the mature cell types that occupy the villus surface (Cheng and Leblond, 1974a). The terminally differentiated cells continue their migration towards the villus tip and eventually undergo apoptosis or are sloughed off into the lumen, where they undergo anoikis (Hall *et al.*, 1994). As a result of the continuous migration towards the villus tip, virtually all the mature cells in the small intestine are renewed every 5 days in humans and every 3 days in mice (Marshman *et al.*, 2002). The only differentiated cells that escape this upward flow are the Paneth cells that migrate towards the bottom of the crypt (Cheng *et al.*, 1969).

The majority of mature cells in the small intestinal epithelium belong to one of the
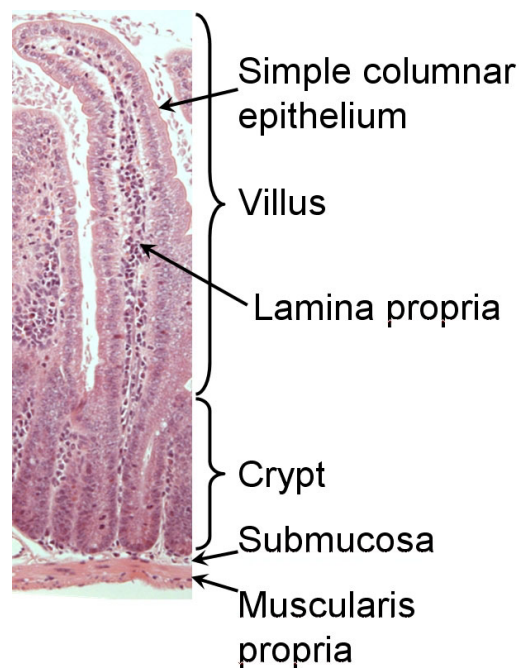
Figure 1.1: Histology of the small intestinal epithelium. The outermost layer of the intestine is represented by the connective tissue of serosa. Underneath the serosa, two layers of muscle (longitudinal and circular) surround the submucosa composed of connective tissue containing blood vasculature and nerves. Finally, the small intestinal mucosa is composed of a muscularis mucosae, a lamina propria and the simple columnar epithelium. The useful surface of the human small intestinal epithelium is increased greatly due to formation of the finger-like projections extended into the lumen, termed villi. At the bottom of the villi epithelium forms pocket-like invaginations into the lamina propria termed crypts of Lieberkühn.

four major cell types. Enterocytes or columnar cells represent the absorptive lineage, while goblet, Paneth and enteroendocrine cells constitute the secretory lineages.

Enterocytes comprise more than 80% of all epithelial cells in the small intestine and are actively renewed with an average turnover time of 3 days. They are positioned along the top of the crypt and over the whole of the villus. The enterocytes are distinguished by a lack of secretory granules and the presence of a tight array of microvilli on their apical membrane that constitute a brush border (Cheng and Leblond, 1974a). The membrane that forms the microvilli harbours numerous hydrolase enzymes that facilitate the final stages of digestion. Various channel proteins located in both the apical and basal membranes of the enterocytes carry out transport of nutrients from the gut lumen into the blood and lymphatic vasculature, while also transporting certain ions into the lumen (Smith, 1985).

The most abundant members of the secretory lineages are the mucus secreting goblet cells, although their relative numbers vary between different regions of the small intestine. Mature goblet cells are distributed among the enterocytes from mid-crypt to the villus tip and are renewed at a rate similar to that of the enterocytes (Troughton and Trier, 1969). Goblet cells are characterised by the presence of large mucus containing granules and enlarged rough endoplasmic reticulum. The mucus produced by the goblet cells serves as a lubricant for the passing food and protects the lining of the intestine from mechanical

abrasion, damage by acidic stomach contents and autodigestion by the digestive enzymes (Cheng, 1974).

The Paneth cells represent the second most abundant cell type in the secretory lineage. They differ from all the other mature cell types in their downward migration, maintenance of active Wnt signalling, and substantially slower turnover. Initial estimates of the Paneth cell turnover rate based on labelling with [^{3}H]thymidine have suggested a period of 18-23 days (Cheng *et al.*, 1969). Another study using a similar approach established that label retaining Paneth cells persisted for at least 29 days (Troughton and Trier, 1969). A recent study using an inducible enhanced yellow fluorescent protein (EYFP) reporter has indicated that the turnover rate of the Paneth cells may be as much as 57 days (Ireland *et al.*, 2005). The turnover rate of the Paneth cells, however, is likely to vary between different parts of the intestine. Morphologically, the Paneth cells are characterised by the presence of a large number of apical secretory granules. These granules contain a number of substances with antimicrobial activity. Among these are polypeptides targeted against bacterial cell wall, such as lysozyme, defensins (cryptdins in mice) and phospholipase A2. Other granule components, such as immunoglobulin IgA, pancreatitis-associated protein and secretory leukocyte inhibitor may be involved in the modulation of the immune response (Porter *et al.*, 2002). The Paneth cells are therefore considered to play a crucial role in the regulation of the intestinal microflora. A recent report has also suggested that Paneth cells provide a niche for the intestinal stem cells (Sato *et al.*, 2010). This particular aspect of the Paneth cell physiology is described in greater detail in later sections.

Enteroendocrine cells represent less than 1% of terminally differentiated cells and comprise a family of at least 15 different cell types. These cells differ in the morphology of their secretory granules, the nature of the principal secretory product and expression of specific markers. The unifying feature of all the enteroendocrine cells is expression and secretion of a range of polypeptide hormones. These include serotonine, secretin, substance P, cholecystokinin, gastric inhibitory polypeptide and others (Höcker and Wiedenmann, 1998).

In addition to the main cell types, two minor cell lineages are present in the small intestinal epithelium. M (membranous or microfold) cells are encountered in the epithelium adjacent to the Peyer's patches. Their basolateral membrane forms invaginations occupied by macrophages and T and B lymphocytes. M cells are able to internalise particles and microorganisms from the lumen by endo- or phagocytosis and transport them across the epithelial border, where they are processed by the immune cells (Neutra *et al.*, 1996). Tuft cells (also known as brush, caveolated or fibrillovesicular cells) are distributed throughout organs of the gastrointestinal and respiratory tracts. They are characterised by a goblet-shaped body, the presence of long and blunt microvilli on the apical membrane and numerous vesicles in the apical cytoplasm. Although their role in the small intestine is still undefined, the abundance of the vesicles in the cytoplasm indicates that tuft cells may be involved in the secretion or absorption of certain substances. Studies in other

organs have also suggested that tuft cells may function as pressure or chemoreceptors, however no direct synaptic contact between the tuft cells of the alimentary tract and neurons have been detected (Sato, 2007).

1.1.3   The small intestine epithelial homeostasis

In order to ensure the proper maintenance and function of the intricate cellular architecture described in the previous section, a number of carefully coordinated processes need to take place. Firstly, active but controlled proliferation ensures continuous renewal of the epithelial sheet. Secondly, proliferation is confined to the crypts, where actively dividing cells are protected from exposure to the contents of the gut lumen. Thirdly, migration of the newly produced cells up the crypt-villus axis further contributes to the flow and renewal of the epithelial layer. And finally, differentiation along various cell lineages ensures the appropriate balance between cell types. All these processes are precisely orchestrated by a mesh of signalling pathways including Hedgehog (Hh), platelet-derived growth factor (PDGF), bone morphogenetic protein (BMP), transforming growth factor β (TGFβ), Wnt and Notch (Figures 1.2 and 1.3). This section will briefly describe each of the pathways and the role they play in maintaining the intestinal homeostasis.

1.1.3.1   Epithelium-to-mesenchyme signalling: Hedgehog and PDGF pathways

The importance of the mesenchyme-epithelium interaction for the development and maintenance of the intestinal epithelium has been long established (Kedinger *et al.*, 1986). More recent studies have provided evidence that this interaction is to a large extent mediated by the Hedgehog (Hh), PDGF and TGFβ/BMP signalling pathways. The first two pathways cover the epithelium-to-mesenchyme side of this interaction.

Hh signalling (Figure 1.2) was first described in *Drosophila melanogaster* and has been implicated in a variety of biological processes including development and maintenance of tissue homeostasis, carcinogenesis and tissue repair (Katoh and Katoh, 2006). The Hh pathway ligands in mammals are represented by three paralogues: Sonic hedgehog (Shh), Indian hedgehog (Ihh) and Desert hedgehog (Dhh), the former two being expressed in the intestinal epithelium. In the absence of Hh ligands the Patched (Ptch1 and Ptch2) receptor inhibits transducer of the Hh signalling, the transmembrane receptor Smoothened (Smo). Inactive Smo serves as an assembly core for a complex consisting of Costal-2 (Cos-2) and fused (Fu). Cos-2 further binds to casein kinase 1α (CK1α), glycogen synthase kinase-3β (GSK3β) and protein kinase A (PKA). This complex sequesters and targets for proteasomal degradation Glioblastoma (Gli) transcription factors (Gli1, Gli2 and Gli3). In the gut full length Gli2 and Gli3 act as the major transducers of the Hh pathway. At the same time, proteasomal degradation of Gli3 and (to a lesser extent) Gli2 results in truncated proteins that are able to act as Hh suppressors. Binding of
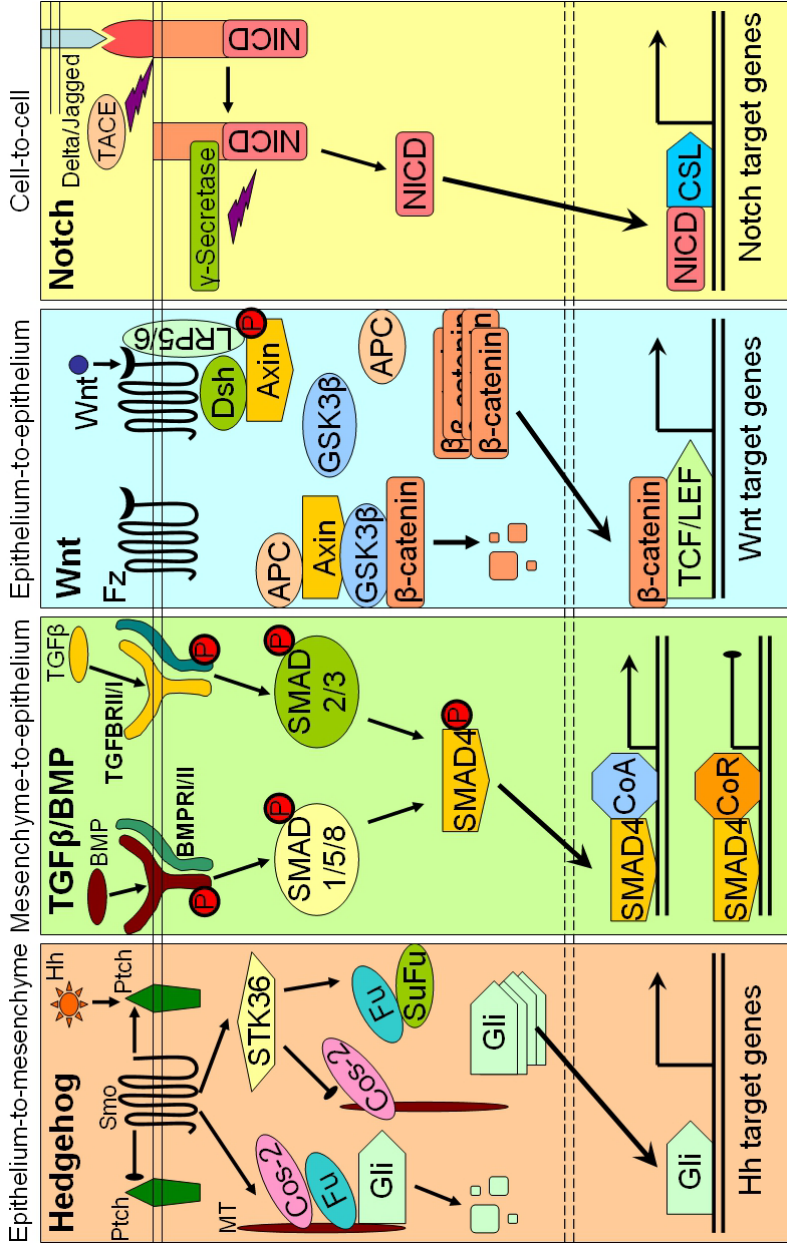
Figure 1.2: Major signalling pathways governing small intestinal homeostasis.
Hedgehog signalling: Unbound patched receptor (Ptch) inhibits the smoothened (Smo) signal transducer allowing formation of Cos2/Fu complex with microtubules (MT), which binds Gli transcription factor sequestering it away from the nucleus and targeting its degradation. Binding of hedgehog ligands to Ptch releases its inhibition of Smo, which in turn activates STK36. Suppressor of fused (SuFu) is activated preventing Cos2/Fu containing complex from being formed. Full length Gli is allowed to accumulate and translocate to the nucleus, where it activates target gene expression.
TGFβ/BMP signalling: BMPs or TGFβs bind to their cognate type I/II receptors resulting in phosphorylation of the type I receptor. BMP signals are transduced through SMAD1/5/8, TGFβs through SMAD2/3. Both result in activation of SMAD4, which translocates to the nucleus and interacts with co-activators and co-repressors to modulate transcription of target genes.
Wnt signalling: Absence of Wnt ligand allows assembly of the β-catenin destruction complex comprised of Axin, Apc and GSK3β, which binds β-catenin and mediates its phosphorylation and proteasomal degradation. Binding of Wnt ligand to Frizzled receptor and LRP5/6 co-receptor results in activation of Dishevelled (Dsh) and phosphorylation of LRP, which inhibit recruits Axin to the receptor thus mediating disassembly of β-catenin destruction complex allowing accumulation and translocation of β-catenin to the nucleus where it binds TCF/LEF transcription factors and activates expression of Wnt target genes.
Notch signalling: Binding of notch receptor by cell surface ligands of the Delta/Jagged family stimulates cleavage of the notch receptor by TACE and γ-secretase. Cleavage by γ-secretase releases the notch intracellular domain (NICD), which translocates to the nucleus and acts with the transcription factor CSL to activate expression of target genes.

Hh ligands to the Ptch receptor releases inhibition of Smo and prevents formation of the Gli destruction complex. Stabilisation of Gli results in its nuclear accumulation and activation of downstream Hh targets (reviewed in Katoh and Katoh, 2006; Lees *et al.*, 2005; van den Brink, 2007).

In the developing murine small intestine, Shh and Ihh are expressed throughout the epithelium. But, in time, with villus morphogenesis their expression becomes progressively confined to the intervillus regions and, at later stages, to the crypts. At the same time, expression of the Hh receptors Ptch1 and Ptch2, and the Hh effectors Gli2 and Gli3, is limited to the underlying stromal cells. The loss of either Shh or Ihh results in gross abnormalities in the epithelial development of the gut (Ramalho-Santos *et al.*, 2000). Loss of Ihh results in perinatal death and is paralleled by reduced proliferation in the crypt region. $Ihh^{-/-}$ mice have also been shown to display a reduction in the enteroendocrine cell markers implying a role for Ihh in cell differentiation. Loss of Shh, while still causing early post-natal lethality, led to an opposite phenotype. $Shh^{-/-}$ mice exhibited overgrown villi in the duodenum suggesting an increase in proliferation (Ramalho-Santos *et al.*, 2000). Despite the overlapping expression of Ihh and Shh, these observations suggested distinct roles for different Hh ligands in the small intestine. In order to explore the combined role of both Hh ligands in adult intestinal homeostasis, Madison *et al.* (2005) specifically blocked Hh signalling in the intestine by overexpression of the Hh inhibitor Hhip in a tissue-specific manner. High expression level of Hhip resulted in a highly proliferative intestinal epithelium with complete abolition of villi. Lower levels of Hh pathway inhibition have been found to produce a milder phenotype, which, nevertheless, was characterised by development of abnormal branched villi with sites of ectopic Wnt activation and proliferation. The model proposed by Madison and colleagues suggested that Shh and Ihh are released in the crypt region and act as paracrine signals for the smooth muscle cells and subepithelial myofibroblasts, which, in turn, inhibit proliferation in the villus epithelium (Madison *et al.*, 2005).

Another pathway that facilitates the flow of signals from epithelium to mesenchyme is the PDGF pathway. Four PDGF ligands (PDGF-A, PDGF-B, PDGF-C and PDGF-D) bind to two related receptor tyrosine kinases, PDGFR-α and PDGFR-β, that transmit the signal to a number of signal transduction pathways, including signal transducer and activator of transcription (STAT), Mitogen-activated protein kinase (MAPK), phosphatidylinositol 3-kinase (PI3K/Akt) and others (reviewed in Andrae *et al.*. 2008). Loss of PDGF-A in murine small intestine has been shown to result in reduction of villus density as well as abnormal villus spacing and morphology (Karlsson *et al.*, 2000). A model proposed to explain the abnormal villus development suggested that PDGF-A expression by epithelial cells (first ubiquitous, then restricted to intervillus regions) drives proliferation and prevents premature differentiation of PDGFR-α positive mesenchymal cells. These cells form so called villus clusters that give rise to fully-formed villi by inducing epithelial folding and blocking the epithelial proliferation in the fold. The loss of PDGF-A

in this scenario leads to the depletion of undifferentiated self-renewing PDGFR-α positive mesenchymal cells and failure to initiate villus clusters, ultimately resulting in fewer, more spaced out villi (Karlsson *et al.*, 2000).

1.1.3.2 Mesenchyme-to-epithelium signalling: TGF-β and BMP pathways

TGF-β signalling (Figure 1.2) regulates a plethora of biological processes such as embryogenesis, wound healing, cell proliferation and differentiation (Shi and Massagué, 2003). The TGF-β family of cytokine molecules is represented by the TGF-β/Activin/Nodal and bone morphogenetic protein (BMP) subfamilies. Both subfamilies of ligands initiate signalling by binding to type I and II receptor serine/threonine kinases. The resulting colocalisation of the two receptors allows phosphorylation of the type I receptor by the type II receptor. This initiates a signalling cascade via phosphorylation of Mothers Against Decapentaplegic (Smad) proteins. The eight Smad family proteins can be divided into three functional classes: the receptor-regulated (R-Smads: Smad1, 2, 3, 5, and 8); the co-mediator (Co-Smad: Smad4); and the inhibitory (I-Smads: Smad6 and 7). Activated type I receptors phosphorylate the R-Smads, which upon activation assemble into heteromeric complexes with Co-Smad. The activated complexes are then translocated to the nucleus, where they regulate expression of the respective target genes. I-Smads compete with R-Smads for receptor binding and Co-Smad thus inhibiting the pathway (reviewed in Shi and Massagué, 2003)

In the intestine, BMP2 and BMP4 ligands are expressed in the mesenchyme, being positively regulated by the Hh pathway (Madison *et al.*, 2005). At the same time, the BMP pathway receptor, Bmpr1a, is expressed in the epithelial cells (Karlsson *et al.*, 2000). Notably, the inhibitor of BMP signalling, Noggin, is expressed in the submucosa around the crypt region, thus blocking BMP signals from mesenchyme in this region (He *et al.*, 2004b). Conversely, epithelial cells of the villi have been shown to display elevated levels of phospho-Smad1, 5 and 8, indicating active BMP signalling (Haramis *et al.*, 2004). Both conditional deletion of Bmpr1a and overexpression of Noggin in mouse intestine resulted in excessive development of aberrant crypt-like structures. Whereas Noggin overexpressing mice developed ectopic crypt structures on the sides of villi (Haramis *et al.*, 2004), loss of Bmpr1a resulted in increased crypt density in the affected areas (He *et al.*, 2004b). Both models developed polyps that were characterised by an expanded proliferative compartment. These observations demonstrate that BMP signalling inhibits ectopic crypt formation and restricts proliferation to the crypt region due to the Noggin availability.

Taken together, the patterns of Hh and BMP signalling provide a model that attempts to explain the crypt-villus self-organisation (Figure 1.3). Hh signalling released by epithelial cells acts upon the underlying mesenchyme, which, in turn, releases BMP ligands. The presence of Noggin in the intervillus region protects crypt from the BMP-mediated inhibition of cellular proliferation. At the same time, BMP signals released by the stroma

underlying the villus epithelium inhibit proliferation and ectopic crypt formation there.
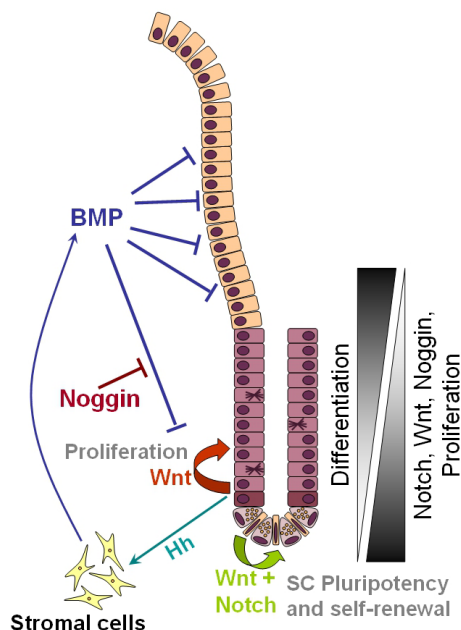
Figure 1.3: Interplay of signalling pathways in maintenance of small intestinal homeostasis. A network of signalling pathways is required to establish and maintain homeostasis of the small intestinal epithelium. High levels of Wnt and Notch signalling in the crypt region maintain the undifferentiated state of intestinal stem and progenitor cells. As cells migrate towards the crypt opening along decreasing gradient of Wnt and Notch signals, progenitor cells loose their proliferative capacity and undergo differentiation. Expression of Hedgehog ligands by epithelial cells activates hedgehog pathway in surrounding stroma and, in turn, activates expression of BMP ligands. Activation of BMP signalling in epithelial cells of the villus prevents cell proliferation in this region. At the same time expression of the BMP antagonist Noggin in the crypt region protects proliferating crypt cells from inhibition by BMP signals.

1.1.3.3   Epithelium-to-epithelium signalling: the Wnt pathway

The Wnt pathway (Figure 1.2) is conserved throughout the animal kingdom from cnidarians through insects and worms to mammals. It plays a crucial role in body patterning and axis formation during development. Importantly, Wnt signalling is also involved in maintenance of adult tissues, and abnormalities in its function are linked to numerous pathological conditions (reviewed in Clevers, 2006).

Wnts are a family of cysteine-rich glycoproteins whose biological activity requires palmitoylation of a conserved cysteine residue during their production and secretion (Willert *et al.*, 2003). Once released into the extracellular space, Wnts can activate their target cells via interaction with a family of Frizzled (Fz) transmembrane proteins (Bhanot *et al.*, 1996). For the activation of the canonical Wnt pathway in vertebrates, Fzs need to cooperate with single-span transmembrane protein LRP5 or LRP6 (Pinson *et al.*, 2000; Tamai *et al.*, 2000). The β-catenin protein is a key player in the canonical Wnt pathway and in the absence of Wnt activation, the pool of free β-catenin is sequestered in the cytoplasm by the so-called destruction complex. The tumour suppressor proteins APC and Axin form the scaffold of this complex and bind free β-catenin enabling its phosphorylation by CK1 at the Ser45 residue (Amit *et al.*, 2002; Liu *et al.*, 2002). Subsequently,

β-catenin is further phosphorylated by GSK3β (Rubinfeld *et al.*, 1996) and recognized by the E3 ubiquitin ligase β-TrCP, which triggers the ubiquitination of β-catenin and its subsequent degradation by proteasomes (Hart *et al.*, 1999).

Binding of Wnts to Fz and LRP5/6 leads to the phosphorylation of the cytoplasmic domain of LRP5/6, which, along with the Fz-bound Dishevelled protein, recruits the Axin protein to the plasma membrane. Axin depletion from the cytoplasm disrupts the integrity of the destruction complex, thus increasing the cytoplasmic pool of free β-catenin (Tamai *et al.*, 2004). Stabilized β-catenin is then translocated to the nucleus, where it binds to members of the Tcf transcription factor family (Waterman, 2002). In a Wnt-inactive cell, Tcf proteins are associated with general transcriptional repressors, such as Groucho, and repress the expression of Tcf-responsive genes (Roose *et al.*, 1998). On the activation of Wnt signalling, β-catenin binding to Tcf proteins displaces Groucho (Daniels and Weis, 2005) and recruits a number of transcriptional coactivators such as BRG1 and the histone acetylase CBP to the Tcf target sites (Barker *et al.*, 2001; Hecht *et al.*, 2000).

Wnt signalling maintains crypt cell proliferation   Numerous lines of evidence have suggested that in the intestinal epithelium Wnt signalling plays a pivotal role in maintaining proliferation, so that pathway inhibition reduces the proliferative compartment, while pathway activation expands it. The importance of the Wnt pathway in the maintenance of the crypt region is highlighted by the expression pattern of its components. Expression of the canonical Wnt pathway ligands (Wnt3, Wnt6 and Wnt9b) and receptors (Fz5, 7 and LRP5, 6) is confined to the proliferative epithelial crypt cells. At the same time, a number of Wnt ligands (Wnt-2b, Wnt-4, Wnt-5a, and Wnt-5b) are expressed in the villus mesenchyme. These ligands induce non-canonical Wnt signalling, which is considered to have an inhibitory effect on the canonical Wnt pathway. Accordingly, Fz4 and 6 are known to mediate non-canonical Wnt signal transduction and are expressed in differentiated epithelial cells of the villus (Gregorieff *et al.*, 2005).

The Wnt pathway inhibition by inactivation of its major downstream effector, Tcf4, have been demonstrated to result in complete abolition of proliferation in the intervillus region of the developing gut (Korinek *et al.*, 1998). Similarly, inducible loss of β-catenin in the adult intestine leads to ablation of cell proliferation, dramatic crypt loss and intestinal failure (Fevr *et al.*, 2007). Conditional Wnt signalling inhibition by overexpression of a Wnt inhibitor Dickkopf 1 (Dkk1) results in a similar phenotype involving depletion of the proliferative compartment, crypt loss and architectural abnormalities, such as reduction in villus size and numbers (Kuhnert *et al.*, 2004; Pinto *et al.*, 2003). Finally, conditional inactivation of a downstream Wnt target c-Myc slows down the cell cycle in the proliferating crypt cells. This leads to gradual elimination of c-Myc deficient crypts and their repopulation with crypts retaining c-Myc expression (Muncan *et al.*, 2006)

Conversely, aberrant activation of the Wnt pathway by either loss of the Wnt pathway negative regulator Apc or by overexpression of a dominant stable form of β-catenin have

been shown to induce expansion of the proliferative compartment and enlargement of crypts (Harada *et al.*, 1999; Sansom *et al.*, 2004). The same studies have shown that Wnt signalling activation impairs cell migration along the crypt-villus axis, indicating increased cell affinity to the proliferative compartment. Notably, whilst pan-epithelial Apc loss activates Wnt signalling in both crypt and villus cells, it does not induce proliferation in the villus, suggesting that other signals are required for the Wnt signalling manifestation (Andreu *et al.*, 2005).

Wnt signalling guides progenitor cells towards the secretory lineage Apart from its function in maintaining proliferation, Wnt signalling has been implicated in the determination of cell fate choices. The most explicit evidence for this comes from Paneth cell differentiation. Unlike other differentiated cells, Paneth cells remain at the bottom of the crypt and display signs of active Wnt signalling (such as nuclear β-catenin). Wnt signalling in Paneth cells has been implicated in the commitment to Paneth cell fate by driving the expression of Paneth cell-specific genes (Andreu *et al.*, 2005; van Es *et al.*, 2005a). The influence of the Wnt pathway on the other cell lineages is less straightforward. Wnt signalling inhibition by Dkk1 overexpression resulted in loss of all the secretory cell lineages without affecting enterocyte differentiation (Pinto *et al.*, 2003). Surprisingly, aberrant activation of Wnt signalling yielded a similar phenotype. Thus, loss of Apc function has been reported to result in general failure to differentiate as evident by the loss of all but Paneth cell differentiation markers (Andreu *et al.*, 2005; Sansom *et al.*, 2004). Together these data suggest that Wnt signalling plays three major roles: maintaining cell proliferation, preventing cell differentiation and directing cells towards the secretory lineage.

Wnt signalling controls cell segregation via the Eph/ephrin system One more function of the Wnt pathway in intestinal homeostasis is spatial segregation of distinct cellular populations. This function is mediated by the expression pattern of the tyrosine kinase guidance receptors EphB2 and EphB3 and their ligand ephrin B1. Wnt signalling stimulates expression of the EphB receptors, while inhibiting ephrin B1 expression. In the intestine of neonatal mice EphB2 and EphB3 are co-expressed in the cells of inter-villus pockets, while ephrin B1 expression is largely limited to the villus cells. In adult intestine EphB3 expression is restricted to the Paneth cells, while EphB2 is expressed in proliferating cells with a decreasing gradient towards the crypt-villus junction. Ephrins B1 and B2 are highly expressed around the crypt-villus junction with a gradual decrease towards the bottom of the crypt in a counter-gradient to EphB2. Loss of either of the EphB receptors has no major effects on intestinal homeostasis, although EphB3 loss does result in mislocalisation of the Paneth cells. The simultaneous loss of EphB2 and EphB3 still allows for near normal development and maturation of the intestinal epithelium, but leads to disruption of the boundaries between cellular compartments and intermingling

of proliferating and post-mitotic differentiated cells (Batlle *et al.*, 2002).

1.1.3.4   Cell-to-cell lateral inhibition: Notch/Delta pathway

The Notch receptors and their respective ligands are represented by a number of trans-membrane proteins that mediate cell-to-cell signal transduction between adjacent cells. The Notch pathway controls a range of biological processes including apoptosis, proliferation, spatial patterning and cell fate determination (Artavanis-Tsakonas *et al.*, 1999). The Notch signalling cascade is initiated after a receptor and a ligand on the surface of the two neighbouring cells come into contact (Figure 1.2). As a result of this receptor-ligand interaction the Notch receptor undergoes two successive proteolytic cleavage events. The first cleavage occurs in the extracellular domain and is mediated by the tumour necrosis factor-α-converting enzyme (TACE) metalloprotease. The second cleavage takes place within the trans-membrane domain and is carried out by a large protein complex termed γ-secretase. The second cleavage releases the Notch intracellular domain (NICD). NICD is translocated to the nucleus, where it binds to the Notch downstream transcription factor CSL (also known as CBF1 in humans and RBP-J in mice). Binding of NICD to CSL displaces co-repressors and recruits co-activators that facilitate transcription of the target genes. One of the best characterised Notch downstream effectors is the hairy enhancer of split (Hes) family of transcriptional repressors that, in turn, regulate expression of a number of target genes (reviewed in Wilson and Radtke, 2006).

In the adult intestine expression of the Notch pathway receptors and ligands is mainly confined to the epithelial cells of the crypt region and, to a lesser extent, the mesenchyme (Schröder and Gossler, 2002). The expression of the Notch downstream target, Hes1, is also limited to the crypt compartment, indicating Notch activation in this cell population (van Es *et al.*, 2005b). Conditional inactivation of CSL in the murine intestine results in the dramatic loss of proliferating crypt cells and their conversion into post-mitotic goblet cells. A similar effect is achieved by blocking Notch signalling with γ-secretase inhibitors (van Es *et al.*, 2005b). A milder inhibition of the Notch pathway by inactivation of the downstream effector Hes1 causes excessive differentiation of enteroendocrine and goblet cells at the expense of enterocytes (Jensen *et al.*, 2000). It appears, therefore, that secretory cell fate is a default choice in the absence of Notch signalling.

Excessive activation of Notch signalling by expression of a dominant active form of NICD impairs differentiation of all the cell lineages, while expanding the proliferative compartment (Fre *et al.*, 2005). Notably, the loss of the transcription factor Mouse atonal homologue 1 (Math1), negatively regulated by Hes1, depletes intestinal epithelium of the secretory cell lineages without affecting enterocyte differentiation (Yang *et al.*, 2001). Together, these observations suggest two primary functions of Notch signalling in intestinal homeostasis: maintenance of the crypt progenitors in the undifferentiated state and determination of the cell fate towards the absorptive lineage. The second function is likely to

be mediated by lateral inhibition. It has been shown that cells committed to the secretory lineage express Notch ligands (Crosnier *et al.*, 2005). These cells, therefore, are able to induce Notch signalling in their neighbours and prevent their commitment towards the secretory lineage via Math1 inhibition.

1.1.4 The small intestinal stem cell

The intestinal epithelium is one of the fastest renewing tissues in the mammalian organism. With the exception of the Paneth cells, all major types of terminally differentiated cells in the small intestinal epithelium are replaced with new cells in a matter of days. The constant renewal of the epithelial sheet is sustained due to the activity of the intestinal stem cell. The stem cells are defined as those cells able to proliferate and self-renew for an unlimited period of time, while generating diverse differentiated progeny specific to the given tissue (Potten and Loeffler, 1990). Considering the central role the stem cells play in epithelial homeostasis, knowledge of intestinal stem cell function and regulation is crucial for our understanding of the normal and pathological processes in the intestinal epithelium.

1.1.4.1 Intestinal stem cell identity and location

The major obstacle in intestinal stem cell research is the lack of definitive markers that would allow identification of the stem cell within the crypt. The exact location of the intestinal stem cell has been disputed over decades (Figure 1.4). A number of recent findings have at last provided functional evidence of stem cell identity, although this has not yet brought the discussion to resolution. This section will discuss the historic views on the stem cell position within the crypt as well as recent advances in the quest for intestinal stem cell markers.

Initial insights into the position of the intestinal stem cell were based on the observation that the proliferative compartment is bound at the bottom by non-proliferating Paneth cells. Downward migration of Paneth cells creates two migration counter-gradients that seemingly originate at the bottom of the migratory column, immediately above the Paneth cells, suggesting it is a likely location for the crypt stem cell (Cairnie *et al.*, 1965). Positioning of the intestinal stem cell immediately above the Paneth cells has been supported by a number of DNA labelling experiments. The rationale for these experiments comes from the observation that at least in some tissues relative quiescence is a definitive characteristic of the stem cell in contrast to its actively proliferating progeny. If an expanding stem cell population is exposed to a DNA labelling agent, the stem cells are able to incorporate and retain the label due to their low proliferation rate. Conversely, active proliferation of the progenitor cells ensures that the label is rapidly diluted and lost. The label-retaining cells (LRCs) can therefore be used to highlight the position of the stem cell and are well characterised in the stem cells of the hair follicle bulge (Cotsarellis *et al.*,
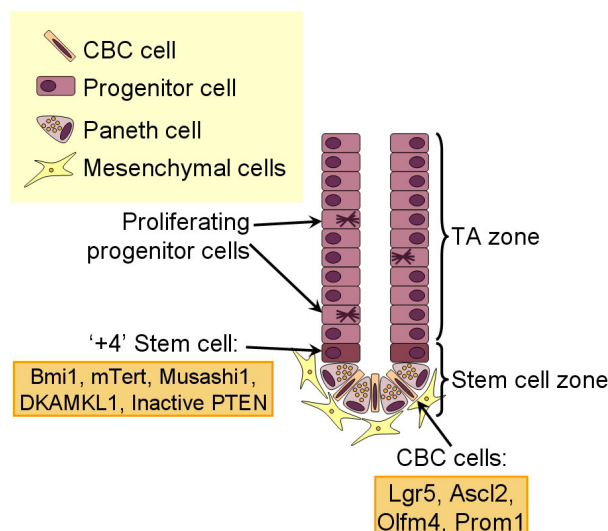
Figure 1.4: Schematic diagram of the small intestinal crypt and candidate locations of the intestinal stem cell. Actively proliferating transit amplifying (TA) zone of the crypt is bound at the bottom by non-cycling Paneth cells. The small intestinal stem cell has been proposed to sit right above Paneth cells (+4 stem cell) or wedged between them (CBC cell). Some evidence suggest that both population can coexist within a crypt. Orange boxes contain the list of proposed stem cell markers for each of the candidate locations. Paneth and mesenchymal cells are proposed to constitute the stem cell niche.

1990) and bone marrow (Cheng *et al.*, 2000), as well as in muscle satellite cells (Boldrin *et al.*, 2010).

Labelling of the intestinal epithelium with tritiated thymidine (^{3}HTdR) has identified a population of slowly cycling cells at position +4, immediately above the Paneth cells. These cells cycled on average once a day, i.e. at half the rate of the rest of the proliferating crypt cells, and were therefore proposed as putative stem cells (Potten *et al.*, 1974). When the label was administered at the time of stem cell expansion, such as during post-irradiation crypt regeneration, the +4 cells were able to retain the label for at least one week post labelling (Potten *et al.*, 1978). Taking into account the 24 hour cell cycle of the +4 cells, they are expected to undergo 8 cell divisions in a week resulting in dilution and loss of the label. The long-term label retention of the +4 cells therefore required an explanation alternative to a merely slower cell cycle. Such an explanation has been proposed by Cairns (1975), who suggested that stem cells may use selective segregation of the parental template and daughter DNA strands to avoid acquisition of mutations during DNA replication. Post-irradiation labelling of the intestinal epithelium with ^{3}HTdR followed by bromodeoxyuridine (BrdU) administration 8 days later has been shown to generate a population of double-labelled cells displaying both ^{3}HTdR and BrdU label (Potten *et al.*, 2002). Of the two DNA strands in a double-labelled cell the template DNA strand contained ^{3}HTdR, while the daughter strand incorporated BrdU. All the double-labelled cells lost BrdU labelling on day 3 after BrdU exposure, while retaining ^{3}HTdR label for at least an extra week. A two day period required for the elimination of the double-labelled cells is consistent with the cell division rate of the +4 cells as two divisions would be necessary to eliminate the freshly synthesised BrdU-labelled strand

(Potten *et al.*, 2002).

Consistent with selective segregation of the template and daughter DNA strands is sensitivity of the +4 cells to extremely low levels of ionising radiation. Even minimal damage to the template DNA strand has been shown to result in altruistic apoptosis rather than an attempt to repair the damage (Potten, 1977). Lost stem cells are then replaced either by clonal expansion of undamaged stem cells or by more repair-proficient progenitor cells retaining a stem-cell potential. Indeed, it has been suggested that every crypt contains a hierarchy of cells able to regenerate a crypt after radioactive damage (i.e. clonogenic cells). The first tier of this hierarchy is represented by the true stem cells highly sensitive to ionising radiation. The second tier contains the immediate progeny of the stem cells and is more resistant to radioactive damage, while the immediate progeny of the second tier cells forms the third, most radioresistant, tier of clonogenic cells (Potten, 1998).

Although the view that the small intestinal stem cell is located at the +4 position has prevailed for decades, an alternative location for the intestinal stem cell was proposed in the same year as for the +4 position. The undifferentiated proliferative crypt-base columnar (CBC) cells intercalated between the Paneth cells at the very bottom of the crypt have been found to be radiosensitive and display signs of active phagocytosis (Cheng and Leblond, 1974b). Upon administration of ³HTdR occasional CBC cells underwent radiation-induced apoptosis and were subsequently phagocytosed by neighbouring CBC cells. Phagosomes containing radioactively labelled nuclei were then used as a marker for tracing the progeny of the CBC cells. ³HTdR containing phagosomes eventually became present in all four mature cell types suggesting that CBC cells have the potential to produce all the differentiated cell types of the intestinal epithelium and are therefore likely candidates for the intestinal stem cell (Cheng and Leblond, 1974b). The proposed role for CBC cells as the intestinal stem cell has been further supported by a number of clonal analysis experiments that suggested the presence of the stem cell zone between cell positions 1-4 at the crypt base (Bjerknes and Cheng, 1981). This alternative candidate location for the intestinal stem cell, however, has been largely overlooked until recently.

An ability to reliably identify the intestinal stem cell would substantially aid in understanding normal intestinal homeostasis and pathogenic processes, such as a disruption of normal homeostasis. It comes as no surprise, therefore, that many efforts have been directed at establishing molecular markers that would distinguish the stem cell from other cells in the crypt (for a list of proposed markers and cells marked by them see Figure 1.4). Early attempts to identify such markers were based on the presumed location of the stem cell and were therefore looking for proteins exclusively expressed in the stem-cell zone. One of the earliest intestinal stem cell markers to be suggested is an RNA-binding protein Musashi-1. It has been found to be expressed at high levels in developing and regenerating crypts as well as in intestinal adenomas of Apc^{MIN} mice, all of which are likely to contain expanded stem cell populations. Musashi-1 expression, however, has been reported in

both +4 and CBC cells as well as in early progenitor cells and therefore cannot be used as an exclusive marker for the intestinal stem cell (Potten *et al.*, 2003).

The inactive (phosphorylated) phosphatase and tensin homologue (Pten) protein has been suggested as another position-based stem cell marker. He *et al.* (2004b) observed co-staining of position +4 BrdU-retaining cells with P-Pten in the intestinal crypts. Consistent with Pten inactivation these cells displayed active PI3K/Akt signalling as well as nuclear localisation of β-catenin indicating active Wnt signalling (He *et al.*, 2004b). These observations, however, have been questioned by Bjerknes and Cheng (2005) who demonstrated that P-Pten staining was not exclusive to +4 cells and was indeed encountered throughout the crypt-villus axis, although at a lower frequency than at the bottom of the crypt. They also observed consistent co-staining of P-Pten with Chromogranin A, which is a specific marker of enteroendocrine cells (Bjerknes and Cheng, 2005).

Similarly, the microtubule-associated kinase doublecortin and CaM kinase-like-1 (Dcamkl-1) protein has been proposed to mark the intestinal stem cell based on its ability to stain individual cells around position +4 (May et al., 2008). Dcamkl-1 has also been shown to mark a very small population of non-proliferating cells in intestinal adenomas from Apc^{MIN} mice, suggesting that Dcamkl-1 marks a quiescent stem cell (May *et al.*, 2008). While May *et al.* did not assess the proliferative state of Dcamkl-1 positive cells in normal tissue, a later study failed to detect any proliferating Dcamkl-1 positive cells irrespective of their position along the crypt-villus axis (Gerbe *et al.*, 2009). Additionally, a number of characteristics have undermined the role of Dcamkl-1 as a classic stem cell marker. Dcamkl-1 positive cells are frequently detected among the villus cells, they are resistant to ionising radiation and do not seem to drive post-irradiation crypt regeneration (May *et al.*, 2008). It has also been demonstrated that all Dcamkl-1 positive cells in the intestinal epithelium express molecular markers of tuft cells, such as cyclooxygenase 1 and 2, and thus mark post-mitotic differentiated tuft cells rather than quiescent stem cells (Gerbe *et al.*, 2009).

All the proposed markers mentioned so far define the stem cell according to its proposed topographical location along the crypt-villus axis. These studies, however do not provide any functional evidence of the 'stemness' of these cells, namely, the ability to self-renew or give rise to the mature epithelial cell lineages. Such evidence has at last been provided by two studies using transgenic techniques (Barker *et al.*, 2007; Sangiorgi and Capecci, 2008). Barker *et al.* reported that a Wnt target gene, leucine-rich-repeat-containing G-protein-coupled receptor 5 (Lgr5), is selectively expressed in rare cells in a range of tissues. In the tissues of the gastrointestinal tract (stomach, small and large intestines) Lgr5 expression is confined to the crypt base. In the small intestine Lgr5 expression specifically marks the CBC cells. Using an inducible Cre-recombinase transgene expressed under the control of the *Lgr5* promoter and the *LacZ* reporter allele, Barker and colleagues demonstrated that Lgr5 expressing (Lgr5$^+$) CBC cells are capable of producing all the mature intestinal cell types and clones generated by these CBC cells persist

in the intestinal epithelium for at least 60 days (Barker *et al.*, 2007). Lgr5$^+$ cells, thus, fulfil both prerequisites of stem cells, namely pluripotency and long-term self-renewal, establishing CBC cells as true intestinal stem cells. Two additional stem cell markers have been proposed based on their co-expression with Lgr5. Achaete scute-like 2 (Ascl2) and Olfactomedin-4 (Olfm4) have been found exclusively expressed in Lgr5$^+$ CBC cells, but not in Paneth or transit amplifying cells (van der Flier *et al.*, 2009).

Although Barker *et al.* convincingly demonstrated the stem cell nature of CBC cells, a study by Sangiorgi and Capecci (2008) has provided functional evidence that the polycomb group protein Bmi1 (a polycomb group ring finger oncogene) also marks true stem cells, but is mainly expressed in position +4 cells, thus introducing an extra degree of complexity into the debate over the intestinal stem cell identity. Activation of the reporter allele in Bmi1 expressing (Bmi1$^+$) cells has established that Bmi1$^+$ cells are able to form long-lasting cell clones that include all the differentiated cell lineages. Additionally, stem cell ablation via selective expression of diphtheria toxin in Bmi1$^+$ cells resulted in a rapid crypt loss (Sangiorgi and Capecci, 2008).

While the position of Bmi1$^+$ cells was the main feature that distinguished them from Lgr5$^+$ cells, a number of other distinct characteristics have been observed. While Lgr5$^+$ cells are ubiquitous throughout the alimentary tract, Bmi1 expression has been detected only in the first 20 cm of the small intestine, indicating that Lgr5 is a more universal stem cell marker, which is consistent with its expression in the putative stem cell zones of other tissues (Barker *et al.*, 2007). It has been claimed that Bmi1$^+$ cells proliferate at a slower rate than CBC cells (Sangiorgi and Capecci, 2008). This claim has been widely used to propose that Bmi1$^+$ and Lgr5$^+$ cells represent two distinct stem cell populations with Bmi1$^+$ cells comprising a quiescent or slow cycling population and Lgr5$^+$ cells representing active stem cells. Coexistence of such populations has been described in other tissues such as hair follicle and bone marrow (reviewed in Li and Clevers, 2010).

Interestingly, while Lgr5$^+$ CBC cells have been described as actively proliferating, initial estimations of their cell cycle suggested that they divide once a day (Barker *et al.*, 2007). More accurate assessment of the Lgr5$^+$ cell proliferation rate has demonstrated that they cycle every 21.5 hours, nearly at half the rate of transit-amplifying cells, which divide every 12 hours (Schepers *et al.*, 2011). The 21.5 hour long cell cycle of Lgr5$^+$ cells is strikingly similar to the 24 hour cell division rate of the classic +4 LRC described by Potten *et al.* (1974), a fact widely overlooked in the literature. On the other hand, no deliberate assessment of the proliferation kinetics of Bmi1$^+$ cells has been performed. The claim that Bmi1$^+$ cells are slow cycling is loosely based on the observation that following activation of the yellow fluorescent protein (YFP) reporter in Bmi1$^+$ cells, occasional doublets of YFP expressing cells are detected as late as 5 days after induction, placing the length of the cell cycle in the order of several days (Sangiorgi and Capecci, 2008). However, essentially identical experiments in the same study using a LacZ reporter have revealed relatively large LacZ positive clones as early as day 2 after induction, indicating

a much faster cell cycle. Another argument in favour of a slower proliferation rate for Bmi1$^+$ cells is the longer time required for the reporter expressing progeny of Bmi1$^+$ cells to expand and populate the crypt, compared to the progeny of Lgr5$^+$ cells. This discrepancy, however, could be explained by the higher abundance of the Lgr5$^+$ cells compared to Bmi1$^+$ cells as evident from expression studies (Barker *et al.*, 2007; Sangiorgi and Capecci, 2008). In view of these observations, and the absence of a careful assessment of the Bmi1$^+$ cell proliferation rate, the claims that Bmi1$^+$ cells divide less frequently than Lgr5$^+$ cells appear to be unsubstantiated.

Notably, it is generally assumed that since Bmi1 is mainly expressed around the +4 position, Bmi1$^+$ cells equate to the classic LRC stem cell. However, no study to date has explicitly shown if Bmi1$^+$ cells are capable of long-term label retention and whether they selectively segregate the template DNA strand. At the same time, it has been demonstrated that Lgr5$^+$ cells segregate their chromosomes at random (Schepers *et al.*, 2011) consistent with the lack of asymmetric division in the CBC cells (Snippert *et al.*, 2010).

A strong argument against Bmi1 expression marking a distinct population of the quiescent stem cells comes from the stem cell ablation experiment. Cre recombinase-mediated induction of diphtheria toxin expression in Bmi1$^+$ cells results in the rapid loss of intestinal epithelium and animal death within 2-3 days after induction, while a lower dose induction protocol aids animal survival, but still causes extensive crypt loss (Sangiorgi and Capecci, 2008). Notably, the low dosage protocol has been reported to induce reporter gene recombination in 10% of the crypts in the first 10 cm of the duodenum and gradually decreases along the length of the small intestine. Although the exact frequency of recombination induced by the high dosage protocol has not been specified, it has been said to be similar to that induced by the low dosage protocol (Sangiorgi and Capecci, 2008). With these observations in mind, it is rather remarkable that expression of diphtheria toxin in a quiescent stem cell population in approximately 10% of the crypts is able to cause such a rapid and severe crypt ablation. If Bmi1 was indeed expressed in 'quiescent' stem cells, the 'active' stem cell population would be expected to maintain normal intestinal homeostasis at least for some time.

Remarkably, a very recent report has attempted to revise the 'reserve stem cell' hypothesis using the reciprocal approach of controlled ablation of the Lrg5$^+$ cells. Tian *et al.* (2011) placed a diphtheria toxin receptor transgene under the control of the *Lgr5* promoter thus conferring diphtheria toxin (DT) sensitivity to Lgr5$^+$ cells. DT treatment of mice carrying this knock-in transgene was found to ablate Lgr5$^+$ cells as determined by the loss of the transgene-controlled reporter and Lgr5 mRNA. The loss of Lgr5 expression in the small intestinal epithelium was accompanied by an apparent loss of CBC cells on electron microphotographs of the crypt bases. To the authors' surprise, the ablation of Lgr5$^+$ cells had no major impact on epithelial architecture and homeostasis for as long as 10 days of DT treatment with the exception of increased apoptosis at the crypt base

for the duration of the treatment. Notably, the frequency of Bmi1$^+$ cells was found to increase substantially upon ablation of Lgr5$^+$ cells. Additionally, lineage tracing experiments detected an expansion of the intestinal crypts populated by descendants of Bmi1$^+$ cells upon ablation of Lgr5$^+$ cells. Together, these observations were used by authors to suggest that Bmi1$^+$ cells are mobilised upon loss of Lgr5$^+$ cells and are able to give rise to all small intestinal cell lineages bypassing the intermediate Lgr5$^+$ state. Finally, lineage tracing with a Bmi1-driven reporter allele was used to demonstrate that Bmi1$^+$ cells are able to give rise to Lgr5$^+$ cells under physiological conditions and upon cessation of DT treatment (Tian *et al.*, 2011).

While the report by Tian *et al.* provides strong evidence in favour of Bmi1$^+$ cells being able to contribute to intestinal homeostasis in the absence of Lgr5$^+$ cells and give rise to Lgr5$^+$ cells both under physiological conditions and following Lgr5$^+$ cell ablation, the methodology used has an innate vulnerability that may undermine the conclusions. Additionally, the authors make a number of unsubstantiated claims, that would require additional experiments to confirm their validity. Firstly, the ablation of Lgr5$^+$ cells using DT treatment depends on the penetrance and levels of transgene expression. It is possible, therefore, that a fraction of Lgr5$^+$ cells fail to express the transgene or express it at levels insufficient to cause cell death. Importantly, analysis of GFP knock-in expression revealed that Lgr5 is expressed in a decreasing gradient along the crypt-villus axis rather than in an on-off pattern (Sato *et al.*, 2009). Tian *et al.*, attempted to address the possibility of rare Lgr5$^+$ cells persisting in largely Lgr5 deficient epithelium by using an inducible reporter allele activated by Cre recombinase expression from the same knock-in transgene as the DT receptor. When no reporter expression was detected upon Cre recombinase induction in DT treated small intestine, the authors claimed that all the Lgr5$^+$ cells had been eliminated and intestinal homeostasis was sustained due to the activity of the 'reserve' stem cell. This approach is, however, innately vulnerable as it equates 'Lgr5 expressing cells' with 'transgene expressing cells'. Additionally, as this experiment required the manipulation of both *Lgr5* alleles and hence compromised animal survival, it had to be carried out in an artificial setting by transplanting pieces of embryonic small intestine under the kidney capsule of immunocompromised mice. While this transplanted intestine formed the crypt-villus architecture and resembled early postnatal epithelium, its homeostasis could differ from that of intact epithelial tissue. It is, therefore, still possible that a population of low-level Lgr5$^+$ cells contributes to the maintenance of intestinal homeostasis in the absence of high-level Lgr5$^+$ cells. This notion is supported by the observation that after 6 days of lineage tracing in DT treated gut, only a third of the crypts were fully populated with descendants of Bmi1$^+$ cells (Tian *et al.*, 2011).

Based on the ability of Bmi1$^+$ cells to mobilise and contribute to intestinal homeostasis, Tian *et al.* claimed that Lgr5$^+$ and Bmi1$^+$ cells represent distinct stem cell populations. The key point in such a claim is a definition of what makes two cell populations distinct. The first definition can be based on the expression of molecular markers, such as Bmi1 or

Lgr5 themselves. However, Tian *et al.*, reported a clear overlap between Bmi1 and Lgr5 expression as double-labelled cells are detected under physiological conditions between positions 1 and 6, consistent with the original report by Sangiorgi and Capecci (2008). Although Tian *et al.* did not explicitly state the frequency of such double-labelled cells, analysis of their quantitative data suggests that about 21% of Bmi1$^+$ cells also expressed Lgr5. While the proportion of Lgr5$^+$ cells expressing Bmi1 is likely to be lower, due to the overall higher number of Lgr5$^+$ cells per crypt, it is clear that Lgr5$^+$ and Bmi1$^+$ cells cannot be regarded as distinct population based on the expression of these molecular markers. The second definition of distinct cell populations could rely on the cell morphology. Although no thorough morphological analysis of Lgr5$^+$ and Bmi1$^+$ cells has been conducted, the former have been strongly associated with a narrow spindle-like shape and an elongated nucleus – a morphology characteristic of the CBC cell. Visual analysis of Bmi1$^+$ cells can distinguish two morphotypes loosely correlated to their location within the crypt. Bmi1$^+$ cells at the bottom of the crypt appear to have a CBC cell-like morphology, while cells higher in the crypt are characterised by a larger and more round nucleus (Sangiorgi and Capecci, 2008; Tian *et al.*, 2011). Consistent with this observation, fluorescence-activated cell sorting (FACS) analysis of intestinal crypt cells distinguished two morphologically distinct populations: the 'main' population consisting of larger cells was largely represented by transit amplifying cells, while the 'small' population was represented by smaller CBC cells. Notably, while Lgr5 expression was strictly confined to 'small' cells, Bmi1 was expressed in both populations (Montgomery *et al.*, 2011). Therefore, based on morphology, Bmi1$^+$ cells not only overlap with CBC cells, but appear to comprise two morphologically distinct populations. Finally, physiological properties can be used to define the stem cell populations. One such property relevant to this dispute is the rate of proliferation. While Tian *et al.* explicitly state that Bmi1$^+$ cell quiescence is yet to be demonstrated, they repeatedly imply that Bmi1$^+$ cells are cycling slower than Lgr5$^+$ cells. However, since no careful analysis of cell cycle kinetics of Bmi1$^+$ cells has been performed to date, this parameter cannot be used to identify Lgr5$^+$ and Bmi1$^+$ cells as two distinct populations. Given the possible definitions of distinct cell populations, even if Lgr5$^+$ and Bmi1$^+$ cells form different populations, these are more likely to represent a continuum rather that distinct populations. Based on the lineage tracing of Bmi1$^+$ cells' descendants and Lgr5 expression in a fraction of these descendants, Tian *et al.* arrived at the conclusion that Bmi1$^+$ cells give rise to Lgr5$^+$ cells under physiological conditions. Based on this conclusion, the authors went on to speculate that Bmi1$^+$ cells take an upstream position in the stem cell hierarchy in relation to Lgr5$^+$ cells. However, the observations that led the authors to conclude a Bmi1$^+$ origin for Lgr5$^+$ cells could be interpreted in a number of ways. For example, 24 hours after the activation of the inducible reporter gene using a Bmi1-driven Cre recombinase, Tian *et al.* observed single cells expressing the reporter. These cells were postulated to be Bmi1$^+$ cells before their first division since labelling. As mentioned above, 21% of these reporter expressing cells

were also found to express Lgr5. Since these Bmi1$^+$ cells had not undergone a division, they represent an overlapping population of Bmi1 and Lgr5 expressing cells and cannot be regarded as Lgr5$^+$ cells that originated from Bmi1$^+$ cells, but rather as a cell population that expresses both markers. Somewhat hastily the authors then stated that the number of the double-labelled cells increased two-fold by 48 hours after reporter activation and concluded that Bmi1$^+$ cells can give rise to Lgr5$^+$ cells under normal physiological conditions. However, the two-fold increase in the number of double-labelled cells is readily explained by the 21.5 hour cell cycle of Lgr5$^+$ cells (Schepers *et al.*, 2011). This notion is consistent with the images provided in the paper that show pairs of double-labelled cells, suggesting that the observed increase in double-labelled cells is due to normal proliferation of the Lgr5$^+$ cell population. Therefore, what these observations appear to suggest is the existence of a cell population that expresses both stem cell markers and proliferates at a rate comparable to that of Lgr5$^+$ cells. Indeed, if Bmi1$^+$ cells truly 'gave rise' to Lgr5$^+$ cells (i.e. underwent a cell division with one daughter cell retaining reporter-only staining and the second daughter cell acquiring Lgr5 expression and becoming a double-labelled cell) a rather different picture is expected. In such a scenario no double-labelled cells would be observed at 24 hours after induction of reporter expression. The first double-labelled cells would appear at 48 hours after induction and ideally would be found in pairs comprised of one reporter-expressing and one double-labelled cell.

Finally, even if one accepts the authors' reasoning that Bmi1$^+$ cells can give rise to Lgr5$^+$ cells, a reciprocal experiment demonstrating that Lgr5$^+$ cells are unable to give rise to Bmi1$^+$ cells is required to support the claim that Bmi1$^+$ cells are upstream of Lgr5$^+$ cells in the stem cell hierarchy. Without such an experiment an equipotent possibility remains that a two-way flow exists between these two populations. Such a possibility is favoured by the presence of a substantial intermediate population expressing both markers.

Taking all these caveats into consideration, Bmi1 is unlikely to specifically mark a population of quiescent stem cells distinct from Lgr5$^+$ cells. It seems more reasonable to conclude that Bmi1 is expressed in, but not limited to, a subset of Lgr5$^+$ cells in the proximal section of the small intestine. However, this does not rule out the existence of the quiescent intestinal stem cell altogether. Notably, a recent report identified a rare population of murine intestinal cells characterised by the expression of mouse telomerase reverse transcriptase (mTert) (Montgomery *et al.*, 2011). These cells were found to be largely quiescent as 90-95% of mTert$^+$ cells failed to exhibit expression of the proliferation marker Ki67. The progeny of mTert$^+$ cells were able to populate the whole crypt over an extended period of time and gave rise to all the intestinal cell lineages. While the descendants of mTert$^+$ cells were found among Lgr5$^+$ cells, whether Lgr5$^+$ cells can contribute to the pool of mTert$^+$ cells was not explored (Montgomery *et al.*, 2011). It, therefore, remains unclear, whether mTert$^+$ cells represent a 'master' stem cell population or whether the two populations exist in a dynamic equilibrium with each population contributing to the other.

Notably, mTert and Lgr5 expression in the crypt intestinal cell populations was found to be mutually exclusive. mTert expression was absent from Lgr5 expressing CBC cells, and *vice versa* no Lgr5 expression was detected in the mTert$^+$ population. Conversely, Bmi1 expression was detected in both of these cellular populations, as well as in cells lacking expression of either of these markers (Montgomery *et al.*, 2011). Bmi1, therefore, appears to mark a diverse population of intestinal cells likely to comprise both 'active' and 'reserve' stem cells as well as some undefined cell population. Thus, designation of Bmi1 as a 'specific' stem cell marker should be used with caution.

A number of reports have also proposed a hematopoietic stem cell marker CD133 (Prominin 1 (Prom1) in mice) as a molecular marker for the intestinal stem cell (Snippert *et al.*, 2009; Zhu *et al.*, 2009). Targeting a reporter gene to the Prom1 locus has indeed demonstrated that Prom1 expression in the small intestine is mainly confined to the CBC cells that are able to give rise to all mature cell lineages (Zhu *et al.*, 2009). However, Snippert *et al.* (2009) have reported a broader expression of Prom1 and a rapid elimination of reporter labelled cells from the intestinal epithelium. They, therefore, concluded that Prom1 expression marks a population of cells mainly composed of early progenitor and, to a much lesser extent, of stem cells (Snippert *et al.*, 2009).

1.1.4.2   Dynamics and homeostasis of the small intestinal stem cell

While a certain degree of controversy remains over which of the newly discovered stem cell markers identify the 'true' stem cell population, and what being a 'true' stem cell population entails, these markers represent powerful tools that enable investigation of many aspects of stem cell biology.

One of the central questions in the intestinal stem cell biology is the number of active stem cells in the crypt. The classic model postulates that the annulus of cells at position +4 contains 16 cells, 4-6 of which are proposed to be the stem cells. Mathematical modelling of the crypt dynamics has further suggested that a steady state crypt contains between 4 and 16 stem cells, while their number can increase up to 30-40 per crypt in response to damage (reviewed in Potten *et al.*, 2009). Consistent with these estimations, Snippert *et al.* have calculated that the crypt base contains between 12 and 16 Lgr5$^+$ cells (Snippert *et al.*, 2010).

The presence of more than 1 stem cell per crypt raises the question of their equipotency. The use of chimeric mice from strains differentially expressing binding sites for lectin has demonstrated that while crypts of neonatal mice were composed of cells derived from both parental strains, the crypts of mice older than 2 weeks were monoclonal (Schmidt *et al.*, 1988). These results were consistent with a number of other studies exploiting various approaches that concluded that crypts of adult mice are derived from a single 'founder' cell (Ponder *et al.*, 1985; Winton *et al.*, 1988). A number of reports exploiting mutagenesis to randomly interrupt otherwise uniform expression of a reporter gene have demonstrated

mosaic reporter expression in crypts shortly after mutagenesis. Long-term observations of such crypts have revealed a gradual increase in the number of uniformly expressing (or not expressing) crypts coincident with the loss of mosaic crypts, a process termed 'monoclonal conversion' (Park *et al.*, 1995; Williams *et al.*, 1992; Winton *et al.*, 1988). These observations raise the possibility of a single 'master' stem cell producing the rest of the stem cells. In this scenario, if the inactivating mutation occurs in the 'master' stem cell the whole crypt eventually becomes mutant. Conversely, mutations in the shorter-lived 'slave' stem cells are eventually lost, returning the crypt to the uniform expression of the intact reporter. An alternative model has proposed the existence of several equipotent stem cells that stochastically undergo symmetric division, which could equally explain the observed return to monoclonality (Loeffler *et al.*, 1997). Symmetric division gives rise to either two new stem cells or two partially committed progenitors. However, asymmetric divisions are postulated to predominate in the intestinal stem cell population, with the daughter cells adopting divergent fates (i.e. one stem and one committed progenitor) (Scoville *et al.*, 2008).

Two recent studies have demonstrated that, contrary to the widespread confidence in prevalence of asymmetric stem cell division, the majority of intestinal stem cell divisions occur in a symmetric fashion thus creating a steady-state asymmetry on the populational level. Lopez-Garcia *et al.* (2010) and Snippert *et al.* (2010) have conducted mathematical analyses of long-term lineage tracing of recombination events resulting in reporter gene activation. The observed patterns of clonal expansion and monoclonal conversion are consistent with the existence of equipotent stem cell populations predominantly undergoing symmetric divisions. In this scenario, stem cell loss due to production of two committed progenitor cells is compensated by symmetrical divisions generating two stem cells. As a result, monoclonal conversion is achieved due to neutral competition between the existing stem cells rather than expansion of the 'master' stem cell (Lopez-Garcia *et al.*, 2010; Snippert *et al.*, 2010). While both groups have stated that their conclusions do not disprove the existence of a hypothetical quiescent 'master' stem cell, its activity does not seem to have a substantial influence on the steady-state homeostasis of the crypt stem cell population. Notably, while Snippert *et al.* have used Lgr5-driven Cre recombinase to activate the reporter gene, Lopez-Garcia *et al.* have employed the AhCre^{ER} recombinase, which is expressed in wider stem and progenitor cell populations. The similarity between the two models derived from these experimental approaches implies that even if Lgr5$^+$ cells are not the only stem cells in the crypt, they represent the major driving force behind the crypt repopulation.

The prevalence of symmetric divisions within the stem cell population has challenged another common view. It has been generally agreed that certain mechanisms are required to protect the stem cell DNA from the inevitable errors during replication and environment-induced mutagenesis. Two such mechanisms have been observed in other stem cell systems. The first mechanism involves a very slowly cycling stem cell, which

produces actively proliferating progeny. The stem cell thus undergoes a limited number of cell divisions during the lifetime of an organism and in that way is protected from replication-induced mutagenesis. Such a mechanism has been reported in the bone marrow (Cheng *et al.*, 2000). An alternative mechanism first proposed by Cairns (1975) involves an asymmetric division and retention of the 'immortal' DNA strand by the newly formed stem cell. In this way, the original DNA template is maintained unchanged in the stem cell and thus prevents the accumulation of the errors produced during replication (Cairns, 1975). Such a system has been proposed in a number of tissues including mammary epithelium, brain and muscle (Karpowicz *et al.*, 2005; Shinin *et al.*, 2006; Smith, 2005). As mentioned earlier, label retaining cells have been observed in the small intestinal epithelium, where they have been demonstrated to segregate their parental and newly synthesised DNA strands (Potten *et al.*, 2002). However, in view of the lack of asymmetric stem cell division reported recently, it is unlikely that retention of the 'immortal' DNA strand takes place, at least in the majority of the intestinal stem cells. Consistent with this, Schepers *et al.* (2011) have reported that Lgr5 expressing CBC cells segregate chromosomes between the daughter cells at random. Additionally, a recent report has provided conclusive evidence that both CBC cells and position +4 cells (defined as the first cell just above Paneth cells) segregate their chromosomes randomly (Escobar *et al.*, 2011). Moreover, post-irradiation DNA label retention in this study has demonstrated that the only crypt cells retaining high levels of the label at day 9 post labelling were represented by the mature cell types. Conversely, CBC and position +4 cells displayed heavily diluted label at day 9 that was completely lost by day 18 post labelling (Escobar *et al.*, 2011). Intestinal stem cells or at least the majority of them, therefore, represent an unusual stem cell population. They are relatively fast-cycling, predominantly undergo symmetric divisions and segregate their chromosomes at random. Yet, the stem cell population persists for the lifetime of an organism, undergoing 700-1000 cell divisions, while demonstrating reasonably low mutability (Scheppers *et al.*, 2011). Therefore in the current absence of evidence in favour of a quiescent 'master' stem cell new mechanisms are necessary to explain the protection of the stem cell genome integrity.

In addition to the lack of definitive stem cell markers, the absence of a defined *in vitro* system to culture intestinal crypts has hindered the progress in understanding the pathways involved in intestinal stem cell homeostasis. A number of attempts to develop such a system have provided insights into the factors and pathways required for stem cell maintenance. These insights have been consolidated by Sato *et al.* (2009), who generated an *in vitro* system capable of supporting the development and long-term growth of intestinal organoids composed of crypt and villus-like domains encompassing a central lumen. This system makes use of laminin-rich matrigel media to avoid detachment-induced apoptosis (anoikis) and contains the Wnt agonist R-spondin, epidermal growth factor (EGF), the Notch ligand Jagged and the BMP antagonist Noggin (Sato *et al.*, 2009). The components of this system therefore define the requirements for the intestinal

stem cell niche. In order to sustain the long-term growth of the epithelium the intestinal stem cells require the presence of the laminin-containing basal membrane, activated Wnt and Notch pathways, activation of the EGF receptor and inhibition of BMP signalling. Notably, the named components are sufficient to support the development of the crypt-villus organoids from a single Lgr5 expressing cell further supporting the significance of Lgr5 as a marker of the functional stem cell (Sato *et al.*, 2009).

The mesenchymal tissue underlying the epithelial sheet has been proposed to provide a cellular niche for the intestinal stem cell (reviewed in Shaker and Rubin, 2010). In terms of the particular signals required for intestinal stem cell function, mesenchymal cells contribute some of the basal membrane components, such as collagen IV, laminin and nidogen, providing structural support and the base for cell adhesion (Paulsson, 1992). Additionally, stromal cells adjacent to the crypt base have been shown to express BMP antagonists such as Noggin, Gremlin and Chordin thus creating a permissive environment for stem cell proliferation (Haramis *et al.*, 2004; Kosinski *et al.*, 2007).

In addition to the suggested role of mesenchymal cells in creating the stem cell permissive environment, it has been demonstrated that within the crypt the stem cell niche is provided by the Paneth cells. Along with the production of antimicrobial substances, Paneth cells have been found to express the Wnt ligands Wnt3 and Wnt11, the EGF receptor ligands Egf and Tgfα as well as the Notch ligand Dll4 (Sato *et al.*, 2010). Signals generated by the Paneth cells thus complement the signals provided by the mesenchyme to generate an environment capable of supporting the intestinal stem cell as outlined earlier. Of note, Lgr5 expressing cells have been found to position themselves so that to maximise their contact area with Paneth cells (Sato *et al.*, 2010). Consistent with the requirement for the signals provided by Paneth cells for stem cell maintenance, Paneth cell ablation via conditional inactivation of the *Sox9* gene has been shown to result in crypt loss coincidental with the expected Paneth cell turnover rate (Sato *et al.*, 2010). Notably, while single Lgr5 expressing cells are able to produce crypt-villus organoids in culture, this happens with a frequency of about 7%. Conversely, heterotypic doublets consisting of one Lgr5 expressing cell and one Paneth cell give rise to intestinal organoids with 60% efficiency (Snippert *et al.*, 2010). The improved plating efficiency of stem cell - Paneth cell tandems could be explained by the Paneth cell-mediated secretion of the Wnt ligands. Consistent with this hypothesis, the presence of the Wnt agonist R-spondin in the culture media only seems able to amplify the pre-existing Wnt response induced by Wnt ligands provided by the Paneth cells. Despite the ubiquitous presence of R-spondin, active Wnt signalling has been found to be confined to the crypt base of the cultured organoids, as assessed by Wnt reporter expression. Conversely, addition of Wnt3 ligand to the media has been shown to induce the organoid-wide expression of the Wnt reporter, coincidental with expansion of the proliferative compartment and the loss of differentiated cell types (Sato *et al.*, 2010).

Finally, *in vitro* culture of the intestinal organoids has highlighted a requirement for

Notch signalling in intestinal stem cell homeostasis (Sato *et al.*, 2010). As mentioned in the previous section, suppression of Notch signalling using γ-secretase inhibitors has been shown to abolish cell proliferation and induce differentiation along the secretory lineage (van Es *et al.*, 2005b). Conversely, expression of constitutively active Notch1 receptor has been reported to induce a dramatic increase in cell proliferation, while suppressing cell differentiation (Fre *et al.*, 2005). However, expression of constitutively active Notch1 receptor in the intestinal epithelium lacking Tcf4 was unable to rescue ablation of the proliferative compartment caused by a dearth of Wnt signalling (Fre *et al.*, 2009). It appears, therefore, that a combination of Wnt and Notch signals is required to maintain cell proliferation in the crypt. Notably, activated Wnt signalling has been reported to induce Notch signalling as judged by the increased expression levels of the Notch target gene Hes1 in intestinal adenomas (van Es *et al.*, 2005b). Conversely, neither blocking nor activation of Notch signalling seems to affect the extent of Wnt pathway activation (Fre *et al.*, 2005; van Es *et al.*, 2005b). Together, these observations suggest a model (Figure 1.3), where high levels of Wnt signalling at the bottom of the crypt induce expression of Notch pathway components. By a yet unknown mechanism, some cells express Notch ligands and thus escape Notch activation. These cells impose lateral inhibition on their neighbours by activating Notch signalling and maintaining their proliferation. As cells migrate up the crypt and down the Wnt ligand gradient, they lose their proliferative potential and differentiate into one of the mature cell types. Those cells that escape Notch activation differentiate along the secretory lineage, while the cells with activated Notch signalling differentiate into enterocytes (reviewed in Crosnier *et al.*, 2006).

1.2 Colorectal cancer

1.2.1 Incidence and environmental risk factors

Colorectal cancer (CRC) is the third most common cancer in UK (excluding non-melanoma skin cancer). CRC is more common in men than women, and its incidence has remained relatively unchanged during the last decade. Although the 10-year survival rate has improved nearly two-fold in the past 40 years, CRC still is the second most common cause of cancer-related mortality after lung cancer (Cancer Research UK). Environmental factors suggested to increase the risk of developing CRC include diet rich in red and processed meat (Norat *et al.*, 2000) and poor in natural fibres (Park *et al.*, 2005), lack of physical activity (Wolin *et al.*, 2011), obesity (Moghaddam *et al.*, 2007), smoking (Liang *et al.*, 2009) and alcohol consumption (Fedirko *et al.*, 2011).

1.2.2 Genetic predisposition to CRC

It is estimated that 20-25% of all CRC cases have a familial hereditary origin, while 5-10% of all cases are inherited with a mendelian ratio, indicating an autosomal dominant nature of the mutation (Lynch and de la Chapelle, 2003). Hereditary syndromes conferring susceptibility to CRC development have provided invaluable insights into the causes and natural history of CRC. Hereditary CRC syndromes are classified into two major categories depending on the presence of intestinal polyps. Polyposis syndromes are, in turn subdivided into adenomatous and hamartomatous polyposis based on the predominant tissue within the polyps.

1.2.2.1 Familial adenomatous polyposis (FAP)

The individuals diagnosed with FAP develop hundreds to thousands of florid colonic adenomas at an early age, predominantly composed of epithelial cells. By the mean age of 40 years high adenoma burden results in the development of adenocarcinoma in nearly 100% of cases. Tumours from such patients are commonly characterised by aneuploidy and chromosomal instability. They typically carry mutations in a range of important oncogenes and tumour suppressors such as APC, KRAS and P53 (reviewed in Lynch and de la Chapelle, 2003). In 1991 Groden and colleagues discovered that mutations in *APC* (*adenomatous polyposis coli*) gene are implicated in the development of FAP (Groden *et al.*, 1991). Additionally, APC has been found to be mutated in 80% of early adenomas in sporadic cases of CRC (Nagase and Nakamura, 1993). The position of the mutation within the *APC* gene is known to affect the manifestation of the syndrome. While mutations in the second half of the last *APC* exone result in typical FAP symptoms, mutations earlier in the gene, or in the most 5' region, manifest as attenuated FAP (AFAP) characterised by fewer and more proximal adenomas as well as a delayed adenoma formation (reviewed in Sancho *et al.*, 2004).

1.2.2.2 Hamartomatous polyposis syndromes

Hamartomatous polyposis syndromes are a group of four syndromes characterised by hyperplasia of otherwise normal tissue with predominant stromal component. This group includes the juvenile polyposis syndrome (JPS), the Peutz-Jeghers syndrome (PJS), the Bannayan-Ruvalcaba-Riley syndrome and Cowden's disease (de la Chapelle, 2004). The latter two syndromes are both linked to mutations within the *PTEN* gene and display a substantial symptomatic overlap, suggesting that they might represent different manifestations of the same syndrome (Eng and Ji, 2003). Notably, although these two syndromes have been shown to result in malignant carcinoma in a limited number of cases, gastrointestinal lesions developing in the patients are predominantly benign in nature and the involvement of these syndromes in development of advanced CRC is yet to be conclusively demonstrated (Merg and Howe, 2004). The other two syndromes (PJS and JPS),

despite their low incidence, confer a substantial risk of colorectal cancer (de la Chapelle, 2004).

JPS patients develop between 50 and 200 polyps predominantly in rectosigmoid region of the colon. The polyps in JPS patients differ from florid FAP polyps in a spherical morphology with smooth surface. Histologically, JPS polyps consist of mucous cysts surrounded by stromal tissue with obvious chronic inflammation response (Rashid *et al.*, 2000). The mutations most commonly associated with JPS have been found to occur in *SMAD4* (Howe *et al.*, 1998) and *BMPR1A* (Howe *et al.*, 2001) genes.

Individuals with PJS develop benign hamartomatous polyps in the gastrointestinal tract, which are characterised by cystically dilated glands with a prominent presence of mucus overproducing Goblet cells (Tomlinson and Houlston, 1997). 50% of PJS cases are linked to a mutation in the *LKB1* gene (Lim *et al.*, 2003).

1.2.2.3   Hereditary nonpolyposis colorectal cancer

Hereditary nonpolyposis colorectal cancer (HNPCC) or Lynch syndrome accounts for 2.5-5% of all CRC depending on the definition (de la Chapelle, 2004). This syndrome is characterised by the development of CRC in the absence of marked intestinal polyposis with a relatively late onset (Hampel *et al.*, 2005). A distinctive feature of HNPCC tumours is microsatellite instability (as opposed to chromosomal instability in FAP) (Thibodeau *et al.*, 1993). Consistent with this, HNPCC is strongly associated with mutations in mismatch repair (MMR) genes such as *MLH1*, *MSH2*, *MSH6*, *PMS1* and *PMS2* with the first two genes accounting for 90% of all mutations in HNPCC cases. Microsatellite instability caused by deficiency in MMR is then thought to accelerate the rate of mutagenesis.

These three groups of hereditary syndromes predisposing to colorectal cancer exemplify defects in different functional groups of genes as defined by Kinsler and Vogelstein (1998), namely 'gatekeeper', 'landscaper' and 'caretaker' genes. Malfunction of the gatekeeper genes, such as *APC*, results in large number of benign polyps. As a result of their abundance, some polyps progress to malignant cancer with nearly 100% penetrance. In contrast to this, polyps in individuals with defects in caretaker genes (for instance, MMR system genes) arise at a rate comparable to general population. However, due to the accelerated rate of tumourigenesis, these polyps are more likely to progress towards advanced stages. Finally, defects in the landscaper genes leading to hamartomatous polyposis disrupt the physiological microenvironment of epithelial cells thus creating permissive state for cancer development (Kinzler and Vogelstein, 1998).

1.2.3   Major signalling pathways involved in CRC

Although familial cases of CRCs account only for about 20% of all cases, mutations in the pathways implicated in the hereditary syndromes leading to CRC are commonly detected in sporadic cases of CRC. Research into the causes of CRC-related syndromes, as well as

mutational analysis of sporadic CRCs, has therefore provided insights into the signalling pathways involved in initiation and progression of CRC (reviewed in Sancho *et al.*, 2004).

1.2.3.1 Wnt signalling

Characterisation of the mutations within the *APC* gene in patients with FAP has provided an early link between the Wnt pathway and CRC (Groden *et al.*, 1991). As described earlier in this chapter, APC is a central component of the destruction complex that targets cytoplasmic β-catenin for proteasomal degradation (Figure 1.2). Loss of APC therefore results in an inability to control cytoplasmic levels of β-catenin and, as a result, up-regulation of the canonical Wnt pathway target genes (reviewed in Giles *et al.*, 2003). Although FAP represents a small proportion of all CRC cases, APC mutations are detected in 80% of CRC cases (Nagase and Nakamura, 1993). Additionally, mutations in β-catenin that render it resistant to proteasomal degradation have been observed in 10% of CRC (Morin *et al.*, 1997). Remarkably, mutations in β-catenin and APC appear to be mutually exclusive suggesting complementarity of Wnt activating mutations. However, β-catenin activating mutations are more common in small adenomas and under-represented in invasive carcinomas, indicating that APC might have other tumour suppressor roles in addition to β-catenin degradation (Samowitz *et al.*, 1999). Interestingly, although other Wnt pathway components, such as AXIN and certain WNT ligands, have been found mutated or misregulated in other cancers, the role of these mutations in CRC appears to be insignificant (reviewed in Giles *et al.*, 2003). Notably, mutations leading to aberrant activation of the Wnt pathway are the only genetic aberrations observed in early premalignant stages of CRC such as aberrant crypt foci and early adenomas (Powell *et al.*, 1992). This suggests that aberrant activation of Wnt signalling is an early event in CRC natural history.

A number of animal models targeting Wnt pathway components have been generated in order to recapitulate FAP symptoms and CRC development in a controlled environment (reviewed in Heyer *et al.*, 1999). An N-ethyl-N-nitrosourea (ENU) screen by Su *et al.* (1992) yielded the first mouse model of the intestinal carcinogenesis, termed Multiple Intestinal Neoplasia (MIN). These mice have been found to carry a nonsense-mutation in codon 850 of *Apc* resulting in a truncated protein. Mice heterozygous for the Apc^{MIN} allele have a shortened lifespan and develop numerous adenomas across the gastrointestinal tract (Su *et al.*, 1992). Similarly, mice with a heterozygous truncating mutation in codon 716 of *Apc* gene ($Apc^{\Delta716}$) developed multiple intestinal adenomas (Oshima *et al.*, 1995). Somewhat in contrast to these two studies, mice with a mutation at codon 1638 of *Apc* gene (Apc^{1638N}) developed far fewer intestinal tumours, which were nonetheless capable of progressing towards carcinoma (Fodde *et al.*, 1994). These mice also displayed a range of extra-intestinal phenotypes similar to those found in FAP patients. The observation that distinct mutations in the murine *Apc* gene manifest in different ways reflects

the heterogeneity of the symptoms observed in FAP patients. Deletion of exon 3 of β-*catenin* resulting in dominant stable form of the protein has also been reported to cause an intestinal neoplasia phenotype similar to the one observed in $Apc^{\Delta}716$ mice (Harada *et al.*, 1999). Notably, mutational analysis of adenomas arising in Apc^{1638N} mice have demonstrated that the only mutation consistently present across the majority of tumours is the loss of the intact *Apc* allele, further supporting the idea that aberrant activation of the Wnt pathway is sufficient to initiate CRC (Smits *et al.*, 1997). It should be noted, however, that while in mouse models mutation of the intact *Apc* allele usually results in complete inactivation of Apc tumour suppressor activity, in human cancers selection favours mutations that retain residual β-catenin degradation activity of APC. This relationship between APC mutations and the level of Wnt activation has been formulated into the 'just-right' model, which postulates that an 'optimal' level of Wnt signal is required for tumour development with both 'too-low' and 'too-high' levels of signalling conferring selective disadvantage (reviewed in Fodde *et al.*, 2001).

Notably, all mouse models based on Apc inactivation predominantly develop tumours in the small intestine. This is in contrast to the pattern of intestinal tumourigenesis in humans, where the majority of cancer arise in the large intestine. Additionally, large numbers of polyps arising in these models and extra-intestinal manifestations results in a drastically reduced animal lifespan thus limiting the time available for cancer progression. As a result, only very few adenomas progress to carcinoma stage and virtually no metastatic spread is detected in these animals (Heyer *et al.*, 1999). Generation of a conditional *Apc* allele, whose truncation is induced by the expression of the Cre-recombinase, has made it feasible to overcome these limitations by confining Apc loss to a specific tissue and even to a particular region or cell type within the gastrointestinal tract (Shibata *et al.*, 1997). Indeed, expression of the Cre-recombinase under the control of the CDX2 promoter elements along with a conditional *Apc* allele resulted in preferential adenoma and carcinoma development in the colon and distal small intestine (Hinoi *et al.*, 2007).

1.2.3.2   RAS-RAF-MAPK signalling

Another signalling pathway, whose components are commonly found to be mutated in CRC is the RAS-RAF-MAPK pathway. The Rat Sarcoma viral oncogene homology (RAS) family is represented by Harvey (H-RAS), Kirsten (K-RAS) and neuroblastoma (N-RAS) members. RAS proteins are a group of small G-proteins that are activated by various extracellular stimuli and act as GDP/GTP controlled switches. RAS proteins assume active or inactive states, when bound by GTP or GDP respectively. The GTP-bound active form of RAS is continuously converted to the inactive state via dephosphorylation of GTP to GDP by GTPase Activating Proteins (GAPs). Return to the active state is promoted by Guanine nucleotide Exchange Factors (GEFs) that facilitate exchange of GDP for GTP. Once bound by GTP, the active form of RAS is able to phosphorylate one

of the many downstream effectors. The most characterised pathway downstream of RAS involves sequential signal transduction between RAF, MEK and mitogen-activated protein kinases (MAPK). Phosphorylated MAPK kinases are translocated into the nucleus, where they activate a range of transcription factors resulting in predominantly mitogenic response (reviewed in Malumbres and Barbacid, 2003).

Mutations resulting in constitutively activated K-RAS have been found to occur in over one third of all CRCs (Bos *et al.*, 1987). Additionally, activating mutations in the *B-RAF* gene have been found in 20% of CRC with functional K-RAS (Rajagopalan *et al.*, 2002). Mutations in either K-RAS or B-RAF are predominantly found in tumours larger than 1 cm and are rare in smaller lesions (Vogelstein *et al.*, 1988). This observation suggests that aberrant activation of RAS-RAF-MAPK pathway is more likely to be acquired at later stages of CRC genesis rather than at initiation (Rajagopalan *et al.*, 2002). This notion of K-RAS and B-RAF mutations as drivers of cancer progression have been supported by a number of animal models. Early studies of transgenic expression of oncogenic forms of k-Ras in postmitotic villus as well as proliferating crypt cells has revealed no increase in tumourigenesis (Coopersmith *et al.*, 1997; Kim *et al.*, 1993). In contrast, a report from Janssen *et al.* (2002) has shown that transgenic expression of oncogenic k-Ras under the control of *Villin* promoter in murine intestine resulted in a limited number of tumours ranging from ACF to invasive adenocarcinomas (Janssen *et al.*, 2002). However, expression of a k-Ras oncogene from the *Villin* promoter results not only in activation of k-Ras, but also its over-expression. Expression of a k-Ras oncogene from the endogenous promoter would, therefore, represent a more genuine model of k-Ras activation. Indeed, expression of an oncogenic k-Ras at endogenous locus has failed to alter normal homeostasis of the intestinal epithelium (Guerra *et al.*, 2003). However, conditional expression of the same oncogenic form of k-Ras in the context of heterozygous Apc loss accelerated Wnt-driven tumourigenesis and conferred more invasive phenotype compared to tumours with native k-Ras (Sansom *et al.*, 2006). Together, these observations further support the notion that aberrant activation of RAS-RAF-MAPK pathway plays a crucial role in progression of pre-existing tumours.

1.2.3.3 TGFβ and BMP signalling

As described earlier, TGFβ and BMP ligands are both members of a larger family of TGFβ cytokines. Although TGFβ and BMP ligands differ in the receptor affinities and preferential activation of receptor regulated R-SMAD proteins, they share the same signal transduction machinery in the form of the SMAD4 effector protein (Shi and Massagué, 2003). BMP and TGFβ signalling, therefore, exert a similar anti-proliferative, pro-apoptotic and pro-differentiation effect on the target tissue (Waite and Eng, 2003). Consistent with this, mutations in the BMP receptor BMPR1A and SMAD4 have been implicated in Juvenile polyposis syndrome associated with increased risk of CRC (Chow

and Macrae, 2005). Additionally, TGFβ mutations are frequently acquired in the course of adenoma-carcinoma progression (Fearon and Vogelstein, 1990). The most commonly inactivated component of TGFβ in CRC is the TGFβ receptor type II (TGFβR2) (Grady *et al.*, 1999; Markowitz *et al.*, 1995). SMAD proteins 2 and 4 have also been found to be mutated in 6% and 16% of colon carcinomas respectively (Eppert *et al.*, 1996; Takagi *et al.*, 1996). A number of mouse models targeting components of TGFβ pathway failed to detect an increase in colon neoplasia (reviewed in Dunker and Krieglstein, 2000). The SMAD4 protein represents an exception to this rule as mice with heterozygous loss of SMAD4 have been reported to develop duodenal polyps not dissimilar to polyps in human JPS (Takaku *et al.*, 1999). Similarly, overexpression of the BMP inhibitor Noggin resulted in development of polyps similar to those found in JPS patients (Haramis *et al.*, 2004). Notably, heterozygous loss of SMAD4 and homozygous deletion of TGFβ1 have been reported to accelerate progression of pre-existing lesions towards advanced carcinoma (Engle *et al.*, 1999; Takaku *et al.*, 1998). Taken together, these studies indicate that abrogation of TGFβ and BMP signalling is essential for CRC progression. This idea is consistent with the observation that TGFβR2 mutations are mainly observed in cancers at or after the adenoma/carcinoma transition stage (Markowitz *et al.*, 1995). Remarkably, TGFβ signalling has been reported to have an opposite role in advanced cancer as TGFβ activation has been shown to contribute to metastatic disease (reviewed in Roberts and Wakefield, 2003).

1.2.4 The genetic model of cancer progression

Analysis of the genetic alterations present at various stages of the CRC has revealed a number of commonly recurring mutations. Based on these observations, Fearon and Vogelstein (1990) proposed a model of cancer progression from benign adenoma to carcinoma and, finally, metastatic disease. This model postulates that gradual accumulation of genetic aberrations in a range of tumour suppressor and oncogene genes is required for cancer to progress towards a malignant disease. Although alterations in specific genes are more likely to be found at particular stages, their progressive accumulation is what is required for disease progression, rather than particular chronological order. Nevertheless, the model proposed by Fearon and Vogelstein had suggested a likely sequence of the events based on the likelihood of the genetic alterations. As described earlier, aberrant activation of the Wnt pathway (most frequently due to loss of APC tumour suppressor) is commonly seen as a pivotal event in CRC initiation. Further acquisition of an activating mutation in the RAS oncogene is viewed as the next common step enabling progression to later stages of adenoma. Loss of the long arm of chromosome 18 is also frequently observed towards more advanced stages of adenoma development. This has been associated with the loss of candidate tumour suppressor gene *Deleted in colorectal cancer (DCC)* located on 18q (Fearon *et al.*, 1990). Later studies have also implicated the TGFβ and

BMP pathways effectors SMAD2 and SMAD4 as likely tumour suppressors mapped to chromosome 18q (Eppert *et al.*, 1996; Thiagalingam *et al.*, 1996). Finally, Fearon and Vogelstein proposed the loss of short arm of chromosome 17, which contains the *TP53* locus encoding p53 tumour suppressor, as a final step required for cancer progression towards malignant disease (Fearon and Vogelstein, 1990). Indeed, p53 has been found mutated in nearly 50% of colorectal cancers (reviewed in Iacopetta 2003). Consistent with the model proposed by Fearon and Vogelstein, expression of the mutant form of p53 has been reported in nearly 50% of carcinomas, while in less than 10% of adenomas, supporting the loss of p53 function as a late event in adenoma-to-carcinoma progression (Purdie *et al.*, 1991).

Curiously, even considering the simplified model proposed by Fearon and Vogelstein, for CRC to arise and progress to a malignant disease would require an accumulation of at least seven independent genetic alterations (loss of both copies of three tumour suppressors and an oncogene activation). Based on the mutation rate in normal tissue, this amount of mutations is unlikely to be achieved during the lifetime of an individual (Kinzler and Vogelstein, 1996). However, a mechanism exists that allows cancers to overcome this limitation. In particular, CRCs initiated by APC loss are characterised by 'chromosomal instability' (CIN) that drastically increases the level of chromosomal rearrangements and thus accelerates accumulation of the genetic alterations needed for cancer progression. Moreover, chromosomal instability in these tumours has been directly linked to the loss of APC function (reviewed in Fodde *et al.*, 2001).

An alternative pathway for cancer progression accounting for nearly 15% of CRC cases is exemplified by cancers developed in HNPCC, where microsatellite instability (MIN) due to the defects in mismatch repair system results in mutation rate two to three fold higher that in wild type cells and, as a result, accelerated cancer evolution (Jass *et al.*, 2002). Remarkably, although mutations in MIN cancers affect a set of genes distinct from those in CIN cancer, they tend to target the same four major signalling pathways, namely, Wnt/β-catenin, RAS-RAF-MAPK, TGFβ and p53 further highlighting the importance of these pathways in CRC pathogenesis (reviewed in Laurent-Puig *et al*, 1999).

1.2.5   Cancer stem cell concept and the intestinal stem cell as a cell of origin in CRC

The concept of a cancer stem cell has become increasingly popular over the past five decades (reviewed in Reya *et al.*, 2001; Wicha *et al.*, 2006). This concept has two major implications. The first is the notion that tumours are comprised of heterogeneous cell populations with varying ability to initiate new tumours (clonogenicity). The second implication stems from the hypothesis that cancers arise from cells with stem cell like properties. These two implications are causing a paradigm shift in a number of aspects of cancer biology such as models of carcinogenesis, early cancer detection and prevention,

therapeutic target discovery, drug resistance, metastasis and others (Wicha *et al.*, 2006). A range of cancer stem cell targeting strategies specific for colorectal cancer have been reviewed by de Sousa *et al.* (2011)

The notion that cancer cells have a limited capacity to form colonies in the host environment was first reported in a number of studies using mouse myeloma cells. It has been demonstrated that only a minor fraction of isolated leukaemic cells are able to form colonies both *in vitro* and *in vivo* (Bruce and van der Gaag, 1963; Park *et al.*, 1971). Two alternative explanations were proposed to account for the limited clonogenicity of the leukaemic cells. Either cancer cells in their totality had overall low clonogenic capacity, or a particular small subset of cells was enriched for cancer-initiating cells with the rest of the cells in cancer being non-clonogenic. This duality has been to some extent resolved by Bonnet and Dick (1997). Using human acute myeloid leukaemia (AML) cells, Bonnet and Dick demonstrated that, when transplanted in non-obese diabetic/severe combined immunodeficiency disease (NOD/SCID) mice, AML cells expressing the cell surface marker CD34 but not CD38 ($CD34^+CD38^-$ cells) were the only cell population able to induce AML (Bonnet and Dick, 1997). Although widely accepted in blood cancers, the idea of cancer stem cell in solid cancers is more controversial (reviewed in Hill, 2006). Cancer cells of CRC has proven to be as elusive as from any other solid cancer, if not more so. A number of studies using transplantation of defined populations of CRC cells into NOD/SCID mice have suggested a limited number of cell surface markers alleged to identify cancer stem cells. One of the first markers proposed to define the cancer stem cell population in CRC was CD133 (also known as Prominin 1). Cells expressing CD133 have been found to be 200-fold enriched for cancer initiating cells compared to the $CD133^-$ population (O'Brien *et al.*, 2007; Ricci-Vitiani *et al.*, 2007). A similar study by Dalerba *et al.* (2007) has shown that high expression levels of epithelial cell adhesion molecule (EpCAM) as well as expression of cell surface marker CD44 define a subpopulation of cells with high ability to initiate tumours morphologically comparable to the original lesion (Dalerba *et al.*, 2007). A number of other colorectal cancer stem cell markers such as CD166, CD29, CD24 and Lgr5 have been suggested, based on their expression in spheroid cultures derived from $CD133^+$ cells (Vermeulen *et al.*, 2008). These results, however, should be taken with caution, especially in the light of the recent study by Shmelkov *et al.* (2008). Shmelkov *et al.* have observed wide-spread expression of CD133 in human and mouse metastatic colon cancers, undermining its candidacy as a marker for rare cancer stem cells. Moreover, $CD133^-$ cells from metastatic colon cancer have been found to possess equal if not greater tumourigenic capacity than $CD133^+$ cells (Shmelkov *et al.*, 2008).

Although CRC stem cell surface markers such as CD44, CD166 and others are unlikely to be essential for cancer cell survival and therefore may not represent valuable therapeutic targets, with advances in our understanding of such markers in CRC they may provide a useful tool in developing therapies that would selectively target this cell population.

The second implication of the cancer stem cell concept is that cancers arise from

a particular population of cells with the stem cell-like properties. A number of characteristics make normal tissue stem cells particularly favourable targets for malignant transformation. In fast regenerating tissues, such as intestinal epithelium differentiated cells are replace in a matter of several days. Unlike differentiated sells, adult stem cells are retained in the tissue over longer periods of time, which theoretically enables them to accumulate the mutations required for neoplastic transformation. Furthermore, somatic stem cells are capable of self-renewal, have activated anti-apoptotic pathways, are responsive to growth signals and express telomerase - hallmarks commonly shared by cancer cells (Wicha *et al.*, 2006). A study by Barker *et al.* (2009) has made a strong case in favour of a stem cell origin of CRC. Using a Cre recombinase expressed in Lgr5 positive cells Barker *et al.* have demonstrated that selective induction of Apc loss in the small intestinal stem cells resulted in rapid development of macroscopic adenomas. Conversely, Apc deficient lesions originating from transit amplifying cells displayed impeded growth and rarely progressed beyond the microadenoma stage (Barker *et al.*, 2009). A recent study by Merlos-Suarez *et al.* (2011) have reported that a gene expression signature of normal intestinal stem cells is shared by a subpopulation of CRC cells. This subpopulation has been shown to initiate tumour growth in immunodeficient mice with high frequency. Additionally, cells with this gene expression signature has been shown to be enriched in recurrent and metastatic CRCs (Merlos-Suarez *et al.*, 2011). Together, these observations further support the relevance of the cancer stem cell concept in CRC and could potentially lead to the development of cancer stem cell targeted therapies.

1.2.6   The Wnt pathway as a therapeutic target in CRC

1.2.6.1   Conventional therapies in CRC treatment

The exact treatment plan for CRC patients in UK is normally devised by a multidisciplinary team of specialists including surgeons, oncologist, histopathologist, radiologist and others. The treatment plan is based on the range of factors such as stage and location of the tumour as well as fitness of the patient (NICE guidelines, 2004). Invasive surgery to remove the tumour is undertaken in approximately 80% of cases and is the primary option in CRC management. Although not used routinely, pre-operative radiotherapy in a small number of cases has been shown to substantially reduce the risk of local recurrence. However, its use is limited by radiotherapy-related adverse effects. Adjuvant chemotherapy is recommended in invasive cancers that have spread to local lymph nodes. In cases of advanced cancer with metastatic spread surgical removal of the primary tumour may be recommended to alleviate symptoms such as bowel obstruction or substantial rectal bleeding as well as palliative chemotherapy. In a limited number of cases metastatic spread to the liver is also managed by surgical resection of the liver (NICE guidelines, 2004).

The standard chemotherapy for CRC involves six month intravenous treatment with 5'-fluorouracil and folinic acid (FUFA) (NICE guidelines, 2004). Two other drugs commonly

used in treatment of advanced CRC are topoisomerase I inhibitor Irinotecan and platinum-based alkylating agent Oxaliplatin (Cancer Research UK). General cytotoxicity caused by these drugs during the treatment is often accompanied by substantial side effects. A number of novel therapies targeting specific signalling pathways are being introduced in an attempt to reduce the off-target side effects. Examples of such drugs approved for CRC treatment include a monoclonal antibody against epidermal growth factor receptor (EGFR), Cetuximab, and an EGFR tyrosine kinase domain inhibitor, Gefitinib (Cancer Research UK).

1.2.6.2   Wnt signalling as a therapeutic target

Despite the Wnt pathway being aberrantly activated in 90% of CRC cases, therapies targeting the Wnt pathway remain very limited (Gehrke *et al.*, 2009). A number of factors contribute to the lack of the Wnt targeting therapies, such as potentially high toxicity and the complexity of pathway regulatory mechanisms. At the same time, the modular nature of the Wnt pathway provides multiple points of intervention to alter the level of signalling. Wnt signalling, therefore, may be potentially modulated at many levels, such as ligand expression, processing and secretion, ligand binding to the receptor complex, β-catenin degradation, formation of the nuclear complex between β-catenin and transcription factors as well as expression of downstream Wnt targets.

Although Wnt activation in the majority of CRCs is due to defects in the mechanisms regulating β-catenin degradation, a number of studies have also observed elevated levels of Wnt ligand expression in CRC cell lines (Bafico *et al,*. 2004; Gregorieff *et al.*, 2005; Holcombe *et al.*, 2002). The use of a monoclonal antibody against WNT-1 has been demonstrated to induce an apoptotic response in CRC cells even in the presence of downstream mutations in APC or β-catenin (He *et al.*, 2004a). Further, soluble Wnt inhibitors such as secreted frizzled-related proteins (SFRPs) capable of binding Wnt ligands and preventing their interaction with the receptor complex have been found to be epigenetically silenced in a range of CRC cells and primary tumours. Notably, restoration of SFRP function in CRC cells with mutations in either APC or β-catenin have been found to attenuate Wnt signalling and inhibit colony formation (Suzuki *et al.*, 2004). Another Wnt inhibitor family of proteins Dikkopf (DKK) has been found silenced in CRC cells and primary cancers. Over-expression of DKK in CRC cells even with mutations in APC and β-catenin has been demonstrated to suppress Wnt signalling and impair colony formation (Sato *et al.*, 2007). It should be noted, however, that the above studies used endogenous expression of the Wnt inhibitors. It is unclear, therefore, if treatment with exogenous inhibitors would yield comparable results.

A number of approaches targeting the components of the Wnt receptor complex, such as Frizzled and Dishevelled proteins, have been found effective in suppressing tumourigenesis in a range of cancer cell lines of various tissue origin (Fujii *et al.*, 2007; Merle *et al.*,

2004; Nagayama *et al.*, 2005). However, despite increased expression of Frizzled receptors in colon tumours (Holcombe *et al.*, 2002), no studies have yet demonstrated the feasibility of targeting Wnt receptor components in CRC.

Reflecting different mechanisms that lead to β-catenin accumulation (i.e. stabilising mutations in βcatenin or loss-of-function mutations in the components of the destruction complex) therapeutic approaches at the level of β-catenin turnover complex may either target the oncogenic form of β-catenin or aim to restore the function of the β-catenin destruction complex. Both approaches present a significant challenge. In the case of stabilised β-catenin a number of 'proof of concept' studies have demonstrated that selective deletion of stabilised β-catenin in CRC cells can suppress clonal growth (Kim *et al.*, 2002). However, even more interestingly, some cell lines have been found to have lost their reliance on Wnt signalling. In these cells targeting the stabilised β-catenin was successful in suppressing the Wnt pathway, but appeared to have no effect on the cell ability to grow and form tumours in mouse xenografts (Chan *et al.*, 2002; Kim *et al.*, 2002). This observation raises a concern that advanced cancers may overcome their requirement for the activated Wnt signalling by acquisition of additional mutations.

Restoration of functionality to the β-catenin turnover complex is logistically challenging, especially *in vivo*, due to the 'loss of function' nature of the mutations involved. This approach, therefore, would require introduction of a functional protein into cancer cells. A study by Arenas *et al.* (1996) has provided an indication that this approach might prove feasible *in vivo* as liposome-mediated delivery of an Apc-expressing construct suppressed tumour incidence in Apc^{MIN} mice (Arenas *et al.*, 1996). An alternative approach to restoration of the β-catenin turnover complex activity has been recently discovered that bypasses the need for the introduction of the functional version of Apc. Two groups have independently discovered a number of compounds that inhibit Tankyrase, a poly-ADP-ribose polymerase that facilitated ubiquitin-mediated degradation of Axin. Inhibition of Tankyrase by the given compounds results in stabilisation of Axin and the turnover complex thus promoting β-catenin degradation even in cells with APC mutations (Chen *et al.*, 2009; Huang *et al.*, 2009).

Glycogen synthase kinase 3 (GSK3) represents yet another potential target for the regulation of oncogenic β-catenin. Activation of GSK3β by differentiation-inducing factors (DIFs) from *Dictyostelium discoideum* has been found to inhibit expression of the Wnt target gene *Cyclin D1* and suppress proliferation in a number of CRC cell lines including those bearing activating mutations in β-catenin (Takahashi-Yanaga and Sasaguri 2009).

A number of alternative pathways of β-catenin degradation have been proposed as therapeutic targets in Wnt-driven neoplasia. Chemically induced expression of Siah1, a ubiquitin-ligase binding protein, has been shown to promote β-catenin degradation in a GSK3β-independent manner and suppress proliferation of CRC cells bearing an oncogenic form of β-catenin (Park *et al.*, 2006). It should be noted, however, that Siah1 mediated degradation still relies on functional APC and thus is unlikely to be effective in APC

deficient cancers. Conversely, a small molecule compound Murrayafoline A has been found to facilitate proteasomal degradation of β-catenin independent of GSK3β and APC activity. Murrayafoline A has been found to be effective in suppressing Wnt target gene expression and proliferation of a number of CRC cell lines regardless of their APC status (Choi *et al.*, 2010).

In order to initiate transcription, the β-catenin/TCF complex interacts with a number of transcriptional co-activators, such an acetyletransferases p300 and CBP (CREB binding protein). Targeting the interactions between β-catenin and TCF as well as various co-activators and co-repressors may prove an attractive therapeutic approach for Wnt signalling suppression. An obvious benefit of targeting the Wnt pathway at such a late stage is that it would allow modulation of the pathway even in the presence of upstream APC and β-catenin mutations. A number of small-molecule compounds targeting β-catenin/TCF interaction have been demonstrated to repress Wnt target genes and induce apoptosis in CRC cells (Leproucelet *et al.*, 2004). Similarly, the flavonoid quercetin has been shown to repress Wnt target genes by disrupting the interaction between β-catenin and TCF. As a result, quercetin suppresses cell proliferation and promotes apoptosis in CRC cells in a dose-dependent manner (Shan *et al.*, 2009). Accordingly, quercetin has been previously shown to reduce the number of chemically induced aberrant crypt foci in rats (Matsukawa *et al.*, 1997). A small molecule compound that disrupts interaction between CBP and β-catenin has been shown to induce apoptosis in CRC cells and suppress polyp formation in Apc^{MIN} mice (Emami *et al.*, 2004).

Downstream Wnt target genes represent attractive therapeutic targets for the same reasons that apply to the β-catenin/TCF nuclear complex. Targeting genes commonly up-regulated in Wnt driven neoplasia may provide a tool to manipulate oncogenic effects of aberrant activation of the pathway rather than the pathway itself, thus reducing toxicity and bypassing the upstream mutations. Concurrent inactivation of the Wnt target gene *c-Myc* and *Apc* in transgenic mice has been found to attenuate the intestinal effects of Apc loss, such as increased proliferation and disruption of cell migration and differentiation (Sansom *et al.*, 2007b). Furthermore, antisense morpholino oligomer targeted against c-Myc has been found effective in suppressing the growth of lung and prostate cancer cells in mouse xenografts, while being well tolerated by healthy individuals (Iversen *et al.*, 2003; Sekhon *et al.*, 2008). Adenomas from Apc^{MIN} mice have been demonstrated to express high levels of matricellular protein Sparc, suggesting its Wnt-induced expression. In line with this observation, Sparc deficiency in Apc^{MIN} mice greatly reduced polyp formation, most likely due to enhanced cell migration in normal small intestinal mucosa (Sansom *et al,*. 2007a).

Advances in our understanding of the intestinal stem cell biology may lead to the development of novel therapies targeted at the CRC stem cells. Wnt target genes proposed as the intestinal stem cell markers, such as *LGR5* and *ASCL2* have been found expressed in a fraction of cells in CRC, suggesting a possible overlap between normal and cancer

stem cell marker genes (Becker *et al.*, 2008; Jubb *et al.*, 2006). Notably, ASCL2 knock-down has been shown to induce cell cycle arrest in ASCL2 expressing CRC cells lines (Jubb *et al.*, 2006).

Epigenetic silencing of negative Wnt signalling regulators due to promoter hyperme-thylation has been demonstrated to contribute towards aberrant activation of the Wnt pathway. Particularly, a number of soluble Wnt inhibitors, such as DKKs, SFRPs or WIF, have been shown to be epigenetically silenced in a range of cancers (See Ewan and Dale (2008) for a summary). The use of DNA-methylation inhibitors may, therefore, have a therapeutic benefit in Wnt driven neoplasms. It should be noted, however, that the comprehensive effect of such a therapy is likely to affect cellular processes beyond the Wnt pathway. For instance, activation of silenced tumour suppressors may enhance the anti-oncogenic effect of Wnt signalling suppression.

Inhibition of the DNA methyl transferases (DNMTs) is a common approach used in the reversion of aberrant DNA methylation. However, the use of DNMT inhibitors is primarily restricted to blood cancers due to poor bioavailability in solid tumours (reviewed in Sharma *et al.* 2010). Gene silencing caused by promoter methylation is mediated by a group of methyl-DNA binding domain (MBD) proteins. These proteins bind to methylated CpGs and recruit a range of proteins, such as histone methyl transferases and histone deacetylases, which, in turn, establish repressive histone signature (reviewed in Klose and Bird, 2006). Constitutive deletion of some MBD proteins (Mbd2 and Kaiso) in Apc^{MIN} mice have been shown to extend animal survival and suppress tumour formation and growth (Prokhortchouk *et al.* 2006; Sansom *et al.*, 2003). Of importance, mice deficient for Mbd2 or Kaiso showed no serious abnormalities, which makes MBD proteins favourable potential therapeutic targets.

1.2.7 Use of mouse models in development of novel therapies

One of the obstacles slowing the development of therapies targeting Wnt signalling is the lack of appropriate models for the drug target discovery, validation and testing. Over the decades various human CRC cell lines have served as a platform for target validation and drug testing. In order to assess the validity of a protein as a therapeutic target or the efficiency of a drug, a number of cellular characteristics are examined in the re-sponse to drug administration. These include cell proliferation, apoptosis, clonal survival, anchorage-independent growth and the ability to form tumours when transplanted into immunodeficient mice. These approaches, however, suffer from a range of shortcomings. Some of the CRC cell lines were isolated decades ago and maintained in culture ever since. Considering the high inherent mutation rate and genomic instability in cancer cells, it is likely that these cell lines have acquired numerous mutations and chromosome rearrangements and only remotely resemble the original cancers they were isolated from. Additionally, *in vitro* conditions lack a range of factors that cancer cells are exposed to

in vivo. A cocktail of growth factors, interactions with stromal cells and extracellular matrix all can affect cancer cell survival and modulate the effects of the treatment and should be taken into account during testing of novel therapies. This is considered to be of particular importance for cancer stem cells (Watt and Driskell, 2010)

While transplantation of cancer cells into immunodeficient mice addresses some of the limitations of the *in vitro* conditions, it is not sufficient to recapitulated the native microenvironment of the cancer. The standard xenotransplantation procedure involves CRC cells being injected subcutaneously into mouse flanks. While this might, to some extent, model the process of metastatic spread, the interactions between the xenograft and surrounding tissue are likely to differ significantly from those observed between a primary tumour and its microenvironment in the tissue of origin. Physiological processes, such as angiogenesis, immune response and secretion of the growth regulating factors by the stromal cells play a crucial role in cancer survival. Due to these factors, naturally arising tumours are likely to have a number of advantages over a xenograft in terms of modelling the tumour response. This is particularly relevant when transplanting human cancer cells into mice as mouse tissue may lack the whole range of factors needed for human cell survival (Kelly *et al.*, 2007). As a result, xenotransplanted cells may be more susceptible to the anti-cancer therapy and their extensive use as a testing platform may account for a high failure rate of novel anti-cancer drugs at the transition between animal and human studies (Olive *et al.*, 2009).

The combination of these factors highlights the need for the models that would faithfully recapitulate the microenvironment and evolution of human cancer in animal models. Despite clear differences in physiology and genetics, mice represent an ideal organism to model human neoplasia due to well establishes transgenic approaches and their relatively short reproductive period. A good genetic model of mouse colorectal carcinogenesis should reproducibly generate tumours within a short time frame, which are able to progress through all the stages of carcinoma development to metastatic disease and recapitulate the evolutionary history of human neoplasia in terms of the accumulated mutations.

A number of mouse models that make use of germline mutations in *Apc* gene have been described earlier in this chapter. While the Apc^{MIN} mouse in particular has made an invaluable contribution to our understanding of CRC initiation and development, a substantial differences exist between carcinogenesis in Apc^{MIN} and human intestine. The major differences concern the tumour distribution and extent of progression to advanced stages (reviewed in Heyer *et al.*, 1999). In response to these differenced more advanced models combining mutations in different genes are being constantly generated in order to 'humanise' mouse cancer.

1.2.7.1 Constitutive transgenesis

Generation of targeted deletion of hypoxanthine-guanosine phosphoribosyl transferase (HPRT) in 1987 marked the beginning of targeted transgenesis technology in mice (Kuehn *et al.*, 1987). Numerous mouse models of constitutive gene deletion have been generated since in order to model various conditions and study gene function *in vivo*. While constitutive transgenesis has provided many insights into the physiological role of numerous genes, it has also revealed a number of intrinsic limitations associated with constitutive gene loss.

The first limitation is concerned with the absolute requirement of many genes for normal embryonic development. As a result, constitutive loss or activation of an important developmental regulator is likely to prevent the study of its function in adult tissues. This is particularly relevant in cancer, where many tumour suppressors and oncogenes are vital for normal development. The second limitation is associated with pan-organism loss of the targeted gene. This makes it difficult to study the effects of gene loss in a particular tissue if the gene inactivation causes severe complications elsewhere in the organism. Finally, targeting a gene in all cells of the organism is likely to mask the effects of gene loss in specific cell types as well as affect the interaction between different cell types.

1.2.7.2 Conditional transgenesis

In order to overcome the limitations imposed by constitutive transgenesis, a number of conditional transgenic approaches have been developed, which allow more intricate control over gene manipulation. The simplest case of conditional transgenesis is exemplified by the use of tissue-specific promoters to drive the expression of a gene of interest. This provides spatial control over the gene expression and circumvents the 'side effects' outside the target tissue. Understandably, this approach is mainly restricted to gene overexpression and, therefore, has a limited value for loss-of-function studies. Moreover, in the majority of cases simply expressing a gene in a tissue-specific manner does not provide temporal control and thus does not overcome possible developmental effects. In relation to models of CRC, this approach can be exemplified by expression of the oncogenic form of K-Ras in the murine intestinal epithelium under control of *Villin* promoter (Janssen *et al.*, 2002).

To achieve temporal control over gene loss or activation, a switching mechanism is required that would allow voluntary alteration of gene expression status. A number of systems have been designed to provide such a mechanism. Among the most successful conditional transgenesis systems are Cre-loxP (Causes recombination (Cre) - Locus of crossover of bacteriophage P1 (loxP)), TetO (tetracycline operator) and Flp-Frt (Flp-Flp recognition target). The basis of all these systems lies in two principal elements: the inducible 'effector' and the targeted gene. In the case of the Cre-loxP system the effector component is represented by Cre recombinase. Cre is a DNA recombinase able to specifically recognise 34 bp long nucleotide sequences from bacteriophage P1 and facil-

itate recombination between them (Sternberg and Hamilton, 1981). Depending on the loxP sites orientation, recombination results in either inversion or excision of the DNA fragment enclosed between the sites. When loxP sites are placed unidirectionally so that they flank a crucial part of a gene or a whole gene, Cre recombinase expression would result in excision of that locus effectively rendering the gene inactive. The Cre-loxP system can equally be used to express constitutively activated oncogenes. To this end, a transcription terminating stop-cassette flanked by loxP sites is inserted before the gene, whose expression needs to be induced. When needed, Cre recombinase mediated excision of the loxP flanked region eliminates the stop cassette and allows gene expression to resume.

Two main approaches are commonly exploited to control Cre recombinase activity. Transcriptional control makes use of inducible promoters, while post-translational approaches mainly rely on ligand-mediated activation of the pre-existent recombinase. Of the transcriptionally inducible Cre-recombinases used in the intestinal epithelium, AhCre recombinase is arguably one of the most commonly utilised. It exploits regulatory elements of the rat cytochrome P4501A1 gene (*Cyp1A1*). Under normal physiological conditions *Cyp1A1* is transcriptionally silent. Interaction of certain lipophilic xenobiotics (e.g. β-naphthoflavone) with the cytoplasmic aryl hydrocarbon receptor results in translocation of the latter to the nucleus, binding to *Cyp1A1* promoter and *Cyp1A1* transcription initiation (Ireland *et al.*, 2004).

AhCre recombinase expression is limited to a finite number of epithelial tissues and thus confers a degree of tissue specificity. However, in order to make this approach applicable to a large number of tissues would require finding an inducible gene-expression system for every tissue of interest. On the other hand, post-translational activation of Cre recombinase activity allows the combination of tissue-specificity with inducibility. The most common approach to post-translational regulation of Cre recombinase is the use of a fusion protein between the recombinase and mutated ligand binding domain of human oestrogen receptor (ER) that selectively binds to the oestrogen antagonist tamoxifen, but not endogenous oestrogen (Feil *et al.*, 1997). In the absence of tamoxifen, the fusion Cre-ER protein is sequestered in the cytoplasm preventing it from accessing loxP sites. Tamoxifen binding to the ER domain of the fusion protein reveals a nuclear localisation signal and permits Cre recombinase transport to nucleus, where it can recognise and recombine the loxP sites. Expression of the Cre-ER fusion protein under the control of a tissue specific promoter thus provides a means of tissue-specific inducible deletion or activation of a given targeted gene. As an example of post-translational Cre recombinase regulation, expression of the Cre-ER recombinase protein from the *Villin* locus has been shown to controllably drive recombination in the intestinal epithelium (el Marjou *et al.*, 2004).

Finally, a combination of transcriptional and post-translational approaches creates an opportunity for more stringent control over the Cre recombinase regulation. The use of the Cre-ER fusion protein expressed from *Cyp1A1* promoter overcomes undesired

expression of AhCre recombinase during embryonic development. The resulting AhCreER recombinase requires two ligands, β-naphthoflavone and tamoxifen, for its activation and thus provides a tighter regulatory mechanism (Kemp *et al,.* 2004).

The mechanism of action of the Flp/FRT recombination system derived from Saccharomyces cerevisiae is, in essence, very similar to Cre-loxP system (Dymecki, 1996). Since wild type Flp is characterised by a substantial thermolability and limited activity at 37 °C, an enhanced Flp variant termed Flpe has been created to increase the recombination efficiency in mice (Buchholz *et al.*, 1998).

One of the disadvantages of both the Cre/loxP and Flp/FRT systems is the irreversible nature of the genetic alterations driven by the excision of the targeted region. This limitation has been to some extent resolved in Tetracycline-controlled gene expression systems. Based on the Tet repressor protein from Escherichia coli, Bujard and colleagues have designed Tet-On and Tet-Off expression systems that induce or suppress a targeted gene expression respectively in response to administration of the tetracycline derivative doxycycline (Gossen and Bujard, 1992; Gossen *et al.*, 1995).

The availability of the various conditional transgenesis systems creates a potential for the development of the 'multi-stage' models with several levels of gene manipulation. The first stage of such a model would involve 'cancer initiating' mutations (Apc, β-catenin, K-RAS, p53, etc) being triggered by Cre recombinase. At the second stage a 'therapeutic' gene would be depleted or activated via Tet-regulated system. Combined with new developments in CRC mouse models such an approach may be particularly useful in assessment of the therapeutic potential of novel targets in advanced tumours. Implementation of such a model, however, would require reliable activity of the stage-two targeting system within malignant tissue.

1.3 Brg1 as a therapeutic target candidate for Wnt-driven tumourigenesis

DNA comprising the genome of eukaryotic cells is tightly packaged into chromatin in order to be accommodated within the relatively small boundaries of the nucleus. The basic unit of chromatin is represented by a nucleosome core comprised of DNA wrapped around the octamer of histone proteins. Nucleosomal organisation of chromatin poses substantial challenges for processes that require access to DNA, such as transcription and DNA repair. At the same time, control over the 'chromatin barrier' provides diverse mechanisms for the regulation of the aforementioned processes. Chromatin remodelling complexes capable of shifting and displacing nucleosomes constitute one of these mechanisms. Chromatin remodelling activity thus maintains chromatin in a dynamic state and aids in the interpretation of the variety of inter- and intracellular cues, both normal and neoplastic (For the extensive review of chromatin remodelling complexes see de la Serna

et al., 2006; Roberts and Orkin, 2004; Workman and Kingston, 1998). This section will describe the chromatin remodelling factor BRG1 and its role in mammalian development and tumourigenesis.

1.3.1 Discovery and functional redundancy between paralogues

Brahma related gene 1 (*BRG1*, also known as SWI/SNF related, matrix associated, actin dependent regulator of chromatin, subfamily a, member 4 (*SMARCA4*)) is one of the two mutually exclusive ATPase subunits characteristic of the SWItch/Sucrose Non-Fermentable (SWI/SNF) class of chromatin remodelling complexes in mammals. Human BRG1 and its paralogue human Brahma (BRM) have been independently discovered based on the sequence similarity to their homologues in yeast (SWI2/SNF2) and Drosophila (Brahma) (Khavari *et al.*, 1993; Muchardt and Yaniv, 1993). BRG1 and hBRM have been found to share domain structure with their yeast and Drosophila homologues, including acetyl-lysine binding bromodomain and DNA unwinding helicase motifs (Chiba *et al.*, 1994). Both BRG1 and hBRM have been reported to be enzymatically active and protein complexes containing either of the subunits are capable of remodelling nucleosomes *in vitro* (Phelan *et al.*, 1999). However, a number of studies have reported substantial differences in the expression patterns and function of BRG1 and hBRM, suggesting a lack of functional redundancy between the two ATPases. Analysis of expression patterns has revealed that hBRM is predominantly expressed in tissues with low proliferation rates such as liver, brain, fibromuscular and endothelial cells. Conversely, BRG1 expression has been found to be mainly confined to tissues with high cell turnover, such as epithelial tissues of the gastrointestinal tract, skin, etc. (Reisman *et al.*, 2005). Functional differences between BRG1 and hBRM have been highlighted by the effects of the respective constitutive knock-out mouse models. hBRM null mice have been reported to be viable and fertile, albeit displaying increased cell proliferation (Reyes *et al.*, 1998). Conversely, *BRG1* homozygous null embryos have been found to die *in utero* prior to implantation, while heterozygous knock-outs often display exencephaly and are predisposed to tumourigenesis (Bultman *et al.*, 2000). Furthermore, BRG1 and hBRM have been reported to exhibit antagonistic roles in some processes, for instance osteoblast differentiation (Flowers *et al.*, 2009). This functional diversity is likely to be facilitated by interactions with distinct non-overlapping protein populations. Indeed, both BRG1 and hBRM have been found to contain unique domains not present in the other paralogue that could allow preferential interaction with distinct classes of transcription factors (Kadam and Emerson, 2003).

1.3.2 Physiological functions of BRG1

1.3.2.1 BRG1 protein-protein interactions

Since the SWI/SNF chromatin remodelling complex does not possess an intrinsic DNA binding ability, its recruitment to DNA is accomplished via interaction with transcription factors (Kwon and Wagner, 2007). While BRG1 has no DNA binding ability either, its bromodomain enables BRG1 recruitment to acetylated lysines on histone tails. BRG1, therefore, may serve as an interpreter of the chromatin epigenetic signature for the SWI/SNF complex (Shen *et al.*, 2007). Due to its role as a recruitment platform, BRG1 has been found to mediate the interaction of the SWI/SNF complex with a number of nuclear receptors. Among those are the oestrogen receptor (Chiba *et al.*, 1994), glucocorticoid receptor (Trotter *et al.*, 2008), androgen receptor (Link *et al.*, 2005), retinoid acid receptor (Dilworth *et al.*, 2000), peroxisome proliferator-activated receptor γ (Debril *et al.*, 2004) and vitamin D3 receptor (Kitagawa *et al.*, 2003).

In addition to SWI/SNF complex, BRG1 and BRG1-associated factors (BAFs) have been found to participate in other complexes with activities as diverse as transcriptional control, DNA replication, recombination and repair. Examples of BRG1 and BAFs containing complexes include WINAC (WSTF including nucleosome assembly complex) involved in nuclear receptor mediated transcription regulation and chromatin assembly after DNA replication (Belandia and Parker, 2003); the NUMAC complex (nucleosomal methylation activation complex) containing the histone methylating enzyme CARM1 (coactivator-associated arginine methyltransferase-1) (Xu *et al,*. 2006); and the NCoR-1 complex (Nuclear receptor corepressors-1) containing histone deacetylase 3 (HDAC3) and the transcriptional corepressor KAP-1 (Krab associated protein 1) (Underhill *et al.*, 2000). For an extensive list of BRG1 mediated protein interactions and their respective effect on transcription see Trotter and Archer, 2008.

1.3.3 The role of BRG1 in mammalian development

Taking into account the vast network of protein interactions involving BRG1, it is hardly surprising that BRG1 has been implicated in the regulation of various physiological processes. Early developmental failure of Brg1 deficient mice indicates an essential role played by Brg1 during the very early stages of embryonic development (Bultman *et al.*, 2000). The earliest developmental event that has been found to require Brg1 is zygotic genome activation – reprogramming of the transcriptional signatures upon zygote formation, which is crucial for establishment of totipotency and development initiation (Bultman *et al.*, 2006). The first cell-fate decision event in mammalian development occurs at the blastocyst stage. Cells located within the blastocyst termed inner cell mass (ICM) cells are destined to become the proper embryo, while external cells give rise to the trophectoderm that produces the embryonic portion of placenta. The segregation between ICM

and trophectoderm is controlled by the activity of two transcription factors: Oct4 and Cdx2. During the segregation event, Oct4 transcription becomes limited to ICM, while Cdx2 becomes exclusively expressed in trophectoderm (Nichols *et al.*, 1998; Strumpf *et al.*, 2005). Transcriptional repression of Oct4 in trophectoderm has been shown to be mediated by Cdx2 and require Brg1, thus implicating Brg1 in ICM-trophectoderm differentiation (Wang *et al.*, 2010). The ICM cells from a mouse embryo can be successfully maintained in culture and re-introduced into a new blastocyst contributing to all three germ layers of the resulting chimaera embryo (Evans and Kaufman, 1981). These pluripotent cells have been termed embryonic stem (ES) cells and have had an immense impact on the understanding of early stages of embryonic development and generation of transgenic techniques. The ability of ES cells to maintain pluripotency and self-renewal has been largely attributed to the activity of two key transcription factors: Nanog and Oct4 (Chambers *et al.*, 2003; Nichols *et al.*, 1998). Of these, Nanog has been demonstrated to directly interact with Brg1 in mouse ES cells (Liang *et al.*, 2008). This interaction has been proven to be functional as Brg1 has been found to co-localise with both Nanog and Oct4 as well as Sox2, Stat3 and Smad1 at the promoters of their target genes and thus contribute to regulation of ES cell pluripotency and self-renewal (Ho *et al.*, 2009). Furthermore, Brg1 has also been demonstrated to occupy promoters of these transcriptional regulators (Oct4, Sox2, Nanog, Sall4 and others) and regulate their expression both in ES cells and in the blastocyst (Kidder *et al.*, 2009). Taken together, these observations suggest that Brg1 plays a crucial role in the maintenance of ES cell self-renewal and pluripotency by regulating expression of key transcriptional regulators and their respective target genes.

In addition to its role in ES cell physiology, Brg1 has been implicated in various processes at later stages of embryonic development, mainly in aiding differentiation along various cell lineages. Indeed, the components of the SWI/SNF remodelling complex have been found to participate in the majority of differentiation events examined (de la Serna *et al.*, 2006). The developmental processes that have been found to require Brg1 include skeletal and cardiac muscle differentiation (Hang *et al.*, 2010; Ohkawa *et al.*, 2006; Stankunas *et al.*, 2008), active albumin expression during liver development (Inayoshi *et al.*, 2006), erythropoesis (Bultman *et al.*, 2005; Griffin *et al.*, 2008; Xu *et al.*, 2006), T-cell differentiation and activation (Chi *et al.*, 2003; De *et al.*, 2011), vascular remodelling of the yolk sac (Griffin *et al.*, 2008), limb patterning and keratinocyte differentiation (Indra *et al.*, 2005). Brg1 has also been found involved in maintenance and differentiation of certain somatic stem cells including neural (Matsumoto *et al.*, 2006) and mesenchymal stem cells (Alessio *et al.*, 2010; Napolitano *et al.*, 2007).

1.3.4 The role of BRG1 as a tumour suppressor

Consistent with its importance for precise regulation of various cellular processes, malfunction of BRG1 has also been implicated in a number of pathological conditions, par-

ticularly in neoplasia. BRG1 is widely considered to act as a tumour suppressor in a range of tissues. *BRG1* is located within 19p13.2 locus, which it shares with another tumour suppressor, *LKB1*, and which is frequently lost in certain cancers (Rodriguez-Nieto and Sanchez-Cespedes, 2009). A number of studies have reported *BRG1* mutations in numerous human cancer cell lines as well as in primary and metastatic cancers (Becker *et al.*, 2009; Reisman *et al.*, 2003; Wong *et al.*, 2000). In lung cancer BRG1 mutations have been detected in nearly a quarter of the screened cell lines making it the fifth most common mutation in non-small cell lung cancer (NSCLC) cell lines (Medina *et al.*, 2008). Despite the apparently low incidence of BRG1 mutations in primary lung cancers (Medina *et al.*, 2004) analysis of BRG1 expression in primary NSCLCs has detected loss of BRG1 expression in nearly 30% of tumours (Fukoka *et al.*, 2004; Reisman *et al.*, 2003). This discrepancy has been rectified using ultra-deep pyrosequencing, a more sensitive sequencing technique able to detect under-represented mutations. The pyrosequencing analysis of a panel of primary lung cancers has now detected biallelic *BRG1* inactivation in a substantial portion of tumours (Rodriguez-Nieto *et al.*, 2011).

A number of mouse models have also suggested that Brg1 may act as a tumour suppressor. Heterozygous constitutive *Brg1* knock-out mice have been shown to be susceptible to tumourigenesis in the mammary gland epithelium (Bultman *et al.*, 2007). Notably, mammary gland tumours that arise in mice with heterozygous Brg1 loss have been found to retain expression of the remaining functional copy of *Brg1*. This observation suggests that the oncogenic effects of Brg1 loss are likely to be due to Brg1 haploinsufficiency rather that loss of heterozygousity (Bultman *et al.*, 2007). Consistent with this observation, conditional inactivation of a single *Brg1* allele has been reported to promote chemically induced lung carcinogenesis in mice. At the same time, no increase in the number of tumours has been observed in mice with both *Brg1* alleles inactivated. Conversely, inactivation of both *Brg1* alleles after tumour initiation has been shown to result in increased tumour burden (Glaros *et al.*, 2008). Together with frequent biallelic loss of *BRG1* in human lung cancers, these observations indicate that partial and complete loss of Brg1 may have different effects at various stages of tumour initiation and progression.

Interestingly, another member of the SWI/SNF complex (SNF5/INI1) has been found to act as a tumour suppressor. The gene encoding the *SNF5/INI1* subunit has been found to undergo biallelic inactivation in human malignant rhabdoid tumours (MRT) and less frequently in other cancers (Roberts and Orkin, 2004). Similarly to $Brg1^{-/-}$ animals, $Snf5^{-/-}$ null mice die *in utero* due to early developmental failure, while mice with heterozygous loss of *Snf5* are prone to tumourigenesis. However, despite being components of the same complex the tumours arising in these two models exhibit very distinct phenotypes. $Snf5^{+/-}$ mice have been found to develop multiple tumours that resemble human MRTs (Roberts *et al.*, 2000). These tumours develop more rapidly and are more aggressive compared to mammary tumours from $Brg^{+/-}$ animals. Even more curiously, MRT-like tumours in $Snf5^{+/-}$ mice display loss of the functional copy in the malignant tissue and

thus arise via loss-of-heterozygousity (LOH). These observations represent a peculiar case that genetic aberrations within components of the same regulatory system may give rise not only to morphologically distinct tumour types, but also lead to tumourigenesis via different paths (i.e. single-hit (haploinsufficiency) and two-hit (LOH)).

A number of mechanisms have been suggested to account for the apparent tumour suppressor role of BRG1. One of the putative mechanisms has been proposed to rely on the interaction between BRG1 and the retinoblastoma protein (pRB) repressive complex. BRG1 activity has been found to be essential for pRB complex ability to repress the function of the E2F1 transcription factor (Trouche *et al.*, 1997). An alternative pRB-mediated mechanism of BRG1 tumour suppressor function has been proposed that involves the Cdk inhibitor p21 (also known as CIP1 or WAF). BRG1 has been demonstrated to up-regulate p21 expression, which, in turn, leads to hypophosphorylation of pRB and repression of E2F1 activity (Kang *et al.*, 2004). Although the majority of mutations targeting BRG1 result in abrogated expression, a range of cell lines have been found to bear point mutations in BRG1 leading to single amino acid substitutions. Functional analysis of such mutations has revealed that mutant BRG1 subunits are still capable of interacting with other members of the chromatin remodelling complex and can bind to the promoters of at least some target genes. However, cells bearing mutant BRG1 have been found to be unable to respond to RB-mediated cell cycle arrest, indicating BRG1 failure to facilitate RB-driven transcription (Bartlett *et al.*, 2011).

The interaction of BRG1 with the known tumour suppressor BRCA1 has been suggested as another putative mechanism of BRG1 mediated tumour suppression. BRCA1 has been found to co-purify with the SWI/SNF chromatin remodelling complex via direct interaction with BRG1. Furthermore, BRCA1 activity as a transcriptional regulator has been shown to rely on this interaction as BRG1 and BRCA1 mutations disrupting this interaction result in an inability of BRCA1 to stimulate p53-dependent transcription (Bochar *et al.*, 2000). In addition to regulation of BRCA1 mediated p53-dependent transcription, BRG1 has been shown to directly interact with p53. Overexpression of a dominant negative form of BRG1 protein has been found to result in repression of p53 mediated transcription and an inhibition of p53's ability to induce apoptosis and cell growth arrest (Lee *et al.*, 2002). This picture, however, has been complicated by a contrasting study suggesting an opposing role of BRG1 in p53 regulation as BRG1 has been found to cooperate with the histone acetyl transferase protein, CBP, to destabilise p53 by promoting poly-ubiquitination of the latter (Naidu *et al.*, 2009).

Transcriptional regulation by the SWI/SNF complexes involves both stimulation and repression of gene expression. In line with this, BRG1 has been shown to repress transcription of the *c-Fos* oncogene, with this repression being abrogated by an inactivating mutation in the ATPase domain of BRG1 (Murphy *et al.*, 1999).

This relatively simple portrayal of BRG1 as a *bona fide* tumour suppressor is complicated by a number of studies reporting positive correlations between increased BRG1

expression and more advanced, invasive disease in melanoma and prostate cancer (Lin *et al.*, 2010; Saladi *et al.*, 2007; Sun *et al.*, 2007). The requirement of BRG1 for trans-activation of the Wnt pathway target genes described in the following section further contributes to the complexity of the involvement of BRG1 in tumourigenesis.

1.3.5   BRG1 as a mediator of the Wnt pathway - the oncogenic face of BRG1

In contrast to the evidence from the animal models and cancer cell line studies implicating BRG1 as a tumour suppressor in cancers as varied as melanoma, mammary and lung, BRG1 has been found to facilitate activation of the Wnt pathway in CRC cell lines. Further, yeast two-hybrid screening for proteins interacting with β-catenin has detected an interaction between BRG1 and β-catenin, which was confirmed by co-purification experiments (Barker *et al.*, 2001). Upon the discovery of the β-catenin-BRG1 interaction Barker *et al.* conducted a series of experiments to examine the possibility of BRG1 being recruited to TCF target genes and contributing to Wnt mediated transcriptional activation. Reintroduction of functional BRG1 into BRG1 deficient cell lines, along with simultaneous activation of the Wnt pathway, has been found to double the level of TCF-reporter gene expression compared to the Wnt pathway activation in BRG1 deficient controls. The described increase in reporter gene activity has been shown to require the optimal TCF-recognition site sequence, suggesting that TCF binding to its target site is essential for the recruitment of the β-catenin-BRG1 complex. Additionally, overexpression of a dominant negative form of BRG1 in colon carcinoma cell lines has been demonstrated to inhibit both TCF reporter gene and endogenous Wnt target genes expression.

Two independent reports have demonstrated that Brg1 positively regulates expression of two Wnt target genes, *CD44* and *Cyclin D1*. Ectopic BRG1 expression in BRG1 deficient cell lines derived from cervical carcinoma and adenocarcinoma has been observed to restore CD44 expression otherwise suppressed in those cells (Strobeck *et al.*, 2001). High levels of BRG1 expression have also been found to positively correlate with expression of the Wnt target gene Cyclin D1 in human CRC samples. Positive regulation of Cyclin D1 expression has been proposed to rely on BRG1 mediated suppression of tumour suppressor phosphatase and tensin homolog (PTEN) and subsequent activation of PI3K-AKT signalling (Watanabe *et al.*, 2010). It should be noted, however, that explicit interaction between BRG1 and Wnt signalling has not been explored in these studies, although it cannot be ruled out. As a more direct indication of BRG1-Wnt pathway interaction, BRG1 has been found to cooperate with telomerase reverse transcriptase (TERT), a component of the telomerase complex, at the promoter regions of Wnt target genes and activates Wnt-dependent reporters, both in cultured cells and *in vivo* (Park *et al,.* 2009). Finally, the Wnt target gene c-MYC has been found to interact with BRG1 and rely on this interaction for trans-activation of its transcriptional targets (Cheng *et al,.* 1999).

1.4 Aims and objectives

The main objective of this thesis is to explore the possibility of epigenetic modulation of the Wnt pathway and its potential therapeutic benefits. This objective is based on the pivotal role of the Wnt pathway in the intestinal physiology and pathophysiology as well as an apparent requirement of a chromatin remodelling ATPase subunit BRG1 for execution of the Wnt pathway transcriptional programme. Numerous lines of research have proposed aberrant activation of Wnt signalling as a key initiation step in intestinal tumourigenesis. The previously published study by Barker *et al.* (2001) have reported suppression of Wnt target genes upon inhibition of BRG1 function in CRC cell lines. This project thus aims to further explore the possibility of epigenetic therapy of Wnt-driven neoplasia in mouse models of CRC using conditional transgenesis.

Brg1 loss and haploinsufficiency have been implicated in tumourigenesis in a range of tissues, which could potentially undermine its use as a therapeutic target. In order to investigate potential contraindications of targeting Brg1, the effects of heterozygous and homozygous Brg1 loss will be studied in the context of normal small intestinal epithelium as a tissue of choice for modelling Wnt-driven intestinal neoplasia in mice. To achieve this objective Brg1 will be conditionally inactivated using a selection of Cre recombinases. This work is described in Chapter 3. Additionally, the consequences of Brg1 haploinsufficiency and loss of function will be analysed in a range of other tissues both within and outside of the gastrointestinal tract. This part of the project is outlined in Chapter 4.

In order to address any potential therapeutic advantage of epigenetic modulation of Wnt signalling by Brg1 loss, Brg1 deficiency will also be placed in the context of aberrant Wnt signalling by conditional inactivation of the *Apc* gene. The outcomes of Brg1 loss in the context of Wnt-driven neoplasia will be characterised in the small intestinal epithelium as well as a range of other epithelial tissues. These studies are presented in Chapters 5 and 6.

Chapter 2

Materials and Methods

2.1 Experimental animals

All animal experiments were carried out in accordance with UK Home Office regulations, under valid personal and project licenses.

2.1.1 Transgenic constructs and animals used in the project

A number of transgenic mouse lines were used in this project. These include mice bearing tissue-specific inducible transgenes driving expression of a Cre recombinase as well as loxP targeted native alleles and reporter constructs. Mice bearing the *Tg(Cyp1a1-cre)1Dwi* transgene (abbreviated here as AhCre), which can be induced by β-naphthoflavone treatment in a range of tissues including the intestinal epithelium, stomach and bladder, were generated by Ireland *et al.* (2004). The *Tg(Cyp1a1-cre/ESR1)1Dwi* transgene (abbreviated here as AhCreER), expresses a fusion protein in which Cre recombinase and a mutated oestrogen receptor are fused and thus provides additional control over Cre recombinase activation (Kemp *et al.*, 2004). The *Tg(Vil-cre/ESR1)23Syr* transgene (further abbreviated as VillinCre) expresses a tamoxifen-dependent Cre recombinase-ER fusion protein under the transcriptional control of the *Villin1* promoter (el Marjou *et al.*, 2004). Mice bearing *Lgr5-EGFP-IRES-creERT2* knock-in transgene (further abbreviated as Lgr5CreER) expressed from *Lgr5* locus were provided by Owen Sansom (Barker et al., 2007). The targeted *Brg1* allele bearing loxP sites flanking exons 2 and 3 (Figure 2.1a) was provided by Pierre Chambon (Sumi-Ichinose *et al.*, 1997). The targeted *Apc* transgene with loxP sites positioned within the introns surrounding exon 14 (Figure 2.1b) was generated by Shibata *et al.*, (1997).
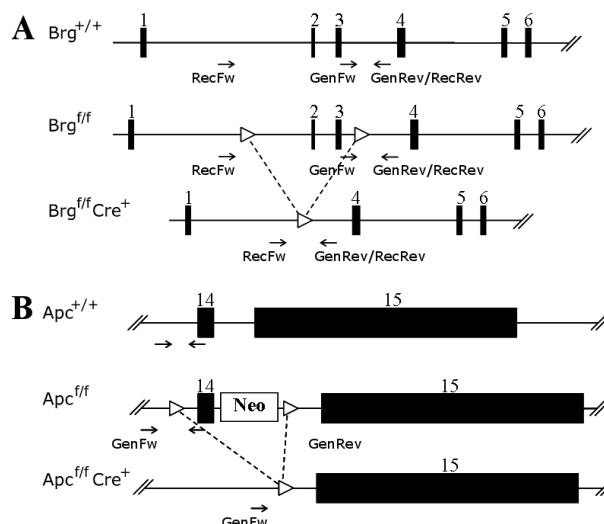
Figure 2.1: Schematic representation of the loxP targeted alleles and primer positions. **(a)** Two loxP sites are placed in *Brg1* gene so that they flank exons 2 and 3. Primers specific to regions either side of the second loxP site (GenFw-GenRev) enable PCR detection of the animal genotype. Primers specific to regions upstream of the first loxP site and downstream of the second site (RecFw-RecRev) allow for PCR-mediated detection of recombination events (Sumi-Ichinose et al., 1997). **(b)** Two loxP sites are placed either side of exon 14 of *Apc* gene. Primers specific to regions either side of the first loxP site (GenFw-GenRev) enable PCR-mediated detection of the transgene in the animal genome (Shibata et al., 1997).

2.1.2 Animal husbandry

2.1.2.1 Colony maintenance

Mice were housed in a standard facility and had access to the Harlan standard diet (Scientific Diet Services, RM3(E)) and water *ad libitum*.

2.1.2.2 Breeding

All mice were maintained on a mixed background. Adult animals (6 weeks and older) of known genotype were mainly bred in trios (one male with two females). Pups were left with their mothers until capable of feeding independently. They were weaned on average at four weeks of age.

2.1.2.3 Identification, ear and tail biopsies

At the time of weaning animals were sexed and separated. Ear clipping was employed for animal identification. The resulting ear pinna was used for DNA extraction and genotyping (described below). When required surgical biopsy of 3–5 mm of the tail tip was taken under local anaesthetics.

2.1.3 Experimental Procedures

Unless otherwise specified, animals were aged to at least 10 weeks before being subjected to any experimental procedures. Intraperitoneal injections were performed using 1 ml

syringe (BD Plastipak) and 25G needle (BD Microlance 3)

2.1.3.1 Injection of β-naphthoflavone

Expression of the AhCre recombinase was induced by administration of β-naphthoflavone (bNF, Sigma) in corn oil (Sigma). Powdered bNF to a concentration of 10 mg/ml was added to corn oil in an amber bottle in order to protect bNF from light exposure. The solution was heated to $80\,^{\circ}$C and stirred vigorously to aid complete dissolution of bNF. Aliquots of bNF solution were frozen and stored at $-20\,^{\circ}$C until required. Prior to injection, aliquots were thawed, heated to $80\,^{\circ}$C and kept at that temperature until immediately before injection to prevent bNF precipitation out of the solution. bNF was injected intraperitoneally (IP) at a dose of 80 mg of bNF per kg of body weight. This dose was repeated thrice with 8 hour interval between injections (4 injections in total). During a single course of injections solution was kept in darkness at $4\,^{\circ}$C and then any remaining solution was discarded.

2.1.3.2 Injection of Tamoxifen

Animals expressing the *VillinCre* or *Lgr5CreER* transgenes were induced by administration of Tamoxifen (Sigma) in corn oil. Powdered Tamoxifen was added to corn oil in an amber bottle to final concentration of 10 mg/ml. The solution was heated to $80\,^{\circ}$C with regular shaking to aid Tamoxifen dissolution. Once completely dissolved, the Tamoxifen solution was aliquoted and stored at $-20\,^{\circ}$C. Prior to injection the solution was thawed, heated to $80\,^{\circ}$C and kept at this temperature until immediately before injection. Two distinct induction protocols were used to induce *VillinCre*$^+$ animals. The low-dose protocol involved a single IP injection of 40 mg/kg Tamoxifen. The high-dose protocol involved four daily IP injections at a dose of 80 mg/kg. *Lgr5CreER*$^+$ animals received an initial dose of 120 mg/kg followed by three daily injections at a dose of 80 mg/kg. After the injection, the solution was re-frozen and re-used no more than 3 times to avoid Tamoxifen degradation.

2.1.3.3 Combined injection of bNF and Tamoxifen

Mice bearing the *AhCreER* transgene were induced by combined bNF and Tamoxifen treatment to induce both recombinase expression and activity. Powdered bNF and Tamoxifen were added to corn oil in an amber bottle to the final concentration of 10 mg/ml and heated to $80\,^{\circ}$C with vigorous stirring until complete dissolution. Once dissolved the solution was aliquoted and stored at $-20\,^{\circ}$C. The recombinase was induced by five bi-daily IP injections of combined bNF+Tamoxifen solution at a dose of 80 mg/kg, unless stated otherwise.

2.1.3.4   Injection of 5'-bromo-2-deoxyuridine

Where specified, animals were administered 0.25 ml of 10 mg/ml 5'-Bromo-2-deoxyuridine (BrdU, Amersham Biosciences) either 2 or 24 hours prior to dissection in order to label cells in S-phase of the cell cycle.

2.1.3.5   Whole body γ-irradiation

For the assay of clonogenic repopulation of the intestinal epithelium mice were subjected to whole body gamma irradiation. Animals were restrained using a small well ventilated Perspex chamber. An effective dose of 15 Gy of γ-irradiation was administered by exposure to a Caesium-137 source delivering 2.1 Gy per minute (IBL437C irradiator, RPS Services).

2.1.4   PCR Genotyping

Mice were genotyped by PCR using DNA extracted from ear or tail biopsies at weaning age (four weeks) and confirmed at death. Unless provided by earlier publications, all primers used were designed using Primer3 software at http://fokker.wi.mit.edu/primer3/input.htm, checked for specificity using BLAST engine against Ensembl database (http://www.ensembl.org/Multi/blastview) and synthesised by Sigma Genosys.

2.1.4.1   DNA purification (Puregene method)

Ear or tail biopsy was placed in a 1.5 ml eppendorf tube and stored at $-20\,^{\circ}$C until analysis. For DNA isolation 250 μl of Cell Lysis Solution (Gentra) and 5 μl of 20 mg/ml Proteinase K (Roche) were added to the tissue and incubated overnight at $37\,^{\circ}$C with agitation. The next day the contents of the tubes were cooled to room temperature, mixed with 100 μl of Protein Precipitation Solution (Gentra) and centrifuged at 13000 rpm in a microcentrifuge for 10 min. The supernatant was recovered and mixed with 250 μl of isopropanol in a fresh 1.5 ml eppendorf tube and centrifuged at 13000 rpm for 15 min. The supernatant was carefully discarded, and the tubes were left to air-dry for 1 hour. The DNA was then dissolved in 250 μl of PCR-grade water (Sigma) and 2.5 μl of the resulting solution was used in PCR reactions.

2.1.4.2   Generic protocol for PCR genotyping

PCR reactions were carried out in thin-wall 96-well plates or in thin-wall 0.2 ml strip tubes (Greiner Bio-One) and run using either PTC-100 Peltier (MJ Research), Techne Flexigene (Krackeler Scientific) or GS1 (G-Storm) thermal cycler. Pipetting of the reagents and DNA samples was carried out using filtered pipette tips to avoid aerosol contamination. 2.5 μl of crude genomic DNA extract was loaded into wells using multi-channel pipette. The master-mix containing the remaining components of the reaction (distilled

water, GOTaq 5X PCR buffer (Promega), 25 mM Magnesium Chloride (Promega), 25 mM dNTPs (Bioline), Primers (Sigma-Genosys) and either GOTaq (Promega) or Dream-Taq (Fermentas) DNA Polymerase) was prepared according to Table 2.1. 47.5 μl of the appropriate master-mix were added to each well. 96-well plates were sealed with aluminium foil tape, while strip-tubes were closed with appropriate caps (Greiner Bio-One). The tubes were gently tapped to dislodge air bubbles and ensure the mixture was at the bottom of the well. Reactions were run using cycle conditions outlined in Table 2.1.

The primer sequences used for genotyping of the particular transgenes and the size of respective products are provided in Table 2.2.

2.1.4.3 Visualisation of PCR products

After completion of PCR reactions the products were visualised by agarose gel electrophoresis. The reactions using colourless 5X PCR buffer (Promega) were mixed with 5μl of DNA loading dye (50% Glycerol (Sigma), 50% distilled water, 0.1% (w/v) Bromophenol Blue (Sigma)). All samples and an appropriate marker (e.g. 100 bp ladder (Promega)) were loaded onto 2% agarose gel (4 g agarose (Eurogentech), 200 ml 1X Tris-Borate-EDTA (TBE) buffer (Sigma), 10 μl of 10 mg/ml ethidium bromide (Sigma) or 10μl Safeview (NBS Biologicals)). The products of Ah-Responder PCR were analysed using 4% agarose gel. Gels were run in 1X TBE buffer at 120 V for 30 minutes. Products were visualised in UV light using GelDoc apparatus (BioRad).

2.2 Tissue harvesting and processing

2.2.1 Tissue harvesting

Following a schedule 1 approved method of culling (cervical dislocation), animals were dissected using a micro-dissection kit. The fur was sprayed with 70% ethanol and an incision made along the mid-line of the abdomen, through both, skin and peritoneal wall. Unless otherwise specified the following protocol of harvesting the small intestinal (SI) tissue was adhered to. The small intestine between stomach and caecum was isolated and flushed with ice cold 1X PBS (Invitrogen) using 60 ml syringe (BD Plastipak). The first 8 cm of the SI were 'swiss-rolled' (intestine was opened longitudinally, spread on a flat surface with the epithelium facing up, rolled from end to end using forceps and secured by piercing it with a 23G syringe needle (BD Microlance)). The following 8 cm were cut into four 2 cm pieces and bundled together with surgical microtape. Epithelial and stromal cells from the following 8 cm were separated from muscle wall by scraping with the blunt edge of a scalpel. The scraped off tissue was divided into two equal parts, and used for RNA (section 2.5.1) and protein (section 2.6.1) isolation. The following 8 cm were cut into three equal pieces and bundled with surgical microtape. The rest of the SI was 'swiss-rolled'. The stomach was cut open and flushed with running tap water. It

Table 2.1: Genotyping PCR reaction conditions

	Cre/LacZ	Responder	ApcLoxP	Brg1LoxP	Brg1-Recombined
PCR Reaction Components:					
DNA extract (See section 2.1.4.1)	2.5 µl	2.5 µl	2.5 µl	2.5 µl	2.5 µl
Master Mix:					
PCR-grade H$_2$o (Sigma)	31.5 µl	31.7 µl	31.7 µl	31.7 µl	31.7 µl
GOTaq PCR Buffer (5X, Promega)	10 µl	10 µl	10 µl	10 µl	10 µl
Magnesium Cloride (25 mM, Promega)	5 µl	5 µl	5 µl	5 µll	5 µl
dNTPs (25 mM, Bioline)	0.4 µl	0.4 µl	0.4 µl	0.4 µl	0.4 µl
Forward Primer (100 mM, Sigma Genosys)	2 x 0.1 µl	0.1 µl	0.1 µl	0.1 µl	0.1 µl
Reverse Primer (100 mM, Sigma Genosys)	2 x 0.1 µl	0.1 µl	0.1 µl	0.1 µl	0.1 µl
Taq Polymerase	0.2 µl	0.2 µl	0.2 µl	0.2 µl	0.2 µl
Taq Polymerase Brand	GOTaq	Dream Taq	Dream Taq	GOTaq	GOTaq
Total Reaction Volume:	50 µl	50 µl	50 µl	50 µl	50 µl
Cycling conditions (Time; Temperature)					
Initial denaturation	3 min; 94°C	5 min; 94°C	2.5 min; 95°C	2.5 min; 94°C	2.5 min; 95°C
Cycle number	30	30	30	35	35
Step 1 (Denaturation)	30 sec; 95°C	20 sec; 94°C	30 sec; 95°C	30 sec; 94°C	30 sec; 95°C
Step 2 (Annealing)	30 sec; 55°C	20 sec; 57°C	30 sec; 60°C	30 sec; 60°C	30 sec; 58°C
Step 3 (Elongation)	1 min; 72°C	30 sec; 72°C	1 min; 72°C	1 min; 72°C	40 sec; 72°C
Final Extension	5 min; 72°C	5 min; 72°C	5 min; 72°C	5 min; 72°C	5 min; 72°C
Hold	∞; 15°C	∞; 15°C	∞; 15°C	∞; 15°C	∞; 15°C

Table 2.2: Primer sequences used for PCR genotyping

Gene	Forward Primer Sequence (5-3)	Reverse Primer Sequence (5-3)	Product Size
General Cre	TGACCGTACACCAAAATTTG	ATTGCCCCTGTTTCACTATC	1000 bp
ROSA26:LacZ	CTGGCGTTACCCAACTTAAT	ATAACTGCCGTCACTCCAAC	500 bp
AhCre Non-Responder	AGGTTCCCTGGGACTTGTTT	TCACCAAACCCTCCATCAGT	Responder: 196 bp; Non-responder: 178 bp
ApcLoxP	GTTCTGTATCATGGAAAGATAGGTGGTC	CACTCAAAACGCTTTTGAGGGTTGATTC	WT: 226 bp; Targeted: 314 bp
Brg1LoxP	CCAAGGTAGCGTGTCCTCAT	CACTGCTCAGCTTCACTTGC	WT: 407 bp; Targeted: 500 bp
Brg1-Recombined	TCTTTCCATTTCCTGCCTCA	AGGGCTATCGGGTAACTTCA	Recombined allele: 529 bp

was then folded along the border separating glandular and forestomach sections and fixed with surgical microtape. The pyloric junction including 5 mm of pyloric stomach and first 5 mm of duodenum was cut open, folded along the border between the stomach and small intestine and fixed with surgical microtape. The large intestine between the caecum and the rectum was flushed with ice cold 1X PBS (Invitrogen) and 'swiss-rolled'.

In addition to the gastrointestinal tract tissues, samples of the following tissues were harvested from mice bearing particular transgenes: - *AhCre* and *AhCreER*: liver, pancreas, kidney, bladder, spleen; - *VillinCre*: kidney.

2.2.2 Tissue fixation

Once collected, tissue samples were immersed in ice cold formalin (4% neutral buffered formaldehyde in saline, Sigma) and incubated for 12–24 hours at 4 °C. After initial fixation, samples were either processed straight away as described below or transferred into ice cold 70% ethanol and stored at 4 °C until processing.

Fixation method used for the gut wholemount and β-galactosidase staining is described in section 2.2.5.1.

2.2.3 Tissue processing for light microscopy

2.2.3.1 Tissue dehydration

Tissue samples were arranged in histocasettes and processed using an automatic processor (Leica TP1050). Samples were dehydrated in increasing concentrations of ethanol (70% for 1 hour, 95% for 1 hour, 100% 2 x 1 hour 30 min, 100% for 2 hours), Xylene 2 x 1 hour and paraffin 1 x 1 hour and 2 x 2 hours. After dehydration, samples were embedded in paraffin wax.

2.2.3.2 Tissue sectioning

A microtome (Leica RM2135) was used to cut 5 μm thick sections from paraffin blocks. Sections were then floated onto slides coated with poly-L-lysine (PLL) and baked at 58 °C for 24 hours.

2.2.4 Tissue preservation for RNA, DNA or protein extraction

Tissues intended for RNA or protein extraction were removed and frozen as quickly as possible to avoid RNA and protein degradation, respectively.

2.2.4.1 For RNA extraction

Gut scrapes from the small intestinal epithelium were placed in a screw-cap tubes containing 1.4 mm ceramic beads (Lysing Matrix D tubes, MP biomedical) and 1 ml of Trizol

reagent (Invitrogen). Tubes were shaken briefly to mix the tissue with Trizol and snap frozen by immersion in liquid Nitrogen (LN$_2$). Tissues were removed from (LN$_2$) and stored at $-20\,°C$.

The bladder urothelium tissue was physically separated from the muscle wall (see section 2.2.6.3), placed in a screw-cap tube with ceramic beads and 0.5 ml of Trizol reagent, snap frozen in (LN$_2$) and stored at $-20\,°C$ (see above).

2.2.4.2   For protein extraction

Gut scrapes of the small intestinal epithelium were transferred into 1.5 ml eppendorf tube and quickly immersed and snap frozen by immersion in (LN$_2$). Tissues were removed from (LN$_2$) at convenience and stored at $-80\,°C$ until needed.

2.2.4.3   For DNA extraction

Small samples were removed from tissues intended for DNA extraction. These samples were placed in 1.5 ml eppendorf tube and stored at $-20\,°C$ until DNA extraction (typically within 2 weeks).

2.2.5   Staining of tissue wholemounts

2.2.5.1   LacZ staining of the small intestine wholemount

Specific regions of whole small intestine were removed and flushed with ice cold 1X PBS (Invitrogen) and ice cold X-Gal fixative solution (2% formaldehyde (Sigma), 0.1% glutaraldehyde (Sigma) in 1X PBS). Approximately 7 cm long sections of the small intestine were placed on a set paraffin wax in 15 cm plastic Petri dish (paraffin wax (Sigma), with 10% mineral oil (Sigma)). The intestine then was cut open, spread with epithelial side facing up and pinned down using entomological pins (Watkins & Doncaster). The tissue was then fixed in the X-Gal fixative for at least 1 hour at room temperature, washed in 1X PBS and incubated in demucifying solution (10% glycerol (Sigma), 0.01 M Tris-HCl (pH 8.2), 20% ethanol (Fisher Scientific), 0.9% NaCl, 0.003% (w/v) Dithiothreitol (DTT, Sigma)) for 1 hour. The plate was flooded with 1X PBS and any adhering mucin was washed off the tissue using a plastic Pasteur pipette. The wholemounts were stained using X-Gal staining solution: 1 mM MgCl$_2$ (Sigma), 3 mM potassium ferricyanide (Sigma), 3 mM potassium ferrocyanide (Sigma) in 1X PBS. The solution was stored in a tin foil-wrapped bottle at $-20\,°C$ and stock X-Gal solution (5% in DMF, Promega) 0.02% was added immediately prior to staining. The intestines were incubated with the staining solution overnight or until the sufficient level of staining was achieved. If necessary, fresh solution was added after overnight incubation and incubated for further 4-6 hours. Once stained, tissues were washed with 1X PBS and fixed with formalin to avoid further

staining. When required, formalin-fixed intestines were 'swiss-rolled' and processed for histology as described earlier (section 2.2.3).

Stained wholemounts were illuminated with Leica CLS50X light source and visually analysed under Olympus SZX12 low-magnification stereo microscope. Where needed, pictures were taken with Olympus C4040ZOOM 4.1 Megapixel digital camera.

2.2.6 Isolation of epithelium enriched cell populations

2.2.6.1 Isolation of the intestinal epithelial cells using Weiser solution

The protocol was adapted from (Flint et al., 1991). The first 15 cm of the small intestine from the stomach was flushed with ice cold 1X PBS (Invitrogen), opened longitudinally and placed in 50 ml falcon tube (Greiner Bio-One) containing 15 ml of freshly prepared ice cold modified Weiser chelating solution (5.56 mM disodium hydrogen orthophosphate (Sigma), 8 mM potassium dihydrogen orthophosphate (Sigma), 96 mM sodium chloride (Sigma), 1.5 mM potassium chloride (Sigma), 27 mM tri-Sodium citrate (Sigma), 0.5 mM dithiothreitol (DTT, Sigma), 1.5% sucrose (Sigma), 1% D-sorbitol (Sigma), 6.07 mM EDTA (Sigma), 4 mM EGTA (Sigma), pH 7.3). The intestine was washed in three changes of ice cold Weiser solution by gentle shaking. After the washes, the tube containing 15 ml of Weiser solution was attached to the vortex mixer and shaken at the lowest setting for 15 min. The tube was then shaken vigorously by hand and the solution was transferred into a fresh tube. Fresh 15 ml of Weiser solution was added to the tube containing the intestine and the shaking steps were repeated. Two 15 ml fractions were joined together and the intestine was discarded. 30 ml of Weiser solution containing the epithelial cells were centrifuged at 1500-2000 rpm for 5 min. The resulting pellet was resuspended in 20 ml of ice cold 1X PBS and centrifuged. The wash in 1X PBS was repeated twice, the pellet was resuspended in 3 ml of 1X PBS and aliquoted into three 1.5 ml eppendorf tubes. The tubes were centrifuged using a mini-centrifuge for 1 minute. The supernatant was removed, the pellet was snap-frozen in LN_2 and stored at $-80\,^{\circ}C$ until needed.

2.2.6.2 Epithelial enrichment by gut scraping

In order to enrich the small intestinal tissue sample for epithelium, epithelial and stromal cells were physically separated from the muscle wall. The small intestine was dissected as described earlier (section 2.2.1). The fragment of small intestine intended for RNA and protein extraction was opened longitudinally and spread on a flat surface luminal side facing up. The intestinal mucosa was then gently scraped off the muscle wall using the blunt edge of a scalpel. The scraped material was divided into two equal parts and transferred into 1.5 ml eppendorf tube for protein extraction or screw-cap tube with ceramic beads and 1 ml of Trizol reagent (Invitrogen) for RNA extraction (see sections 2.5.1 and 2.6.1).

2.2.6.3   Isolation of bladder urothelium

In order to obtain an epithelium enriched sample of bladder urothelium, the epithelial sheet was physically separated from the bladder muscle wall. The bladder was isolated from the genitourinary tract and an incision was made into the bladder wall with surgical spring scissors. The epithelial sheet was then pulled from the muscle wall using two microdissection forceps. The bladder urothelium was then preserved for RNA extraction as described in section 2.5.1.

2.3   Histological analysis

2.3.1   Haematoxylin and Eosin (H&E staining of tissue sections)

Slides containing tissue sections were dewaxed and rehydrated as described in section 2.4. Slides were stained for 5 min in Mayer's Haemalum (R. A. Lamb), washed in running tap water for further 5 min followed by 5 min staining in 1% aqueous Eosin (R.A. Lamb) solution. Eosin was washed off by two 15 second washes in water. Stained sections were dehydrated and mounted as described in section 2.4.

2.3.2   Quantitative histological analysis of H&E stained sections

Histological quantification of the tissue sections was carried out using an Olympus BX41 light microscope. Where appropriate, microphotographs were taken with a Colorview III camera (5 megapixel, Soft Imaging Systems) aided with AnalySIS software (v3.2, Build 831, Soft Imaging Systems) or Moticam 5000 camera (5 megpixel, Motic Instruments) aided with Motic Images Advanced software (v.3.2, Motic China Group). Quantitative and statistical analysis of histological parameters was carried out as described in section 2.7.

2.3.2.1   Scoring of crypt length

Crypt length was scored by counting the number of cells from the base of the crypt to the crypt-villus junction. Scoring was carried out for 50 half-crypts per section and average of 50 crypts were scored per mouse.

2.3.2.2   Scoring of villus length

To score villus length, the total number of cells from the crypt bottom to the villus tip were counted on 50 half crypt-villus axes per slide. The average villus length was calculated as average total crypt-villus length minus average crypt length for each mouse.

2.3.2.3   Scoring of Mitotic index

Mitotic figures were scored on H&E stained sections based on their morphological appearance. Number of mitotic figures was counted in 50 half-crypts per slide. Mitotic index was calculated as average number of mitotic figures per half-crypt for each mouse.

2.3.2.4   Scoring of Apoptotic index

Apoptotic bodies were scored based on their characteristic appearance on H&E stained sections. The number of apoptotic bodies was counted in 50 half-crypts per slide. The apoptotic index was calculated as average number of apoptotic bodies per half-crypt for each mouse. Where appropriate the position of apoptotic bodies in the crypt was also scored to assess the distribution of apoptosis within the crypt. The positions were scored from the crypt base, the bottom-most cell being the cell #1. The positional data from all the mice of the same genotype were pooled together and analysed as described in section 2.7.

2.3.3   Use of specific stains for quantification of histological traits

2.3.3.1   Grimelius staining

Grimelius staining was used to identify argyrophilic enteroendocrine cells. All glassware used for the staining was rinsed thoroughly with ultrapure double-distilled (dd) H_2O prior to use. Tissue sections were dewaxed and rehydrated as described in section 2.4. 1% (w/v) silver nitrate (Sigma) was dissolved in Acetate buffer (0.02 M acetic acid (Fisher Scientific), 0.02 M sodium acetate (Sigma) in ddH_2O) and heated to $65\,^\circ$C on a water bath in a coplin jar. Once slides were placed in preheated solution, the coplin jar was sealed, wrapped in tin foil and incubated at $65\,^\circ$C for 3 hours. Slides were then transferred to reducing solution (0.04 M sodium sulphite (Fisher Scientific), 0.1 hydroquinone (Sigma) in ddH_2O) preheated to $45\,^\circ$C and incubated for 5 minutes or until the tissue developed yellow coulour. Stained slides were dehydrated and mounted as described in section 2.4.

Stained sections were examined and the number of enteroendocrine cells were scored in 50 half crypt-villus axes per mouse. The average number of enteroendocrine cells per half crypt-villus axis was calculated for each mouse and analysed as described in section 2.7.

2.3.3.2   Staining with Alcian Blue

Alcian Blue staining was used to identify mucin-containing goblet cells. Tissue sections were dewaxed and rehydrated as described in section 2.4. Slides were immersed in Alcian Blue staining solution (1% (w/v) Alcian Blue (Sigma), in 3% (v/v) acetic acid (Fisher Scientific)) for 30 seconds followed by washing in running water for 5 minutes. Slides were

then counterstained with 0.1% Nuclear fast red (Sigma) for 5 min. Slides were washed in running water for 5 min and then dehydrated and mounted as described in section 2.4.

Stained sections were examined and the number of goblet cells were scored in 50 half crypt-villus axes per mouse. The average number of goblet cells per half crypt-villus axis was calculated for each mouse and analysed as described in section 2.7.

2.3.3.3 Alkaline phosphatase staining

Staining for brush border-specific Alkaline phosphatase was used as a marker of mature enterocytes. Tissue sections were dewaxed and rehydrated as described in section 2.4. Slides were placed in a humidified chamber, tissue sections were overlaid with Fast Red substrate (DAKO) and incubated for 20 min at room temperature. Slides were washed in dH_2O and counterstained in Mayer's Haemalum for 30 seconds followed by a 5 min wash in running water. Slides were then mounted using glycerol (Sigma).

The intensity of the staining and thickness of the brush border were visually analysed using light microscopy.

2.3.3.4 Lysozyme staining

Immunohistochemistry with an anti-lysozyme antibody (see section 2.4) was used to identify Paneth cells. Both Paneth cell number and position was scored. Paneth cell quantity was scored as the number of lysozyme positive cells in 50 half-crypts per section. The average number of Paneth cells per half-crypt was calculated for each mouse and analysed as described in section 2.7. Paneth cell position was counted from the bottom of the crypt, the bottom-most cell being #1. Paneth cell positions from all the mice of the same genotype were pooled together and analysed as described in section 2.7.

2.3.3.5 Ki67 staining

Immunohistochemistry with an anti-Ki67 antibody (see section 2.4) was used to identify proliferating cells as a supplement to the Mitotic index score. Both Ki67 cell number and position was scored to assess the size and distribution of the proliferative compartment of the crypt. The number of proliferating cells was scored as the number of Ki67 positive cells in 50 half-crypts per slide. The average number of Ki67 positive cells per half-crypt was calculated for each mouse and analysed as described in section 2.7. Ki67 positive cell positions were counted from the bottom of the crypt, the bottom-most cell being #1. Ki67 cell positions from all the mice of the same genotype were pooled together and analysed as described in section 2.7.

2.3.3.6 Cleaved Caspase-3 staining

Immunostaining with cleaved caspase-3 antibody (see section 2.4) was used to confirm the morphology-based Apoptotic index. The number of Caspase-3 positive cells was scored

in 50 half-crypts per slide. The average number of apoptotic cells per half-crypt was calculated for each mouse and analysed as described in section 2.7. Where appropriate the position of Caspase-3 positive cells was also scored to assess the distribution of apoptosis within the crypt. The positions were scored from the crypt base, the bottom-most cell being cell #1. The positional data from all the mice of the same genotype were pooled together and analysed as described in section 2.7.

2.3.3.7 BrdU staining

Tissue samples harvested from mice injected with BrdU at 2 or 24 hours prior to dissection were stained with a BrdU antibody as described in section 2.4. The number and position of BrdU positive cells at 2 and 24 hours post labelling were used to assess proliferation activity and cell migration respectively. The number of BrdU positive cells was scored in 50 half-crypts per slide. The average number of BrdU positive cells per half-crypt was calculated for each mouse and analysed as described in section 2.7. The position of BrdU labelled cells was counted from the bottom of the crypt, the bottom-most cell being #1. Cell positions from all the mice of the same genotype were pooled together and analysed as described in section 2.7.

2.4   Immunohistochemistry (IHC)

All IHC was carried out according to the generic protocol outlined below. Specific conditions and modifications for particular antibodies are provided in Table 2.3. Unless otherwise specified, all incubation steps were carried out at room temperature (approximately $22\,^{\circ}\mathrm{C}$) in humidified chamber to avoid drying out of the sections. To contain the applied solutions to the tissue, slides were gently dried around the tissue section with tissue paper and the area surrounding the tissue was circled with a water-resistant ImmEdge pen (Vector Labs) typically before endogenous peroxidase block or serum block stage.

2.4.1   Generic immunohistochemistry protocol

2.4.1.1   Dewaxing and rehydration of tissue sections

Tissue sections were dewaxed by two 5 min washes in xylene (Fisher Scientific) followed by rehydration washes in decreasing concentrations of ethanol (Fisher Scientific): two 3 min washes in 100%, one 3 min wash in 95% and one 3 min wash in 70% ethanol. Slides were then transferred into dH_2O and washed for 5 min.

2.4.1.2   Antigen retrieval

Antigen retrieval was achieved by heating slides in a boiling water bath or microwave in either 1X citrate buffer (LabVision) or custom citrate buffer (10 mM Sodium Citrate

(Sigma), pH 6.0). For water bath incubation slides were immersed in preheated buffer in a Coplin jar (R. A. Lamb) and incubated at 99 °C for the time specified in Table 2.3 (typically 20 min). For microwave antigen retrieval, citrate buffer was placed in either a plastic container or a plastic pressure cooker and preheated in domestic microwav at high power (850 W) for 5 min. Slides held in a plastic slide rack were then immersed in preheated buffer and heated according to conditions specified in Table 2.3. Slides were kept in citrate buffer and allowed to cool at room temperature for 30–60 min followed by 5 min wash in dH_2O. Slides were then washed in washing buffer (either 1X PBS (Invitrogen) or 1X TBS (Sigma) in dH_2O with 0.1% (v/v) TWEEN-20 (Sigma) as specified in Table 2.3).

2.4.1.3   Endogenous peroxidase activity block

Activity of endogenous peroxidases was blocked by incubating tissue sections with hydrogen peroxide. Either 30% hydrogen peroxide (Sigma) diluted in dH_2O to appropriate concentration or a commercial peroxidase blocking solution (Envision+ Kit, DAKO) were used. The appropriate hydrogen peroxide concentrations and incubation times for specific antibodies are provided is Table 2.3. When using commercial peroxidase block, the tissue was circled with water-resistant pen, placed in a slide chamber and enough solution was applied to cover the tissue. When using hydrogen peroxide from the stock solution, slides were placed in a Coplin jar containing enough solution to cover the tissue. After incubation with the peroxidase blocking solution, slides were briefly rinsed in dH_2O and washed 3 x 5 min in washing buffer.

2.4.1.4   Non-specific antibody binding block

To diminish non-specific antibody binding, tissue sections were treated either with normal serum (DAKO) or BSA (Sigma) diluted to an appropriate concentration in washing buffer. The specific blocking agent, concentrations and incubation times for particular antibodies are outlined in Table 2.3. Typically, the serum used for blocking was derived from the species, in which the secondary antibody was raised (i.e. if a secondary antibody was raised in rabbit, normal rabbit serum was used to block non-specific binding). If not already done, the tissue containing area was circled with a water-resistant pen, slides were overlaid with 200 μl of blocking solution and incubated for the time specified.

2.4.1.5   Primary antibody treatment

Following incubation, blocking solution was removed and 200 μl of primary antibody diluted in blocking solution was applied without washing of sides. The dilutions and incubation times used with specific antibodies are outlined in Table 2.3. After incubation with an antibody, the slides were washed 3 x 5 min in washing buffer.

Table 2.3: Antibody-specific conditions for immunohistochemical staining

Primary antibody	Manufacturer	Antigen retrieval	Non-specific block / staining Block	Wash buffer	Primary antibody incubation	Secondary antibody	Signal amplification
Anti-β-catenin	BD Transduction Labs #610154	20 min, 100 °C, W/B, citrate buffer (Thermo)	Peroxidase (DAKO), 5 min, RT; 10% NRS, 30 min, RT (Block)	3 x 5 min TBS/T	1:300 in 10% NRS, O/N at 4 °C	Envision+ conjugated anti-mouse (DAKO), 30 min at RT	N/A
Anti-BrdU	BD Biosciences #347580	20 min, 100 °C, W/B, citrate buffer (Thermo)	Peroxidase (DAKO), 5 min, RT; 1% BSA, 30 min, RT (Block)	3 x 5 min PBS/T	1:150 in 1% BSA, 1 h at RT	Envision+ conjugated anti-mouse (DAKO), 30 min at RT	N/A
Anti-Brg1	Santa Cruz (G-7): sc-17796	20 min, 100 °C, W/B, citrate buffer (Thermo)	Peroxidase (DAKO), 5 min, RT; 10% NRS, 30 min, RT (Block)	3 x 5 min TBS/T	1:200 in 10% NRS, O/N at 4 °C	Envision+ conjugated anti-mouse (DAKO), 30 min at RT	N/A
Anti-Brm	Santa Cruz, (N-19): sc-6450	20 min, 100 °C, W/B, citrate buffer (Thermo)	Peroxidase (DAKO), 5 min, RT; 10% NRS, 30 min, RT (Block)	3 x 5 min TBS/T	1:200 in 10% NRS, O/N at 4 °C	HRP-conjugated rabbit anti-goat (DAKO), 1:200 in 10% NRS, 30 min, RT	N/A
Anti-CD44	BD Pharmigen #550538	20 min, 100 °C, W/B, citrate buffer (Thermo)	1.5% H_2O_2, 15 min, RT; 10% NRS, 35 min, RT	3 x 5 min TBS/T	1:50 in 10% NRS, 1 h at RT	Biotinylated anti-rat (DAKO) 1:200 in 10% NRS, 30 min at RT	ABC Kit (Vector Labs)
Anti-Cleaved Caspase 3	Cell Signalling Technology #9661	Boil in P/C, 15 min under pressure, citrate buffer (Thermo)	3% H_2O_2, 10 min, RT; 5% NGS, 1 h, RT	3 x 5 min TBS/T	1:200 in 5% NGS, 2 days at 4 °C	Biotinylated anti-rabbit (Vector Labs) 1:200 in 5% NGS, 30 min at RT	ABC Kit (Vector Labs)
Anti-c-Myc	Santa Cruz (C-19): sc-788	50 min, 100 °C, W/B, citrate buffer (Thermo)	1.5% H_2O_2, 15 min, RT; 5% NGS, 30 min, RT	3 x 5 min TBS/T	1:200 in 5% NGS, 2 days at 4 °C	Envision+ conjugated anti-rabbit (DAKO), 2 h at RT	N/A
Anti-E-cadherin	BD Transduction Labs #610182	15 min, 100 °C, M/W, 1:100 antigen unmasking solution (DAKO)	0.5% H_2O_2, 20 min, RT; 20% NRS, 20 min, RT	3 x 5 min TBS/T	1:100 in 20% NRS, O/N at 4 °C	Biotinylated anti-mouse (DAKO) 1:200 in 20% NRS, 30 min at RT	ABC Kit (Vector Labs)
Anti-GFP	AbCam, #6556	20 min, 100 °C, W/B, citrate buffer (Thermo)	Peroxidase (DAKO), 5 min, RT; 5% BSA, 30 min, RT (Block)	3 x 5 min TBS/T	1:500 in 5% BSA, 1 h at RT	Envision+ conjugated anti-rabbit (DAKO), 30 min at RT	N/A
Anti-KI67	Vector Labs #VPK452	20 min, 100 °C, W/B, citrate buffer (Thermo)	0.5% H_2O_2, 20 min, RT; 20% NRS, 30 min, RT	3 x 5 min TBS/T	1:20 in 20% NRS, O/N at 4 °C	Biotinylated anti-mouse (DAKO) 1:200 in 20% NRS, 30 min at RT	ABC Kit (Vector Labs)
Anti-Lysozyme	Neomarkers #RB-372-A	20 min, 100 °C, W/B, citrate buffer (Thermo)	1.5% H_2O_2, 15 min, RT; 10% NGS, 30 min, RT	3 x 5 min TBS/T	1:100 in 10% NGS, 1 h at RT	Envision+ conjugated anti-rabbit (DAKO), 30 min at RT	N/A
Anti-p21	Santa Cruz (M-19): sc-471	20 min, 100 °C, M/W, citrate buffer (Thermo)	Peroxidase (DAKO), 20 min, RT; 10% NGS, 45 min, RT (Block)	3 x 5 min TBS/T	1:50 in 10% NGS, 1 h at RT	Envision+ conjugated anti-rabbit (DAKO), 1 h at RT	N/A
Anti-Phospho-S6	Cell Signalling Technology #9204	15 min, 100 °C, M/W, citrate buffer (Thermo)	3% H_2O_2, 20 min, RT; 10% NGS, 45 min, RT	3 x 5 min TBS/T	1:100 in 10% NGS, 2 h at RT	Biotinylated anti-rabbit (DAKO) 1:200 in 10% NGS, 30 min at RT	ABC Kit (Vector Labs)

Key: W/B water bath, M/W microwave, P/C - Pressure Cooker, NRS normal rabbit serum, NGS normal goat serum, BSA bovine serum albumin, RT room temperature, O/N over night, TBS/T tris buffered saline with tween, PBS/T phosphate buffered saline with tween

2.4.1.6   Secondary antibody treatment

The slides were transferred to the slide chamber and enough secondary antibody was applied to cover the tissue. When signal amplification step was required by the protocol, an appropriate biotinylated secondary antibody (DAKO) was diluted 1:200 in blocking solution. Otherwise, an appropriate Horseradish peroxidase (HRP) conjugated secondary antibody (Envision+ Kit, DAKO) was used undiluted. Appropriate secondary antibodies and incubation times for specific primary antibodies are provided in Table 2.3. After incubation, slides were washed 3 x 5 min in washing buffer.

2.4.1.7   Signal amplification

In instances, when anti-mouse or anti-rabbit Envision+ kits (DAKO) could not be used, a signal amplification step was introduced into the protocol. Avidin-Biotin Complex reagent (Vectastain ABC kit, Vector labs) was prepared according to manufacturer's instructions 30 min prior to use and stored at room temperature. Tissue sections were covered with 200 μl of ABC reagent and incubated for 30 min at room temperature, followed by 3 x 5 min washes in washing buffer.

2.4.1.8   Signal visualisation with 3.3'-diaminobenzidine (DAB)

Antibody binding was visualised by colourimetric detection with 3,3'-diaminobenzidine (DAB). Tissue sections were covered with 200 μl of DAB solution (2 drops of DAB chromogen mixed with 1 ml of DAB substrate (Envision+ Kit, DAKO)). Slides were incubated for 5–10 min or until a sufficient level of staining was attained followed by a 5 min wash in dH$_2$O.

2.4.1.9   Counterstaining, dehydration and mounting

Tissue sections were counterstained in Mayers Haemalum (R. A. Lamb) for 30 sec and washed in running tap water for 5 min. Slides were then dehydrated by consecutive washes in increasing concentrations of ethanol (1 x 3 min 70%, 1 x 3 min in 95%, 2 x 3 min in 100%) and 2 x 5 min washes in xylene. Coverslips were mounted over dehydrated sections using DPX mounting medium (R. A. Lamb).

2.5   Gene Expression Analysis

Due care was taken during procedures involving RNA extraction and handling to ensure that all plastic and glass-ware was RNAse free. All solutions were made using RNAse free water (Sigma) or water treated with Diethyl pyrocarbonate (DEPC, Sigma). Working surfaces and pipettes were sprayed with RNaseZAP (Sigma). Sterile filter-tips were used to carry out the procedures.

2.5.1 RNA extraction from tissue samples

2.5.1.1 Homogenisation of tissue samples

Tissue samples were removed from storage and placed in screw-cap tubes containing 1 ml Trizol reagent (Invitrogen) and 1.4 mm ceramic beads (Lysing matrix D tubes, MP Biomedical), unless this was done at the time of dissection. Samples were then homogenised using Precellys24 homogeniser (Bertin Technologies) at 6500 RPM for 2 x 45 second cycles. Tubes were centrifuged at 11000 x g for 10 min at 4 °C to pellet the beads and tissue debris.

2.5.1.2 RNA extraction

Supernatant was transferred into fresh 1.5 ml eppendorf tubes containing 200 μl of chloroform (Fisher Scientific). Tubes were then shaken vigorously by hand for 30 seconds and allowed to stand at room temperature for 3 min. Tubes were centrifuged at 11000 x g for 15 min at 4 °C. The top, aqueous, phase (approximately 400 μl) containing RNA was removed and transferred into fresh 1.5 ml eppendorf tubes containing 400 μl of isopropanol. Tubes were gently inverted until well mixed.

2.5.1.3 RNA purification and DNAse treatment

RNA purification was performed using the RNeasy mini kit (Qiagen) according to the manufacturer's instructions. All centrifugation steps were performed at 11000 x g in a refrigerated bench top centrifuge cooled to 4 °C. The mix from the previous step was transferred into purification columns placed in a collection tubes. Columns were centrifuged for 30 seconds and the flow-through was discarded. On-column DNAse treatment from illustra triplePrep Kit (GE Healthcare) was used to remove DNA contamination according to the manufacturer's instructions. 100 μl of DNAse treatment solution (70 μl RNAse-free dH$_2$O, 20 μl DNAse buffer, 10 μl DNAse I) was pipetted onto columns and allowed to stand for 10 min at room temperature. After DNAse treatment, columns were centrifuged for 30 seconds and the flow-through was discarded. Columns were washed by adding 500 μl of RPE wash buffer (RNeasy kit, Qiagen) and centrifuging for 30 seconds. The flow-through was discarded and the wash was repeated, followed by 2 min centrifugation. The flow-through was discarded and columns were centrifuged once again for 1 min to remove the remnants of the buffer from columns. To elute RNA, columns were placed into fresh 1.5 ml eppendorf tubes, 100 μl of RNAse-free dH$_2$O was pipetted onto columns and allowed to stand for 3 min at 4 °C. Eluate containing RNA was collected by centrifuging columns for 1 min and immediately placed on ice. The concentration and purity of RNA was assessed using NanoDrop 1000 (Thermo Scientific). RNA samples were stored at -80 °C until needed.

2.5.1.4 Determination of RNA quality

The quality of the extracted RNA was analysed using denaturing agarose gel electrophoresis as described in Qiagen Bench Guide (Qiagen). RNA samples containing 2 μg of RNA were mixed with the appropriate amount of RNA 5X loading buffer (0.25% Bromophenol blue (Sigma), 4 mM EDTA (Sigma), 0.9 M formaldehyde (Sigma), 20% glycerol (Sigma), 30.1 % formamide (Sigma), 4X FA gel buffer (see below)), incubated at 65 °C for 3–5 min and quenched on ice. Samples were then loaded onto a denaturing gel (1% agarose (Eurogentech), in 1X FA gel buffer (20 mM 3-(N-Morpholino)propanesulfonic acid (MOPS, Sigma), 5 mM sodium acetate (Sigma), 1 mM EDTA (Sigma), 0.22 M formaldehyde (Sigma), 0.1 μg/ml Ethidium bromide (Sigma) in dH$_2$O)). The gel was run in FA gel running buffer (20 mM 3-(N-Morpholino)propanesulfonic acid (MOPS, Sigma), 5 mM sodium acetate (Sigma), 1 mM EDTA (Sigma), 0.25 M formaldehyde (Sigma) in dH$_2$O) at 50 V for 1 hour. RNA was then visualised under UV light on a GelDoc (BioRad). Assessment of RNA quality was based on the sharpness of 18S and 28S ribosomal RNA bands.

2.5.2 Preparation of cDNA for quantitative analysis

cDNA synthesis was performed as described by Untergasser A. cDNA synthesis using superscript II http://www.untergasser.de/lab/protocols/cdna_synthesis_superscript_ii_v1_0.htm using Superscript II RNAse H reverse transcriptase kit (Invitrogen). 1 μg of RNA was mixed with 5 μl of 100 ng/μl random hexamers (Promega), and made up to 20 μl with DNAse free dH$_2$O (Sigma). The mix was then incubated at 70 °C for 10 min, 25 °C for 10 min and held at 4 °C long enough to add 20 μl of enzyme mix (8 μl 5X First Strand Buffer, 4 μl 0.1 M DTT, 0.8 μl 25 mM dNTPs (Bioline), 1 μl Superscript II enzyme, 6.2 μl RNAse-free dH$_2$O) per reaction. The reaction mix was then incubated at 25 °C for 10 min, 37 °C for 45 min, 42 °C for 45 min, 70 °C for 15 and stored at 4 °C. 160 μl of DNAse free dH$_2$O was added to 40 μl of reaction mix and 2 μl of the resulting cDNA was used per reaction in quantitative RT-PCR. Negative control cDNA samples were synthesised in the same manner but without addition of Superscript II enzyme to the enzyme mix.

2.5.3 Quantitative real-time PCR analysis

2.5.3.1 Primer design for qRT-PCR

Primers for qRT-PCR analysis (unless previously published) were designed using Primer3 software at http://fokker.wi.mit.edu/primer3/input.htm, checked for mispriming using BLAST engine against Ensembl database (http://www.ensembl.org/Multi/blastview) and synthesised by Sigma Genosys. A number of conditions were considered when designing primers. Primers were designed to reside across exon boundaries to avoid amplification of genomic DNA. Primers were to yield a PCR product of 100–200 bp in size and to have an

annealing temperature close to 60 °C. The primer sequences used are specified in Table 2.4.

Table 2.4: Primer sequences used for quantitative RT-PCR analysis

Gene	Forward Primer	Reverse Primer
E-cadherin	CAGATGATGATACCCGGGACAA	GGAGCCACATCATTTCGAGTCA
β-catenin	AGTCCTTTATGAATGGGAGCAA	TCTGAGCCCTAGTCATTGCATA
β-actin	TGTTACCAACTGGGACGACA	GGGGTGTTGAAGGTCTCAAA
CD44	ATCGCGGTCAATAGTAGGAGAA	AAATGCACCATTTCCTGAGACT
C-myc	CTAGTGCTGCATGAGGAGACAC	GTAGTTGTGCTGGTGAGTGGAG
Cyclin D1	ACGATTTCATCGAACACTTCCT	GGTCACACTTGATGACTCTGGA
Axin2	GCAGCTCAGCAAAAAGGGAAAT	TACATGGGGAGCACTGTCTCGT

2.5.3.2   qRT-PCR reaction set-up

All reactions were run on StepOnePlus real-time PCR system supplemented with StepOne software v2.1 (Applied Biosystems). All reactions were run in a minimum of three technical and three biological replicates. Samples devoid of cDNA served as negative controls to test for contamination with genomic DNA. A housekeeping gene (typically $β$-actin) was used in each run as a reference gene.

Reactions were run using either DyNAmo HS SYBR Green qPCR kit (Finnzymes) according to the manufacturer's instructions or a home-made SYBR Green Master Mix (for 100 reactions: 400 μl 5X GOTaq Flexi buffer (Promega), 200 μl 25 mM Magnesium Chloride (Promega), 20 μl 25 mM dNTPs (Bioline), 20 μl SYBR Green solution (2 μl of stock 10000X SYBR Green (Molecular probes) made up in 1320 μl of DMSO (Sigma)), 40 μl 50X ROX dye (Finnzymes), 1068 μl DNAse-free dH$_2$O (Sigma), 12 μl GOTaq polymerase (Promega)). qRT-PCR reactions for the intestinal stem cell markers (Lgr5 and Ascl2) were performed using TaqMan assay (Applied Biosystems) following the manufacturer's instructions and using custom designed TaqMan probes (Applied Biosystems). Forward and reverse primers (100 mM) were mixed in equal quantities and diluted to 10 mM concentration. 0.4 μl of the resulting 10 mM primer mix was then used per reaction. For all reactions 2 μl of cDNA was loaded into a thin wall 96-well PCR plate (Applied Biosystems). 18 μl of Master Mix containing appropriate primers or TaqMan probes were added to cDNA samples and plates were sealed with optically clear sealing film (Applied Biosystems). All SYBR Green reactions were run using the same cycling conditions: 95 °C for 10 min followed by 40 cycles (95 °C for 15 seconds, 60 °C for 30 seconds, 72 °C for 30 seconds), To ensure that a single product was amplified by the primer set, a melting curve was run after cycling from 60 °C to 95 °C with a 0.5 °C increment. TaqMan reactions were run using the following conditions 50 °C for 2 min, 95 °C for 10 min followed by 40 cycles (95 °C for 15 seconds, 60 °C for 1 min).

2.5.3.3   Analysis of qRT-PCR data

Data from the samples with reproducible cycle time (C_t) values and a single peak melting curve (when applicable) were analysed using the $2^{\Delta\Delta C_t}$ method (Livak and Schmittgen, 2001). ΔC_t values were calculated using C_t value of the reference gene from the same sample. Average ΔC_t values were calculated for all control samples and $\Delta\Delta C_t$ value for each individual sample was calculated in reference to the average 'control' ΔC_t. Average $\Delta\Delta C_t$ values were calculated for samples from each biological group and the Mann-Whitney U test was used to test for significant differences between means. The average $\Delta\Delta C_t$ from each biological group was transformed into fold change using formula $2^{\Delta\Delta C_t}$.

2.5.4   PCR analysis of genomic recombination

2.5.4.1   DNA extraction for recombined PCR

Tissue samples for DNA extraction were collected at the time of dissection and DNA was isolated in the same manner as from ear and tail biopsies (section 2.1.4.1). In instances, where fresh tissue was unavailable, DNA was extracted from paraffin embedded tissue. Slides containing tissue sections were dewaxed and rehydrated as for immunohistochemistry (section 2.4). Sections were then briefly counterstained in Mayer's Haemalum (R. A. Lamb) to aid tissue visualisation and washed in running tap water for 5 min. Required tissue was then scraped off from the slides and placed in 1.5 ml eppendorf tube followed by the previously described DNA extraction procedure (section 2.1.4.1). At the final step, the DNA pellet was resuspended in 100 μl and stored at 4 °C until needed.

2.5.4.2   Brg1 recombined PCR

Primers for Brg1 recombined PCR were designed using Primer3 software at http://fokker.-wi.mit.edu/primer3/input.htm, checked for mispriming using the BLAST search engine against Ensembl mouse database (http://www.ensembl.org/Multi/blastview) and synthesised by Sigma Genosys. Primers specific for recombination product (see Table 2.2) amplified a product of 529 bp from a DNA template that underwent recombination between loxP sites. The unrecombined template would yield a product of 2723 bp that could not be amplified under the reaction conditions (40 seconds amplification time). A parallel PCR reaction with primers used for Brg1 genotyping was carried out to ascertain DNA presence in samples and confirm the animal genotype. The PCR reaction was set up and run under the conditions outlined in Table 2.1. PCR products were visualised as described in section 2.1.4.3.

2.5.5   In situ hybridisation

In situ hybridisation was used to examine the expression of the intestinal stem cell marker *Olfm4*. This technique utilised digoxigenin (DIG) labelled anti-sense RNA probes (ribo-

Table 2.5: Reaction constituents for DIG labelling

Component	Volume
RNase Free H2O	12 μl
Transcription Buffer (10X) (Roche)	2 μl
DIG RNA Labelling mix (Roche)	2 μl
RNasin (Promega)	1 μl
T7 RNA Polymerase (Roche)	2 μl
DNA (1 μg/μl)	1 μl

probes) complementary to *Olfm4* mRNA sequence. Probe binding was detected using an anti-digoxigenin alkaline phosphatase-conjugated antibody by development of purple staining. The probe for *Olfm4*, cloned in a pBluescript II SK+ vector, was provided by Hans Clever's group (Hubrecht Institute, Netherlands). All glassware used in the protocol was heat-treated by baking at 200 °C overnight and RNAse-free (Sigma) or DEPC treated dH$_2$O was used to prepare all solutions.

2.5.5.1   Probe synthesis

The *Olfm4* probe was synthesised by linearisation of plasmid DNA, RNA polymerase reaction from the T7 promoter and DIG labelling. 30 μg of plasmid DNA was linearised by restriction digest with NotI restriction enzyme (NEB) according to manufacturer's instructions. The restriction digest was carried out overnight at the appropriate temperature, and 5 μl of reaction was run on an agarose gel alongside undigested vector to confirm complete linearisation. Linearised DNA was then purified using DNA purification columns (Qiagen). DNA concentration of the purified plasmid was determined using NanoDrop 1000 (Thermo Scientific), and adjusted to 1 μg/μl using 10 mM Tris (pH 8.0) as required. The linearised plasmid DNA was used as a template for the transcription of DIG-labelled riboprobes using T7 RNA polymerase (Roche). The components of the riboprobe-labelling reaction are outlined in Table 2.5.

The labelling reaction was carried out for 2 hours at 37 °C, followed by DNA template digestion by incubation with 20 units of DNaseI (Ambion) for 15 minutes at 37 °C. Riboprobes were purified using the RNeasy Mini kit (Qiagen) according to manufacturer's instructions. Probes were eluted with 100 μl of RNAse-free H$_2$O and divided into 10 μl aliquots, which were transferred to storage at -80 °C.

2.5.5.2   Probe hybridisation

Slides were dewaxed in 2 x 10 min changes of xylene, and rehydrated by 1 min washes in ethanol of decreasing concentration: 2 x 100%, 95%, 85%, 75%, 50% and 30%. Slides were incubated in 1X saline for 5 min followed by 5 min wash in 1X PBS. Endogenous alkaline phosphatase activity was blocked by a 30 min incubation in 6% hydrogen peroxide (in 1X

PBS) at room temperature. Slides were washed 2 x 5 min in 1X PBS, fixed in ice cold 4% PFA (Sigma) (in 1X PBS) for 20 minutes followed by 2 x 5 min washes in 1X PBS. Slides were incubated in Proteinase K (Roche) (20 μg/ml Proteinase K, 50 mM Tris, 5 mM EDTA in dH$_2$O) for 5 min at room temperature, washed for 5 min in 1X PBS, post-fixed in 4% PFA for 5 minutes followed by 2 min wash in DEPC treated H$_2$O. To reduce non-specific probe binding, slides were incubated with acetic anhydride (0.01 M acetic anhydride (Sigma), in 0.1 M triethanolamine hydrochloride (Sigma)), for 10 min at room temperature. Slides were then consecutively washed in 1X PBS and 1X saline for 5 min at room temperature. Slides were rehydrated through 1 min washes in 30%, 50%, 70%, 85%, 95% and 2 x 100% EtOH solutions (70% ethanol wash was carried out for 5 min to prevent salt precipitation). Slides were air dried for 30 minutes and transferred into sealable boxes lined with tissue paper saturated in moisture buffer (5X saline sodium citrate (SSC) buffer (Sigma), 50% (v/v) formamide (Sigma) in dH$_2$O). The probe was heated at 80 °C for 3 minutes, and quenched on ice, and hybridisation buffer (5X SSC, 50% formamide, 1% SDS, 0.05 mg/ml heparin (Sigma), 0.05 mg/ml calf liver tRNA (Merck) in dH$_2$O) was thawed at 80 °C. Adequate amounts of probe and hybridisation buffer were mixed (1 μl probe per 100 μl hybridisation buffer per slide), and applied to slides. A piece of parafilm was placed on top of the slide to prevent probe mixture evaporation. The box was sealed with electrical tape and incubated at 65 °C overnight in a water bath.

2.5.5.3 Post-hybridisation treatment

Slides were removed from the box and incubated in pre-warmed 5X SSC buffer at 65 °C for 30 minutes. Slides were then washed 2 x 30 min in solution I (50% formamide, 5X SSC, 1% (v/v) SDS (Sigma)) pre-warmed to 65 °C followed by 3 x 10 min washes in solution II (0.5 M NaCl (Sigma), 0.01 Tris pH 7.5 (Sigma), 0.1% TWEEN-20 (Sigma)) at room temperature. Unhybridised probe was digested by a 45 min incubation with RNase A (Roche) (0.02 mg/ml in solution II) at 37 °C, followed by a 10 min wash in solution II at room temperature. Slides were washed 2 x 30 min in solution III (50% formamide, 5X SSC) preheated to 65 °C. Slides were washed 2 x 10 min in PBS/T (0.1% TWEEN-20 in 1X PBS) and pre-blocked in 10% heat-inactivated sheep serum (DAKO) in PBS/T for 3 hours, covered with a piece of parafilm to prevent drying up of the solution. Anti-DIG alkaline phosphatase conjugated antibody (Roche) was pre-absorbed in 1% heat inactivated sheep serum in PBS/T containing 6 mg/ml small intestine tissue powder for 3 hours at 4 °C and diluted to a final concentration of 1:2000 in 1% sheep serum in PBS/T. Slides were washed in PBS/T for 5 min, overlaid with 100 μl of antibody solution, covered with a piece of parafilm, and incubated overnight at 4 °C.

2.5.5.4 Signal detection

Slides were washed in PBS/T for 5 min, followed by 2 x 5 min and subsequent 3 x 30 min washes in PBS/T. Slides were preconditioned in 3 x 5 min washes of NTMT (0.1 M sodium chloride, 0.1 M Tris pH 9.5, 0.05 M magnesium chloride (Sigma), 0.1% TWEEN-20) containing 2 mM Levamisole (Sigma). Slides were completely covered with BM Purple substrate (Roche), sealed in a dark box and incubated at room temperature until the desired level of signal was developed. Slides were then washed in PBS/T for 10 min, followed by a 30 min wash in dH$_2$O, and counterstained by immersion in Eosin Y Solution (Sigma) for up to 10 seconds. Excess eosin was washed off under running tap water and slides were air dried for 30 min. Slides were washed briefly in xylene and mounted in DPX mounting media (R. A. Lamb).

2.6 Quantitative Protein Analysis

2.6.1 Protein extraction from tissue samples

Epithelium enriched tissue samples were removed from storage at -80 °C and placed on ice. 200 μl of cell lysis buffer (20 mM Tris-HCl pH 8.0,, 2 mM EDTA pH 8.0, 0.5% (v/v) NP-40 (Sigma)) containing protease inhibitors (complete mini protease inhibitor cocktail tablets (Roche)) and phosphatase inhibitors (25 mM sodium β-glycerophosphate, (Calbiochem), 100 mM sodium fluoride (Sigma), 20 nM Calyculin A from Discodermia calyx (Sigma), 10 mM sodium pyrophosphate (Sigma)) were added to the pellet and mixed by pipetting until the pellet was thawed. Cells were sheared by passing through a syringe needle (23G) at least 20 times. Tubes containing lysate were then centrifuged in a refrigerated centrifuge (Legend Micro 17R, Thermo Scientific) at 9500 x g for 10 min at 4 °C to remove residual insolubles. The supernatant was aliquoted into 0.5 ml tubes, snap frozen in LN$_2$ and stored at -80 °C until needed.

2.6.2 Quantification of protein concentration

The protein concentration in the samples was determined using the Pierce BCA (Bicinchoninic acid) kit (Thermo Scientific). Serial dilutions of BSA (from 5 μg/ml to 25 μg/ml) in 1X PBS (Invitrogen) were prepared along with serial dilutions of protein extract samples (1:100, 1:200 and 1:400 in 1X PBS) and blank solutions containing 1X PBS. All solutions were loaded in duplicates onto 96-well microtitre plate. BCA kit reagents A and B were mixed in 50:1 ratio. 100 μl of the mix was added to each well and mixed by pipetting. The plate was then sealed with aluminium foil tape (Greiner Bio-One) and incubated at 37 °C for 1 hour or at room temperature overnight. Plates were read at 590 nm on a microplate reader (BioTek). A standard curve was generated using serial dilutions of BSA and respective protein concentrations in extracted samples were calculated.

Protein concentration was equalised between samples with cell lysis buffer.

2.6.3 Western-blotting analysis

2.6.3.1 Protein sample preparation

Samples were removed from storage at -80 °C, placed on ice and allowed to defrost. An aliquot of the protein extract containing 30 μg of protein was transferred into a fresh 1.5 ml eppendorf and made up to 25 μl with Laemmi buffer (0.125 M Tris-HCl pH 6.8, 4% (w/v) sodium dodecyl sulphate (SDS, Sigma), 40% (v/v) glycerol (Sigma), 0.1% (w/v) Bromophenol Blue (Sigma), 6% β-mercaptoethanol (Sigma), in ddH$_2$O). Proteins were denatured by heating samples at 95 °C for 5–10 min and quenching on ice just prior to loading.

2.6.3.2 Casting of polyacrylamide gels

Polyacrylamide gels were set in Mini-Potean III (Bio-Rad) gel casting apparatus with 1.5 mm spacers. Solutions for resolving (10%) and stacking (5%) gels were prepared according to Table 2.6, but without addition of TEMED. Casting plates were thoroughly cleaned before use with ddH$_2$O and 70% ethanol. Resolving gel solution was mixed with the appropriate amount of TEMED and poured into the casting immediately leaving approximately 1.5 cm from the top of the prospective gel. Resolving solution was overlaid with 500 μl of ddH$_2$O. After the gel had set the water was drained onto tissue paper. The stacking solution was then mixed with an appropriate amount of TEMED and poured into the casting followed by inserting a 10-well comb. After the stacking gel had set, the plates containing the gels were removed from the casting apparatus, combs were removed and the wells were rinsed with ddH$_2$O.

Table 2.6: Solutions used for quantitative protein analysis

5% stacking polyacryalmide gel (2 gels)	10% resolving polyacrylamide gel (2 gels)
6.9ml Ultrapure double deionised H2O	6.8ml Ultrapure double deionised H2O
1.7ml 30% acrylamide/bisacrylamide (Sigma)	8.4ml 30% acrylamide/bisacrylamide (Sigma)
1.3ml 1M Tris-HCl pH6.8	9.4ml 1M Tris-HCl pH8.8
100μll 10% [w/v] SDS (Sigma)	250μll 10% [w/v] SDS (Sigma)
66μll 25% [w/v] Ammonium persulphate (Sigma)	72μll 25% [w/v] Ammonium persulphate (Sigma)
13.2μll N,N,N,N-tetramethylethylenediamine (TEMED, Sigma)	13.2μll N,N,N,N-tetramethylethylenediamine (TEMED, Sigma)
5X Running buffer (1L)	**1X Transfer buffer (1L)**
950ml deionised H2O	800ml deionised H2O
15.1g Tris base (Sigma)	200ml Methanol (Fisher)
94g Glycine (Sigma)	2.9g Tris base (Sigma)
50ml 10% [w/v] SDS (Sigma)	14.5g Glycine (Sigma)

2.6.3.3 Protein separation by SDS-PAGE

Gels were assembled in the Mini-Protean III (Bio-Rad) electrophoresis tank and filled with a sufficient amount of SDS-PAGE running buffer (see Table 2.6). Protein samples were loaded into the wells, along with full-range Rainbow molecular weight marker (Amersham). Gels were run at 120V until the dye front reached the end of the gel.

2.6.3.4 Protein transfer to nitrocellulose membrane

After electrophoresis completion the gels were removed from the plates and immersed in Transfer buffer (see Table 2.6). Amersham Hybond-ECL nitrocellulose membrane (GE Healthcare) was soaked in transfer buffer prior to use. The nitrocellulose membrane was placed on top of the polyacrylamide gel and sandwiched between two sheets of 3MM blotting paper (Whatman) and sponge, each pre-soaked in transfer buffer. This assembly was then placed into a wet electroblotting system (Flowgen Biosciences). The blotting tank was fitted with blots so that the current runs through gel towards the filter, filled with transfer buffer and placed in a polystyrene box containing ice. The transfer was run at 100 V for 1 hour.

Table 2.7: Antibody-specific conditions for Western blotting analysis

Primary Antibody	Manufacturer	Primary antibody conditions	Secondary antibody conditions
Anti-Active-β-Catenin	Millipore #05-665	1:2000 in 5% milk in TBS/T, O/N at 4 °C	HRP-conjugated anti-mouse (GE Healthcare) 1:3000 in 5% milk in TBS/T, 1 h at RT
Anti-β-actin	Sigma #A5316	1:5000 in 5% milk in TBS/T, 1 h at RT	HRP-conjugated anti-mouse (GE Healthcare) 1:2000 in 5% milk in TBS/T, 1 h at RT

Key: TBS/T Tris buffered saline with 0.1% Tween 20, RT room temperature, O/N overnight

2.6.3.5 Generic protocol for membrane probing

Once the transfer was completed, membranes were removed from the blots and washed briefly in TBS/T. To prevent non-specific binding of antibodies, the membranes were blocked in 5% skimmed milk powder in TBS/T with agitation for 1 hour at room temperature. Membranes were incubated with agitation in blocking solution containing the appropriate dilution of primary antibodies under conditions specified in Table 2.7. Membranes were then washed in TBS/T 3 x 10 min. Secondary HRP-conjugated antibody was diluted to the appropriate concentration with blocking solution and applied to the membranes with agitation according to Table 2.7 followed by 3 x 10 min washes in TBS/T.

Appropriate amount of ECL reagent kit (Amersham) was used to develop membranes according to manufacturer's instructions. After incubation, ECL reagent was drained from membranes, which were then wrapped in cling film prior to signal detection.

2.6.3.6   Signal detection

Chemiluminescent signal generated by antibody-conjugated HRP processing of ECL reagent was detected by radiograph exposure. X-ray film (FujiFilm Super RX blue background) was exposed to blots in the darkness for various lengths of time to obtain clear images. Exposed film was processed on an automatic X-ray film processor (Xograph Compact X4). Processed films were aligned with the original blot and the positions of molecular weight markers were marked on the film to identify target proteins.

2.7   Quantitative and statistical analysis of data

2.7.1   Quantitative analysis of histological parameters

Quantitative analysis of tissue sections was carried out using an Olympus BX41 light microscope. Sample IDs were covered on all slides before scoring to avoid possible bias. Areas to be quantified were carefully selected to ensure that they belong to approximately the same region of the intestine and are free of sectioning artefacts. Quantifiable traits, such as crypt and villus length, mitosis and apoptosis levels, number of differentiated cells of particular types, etc. were scored on appropriately stained tissue sections. A minimum of 50 half-crypt or half-crypt-villus axes were stained per mouse and at least 3 different animals per genotype were examined to allow for statistical analysis. Individual 'crypt' scores were averaged to generate a 'mouse' score. And scored from all mice of the same genotype were used to calculate average 'group' value as well as standard deviation. Average 'group' values were plotted as histograms with error bars representing standard deviation within each group. MS Excel 2003 was primarily used for graphical representation of the data. Individual 'mouse' values were also used to test for significant difference between means as described below. For all tests, the use of one- or two-tailed test was decided on a case-by-case basis, depending on the appropriate null hypothesis.

2.7.2   Comparison of means

Quantitative data was first tested for normal distribution using normal plot of residuals and Anderson-Darling test in Minitab statistical analysis software (version 15.1.30.0). Normally distributed data (Anderson-Darling test $p \geq 0.05$) was then tested for significant difference between means using One-Way ANOVA using SPSS sowtware (version 16.0.2). If data from more than two groups were compared, One-Way ANOVA test was used to establish the difference across all the groups and Post-Hoc Tukey's test was subsequently

employed to perform pair-wise comparisons between groups. These tests were carried out using SPSS software. A significant difference between means was accepted, when p value was equal or less than 0.05.

Non-normally distributed data (Anderson-Darling test p$\leq$0.05) was tested for significant difference between means using Mann-Whitney U test. The test was performed in SPSS software. A significant difference between means was accepted, when p value was equal or less than 0.05.

2.7.3   Comparison of medians

Measured (as opposed to scored) parameters, such as tumour size and position, were tested for significant difference between medians rather than means. Mood's Median Test was performed on such datasets using Minitab software. A significant difference between medians was accepted, when p value was equal or less than 0.05.

2.7.4   Kolmogorov-Smirnov Z test

Kolmogorov-Smirnov Z test was used to test for the significant difference in distribution between two data sets. To assess the distribution of specific cells (i.e. BrdU positive, Ki67 positive, Caspase-3 positive, apoptotic or Paneth cells) the positions of positive cells were recorded using a following method. Each half-crypt was represented as a column of numbers in a spreadsheet with positive cells recorded as 1 and negative cells recorded as 0. Counting was started from the crypt-base so that the row in the column corresponded to cell position on the crypt-villus axis. This was repeated for 50 half-crypts per mouse. The sum of all 1 and 0 in any given row (at any given position) in every mouse was calculated and sums of all the mice of the same genotype were pooled together. These intermediate data sets were used to build graphs of cumulative frequency of positive cells using SPSS 16.0.2.

To test for the difference in distribution between the biological groups, the intermediate data set was transformed using a custom-written KST (Kolmogorov-Smirnov Transformation) program (http://bio.bsu.by/t/temp/holik/KST/). KST was used to transform the number of instances of cells at a given position in a sequence of numbers corresponding to this position. For instance, number 43 in row 7 of the intermediate data set would mean that out of all half-crypts in all the mice of a given genotype, 43 half-crypts contained a positive cell at position 7. After transformations with KST, number 43 in row 7 would be represented by 43 instances of number 7 and so on. Transformed data sets for each mouse were then subjected to Kolmogorov-Smirnov Z test using SPSS software. The two-tailed test was used throughout and statistically significant difference between distributions was accepted, when p value was less or equal 0.05.

2.7.5   Kaplan-Meier survival analysis

Survival analysis and generation of survival curves was performed using the Kaplan-Meier method with the aid of MedCalc software (version 8.2.1.0). Statistical significance between survival time of different experimental cohorts was assessed using the Log-Rank method. Differences in survival probability were accepted as significant, when p value was less or equal 0.05.

Chapter 3

Investigating the effects of Brg1 loss in the small intestinal epithelium

3.1   Introduction

Brg1 has been implicated in a diverse range of physiological and pathological processes at both the cellular and organismic levels consistent with its involvement in mediation of various signalling pathways (Trotter and Archer, 2008). Of particular interest is the involvement of Brg1 in mediation of the Wnt signalling pathway. As has been previously mentioned, a number of studies have implicated Brg1 in the trans-activation of Wnt pathway target genes in both physiological and pathological environments (Barker et al., 2001; Griffin et al., 2008; Park et al., 2009). The observation that suppression of Brg1 function impaired the expression of Wnt target genes in colorectal cancer cells (Barker et al., 2001) positions Brg1 as a potential therapeutic target for Wnt driven neoplasia. However, there is a concern that targeting Brg1 may have adverse effects, particularly in tissues that rely on Wnt signalling to maintain homeostasis. The small intestinal epithelium has long been known to require Wnt signalling for its maintenance (Korinek et al., 1998). More specifically, the intestinal stem cells have been shown to depend on active Wnt signalling for their self-renewal (Fevr et al., 2007). The small intestinal epithelium, therefore, represents a suitable tissue to analyse the effects of Brg1 loss in a cellular environment reliant on Wnt signalling for its homeostasis. Furthermore, the murine small intestinal epithelium is commonly used as a model tissue to study human CRC (reviewed in Heyer et al., 1999). It, therefore, appears appropriate to investigate the consequences of Brg1 deficiency in the normal small intestinal epithelium in order to explore its suitability as a potential therapeutic target for the Wnt-driven neoplasia.

Conversely, Brg1 loss (Becker et al., 2009; Reisman et al., 2003; Wong et al., 2000) and haploinsufficiency (Bultman et al., 2007, Glaros et al., 2008) have been suggested to contribute to tumourigenesis in a range of tissues. Targeting Brg1, therefore, may have a potential oncogenic effect and thus undermine the value of Brg1 as a therapeutic target

in cancer.

This chapter aims to characterise the effects of Brg1 deficiency and haploinsufficiency in the small intestinal epithelium using a range of conditional transgenic approaches.

3.2   Results

3.2.1   Generation of small intestinal specific conditional Brg1 knock-out models

In order to investigate the effects of Brg1 loss in the small intestinal epithelium, I exploited Cre recombinase conditional knock-out system using targeted *Brg1* alleles with loxP sites flanking exons 2 and 3 (Figure 2.1a, Sumi-Ichinose *et al.*, 1997). Recombination between the loxP sites within *Brg1* alleles was achieved using a number of different Cre recombinases with distinct expression patterns and means of regulation. Initially, animals carrying loxP targeted *Brg1* alleles were intercrossed with mice bearing the *Tg(Cyp1a1-cre)1Dwi* transgene (abbreviated here as AhCre) (Ireland *et al.*, 2004). AhCre recombinase is expressed under control of an *Aryl hydrocarbon (Ah)* promoter element derived from the rat cytochrome *P4501A1* gene, which is induced by intraperitoneal administration of beta-naphthoflavone in a range of tissues, such as intestinal epithelium, liver, pancreas and others (Ireland *et al.*, 2004). In the small intestinal epithelium the expression of the AhCre recombinase is confined to the bottom of the crypt, where it is primarily expressed in the stem cell and early progenitor cell populations (Figure 3.1b). Expression of AhCre recombinase in the small intestinal epithelium was confirmed using the *Gt(ROSA)26Sor* (further referred to as *LacZ*) reporter allele to drive expression of *β-galactosidase* gene upon Cre recombinase mediated removal of a loxP flanked stop-cassette (Soriano, 1999). Positive staining for *β*-galactosidase activity was detected in nearly 100% of the small intestinal epithelium upon induction of AhCre recombinase (Figure 3.1a).

Unfortunately, due to off-target-tissue expression of AhCre recombinase during embryonic development loxP targeted *Brg1* alleles conferred embryonic lethality. In order to overcome undesirable consequences of off-target AhCre recombinase expression, I employed *Tg(Cyp1a1-cre/ESR1)1Dwi* transgene (abbreviated here as AhCreER) (Kemp *et al.*, 2004). While AhCreER recombinase shares the expression pattern with AhCre (Figure 3.1b), the synthesised protein is sequestered in the cytoplasm due to the presence of a modified hormone-binding domain of the oestrogen receptor (ER). AhCreER recombinase therefore requires additional activation with tamoxifen, binding to which allows the recombinase to be translocated to nucleus, where it is able to facilitate recombination between the loxP sites. Introduction of the oestrogen receptor domain therefore provides additional level of control over the recombinase activity. Staining for *β*-galactosidase activity revealed that tighter regulation of the recombinase activity resulted in a lower recombination frequency in the small intestine of $AhCreER^{+}LacZ^{+}$ mice compared to
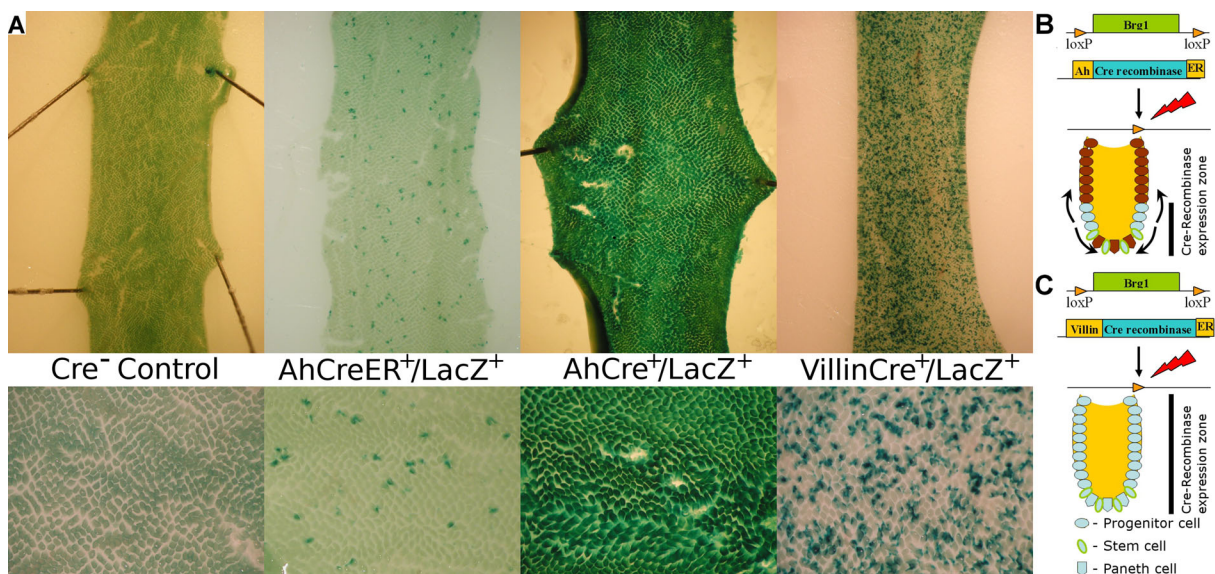
Figure 3.1: Comparative assessment of Cre recombinase efficiency in the small intestinal epithelium. **(a)** Analysis of Cre recombinase efficiency was conducted using the *ROSA26R/LacZ* transgene preceded by the loxP targeted PGK-Neo-STOP cassette. Induction of Cre recombinase activity results in PGK-Neo-STOP cassette excision and expression of the *LacZ* gene. Expression of the latter can be visualised by staining tissues of interest with X-gal substrate. Animals carrying the *ROSA26R/LacZ* reporter and Cre recombinase were induced using different induction protocols dependent on Cre recombinase present (VillinCreER recombinase was induced using low-dose protocol). *Cre⁻* mice induced with respective induction methods were used as negative controls. Mice were aged for between 15 and 30 days, when they were dissected and the third 8 cm region of the small intestinal epithelium was harvested and stained with X-gal. Analysis of LacZ expression in *AhCreER⁺/LacZ* mice revealed rare blue crypt-villus structures at variable frequencies. LacZ staining of *AhCre⁺/LacZ* intestine displayed near 100% efficiency of recombination. Intestine of *VillinCre⁺/LacZ* mice induced with the low-dose protocol, revealed LacZ positive staining in approximately 50% of crypt-villus structures. No LacZ positive staining was detected in *Cre⁻* animals. **(b-c)** Schematic representation of differences between recombination patterns induced by AhCreER and VillinCre recombinases in the small intestinal epithelium. **(b)** AhCreER recombinase drives recombination of targeted alleles in stem and early progenitor cells, progeny of which then can populate the rest of the crypt and an associated villus **(c)** VillinCre recombinase drives recombination of the targeted alleles in all epithelial cells of the small intestinal epithelium thus causing simultaneous gene deletion in all cell populations.

$AhCre^{+}LacZ^{+}$ animals (Figure 3.1a).

In order to obtain a further increase in the recombination efficiency, while avoiding off-target recombination, I also interbred mice harbouring targeted *Brg1* alleles with animals expressing Cre recombinase under the control of *Villin1* promoter (*Vil1*) (el Marjou *et al.*, 2004). *Tg(Vil-cre/ESR1)23Syr* transgene (further abbreviated as VillinCre) is expressed along the entire length of the small and large intestine and its nuclear activity is induced by intraperitoneal administration of tamoxifen. In contrast to AhCre and AhCreER recombinases, VillinCre recombinase is expressed in all the cells comprising the intestinal epithelium, both in the crypt and villus (Figure 3.1c). LacZ staining of the small intestinal epithelium from $VillinCre^{+}LacZ^{+}$ mice induced with the low-dose protocol (2.1.3.2) demonstrated efficient recombination in more then 50% of small intestinal crypts (Figure 3.1). At the same time, high-dose induction protocol was able to drive near 100% efficient recombination in the small intestine of $VillinCre^{+}LacZ^{+}$ mice (not shown).

3.2.2 Brg1 loss under the control of AhCre recombinase results in embryonic lethality

I initially attempted to delete Brg1 under the control of AhCre recombinase. However, animals carrying both Brg1 loxP targeted alleles and the AhCre recombinase transgene ($AhCre^{+}Brg^{fl/fl}$) were significantly under-represented at weaning age (Chi-square test, p<0.01). In order to investigate the disproportionately low numbers of $AhCre^{+}Brg^{fl/fl}$ animals at this time point I assessed the relative frequency of $AhCre^{+}Brg^{fl/fl}$ genotype at different stages of development. Genotyping of 38 embryos at E19.5 failed to detect any embryos with the $AhCre^{+}Brg^{fl/fl}$ genotype (expected frequency 25%). This indicated that off-target expression of AhCre recombinase could cause embryonic lethality of $AhCre^{+}Brg^{fl/fl}$ mice. Genotyping of 20 embryos at E15.5 demonstrated that $AhCre^{+}$-$Brg^{fl/fl}$ mice were present at the expected frequency, suggesting that $AhCre^{+}Brg^{fl/fl}$ animals died *in utero* between E15.5 and E19.5. Histological inspection of paraffin embedded embryos at E15.5 revealed that $AhCre^{+}Brg^{fl/fl}$ embryos were consistently smaller in size and underdeveloped compared to $AhCre^{-}Brg^{fl/fl}$ littermates (Figure 3.2a). Since embryonic lethality was most likely caused by the loss of Brg1 in tissues with non-specific expression of AhCre recombinase, I stained paraffin embedded sections of the embryos at day E15.5 with antibodies against Brg1. The staining revealed areas of Brg1 loss in regions of the choroid plexus, hind limb and tail (Figure 3.2b, white arrowheads) of $AhCre^{+}Brg^{fl/fl}$ embryos, while Brg1 was ubiquitously expressed in control embryos (Figure 3.2a and b). Although this observation confirmed alternative sights of Brg1 loss during embryonic development, the limited pattern of Brg1 loss failed to explain *in utero* lethality. It is plausible, however, that Brg1 deficient cells are rapidly eliminated and that the areas of Brg1 loss detected in E15 $AhCre^{+}Brg^{fl/fl}$ embryos represent only those Brg1 deficient cells with a slower elimination rate.
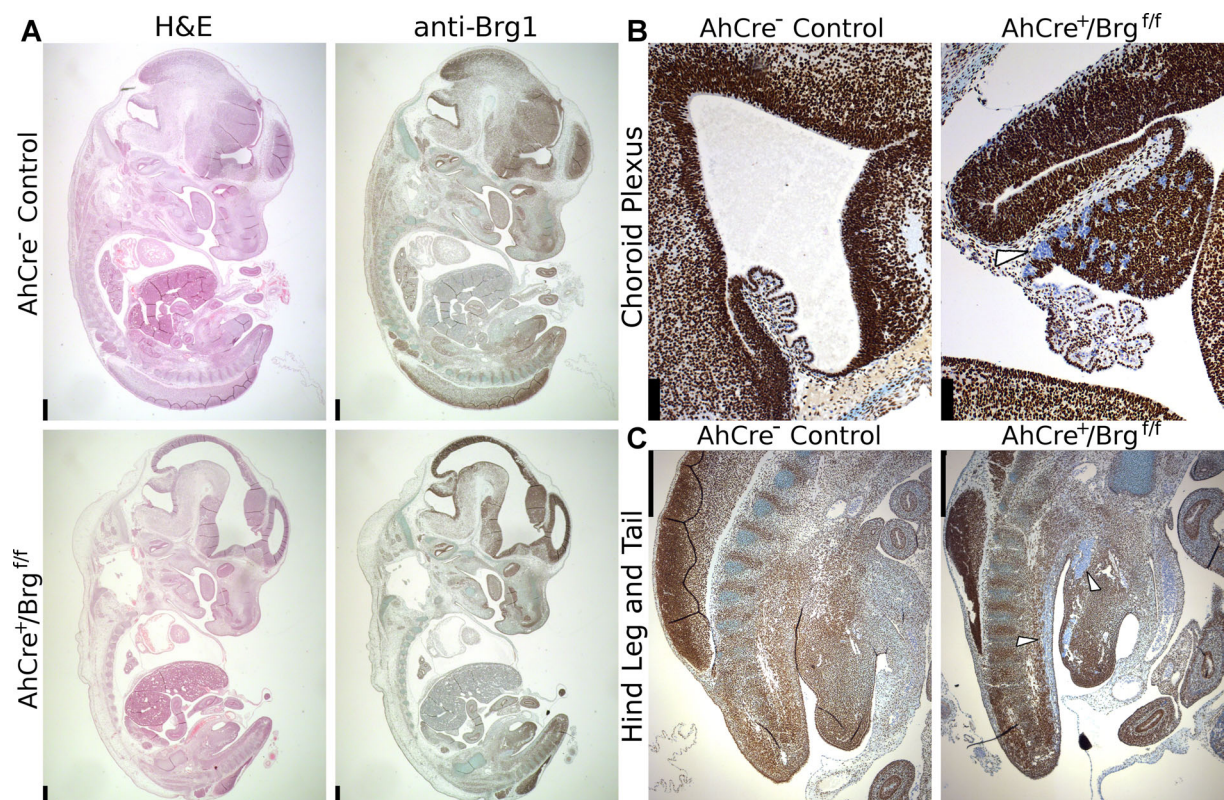
Figure 3.2: AhCre recombinase drives off-target Brg1 loss during embryonic development. Pregnant dams were dissected at day 16 after discovery of the plug. Embryos were harvested, fixed in ice cold formalin and processed for histological analysis. **(a)** Left panels: Visual inspection of H&E stained sections of $AhCre^+Brg^{fl/fl}$ embryos at day E15.5 revealed a consistently smaller size, delayed development and dilated cerebral ventricles compared to $AhCre^-$ controls. Right panels: Immunostaining of embryo sections with Brg1 antibody revealed ubiquitous Brg1 expression. **(b, c)** Closer inspection of Brg1 stained sections of embryos at day E15.5 revealed loss of Brg1 expression in the vicinity of the choroid plexus **(b)** and hind limb **(c)**. Error bars represent 500 μm (a, c), 100 μm (b).

3.2.3 $AhCre^+Brg^{+/fl}$ mice are viable and not prone to intestinal tumourigenesis

While $AhCre^+Brg^{fl/fl}$ mice died *in utero*, heterozygous $AhCre^+Brg^{+/fl}$ pups were present at the expected ratio at the time of weaning and were viable and fertile. Mice with heterozygous loss of Brg1 have been reported to be prone to mammary and lung tumourigenesis (Bultman *et al.*, 2007; Glaros *et al.*, 2008). Notably, tumours developing in those mice retained a functional copy of *Brg1*, indicating that Brg1 haploinsufficiency rather than loss of heterozygousity contributed to tumourigenesis. In order to investigate the effects of Brg1 haploinsufficiency on intestinal tumourigenesis a cohort of $AhCre^+Brg^{+/fl}$ (n=10) animals was aged along with $AhCre^+Brg^{+/+}$ controls (n=9). Mice from both groups were induced with four intraperitoneal injections of 80 mg/kg β-naphthoflavone at 8 hour intervals and regularly inspected for signs of intestinal tumourigenesis. All mice were sacrificed at 600 days post induction (PI) or earlier if found to display signs of ill health. To confirm that the targeted *Brg1* allele was deleted upon activation of the AhCre recombinase, DNA was extracted from the small intestinal samples of $AhCre^+Brg^{+/fl}$ mice. Recombined PCR performed on the intestinal samples revealed the presence of the recombinant product as late as day 600 PI (Figure 3.3), indicating long-term retention of the Brg1 heterozygous cells in the small intestinal epithelium.
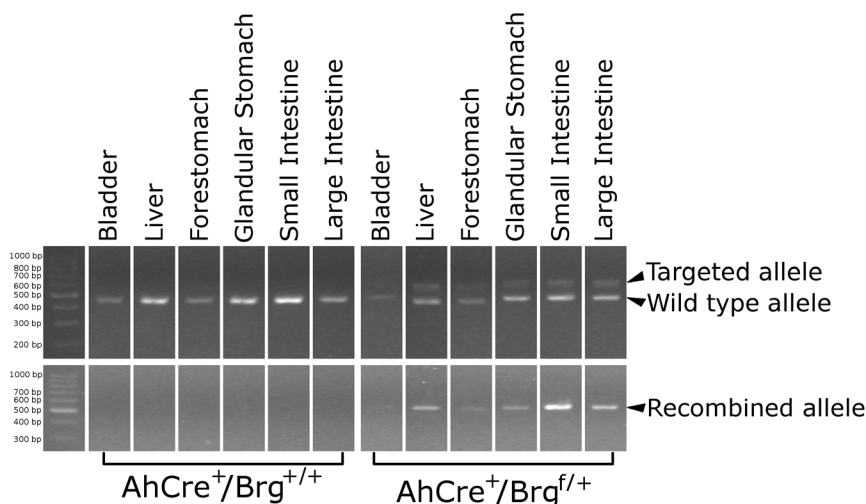
Figure 3.3: Brg1 heterozygous cells are retained in AhCre expressing tissues over a long time. A PCR reaction designed to detect the product of recombination of loxP sites in the targeted *Brg1* allele was carried out using DNA extracted from formalin fixed tissue sections of $AhCre^+Brg^{+/fl}$ and $AhCre^+$-$Brg^{+/+}$ mice at day 600 PI. At least two mice per group were genotyped. Primers used for routine genotyping were used as a positive control to test for the presence of DNA in the sample and to confirm the genotype of the animal (407 bp and 500 bp products are amplified from the wild type and targeted *Brg1* alleles respectively, top section). Recombination-specific product (529 bp, bottom panel) was detected in all tissues from $AhCre^+Brg^{+/fl}$ mice with the exception of the bladder urothelium. No recombination-specific product was detected in any of the DNA samples extracted from $AhCre^+Brg^{+/+}$ animals.

Survival analysis of $AhCre^+Brg^{+/fl}$ (n=10) and control (n=9) animals demonstrated no significant difference between the cohorts (Figure 3.4, p=0.097 Log-Rank test, n≥9). Notably, $AhCre^+Brg^{+/fl}$ mice that became ill and had to be sacrificed prior to 600 days

PI displayed no symptoms of intestinal tumourigenesis, such as pale feet, loss of weight or faecal blood. Coincidentally, macro- and microscopic examination of the small intestine from the animals with heterozygous Brg1 loss did not detect any signs of tumourigenesis.
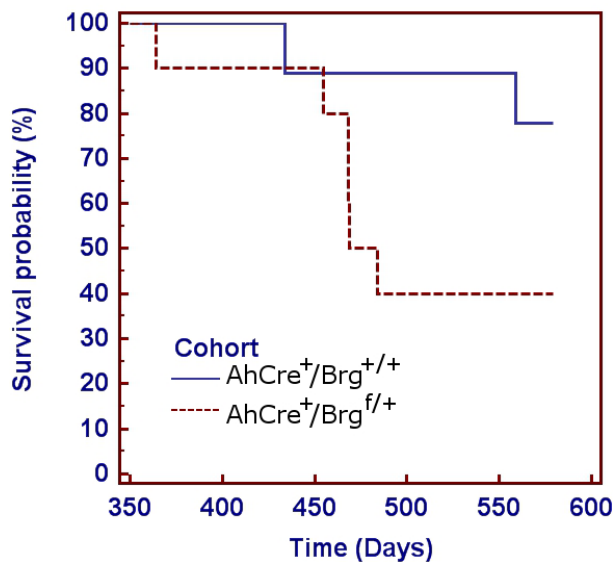
Figure 3.4: Heterozygous loss off Brg1 does not impair animal survival. Cohorts of $AhCre^+Brg^{+/fl}$ (n=10) and $AhCre^+Brg^{+/+}$ mice (n=9) were induced with an appropriate protocol and aged for 600 days or until developed signs of ill health. Survival data was presented as a Kaplan-Meyer plot. No significant difference in survival probability was observed between the cohorts (Log-Rank test p=0.097, n≥9)

3.2.4 AhCreER recombinase drives mosaic loss of Brg1 in $AhCreER^+$-$Brg^{fl/fl}$ mice

In order to overcome the embryonic lethality of Brg1 deficient animals caused by off-target expression of AhCre recombinase animals bearing targeted *Brg1* alleles were intercrossed with mice bearing AhCreER recombinase. The resulting $AhCreER^+Brg^{fl/fl}$ mice were viable and fertile.

To inactivate Brg1 in the small intestine under the control of AhCreER recombinase, a cohort of $AhCreER^+Brg^{fl/fl}$ mice along with $AhCreER^-Brg^{fl/fl}$ controls were induced by five intraperitoneal bi-daily injections of 80 mg/kg β-naphthoflavone and tamoxifen. Immunohistochemical analysis of Brg1 expression in the intestinal epithelium of $AhCreER^+Brg^{fl/fl}$ mice detected Brg1 deficient cells as early as day 3 PI (Figure 3.5, black arrowheads). Consistent with the expression pattern of AhCreER recombinase, Brg1 deficient cells were mainly detected within the crypts or at the bottom of villi. Reflecting the low frequency of AhCreER recombinase activation, Brg1 loss in the small intestinal epithelium was mosaic with the majority of Brg1 negative cells found in small clusters rather than populating full crypts (Figure 3.5, black arrowheads).

<center>Control   AhCreER$^+$/Brg$^{f/f}$</center>
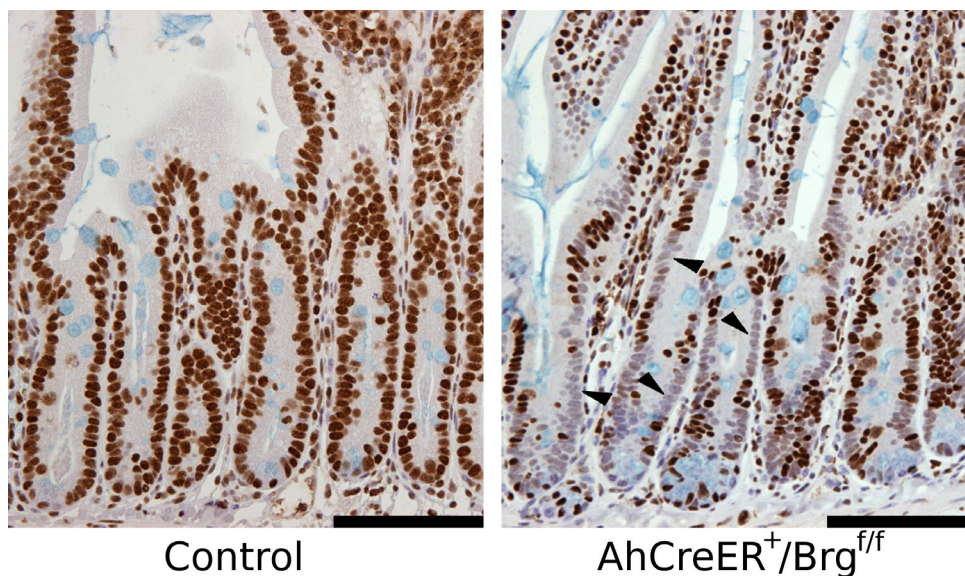
Figure 3.5: AhCreER recombinase drives mosaic loss of Brg1 in the small intestinal epithelium. $AhCreER^+Brg^{fl/fl}$ mice along with $AhCreER^-Brg^{fl/fl}$ controls were induced with an appropriate protocol and dissected at day 3 PI. Immunohistochemical analysis of Brg1 expression revealed mosaic loss of Brg1 in the small intestinal epithelium of $AhCreER^+Brg^{fl/fl}$ mice (black arrowheads). No extensive areas of Brg1 loss were detected in the small intestine of control mice. Scale bars represent 100 μm.

3.2.5   Brg1 deficient cells are repopulated with wild type cells in $AhCreER^+Brg^{fl/fl}$ mice

To analyse long-term fate of Brg1 deficient cells in the small intestinal epithelium, $AhCreER^+$-$Brg^{fl/fl}$ mice and $AhCreER^-Brg^{fl/fl}$ controls were dissected at various time points after induction. Sections of the small intestine taken from these mice were stained with Brg1 antibody and inspected for the presence of Brg1 deficient cells. Quantification of the crypts retaining Brg1 deficient cells revealed a steady decrease in the frequency of such crypts with time (Figure 3.6a and b). By day 15 PI the majority of Brg1 deficient cells were eliminated and replaced with cells retaining intact *Brg1* alleles (Figure 3.6a). Immunohistochemical analysis of Brg1 expression in the small intestinal epithelium of $AhCreER^+Brg^{fl/fl}$ mice 35 days PI failed to detect any Brg1 deficient cells indicating that the epithelium was entirely repopulated with wild type cells.

3.2.6   AhCreER recombinase drives recombination in the stem cell compartment

Gradual elimination of Brg1 deficient cells could be explained by Brg1 loss being limited to short-lived progenitor cells as opposed to the stem cells. If AhCreER recombinase activity induces Brg1 loss only in progenitor cells, such as those residing in the TA zone, eventual exhaustion of the proliferative potential of Brg1 deficient cells would cause their migration towards the villus tip and gradual disappearance. Conversely, if AhCreER drives loss of Brg1 in the stem cell compartment, Brg1 deficient cells are expected to
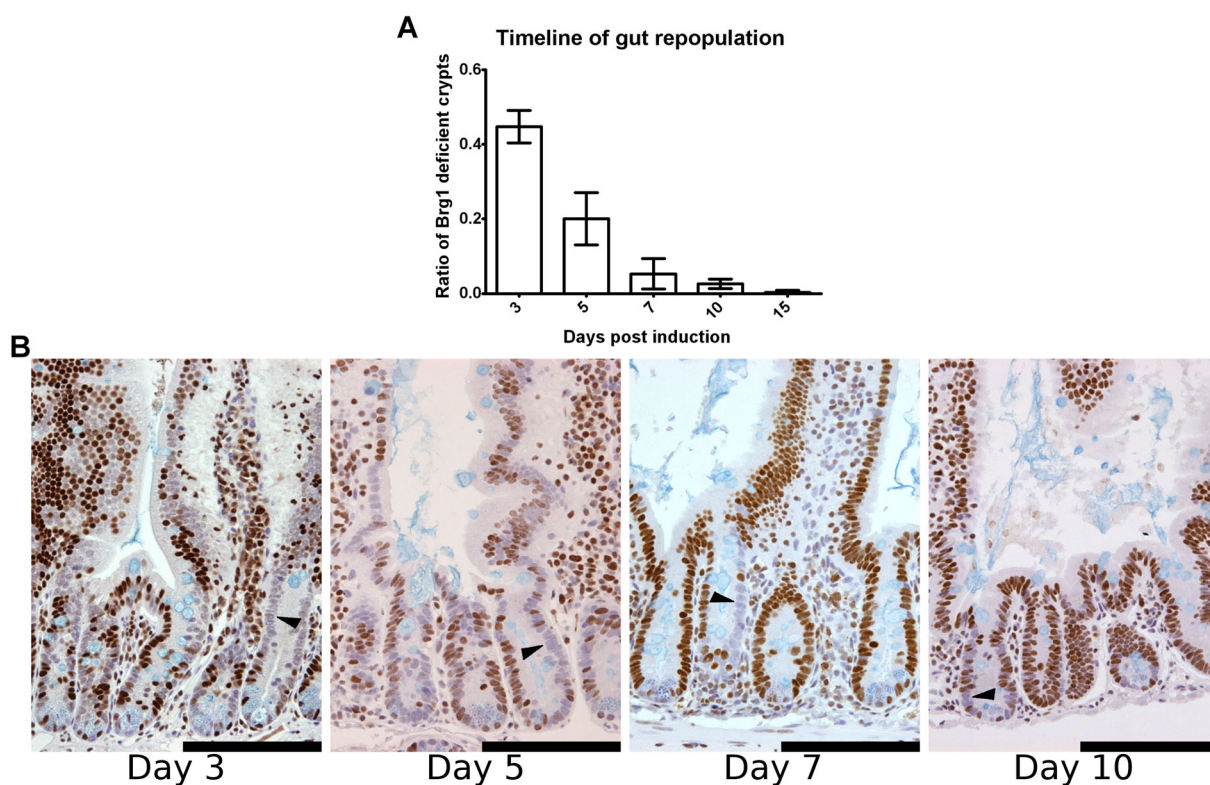
Figure 3.6: Brg1 deficient cells are repopulated with wild type cells in $AhCreER^+Brg^{fl/fl}$ small intestine. $AhCreER^+Brg^{fl/fl}$ mice were induced with an appropriate protocol and dissected at days 3, 5 , 7, 10 and 15 PI. Small intestinal samples harvested at each time point were subjected to immunohistochemical analysis of Brg1 expression. The number of crypts with more than 5 Brg1 deficient cells (b, black arrowheads) was scored per total number of crypts. Both quantitative (**a**) and visual (**b**) analysis of Brg1 expression revealed a gradual decrease in the number of Brg1 deficient crypts, which almost completely disappeared by day 15 PI. A minimum of 3 mice per time point was analysed. Scale bars represent 100 μm.

persist in the small intestinal epithelium over an extended period of time. Although AhCreER recombinase has been previously reported to drive recombination of loxP targeted alleles in intestinal stem cells (Kemp *et al.*, 2004), differences in genetic background of the animals could affect its efficiency. I, therefore, aimed to validate whether the present induction protocol induced AhCreER recombinase activity in the intestinal stem cell population. In order to trace recombination events, I employed the *LacZ* reporter allele expressing *β-galactosidase* gene from *ROSA26* locus (Soriano, 1999). Presence of loxP flanked STOP-cassette upstream of *β-galactosidase* sequence facilitates Cre-recombinase mediated activation of the reporter expression. $AhCreER^+LacZ^+Brg^{+/+}$ animals were induced with five bi-daily intraperitoneal injections of 80 mg/kg $β$-naphthoflavone and tamoxifen and the small intestines were harvested 30 days later. Consistent with previous reports (Kemp *et al.*, 2004), staining for $β$-galactosidase activity revealed the presence of positively stained crypts in the small intestine of $AhCreER^+, LacZ, Brg^{+/+}$ animals albeit at low frequency (Figure 3.7). This observation suggested that elimination of Brg1 deficient cells was not due to lack of recombination in the stem cell compartment.
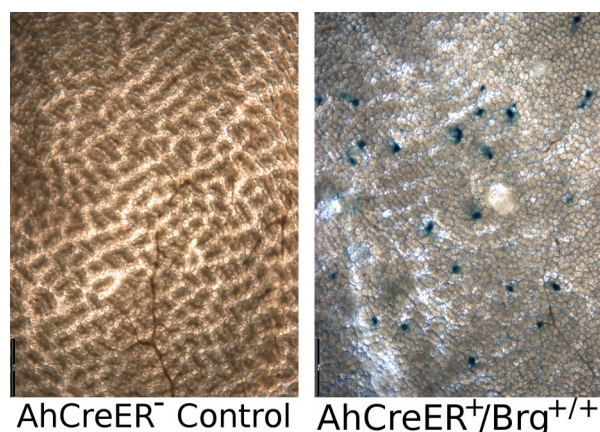
Figure 3.7: AhCreER recombinase drives recombination in the stem cell compartment. $AhCreER^+LacZ^+Brg^{+/+}$ were induced with an appropriate protocol along with $AhCreER^-$ controls. Animals were aged for 30 days PI, at which point the small intestinal tissue was harvested and stained with X-gal substrate in order to visualise expression of the LacZ reporter. Analysis of X-gal staining revealed LacZ positive crypts in the small intestinal epithelium of $AhCreER^+LacZ^+Brg^{+/+}$ mice, confirming recombination event in long-term surviving stem cells. Frequency of LacZ positive crypts, however was low and highly variable between different animals as well as between different sections of the small intestinal epithelium. No LacZ positive crypts were observed in the small intestine of control $AhCreER^-$ animals.

3.2.7 Low-dose induction of VillinCre recombinase drives partial loss of Brg1 and subsequent repopulation with wild type cells

While tighter regulation of AhCreER recombinase activity overcame embryonic lethality, the low frequency of Brg1 loss made it impossible to analyse the mechanism behind elimination of Brg1 deficient cells in $AhCreER^+Brg^{fl/fl}$ intestine. To avoid non-specific

recombinase expression while maintaining high levels of recombination I intercrossed mice carrying targeted *Brg1* alleles with mice expressing VillinCre recombinase. The resulting $VillinCre^+Brg^{fl/fl}$ mice were viable and fertile.

In order to recapitulate elimination of Brg1 deficient cells observed in $AhCreER^+$-$Brg^{fl/fl}$ epithelium, Brg1 loss was induced in $VillinCre^+Brg^{fl/fl}$ mice at low frequency by single intraperitoneal injection of 40 mg/kg tamoxifen. Small intestine samples were harvested 5 and 30 days PI. Immunohistochemical analysis of Brg1 expression at day 5 PI revealed mosaic loss of Brg1 with clusters of Brg1 deficient cells detected both in the crypts and villi of the small intestine of $VillinCre^+Brg^{fl/fl}$ mice (Figure 3.8). However, by day 30 PI the small intestinal epithelium of $VillinCre^+Brg^{fl/fl}$ mice was predominantly composed of Brg1 positive cells, once again indicating strong selective pressure against Brg1 deficient cells (Figure 3.8). The only cells retaining Brg1 deficient status at 30 days PI were Paneth cells, consistent with their low turnover rate (Figure 3.8, inset).
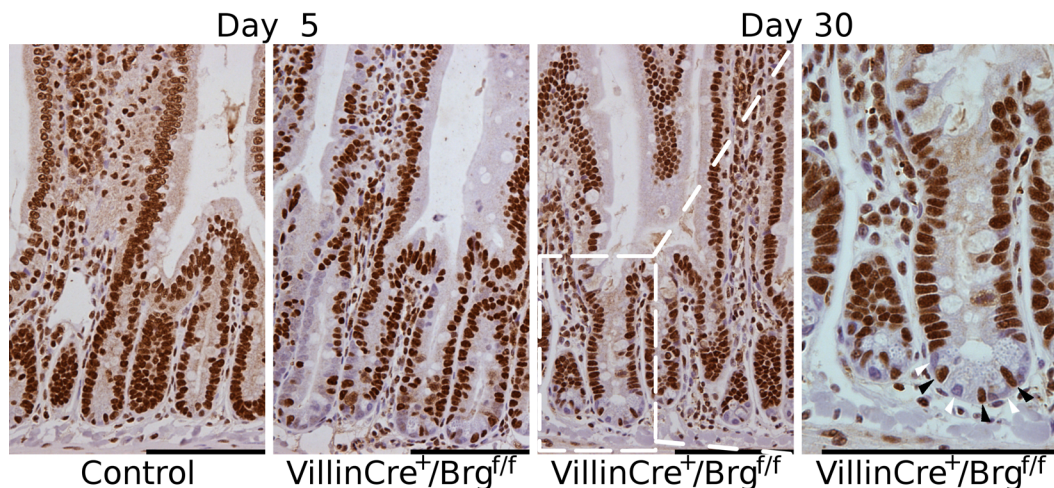
Figure 3.8: Low-dose induction of VillinCre recombinase drives partial loss of Brg1, which are subsequently repopulated with wild type cells $VillinCre^+Brg^{fl/fl}$ were induced with the low-dose protocol along with Cre^- controls and the small intestine samples were harvested at 5 and 30 days PI. Immunohistochemical analysis of Brg1 expression revealed a mosaic pattern of Brg1 loss in the small intestine of $VillinCre^+Brg^{fl/fl}$ mice at day 5 PI. Brg1 deficient cells, however, were largely eliminated from $VillinCre^+Brg^{fl/fl}$ small intestine at day 30 PI. The only Brg1 deficient cells present at day 30 PI were represented by the Paneth cells (inset, white arrowheads) intercalated between Brg1 positive CBC cells (inset, black arrowheads). No extensive clusters of Brg1 deficient cells were detected in the small intestine of control mice at any time point.

To indirectly confirm the selective pressure against Brg1 deficient cells I used the *LacZ* reporter allele to trace recombination events through the expression of β-galactosidase. Mice carrying *VillinCre*, *LacZ* and either two wild type or two targeted *Brg1* alleles were induced with a low-dose protocol and the small intestine was harvested 30 days after induction. Staining for β-galactosidase activity revealed a substantial number of LacZ positive crypt-villus units (approximately 65%) in animals bearing intact *Brg1* alleles, indicating that induction using the low-dose protocol was sufficient to cause recombination in a substantial proportion of the intestinal stem cells (Figure 3.9, middle panel). However, consistent with the apparent selection against Brg1 deficient cells, the number of

LacZ positive crypt-villus units was reduced in the intestine of $VillinCre^+LacZ^+Brg^{fl/fl}$ mice approximately five-fold compared to $VillinCre^+LacZ^+Brg^{+/+}$ intestines (Figure 3.9, right panel), suggesting that a large proportion of stem cells that had undergone deletion of Brg1 were subsequently eliminated and replaced with wild type counterparts. This observation implies incompatibility of Brg1 loss with long-term stem cell retention in the small intestinal epithelium.

VillinCre⁻ Control   VillinCre⁺/Brg⁺/⁺   VillinCre⁺/Brg^f/f
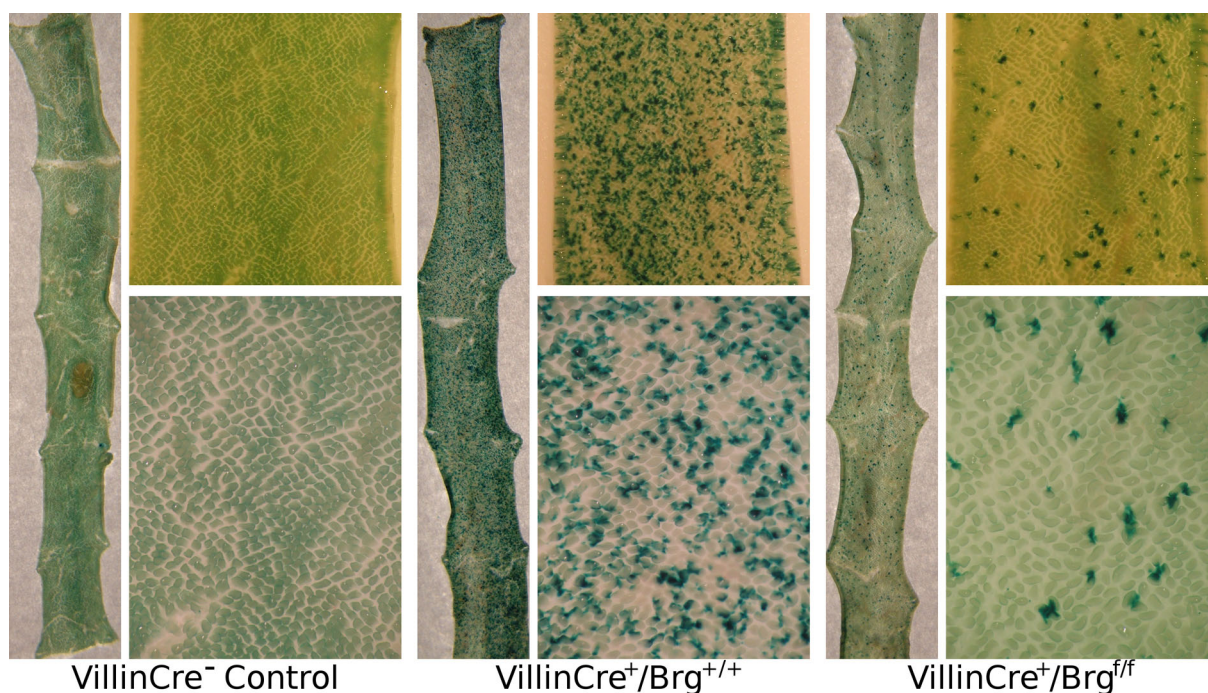
Figure 3.9: Brg1 deficient cells are repopulated with wild type cells in the small intestinal epithelium of $VillinCre^+Brg^{fl/fl}$ mice. The LacZ reporter was used to indirectly confirm elimination of Brg1 deficient cells from the small intestinal epithelium. $VillinCre^+LacZ^+Brg^{fl/fl}$ mice were induced with the low-dose protocol along with positive $VillinCre^+LacZ^+Brg^{+/+}$ and negative Cre^- controls. Mice were dissected at day 30 PI and LacZ expression was visualised in the whole mounted small intestine by staining with X-gal substrate. LacZ expression was observed in approximately 50% of crypt-villus structures in $VillinCre^+Brg^{+/+}$ intestine indicating effective recombination in the stem cell compartment. Positive crypts were largely lost in the small intestine of $VillinCre^+Brg^{fl/fl}$ mice indicating negative selection against retention of Brg1 deficient stem cells. No LacZ expression was observed in the small intestine of Cre^- control mice.

3.2.8   High-dose induction of VillinCre recombinase drives complete loss of Brg1

In order to dissect the mechanism behind elimination of Brg1 deficient cells and further investigate the immediate effects of Brg1 loss on small intestinal homeostasis, I attempted to drive complete loss of Brg1 in the intestinal epithelium. Cohorts of experimental $VillinCre^+Brg^{fl/fl}$ and control $VillinCre^-Brg^{fl/fl}$ animals were induced with 4 daily intraperitoneal injections of tamoxifen. Animals were sacrificed and small intestines harvested at 4 days PI. At the time of dissection, the intestinal morphology was indistinguishable between control and experimental animals. Immunohistochemical analysis of

Brg1 expression at 4 days PI revealed near complete loss of Brg1 in the epithelial compartment of the small intestine of $VillinCre^{+}Brg^{fl/fl}$ mice (Figure 3.10). Brg1 expression was however retained in the stromal compartment, consistent with the expression pattern of VillinCre recombinase (el Marjou *et al.*, 2004). Microscopic examination of H&E-stained sections of the small intestine revealed no difference in histological appearance between animals from control and experimental cohorts. Gross intestinal architecture appeared indistinguishable between the two cohorts (Figure 3.10).
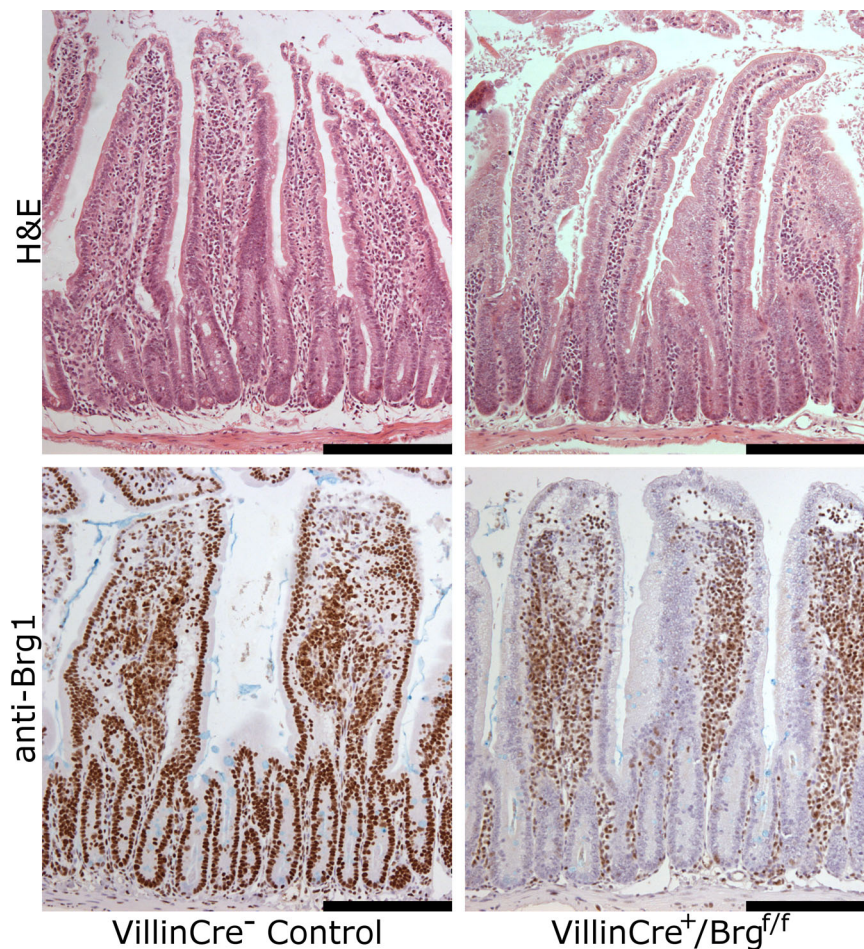
Figure 3.10: High-dose induction of VillinCre recombinase drives complete loss of Brg1. $VillinCre^{+}$-$Brg^{fl/fl}$ mice were induced with high-dose protocol along with Cre^{-} controls. Analysis of H&E stained small intestinal sections revealed no gross differences in epithelial morphology between Brg1 control and Brg1 deficient epithelium at day 4 PI (top panels). Immunohistochemical analysis of Brg1 expression revealed near complete loss of Brg1 expression in the small intestinal epithelium of $VillinCre^{+}Brg^{fl/fl}$ mice at day 4 PI (bottom panels). Scale bars represent 200 μm.

3.2.9   Brg1 loss has mild immediate effects on small intestinal homeostasis

Although Brg1 deficient epithelium did not display obvious morphological abnormalities, quantitative analysis of histological and functional parameters of the intestinal epithelium revealed a number of subtle differences between Brg1 deficient and control animals. The

results of quantitative analysis of histological parameters in control and $VillinCre^+$-$Brg^{fl/fl}$ animals are collated in Table 3.1.

Table 3.1: Quantitative analysis of the effects of Brg1 loss on the small intestinal histology

Parameter	Cohort	Mean	SD	p Value
Crypt Length (cells)	Control	27.48	1.86	0.570
	Brg1 KO	28.13	1.78	
Villus Length (cells)	Control	76.11	3.26	0.003
	Brg1 KO	67.31	3.82	
Apoptosis per half-crypt	Control	0.14	0.09	0.005
	Brg1 KO	0.41	0.14	
Caspase positive cells per half-crypt	Control	0.11	0.04	0.073
	Brg1 KO	0.29	0.16	
Mitosis per half-crypt	Control	0.25	0.05	0.054
	Brg1 KO	0.34	0.08	
Ki67 positive cells per half-crypt	Control	17.28	4.28	0.475
	Brg1 KO	15.29	2.98	
BrdU positive cells per half-crypt	Control	8.41	0.90	0.038
	Brg1 KO	9.77	0.61	

Small intestinal tissue samples from $VillinCreER^-$ (marked here as **Control**) and $VillinCreER^+Brg^{fl/fl}$ (marked here as **Brg1 KO**) mice were collected at day 4 PI. Histological parameters, such as crypt and villus length, apoptosis, proliferation and BrdU incorporation were quiantified and compared between the two cohorts.

Crypt and villus lengths were scored on H&E stained sections as the average number of cells ($\pm$ standard deviation) between the crypt base and the crypt-villus junction and between the crypt-villus junction and the tip of the villus respectively. Crypt size was found to be unaltered in control versus Brg1 deficient epithelium (27.48$\pm$1.86 and 27.13$\pm$1.78, p=0.57, n$\geq$5, Figure 3.11a). Conversely, quantification of the villus length detected a small decrease in the villus size of $VillinCre^+Brg^{fl/fl}$ mice (76.11$\pm$3.26 and 67.31$\pm$3.82, p=0.003, n$\geq$5, Figure 3.11b).

Apoptosis and mitosis levels were scored on H&E stained sections as the average number ($\pm$ standard deviation) of apoptotic bodies and mitotic figures per half-crypt respectively. Quantification of apoptotic bodies within the crypts revealed a statistically significant elevation of apoptosis levels in Brg1 deficient intestine (0.14$\pm$0.09 and 0.41$\pm$0.14, p=0.005, n$\geq$5, Figure 3.11c). This observation, however, was not confirmed by scoring of cleaved Caspase-3 positive cells as no significant difference was detected between the control and experimental animals (0.11$\pm$0.04 and 0.29$\pm$0.16, p=0.073, n=4, Figure 3.11c).

Scoring of mitotic figures revealed no difference in mitosis levels in control versus experimental animals (0.25$\pm$0.05 and 0.34$\pm$0.08, p=0.054, n$\geq$5, Figure 3.11e). In order to
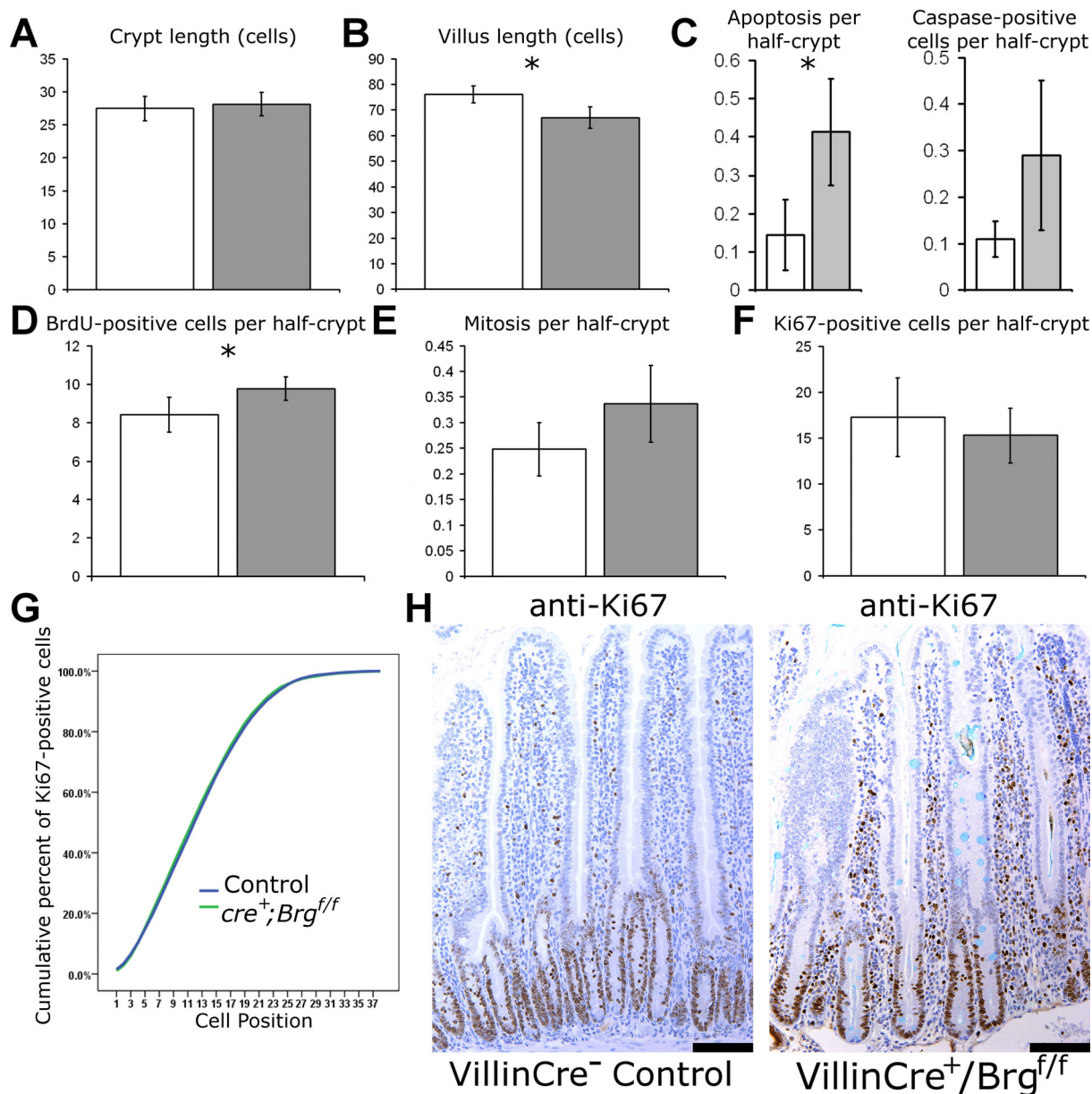
Figure 3.11: Histological analysis of the effects of short-term Brg1 deficiency in the small intestinal epithelium. Control Cre^- and experimental $VillinCre^+Brg^{fl/fl}$ mice were induced with the high-dose protocol and samples of the small intestinal epithelium were harvested at day 4 PI. **(a-f)** Histological parameters such as crypt length **(a)**, villus length **(b)**, apoptosis (**(c)**, left panel) and mitosis **(e)** were scored on H&E stained sections from control (white bars) and $VillinCre^+Brg^{fl/fl}$ (grey bars) small intestines. The average number of BrdU **(d)**, cleaved Caspase3 (**(c)**, right panel) and Ki67 **(f)** positive cells was scored on respective immunostained sections. Error bars represent standard deviation. Asterisks mark histological parameters, which displayed a statistically significant difference (p value <0.05) between the groups. Exact values, standard deviations, respective p values and number of animals analysed are provided in Table 3.1; **(g)** Cumulative frequency analysis revealed no difference in positional distribution of Ki67 positive cells between control and experimental animals (Kolmogorov-Smirnov Z test p=0.676, n=4); **(h)** Immunohistochemical analysis of Ki67 expression revealed no gross changes between proliferative compartments of control and $VillinCre^+Brg^{fl/fl}$ small intestines. Scale bars represent 100 μm.

validate mitosis levels obtained from quantification of mitotic figures, sections of the Brg1 deficient and control intestine were stained with the cell proliferation marker Ki67. Quantification of the cells stained positive for Ki67 detected no change in the average number of proliferating cells per half-crypt in control versus Brg1 deficient samples (17.28 ± 4.28 and 15.29 ± 2.98, p=0.475, n=4, Figure 3.11f). Additionally, distribution of the Ki67 positive cells was analysed in order to assess the shape of the proliferative compartment. Analysis of the cumulative frequency of Ki67 positive cells in the crypt showed no difference in distribution of proliferating cells (Kolmogorov-Smirnov Z test p=0.676, n=4, Figure 3.11g and h).

Finally, the number of cells in S-phase of the cell cycle was estimated using the DNA labelling agent BrdU. $VillinCre^+Brg^{fl/fl}$ and control mice were treated with BrdU reagent 2 hours prior to dissection. Small intestinal sections from treated mice were then stained with antibodies against BrdU. In contrast to proliferation levels derived from quantification of mitotic figures and Ki67 expression, analysis of BrdU incorporation 2 hours post labelling demonstrated a significant increase in the average number of BrdU positive cells per half-crypt in $VillinCre^+Brg^{fl/fl}$ mice (8.41 ± 0.9 and 9.77 ± 0.61, p=0.038, n≥4, Figure 3.11d).

Overall, quantitative analysis of the morphological and functional parameters of the small intestinal epithelium demonstrated that Brg1 loss had a mild effect on small intestinal homeostasis slightly decreasing villus length, apoptosis levels and cell entry into the S-phase of the cell cycle.

3.2.10   Brg1 loss impairs migration of the intestinal epithelium

In order to analyse the effects of Brg1 loss on epithelial cell migration a BrdU pulse-chase experiment was carried out. Cohorts of $VillinCre^+Brg^{fl/fl}$ and control animals (n≥3) were treated with BrdU reagent on day 4 PI. One group of mice from both cohorts was then dissected 2 hours after BrdU administration to assess the number of cells in S-phase. Another group of mice was left for 24 hours after BrdU administration and dissected at day 5 PI to assess cell migration. In order to quantify migratory ability of the epithelial cells in Brg1 deficient and control intestine, I scored positions of the BrdU-labelled cells and analysed their cumulative frequency, Positional quantification of BrdU positive cells 2 hours after labelling detected BrdU labelling to be mainly restricted to the crypt, consistent with the location of the proliferative compartment (median position 10.5 cells for experimental and control animals, Figure 3.12a).

Despite identical median position of BrdU positive cells, distributional analysis of BrdU-incorporation 2 hours post labelling revealed a significant difference in distribution of BrdU positive cells between control and experimental animals (Kolmogorov-Smirnov Z test p=0.005, n≥4, Figure 3.12a). The frequency of BrdU-labelled cells in Brg1 deficient epithelium was increased towards the top of the crypt (Figure 3.12a). On contrary, Brg1
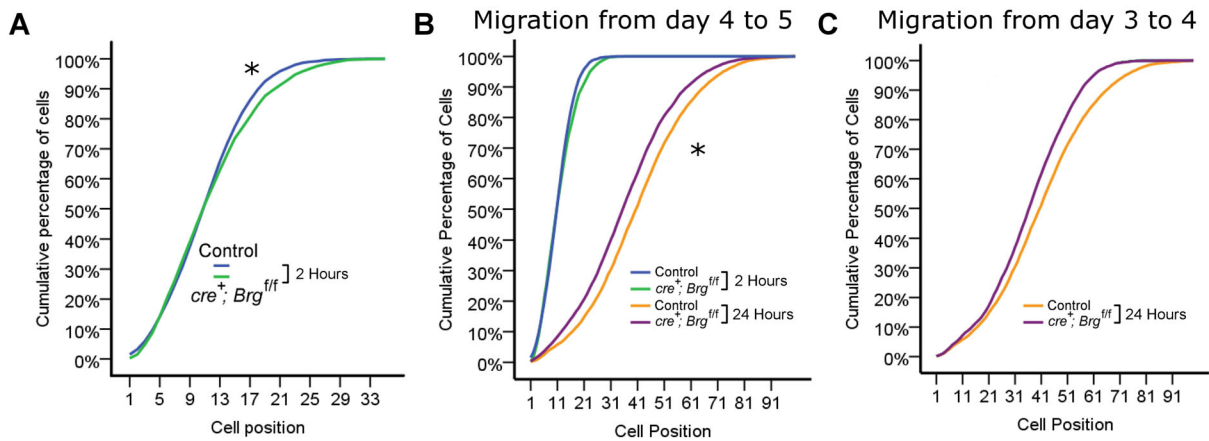
Figure 3.12: Short-term Brg1 deficiency expands the population of BrdU positive cells and impairs cell migration **(a)** Cumulative frequency analysis of BrdU immunostaining 2 hours post labelling revealed a significant difference in distribution of BrdU positive cells between $VillinCre^+Brg^{fl/fl}$ and control animals at day 4 PI (Kolmogorov-Smirnov Z test p=0.005, n≥4). While the median position of BrdU positive cells was unaffected, Brg1 deficient epithelium displayed an expansion of BrdU positive cells towards the top of the crypt. Although less pronounced, a lack of BrdU positive cells was also observed at the crypt base of $VillinCre^+Brg^{fl/fl}$ mice. **(b)** Cumulative frequency analysis of BrdU immunostaining 24 hours post labelling revealed a significantly impaired cell migration in the small intestinal epithelium of $VillinCre^+Brg^{fl/fl}$ (median migration distance 24.54 cells) compared to control mice (median migration distance 30.39 cells) over a 22 hours period between days 4 and 5 PI (Kolmogorov-Smirnov Z test p<0.001, n ≥3). **(c)** A similar pattern of impaired cell migration in the small intestine of $VillinCre^+Brg^{fl/fl}$ mice was observed when migration of BrdU positive cells was traced between days 3 and 4 PI.

deficient epithelium displayed a marked reduction in number of BrdU-labelled cells towards the crypt base, suggesting a decrease in proliferative activity in this region (Figure 3.12a).

Immunohistochemical analysis of BrdU incorporation 24 hours post labelling revealed the extent of migration of the BrdU-labelled cells in both control and experimental animals. Cumulative frequency analysis of BrdU-labelled cells 24 hours post labelling revealed a significantly impaired migratory ability of the Brg1 deficient epithelium (Figure 3.12b). Median migration distance of BrdU-labelled cells in Brg1 deficient epithelium was found to be 24.54 cells compared to 30.39 cells in control mice (Kolmogorov-Smirnov Z test p<0.001, n ≥3). Analysis of cell migration between day 3 and 4 PI revealed a similar pattern of impaired cell migration in the small intestinal epithelium of $VillinCre^+Brg^{fl/fl}$ mice (Figure 3.12c).

3.2.11   Brg1 loss affects differentiation of the certain cell types

The signalling networks that control intestinal homeostasis tightly regulate both, cell proliferation and differentiation. Therefore, to further characterise the effects of Brg1 loss on small intestinal homeostasis I carried out quantitative analysis of the major differentiated cell types present in the small intestinal epithelium in Brg1 deficient and control mice at day 4 PI (Figures 3.13 and 3.14. The results of quantitative analysis of differentiated cells in control and $VillinCre^+Brg^{fl/fl}$ animals are collated in Table 3.2.

Table 3.2: Quantitative analysis of Brg1 deficiency effects on cell differentiation in the small intestinal epithelium

Parameter	Cohort	Mean	SD	p Value
Goblet cells per half-crypt	Control	4.85	0.85	0.212
	Brg1 KO	3.74	1.34	
Enteroendocrine cells per half-crypt	Control	0.76	0.09	0.005
	Brg1 KO	0.49	0.09	
Paneth cells per half-crypt	Control	1.13	0.31	0.416
	Brg1 KO	1.37	0.47	

Small intestinal tissue samples from $VillinCreER^-$ (marked here as **Control**), and $VillinCreER^+$-$Brg^{+/+}$ (marked here as **Brg1 KO**) mice were collected at day 4 PI. Cell type-specific stains were used to detect major cell types of the small intestinal epithelium. Frequency of Goblet, Enteroendoctine and Paneth cells was quantified and compared between the two cohorts.

The majority of the cells in the villus are represented by the only member of the absorptive lineage - enterocytes. In order to investigate the state of the enterocytes in the Brg1 deficient epithelium I carried out specific staining for alkaline phosphatase, which marks the brush border of the enterocytes. A consistent decrease in staining was observed among Brg1 deficient mice compared to the intestines of control mice (Figure 3.13a).

The second most abundant cell type in the small intestinal epithelium are Goblet cells. To assess changes in Goblet cell differentiation upon Brg1 loss, Alcian blue staining was carried out on small intestinal sections from experimental and control animals (Figure 3.13b). Scoring of the cells stained with Alcian blue showed no difference between control and experimental animals (4.85±0.85 and 3.74±1.34 Goblet cells per half-crypt respectively, p=0.212, n=4, Figure 3.14b).

Enteroendocrine cells represent another secretory cell lineage of the small intestinal epithelium. Grimelius staining was carried out to assess the frequency of enteroendocrine cells in the Brg1 deficient epithelium (Figure 3.13d). Quantification of the positively stained cells revealed significantly reduced number of enteroendocrine cells per half-crypt in Brg1 deficient intestine compared to control animals (0.76±0.09 and 0.49±0.09 in control and Brg1 deficient intestine respectively, p=0.005, n=4, Figure 3.14b).

The last member of the secretory cell lineage is represented by Paneth cells. Lysozyme expression was used as a marker to measure the frequency of this cell type (Figure 3.13c). Scoring of lysozyme positive cells showed no difference in the Paneth cell numbers between control and experimental animals (1.13±0.31 and 1.37±0.47, p=0.416, n=4, Figure 3.14c). Since localisation of the Paneth cells within the crypt is tightly regulated by the Eph/Ephrin system, it serves as a sensitive indicator of the Wnt pathway deregulation. I therefore analysed the position of the lysozyme positive cells. The analysis of cumulative frequency of the Paneth cells revealed no difference between the Brg1 deficient and control intestine (Figure 3.14d, Kolmogorov-Smirnov Z test p=0.7, n=4).
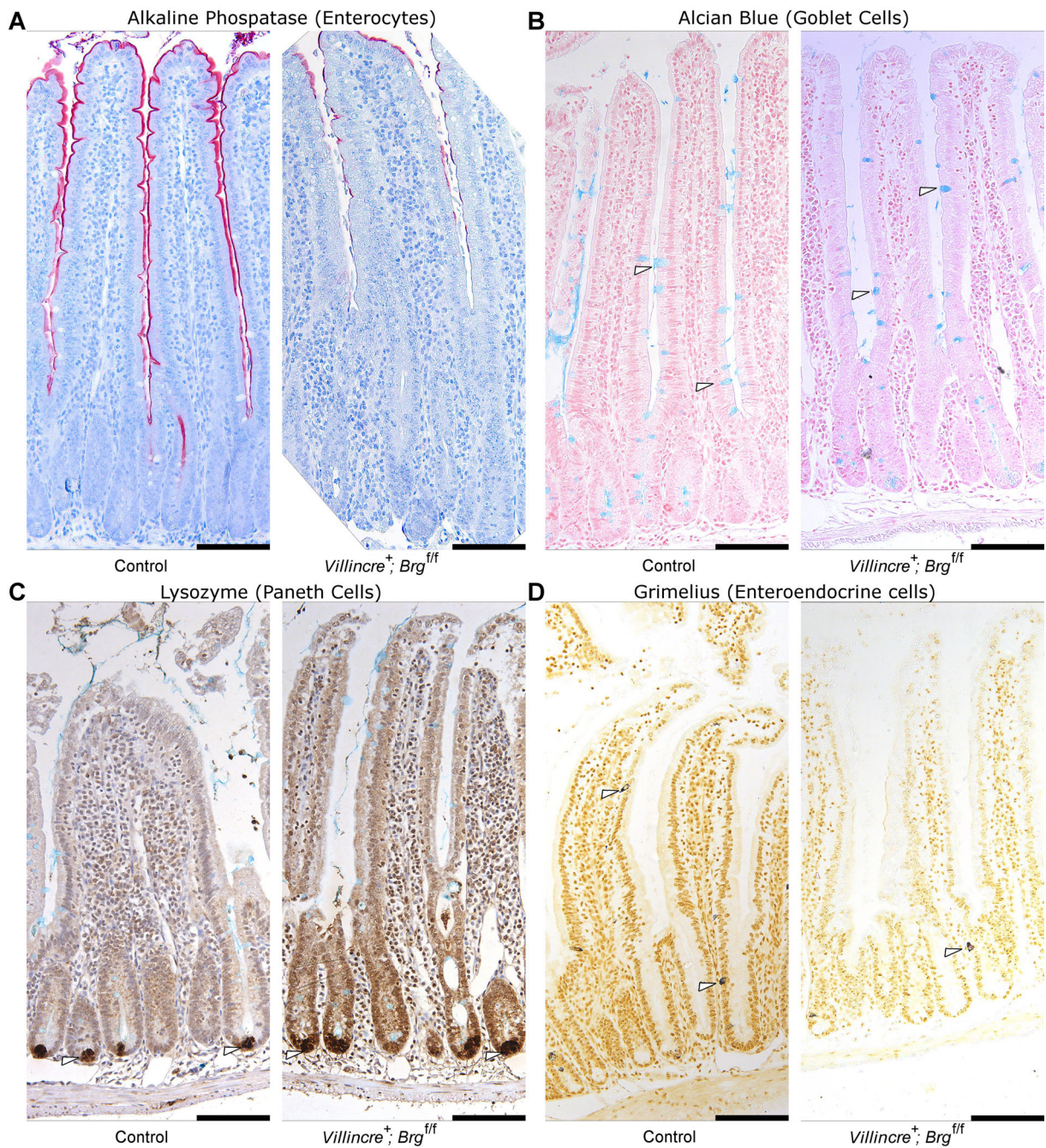
Figure 3.13: Qualitative analysis of cell differentiation upon loss of Brg1 within the small intestine. Small intestinal sections of $VillinCre^+Brg^{fl/fl}$ and Cre^- control animals at day 4 PI were subjected to cell type-specific stains to visualise Enterocytes **(a)**, Goblet cells **(b)**, Paneth cells **(c)** and Enteroendocrine cells **(d)**. Alkaline phosphatase staining revealed a substantially diminished brush border in the small intestine of $VillinCre^+Brg^{fl/fl}$ mice **(a)**. No gross changes were observed in differentiation of secretory cell lineages upon Brg1 loss (b-d). Lysozyme staining revealed normal localisation of the Paneth cells at the crypt base **(c)**. Arrows mark positive cells for each staining method. Scale bars represent 100 μm.
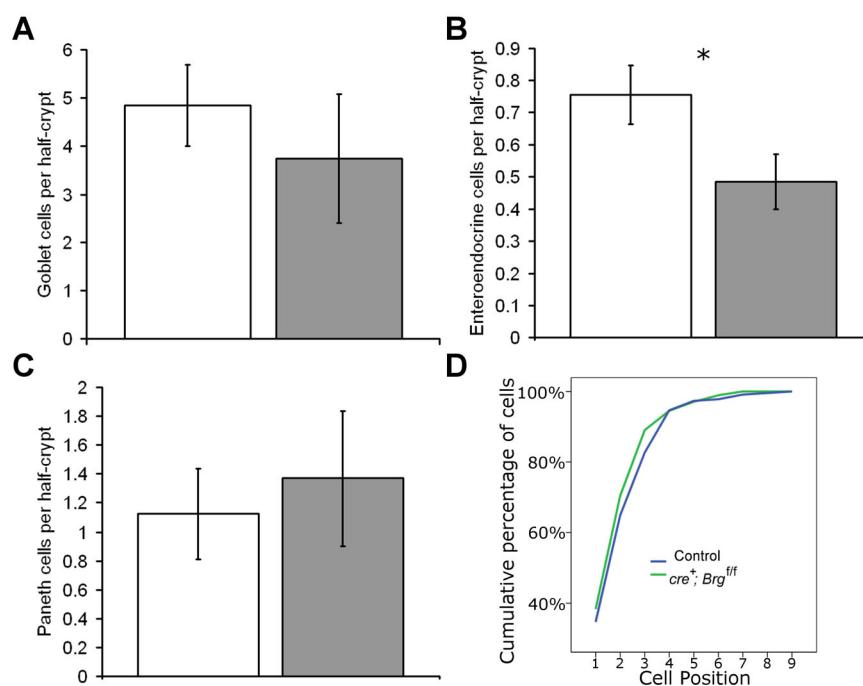
Figure 3.14: Quantitative analysis of cell differentiation upon loss of Brg1 within the small intestine.
(a-c) The average number of Goblet **(a)**, Enteroendocrine **(b)** and Paneth **(c)**, cells per half-crypt and
associated villus was scored in the small intestine of control (white bars) and $VillinCre^+Brg^{fl/fl}$ (grey
bars) animals at day 4 PI. No significant difference was observed in the numbers of Goblet **(a)** and Paneth
(c) cells between control and experimental mice. Quantification of cells stained positive with Grimelius
staining revealed a significant decrease in the number of Enteroendocrine cells in $VillinCre^+Brg^{fl/fl}$
small intestine **(b)**; **(d)** Cumulative frequency analysis of Paneth cell distribution revealed no significant
difference between control and $VillinCre^+Brg^{fl/fl}$ mice. Error bars represent standard deviation. Exact
values, standard deviations, respective p values and number of animals analysed are provided in Table
3.2.

3.2.12   Brg1 loss leads to rapid disruption of intestinal architecture

In order to investigate the long-term effects of complete Brg1 loss in the small intestine I attempted to age a cohort of $VillinCre^+Brg^{fl/fl}$ mice induced with the high dose protocol. Surprisingly, considering the relatively mild effects of Brg1 loss at day 4 PI, $VillinCre^+Brg^{fl/fl}$ mice displayed severe symptoms of ill health by day 8 PI and had to be sacrificed. Histological analysis of the H&E stained sections of the small intestine revealed a slightly perturbed crypt-villus architecture as early as day 5 PI (Figure 3.15a). These mild alterations to epithelial architecture progressed to severe crypt loss and complete abrogation of the normal intestinal morphology by day 8 PI (Figure 3.15a). Notably, occasional crypts retaining Brg1 expression were present in the disrupted epithelium at day 8 after induction. These crypts were commonly seen to undergo crypt fission, a process characteristic of regenerating intestinal epithelium after exposure to ionising radiation (Figure 3.15b).
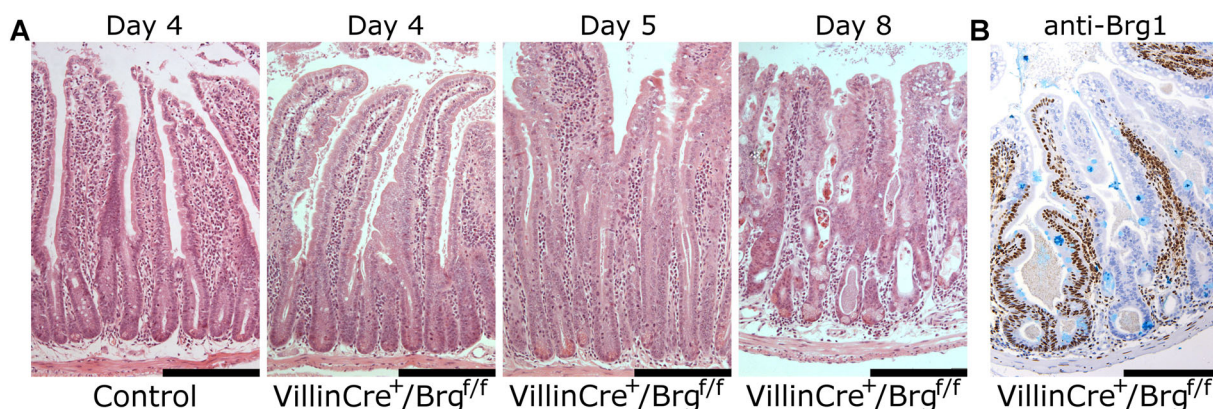
Figure 3.15: Long-term Brg1 loss in the small intestinal epithelium results in crypt ablation. $VillinCre^+Brg^{fl/fl}$ and control Cre^- mice were induced with the high-dose protocol and small intestinal samples were collected at various time points. **(a)** Histological analysis of H&E-stained sections of the small intestine of $VillinCre^+Brg^{fl/fl}$ mice at day 5 PI detected a partial loss of crypt-villus differentiation. This was followed by severe crypt loss by day 8 PI; **(b)** Immunohistochemical analysis of Brg1 expression in the small intestinal epithelium detected rare Brg1 positive crypts in predominantly Brg1 deficient deteriorating epithelium. Brg1 positive crypts had an enlarged appearance and were often found to be undergoing crypt fission. Scale bars represent 200 μm.

3.2.13   Brg1 loss depletes the proliferative compartment

The intestinal epithelium of $VillinCre^+Brg^{fl/fl}$ mice at day 5 PI was characterised by distinctly shortened villi and disappearance of clear crypt-villus junctions (Figure 3.15a). These effects are likely to be caused by impaired proliferation in the crypt. To examine this possibility I analysed the quantity and position of proliferating cells as assessed by expression of Ki67 marker Figure 3.16a. Scoring of Ki67 positive cells at day 5 PI revealed significantly reduced numbers of proliferating cells in Brg1 deficient epithelium compared to control animals. The average number ($\pm$ standard deviation) of Ki67 positive cells

per half-crypt in control versus Brg1 deficient epithelium was 8.84±1.61 and 15.23±1.48 respectively (p=0.03, n≥3, Figure 3.16b). Cumulative frequency analysis of Ki67 positive cell distribution revealed a significant contraction of the proliferative region in Brg1 deficient intestine (Figure 3.16c, Kolmogorov-Smirnov Z test p<0.001, n≥3).
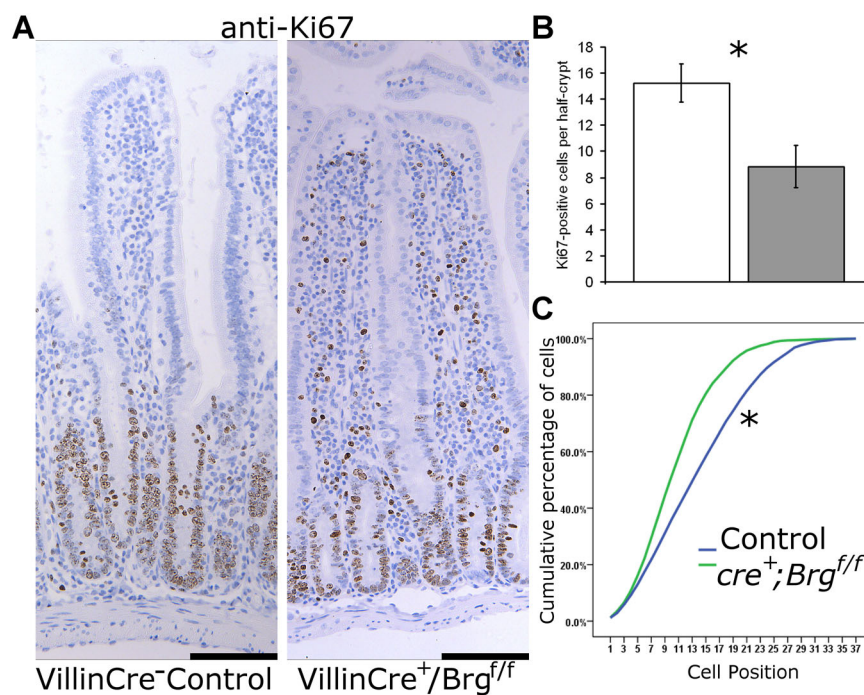
Figure 3.16: Long-term Brg1 loss results in reduction of proliferative compartment. $VillinCre^{+}$-$Brg^{fl/fl}$ and control Cre^{-} mice were induced with the high-dose protocol and small intestinal samples were collected at day 5 PI. (a) Immunohistochemical analysis of Ki67 expression revealed a loss of Ki67 expressing cells in the small intestinal epithelium of $VillinCre^{+}Brg^{fl/fl}$ mice. Scale bars represent 100 μm. (b) Quantification of Ki67 stained sections revealed a significantly reduced number of Ki67 positive cells in the small intestinal epithelium of $VillinCre^{+}Brg^{fl/fl}$ mice (grey bar) compared to control (white bar) animals (p=0.03, n≥3). (c) Cumulative frequency analysis of Ki67 positive cells revealed a significantly contracted proliferative compartment in the small intestinal epithelium of $VillinCre^{+}$-$Brg^{fl/fl}$ mice (Kolmogorov-Smirnov Z test p<0.001, n≥3).

3.2.14 Crypt ablation in Brg1 deficient epithelium is not caused by failure of the cell-adhesion machinery

Loss of the proteins involved in the formation of cell-to-cell adhesions has been shown to disrupt epithelial architecture of the small intestine (Schneider *et al.*, 2010). I therefore assessed whether Brg1 loss affected the expression levels of proteins involved in cell-to-cell adhesion, such as β-catenin and E-cadherin. mRNA was extracted from small intestine epithelial samples of $VillinCre^{+}Brg^{fl/fl}$ and control mice at day 4 PI. qRT-PCR analysis of mRNA levels of *β-catenin* and *E-cadherin* did not reveal significant changes in their expression between experimental and control animals (Figure 3.17a, p>0.05, n≥3). Immunohistochemical analysis of E-cadherin expression at day 4 PI revealed no consistent difference between wild type and Brg1 deficient epithelium (Figure 3.17b). Notably, immunostaining for E-cadherin at day 8 PI demonstrated that even in heavily disrupted

epithelium, E-cadherin was expressed at substantial levels and remained confined to the cellular membrane (Figure 3.17b). Together, these observations indicated that loss of the epithelial architecture in Brg1 deficient intestine was unlikely to be attributed to cell-to-cell adhesion failure.
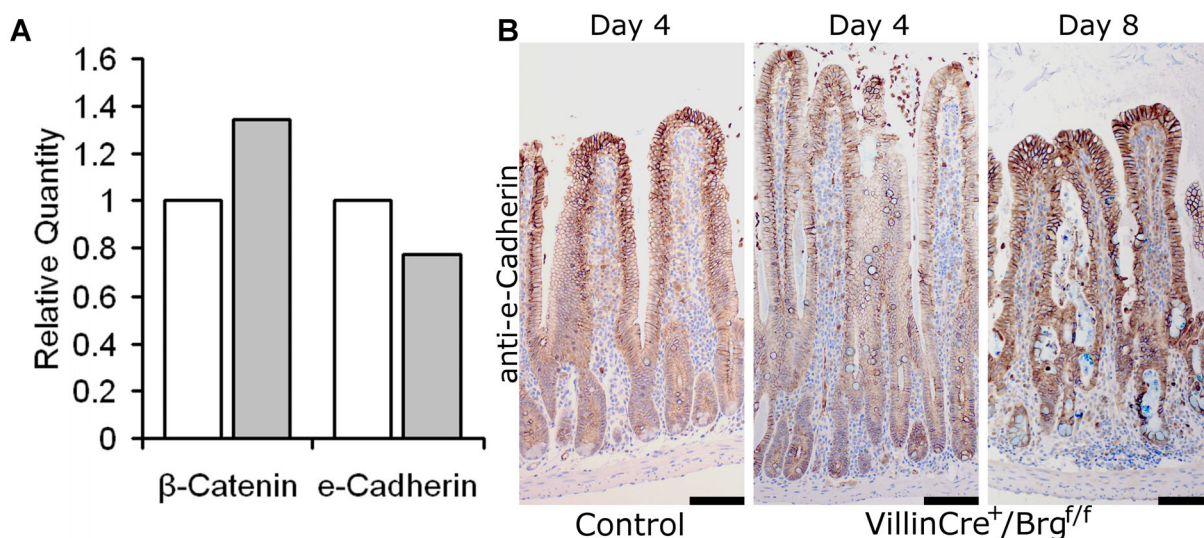
Figure 3.17: Brg1 loss in the small intestinal epithelium does not impair cell-to-cell adhesion machinery. **(a)** Quantitative RT-PCR expression analysis of cell-to-cell adhesion genes β-catenin and E-cadherin revealed no significant difference between the small intestinal epithelium of $VillinCre^+Brg^{fl/fl}$ (grey bars) and control (white bars) mice at day 4 after high-dose induction (p>0.05, n$\geq$3). **(b)** Immunohistochemical analysis of E-cadherin expression in the small intestinal epithelium revealed no difference between $VillinCre^+Brg^{fl/fl}$ and control mice at day 4 PI. Analysis of E-cadherin expression in the small intestine of $VillinCre^+Brg^{fl/fl}$ mice at day 8 PI showed strong membrane-specific staining, despite severely disrupted intestinal architecture. Scale bars represent 100 μm.

3.2.15   Brg1 loss compromises intestinal stem cell function

Delayed depletion of the proliferative compartment leading to severely perturbed epithelial architecture implied that Brg1 could act as a regulator of intestinal stem cell maintenance. In order to explore this hypothesis a series of experiments was conducted to test whether Brg1 loss resulted in depletion of the stem cell population.

To assess the effects of Brg1 loss on the small intestinal stem cell population, I examined the expression levels of the intestinal stem cell markers Ascl2 and Lgr5. Total mRNA was extracted from the intestinal epithelium of $VillinCre^+Brg^{fl/fl}$ and control mice at day 4 PI and used for qRT-PCR. Expression analysis of *Ascl2* and *Lgr5* revealed significantly reduced expression levels of these genes in Brg1 deficient epithelium (7.31- and 4.77-fold downregulation for Ascl and Lgr5 respectuvely, p=0.015, n=4, Figure 3.18a). Since Lgr5 and Ascl2 have been found to be Wnt target genes (Barker *et al.*, 2007; Jubb *et al.*, 2006), it may be argued that their reduced expression levels upon Brg1 loss are merely a result of attenuated Wnt signalling rather than an indicator of the stem cell depletion. In order to overcome this disadvantage of using Lgr5 and Ascl2 as stem cell markers, expression levels of *Olfm4*, a Wnt-independent stem cell marker (van der Flier *et*

al., 2009), were analysed. *In situ* hybridisation using an anti-*Olfm4* probe revealed strong staining around the crypt base of the control epithelium (Figure 3.18b)[1]. Conversely, intestinal epithelium from $VillinCre^+Brg^{fl/fl}$ mice harvested at day 4 PI displayed nearly complete loss of *Olfm4* expression (Figure 3.18b).
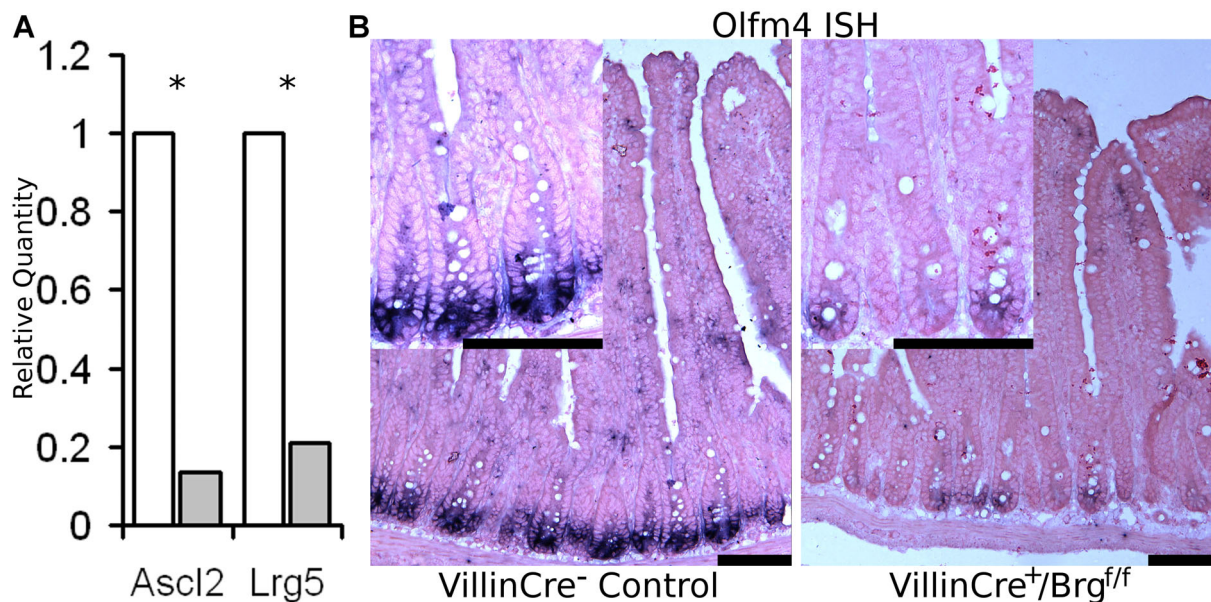
Figure 3.18: Brg1 loss in the small intestinal epithelium depletes the stem cell population. **(a)** Quantitative RT-PCR analysis of the small intestinal epithelium 4 days after high-dose induction revealed significantly reduced expression levels of the intestinal stem cell markers *Ascl2* and *Lgr5* in the small intestinal epithelium of $VillinCre^+Brg^{fl/fl}$ mice (grey bar) compared to control (white bar) animals (for both genes p=0.015, n=4). **(b)** *In situ* hybridisation analysis of the stem cell marker *Olfm4* in the small intestine of $VillinCre^+Brg^{fl/fl}$ and control mice at day 4 PI revealed a severely depleted *Olfm4* expression in Brg1 deficient intestinal epithelium. Scale bars represent 100 μm.

In order to obtain a more direct measure of stem cell depletion in response to Brg1 loss, a Cre recombinase expressed under the control of the *Lgr5* promoter was used to drive recombination of the floxed *Brg1* alleles. Notably, the *Lgr5-EGFP-IRES-creERT2* knock-in allele (further abbreviated as Lgr5CreER) provided extra functionality by driving enhanced green fluorescent protein (EGFP, further referred to as GFP) expression under the *Lgr5* locus control, thus permitting visualisation of the Lgr5 expressing stem cell compartment (Barker *et al.*, 2007). A cohort of $Lgr5CreER^+Brg^{fl/fl}$ mice was induced along with $Lgr5CreER^+Brg^{+/+}$ controls by four daily intraperitoneal tamoxifen injections. Animals were dissected at day 4 PI and small intestine tissue samples were collected. Immunohistochemical analysis of GFP expression revealed positively stained CBC cells at the crypt base of control and experimental animals (Figure 3.19a), consistent with the Lgr5 expression pattern (Barker *et al.*, 2007). Quantitative analysis of the frequency of GFP expressing crypts revealed significantly reduced numbers of GFP positive crypts in the intestinal epithelium of $Lgr5CreER^+Brg^{fl/fl}$ compared to control animals (0.16±0.05 and 0.42±0.09 respectively, p=0.001, n=4, Figure 3.19b). It should be noted,

---

[1]*In situ* hybridisation with anti-*Olfm4* probe was carried out by Maddy Young on intestinal sections provided by me.

however, that both experimental and control animals expressed the transgene at very low frequency. In order to take into account possible fluctuations in the transgene expression frequency, an average number of GFP positive cells per GFP expressing crypt was calculated. In line with the score obtained for the frequency of GFP expressing crypts, the intestinal epithelium of $Lgr5CreER^+Brg^{fl/fl}$ mice displayed significantly reduced number of GFP positive cells per crypt compared to control mice (2.03±0.13 and 2.68±0.27 respectively, p=0.003, n=4, Figure 3.19c).
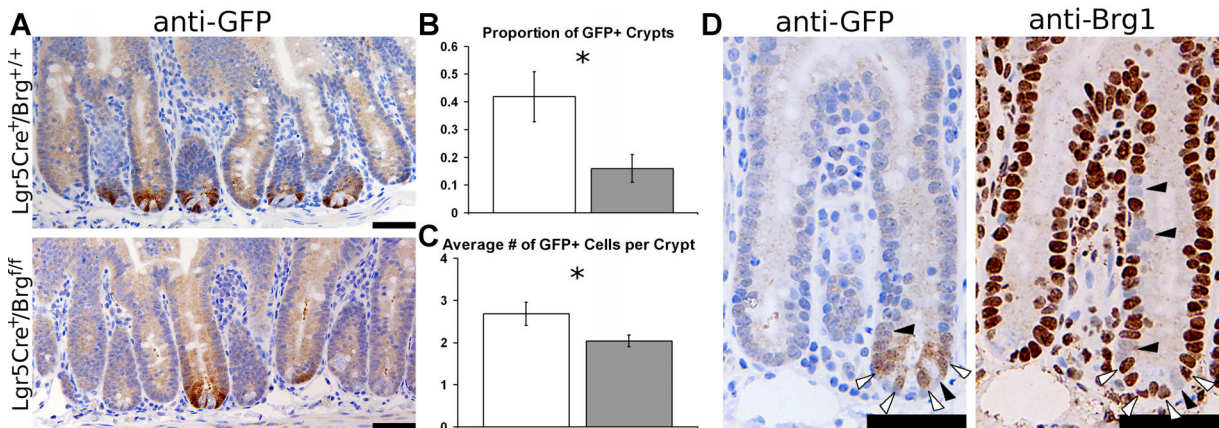
Figure 3.19: Stem cell-specific Brg1 loss abrogates Lgr5 expression and induces terminal differentiation. **(a)** Immunohistochemical analysis of GFP expression in the small intestinal epithelium of $Lgr5CreER^+$-$Brg^{fl/fl}$ mice and $Lgr5CreER^+Brg^{+/+}$ controls revealed positive staining of CBC cells at the crypt base. The frequency of staining was highly variable across the section in both cohorts. **(b)** Quantitative analysis of the number of GFP positive crypts per total number of crypts revealed a significant decrease in the number of GFP positive crypts in $Lgr5CreER^+Brg^{fl/fl}$ (grey bar) small intestine compared to control animals (white bar, p=0.001, n=4). **(c)** Quantitative analysis of the number of GFP positive cells per crypt revealed a significantly reduced number of GFP positive cells in $Lgr5CreER^+Brg^{fl/fl}$ mice compared to control animals (p=0.003, n=4). **(d)** Immunostaining of serial sections with the antibodies against GFP and Brg1 revealed a non-overlapping pattern of Brg1 loss (black arrowheads) and GFP expression (white arrowheads) at the crypt base. Additionally, clusters of Brg1 deficient cells were observed mid-crypt (black arrowheads). Scale bars represent 50 μm.

This observation confirmed that Brg1 loss resulted in depletion of the intestinal stem cell population. In order to assess Brg1 status of the GFP expressing cells that remained present upon induction of Brg1 loss, serial sections of the small intestine were stained with Brg1 and GFP antibodies (Figure 3.19d). Immunohistochemical analysis of Brg1 and GFP expression demonstrated that the remaining GFP positive cells retained Brg1 expression (Figure 3.19d, white arrowheads), indicating that functional Brg1 was essential for expression of the small intestinal stem cell marker Lgr5. Notably, immunohistochemical analysis of Brg1 expression detected clusters of Brg1 deficient cells in GFP expressing crypts (Figure 3.19d , black arrowheads). However, careful examination of such crypts failed to detect Brg1 deficient cells that retained GFP expression (Figure 3.19d).

These observations, along with the severe phenotype caused by extensive Brg1 loss and gradual elimination of Brg1 deficient cells upon partial Brg1 deletion, strongly support an *in vivo* role for Brg1 in maintaining the intestinal stem cell population.

3.2.16   Brg1 haploinsufficiency impairs clonogenic repopulation of the small intestine

High radiosensitivity of the intestinal stem cells results in stem cell ablation upon exposure to ionising radiation. Subsequent regeneration of the intestinal epithelium from post-irradiation damage is driven by surviving clonogenic stem cells and can serve as a readout of intestinal stem cell function (Potten, 1998). The number of surviving clonogens that drive regeneration reflects the number of clonogenic cells in the whole of the intestinal epithelium and therefore can act as a quantitative measure of the stem cell population size. I therefore aimed to assess the effects of Brg1 loss on the regenerative capacity of the intestinal stem cell population. Rapid crypt ablation in response to homozygous loss of Brg1 made it unfeasible to conduct the clonogenic survival assay in $VillinCre^+$-$Brg^{fl/fl}$ mice. It has been reported that heterozygous loss of Brg1 impairs the self-renewal capacity of the embryonic stem cells (Ho *et al.*, 2009). It is therefore possible that Brg1 haploinsufficiency may result in a suboptimal regenerative capacity of the intestinal stem cell population under the stress conditions of DNA damage.
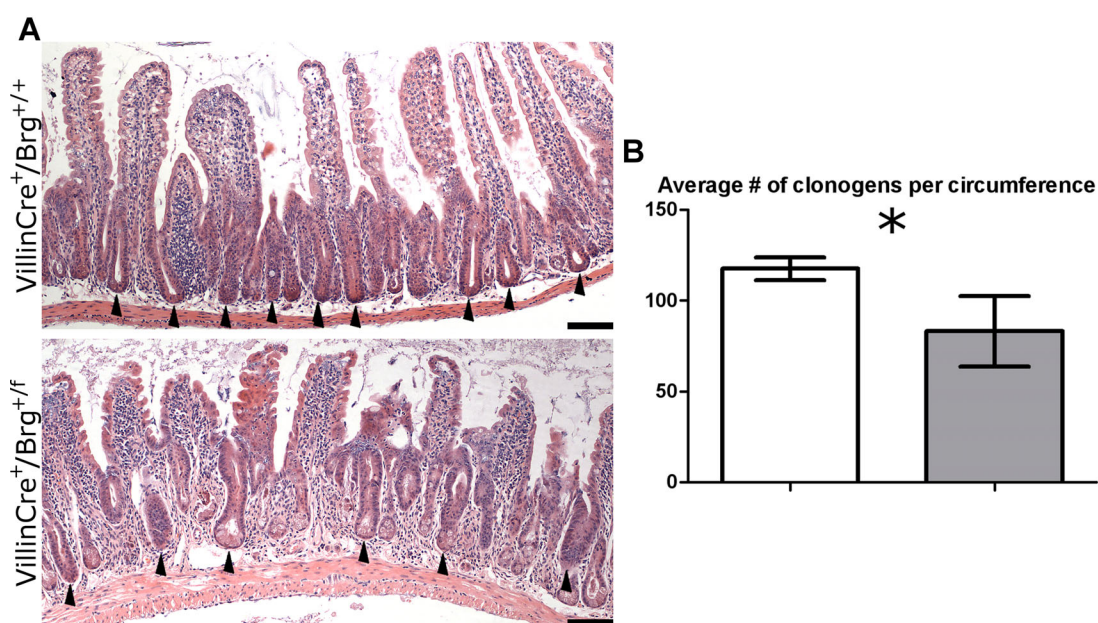
Figure 3.20:   Brg1 haploinsufficiency impairs clonogenic repopulation of the small intestine. $VillinCre^+Brg^{+/fl}$ mice and $VillinCre^-Brg^{+/fl}$ controls induced with high-dose protocol were exposed to gamma irradiation at day 4 PI. Mice were allowed to recover for 72 hours, at which point small intestinal samples were collected. Histological analysis of H&E stained small intestinal sections from $VillinCre^+Brg^{+/fl}$ and control mice displayed numerous clonogens driving epithelial regeneration ((**a**), black arrowheads). Scale bars represent 100 μm. **(b)** Quantitative analysis of epithelial clonogenic capacity revealed significantly reduced number of clonogens per circumference in $VillinCre^+Brg^{+/fl}$ mice (grey bar) compared to control (white bar) animals (p=0.03, n$\geq$3). Error bars represent standard deviation.

In order to investigate this possibility, $VillinCre^+Brg^{+/fl}$ mice along with $VillinCre^-$-$Brg^{+/fl}$ controls were induced with four daily injections of 80 mg/kg tamoxifen. At day 4 PI all mice were subjected to a single dose of 15 Gy of gamma irradiation from a cae-

sium source. Irradiated mice were left for 72 hours for intestinal regeneration to take place. Mice were then sacrificed and small intestinal tissue was harvested. The number of surviving clonogens was scored as the average number of regenerating crypts per radial circumference of the intestine on H&E stained sections (Figure 3.20a, black arrowheads). The average number of surviving clonogens (± standard deviation) in control versus $VillinCre^+Brg^{+/fl}$ mice was found to be 118±6.25 and 83.2±19.3 respectively (p=0.03, n≥3, Figure 3.20b). The reduced number of clonogens in the mice with heterozygous loss of Brg1 shows that Brg1 haploinsufficiency reduces the number of viable clonogens under stress conditions.

3.3   Discussion

Brg1 loss has been extensively reported in cancer cell lines and primary tumours (Becker *et al.*, 2009; Reisman *et al.*, 2003; Wong *et al.*, 2000). Re-expression of Brg1 in Brg1 deficient cancer cell lines has also been reported to induce cell cycle arrest (Hendricks *et al.*, 2004, Wong *et al.*, 2000). It appears, therefore, that Brg1 acts as a tumour suppressor in a range of cancers. However, since these observations were made in late stage cancers, they can not conclusively demonstrate whether Brg1 loss *per se* has an initiating oncogenic effect. Interestingly, insights from the transgenic animal models have suggested that Brg1 haploinsufficiency confers susceptibility to neoplasia at least in mammary and lung epithelial tissues (Bultman *et al.*, 2007, Glaros *et al.*, 2008). At the same time, complete Brg1 loss in lung epithelium was able to facilitate development of existing tumours, but not *de novo* tumourigenesis (Glaros *et al.*, 2008). These observations therefore suggest that, while Brg1 haploinsufficiency may facilitate tumourigenesis in certain tissues, biallelic Brg1 loss seen in human cancers is likely to be acquired at later stages of tumour progression. However, the role of Brg1 in the small intestinal epithelium has not yet been explored. Although not reported to be directly involved in intestinal homeostasis, Brg1 has been implicated as an important factor for the trans-activation of Wnt target genes (Barker *et al.*, 2001). Another indirect link connecting Brg1 to intestinal homeostasis is the tumour suppressor LKB1. LKB1 has been shown to interact with BRG1 and mediate BRG1 induced cell cycle arrest (Marignani *et al.*, 2001). Notably, Lkb1 loss in murine small intestinal epithelium has been found to alter differentiation of Goblet and Paneth cells via increased expression of the Notch pathway target gene *Hes5* as well as suppression of Delta ligand Dll1 in these cell types. Altered Notch signalling upon loss of Lkb1 has been found to result in increased size and perturbed morphology of mucin-secreting cells (Shorning *et al.*, 2009). Given the observed interaction between Brg1 and Lkb1, one could speculate that Brg1 deficiency might recapitulate the small intestinal manifestations of Lkb1 loss.

Bearing in mind the pivotal role of the Wnt and Notch pathways in intestinal homeostasis and intestinal stem cell maintenance, as well as the proposed tumour suppressor

role of Brg1 in other tissues, I aimed to investigate the effects of Brg1 loss and haploinsufficiency in the normal small intestinal epithelium.

In order to dissect the role of Brg1 in normal intestinal homeostasis I attempted to achieve the complete loss of Brg1 in the small intestinal epithelium. I first employed AhCre recombinase (Ireland *et al.*, 2004) to specifically inactivate Brg1 in the stem and progenitor cell compartments of the crypt. Unfortunately, off-target expression of the AhCre recombinase resulted in embryonic lethality of the animals bearing floxed Brg1 alleles and therefore prevented any further exploitation of this model for analysis of Brg1 deficiency. Instead, it was used to analyse consequences of Brg1 haploinsufficiency.

I then employed the AhCreER recombinase transgene (Kemp *et al.*, 2004) to exert a higher degree of control over the recombinase expression and overcome the embryonic lethality. Although the use of AhCreER recombinase proved successful in this aspect, induction of Brg1 deletion occurred at a frequency deemed too low to readily observe any subtle effects or permit the use of whole tissue approaches, such as qRT-PCR or Western blotting.

Finally, I employed the VillinCre recombinase transgene (el Marjou *et al.*, 2004), which is ubiquitously expressed in the small and large intestinal epithelium. High-dose induction of VillinCre recombinase resulted in complete loss of Brg1 in the epithelial compartment of the small intestinal epithelium at 4 days PI, which was confirmed by immunohistochemical staining with anti-Brg1 antibody. Low-dose induction of VillinCre recombinase resulted in mosaic loss of Brg1 in a pattern comparable to that driven by activation of the AhCreER recombinase.

3.3.1 Partial Brg1 loss results in gradual repopulation with wild type cells

Although the frequency of Brg1 inactivation driven by AhCreER recombinase was deemed too low for quantitative characterisation, I aimed to investigate the long-term fate of Brg1 deficient cells. Multiple time point analysis of the frequency of crypts containing Brg1 deficient cells revealed their gradual decline and near complete elimination within 15 days PI. Even though no quantitative analysis of apoptosis levels in Brg1 deficient crypts was performed, no gross signs of increased cell death were apparent. Instead, Brg1 deficient cells were observed to migrate onto the villus and eventually shed into the lumen, while the crypts were repopulated with wild type cells. The small intestinal epithelium of $VillinCre^+Brg^{fl/fl}$ mice induced with a low-dose protocol displayed a similar pattern. Mosaic loss of Brg1 was detected in cells across the crypt-villus axis at 5 days PI. However, 30 days later the intestinal epithelium was found to be fully repopulated with wild type cells. The slightly higher recombination frequency observed in low-dose induced $VillinCre^+Brg^{fl/fl}$ mice allowed me to indirectly confirm elimination of Brg1 deficient cells. Cre recombinase-mediated induction of the *LacZ* reporter gene in control and Brg1

deficient epithelium demonstrated substantially reduced retention rate of LacZ expressing crypts in the latter. Taken together, these data highlight the selective pressure against long-term retention of Brg1 deficient cells in the small intestinal epithelium. However, due to the low frequency of recombination events, these observations provided no explanation of the mechanism behind the repopulation of Brg1 deficient cells.

3.3.2 Complete Brg1 loss has mild immediate effects on intestinal homeostasis

Having established that high-dose induction of VillinCreER recombinase drives complete loss of Brg1 in the intestinal epithelium, I set out to examine the effects of Brg1 deficiency on small intestinal homeostasis.

Histological inspection of the small intestinal mucosa 4 days after high-dose induction revealed no abnormalities in the general crypt-villus architecture despite complete loss of Brg1 from the epithelial cells. However, quantitative analysis revealed a number of subtle alterations to epithelial homeostasis.

Firstly, Brg1 deficient epithelium displayed slightly elevated levels of apoptosis based on morphological appearance. This observation, however was not replicated based of cleaved Caspase-3 staining. Interestingly, although morphology based scoring is able to detect a wider range of apoptosis stages than Caspase-3 staining, both methods produced not only comparable fold change, but also very close average numbers of apoptotic cells. The lack of significant difference in Caspase-3 staining is therefore likely to be attributed to high variation and lower sample size. It should be noted, however, that whilst apoptosis levels in Brg1 deficient epithelium was nearly three times higher than that observed in normal intestine, it still equated to less than one apoptotic cell per crypt. This is considerably less than the elevation in apoptosis levels observed upon loss of proteins involved in cell cycle progression and cell-to-cell adhesion Chk1, Brca2 and E-cadherin (Greenow *et al.*, 2009; Hay *et al.*, 2005, Schneider *et al.*, 2010). Similarly, ablation of Wnt signalling in the intestinal epithelium via deletion of β-catenin or expression of the Wnt antagonist Dickkopf-1 failed to induce significant increase in apoptosis suggesting that Wnt signal abrogation has no pro-apoptotic effect on the intestinal epithelium (Fevr *et al.*, 2007, Kuhnert *et al.*, 2007).

Examination of the proliferative compartment by quantification of mitotic figures and Ki67 positive cells revealed no difference in the number of proliferating cells between Brg1 deficient and control epithelium suggesting that Brg1 is dispensable for the proliferative activity of the majority of crypt cells. In contrast to this observation, conditional loss of β-catenin has been found to result in ablation of the proliferative compartment as early as 2 days after β-catenin deletion (Fevr *et al.*, 2007). Despite this finding, Brg1 deficient intestines displayed a significant increase in the number of BrdU positive cells 2 hours post labelling. The discrepancy between the lack of detectable changes in mitosis levels

on one hand and increased BrdU incorporation on the other, implies a post-S phase cell cycle arrest. Cell cycle arrest at this stage could be an early indicator of the subsequent significant reduction in mitosis levels observed at day five PI. Of interest, while Brg1 loss in normal lung epithelium has been reported to result in increased apoptosis (Glaros *et al.*, 2008), there are no reports to date linking Brg1 loss to the induction of cell cycle arrest *in vivo*. On contrary, numerous reports have demonstrated that Brg1 is required for Rb-mediated cell cycle arrest (Strobeck *et al.*, 2000; Strober *et al.*, 1996; Zhang *et al.*, 2000). As discussed later in this chapter, Brg1 deficiency-induced cell cycle arrest and the subsequent decrease in proliferation may potentially be caused by the exhaustion of the proliferative pool due to the lack of replenishment from the stem cell population.

Analysis of the BrdU positive cell distribution 24 hours post labelling revealed a significantly impaired migration in Brg1 deficient intestine. It should be noted, however, that this observation was based on cell migration over the period spanning the 24 hours between day four and five PI. Importantly, several changes occurred in the biology of the Brg1 deficient epithelium during this time period. While Brg1 deficient intestine at day four PI displayed no changes in mitosis levels compared to control epithelium, a significantly lower proliferation rate was observed in Brg1 deficient crypts at day five PI (discussed later in this chapter). It is therefore difficult to ascertain whether impaired migration apparent at day five PI is a secondary effect of the reduced cell proliferation or a primary effect of Brg1 loss. However, an equivalent experiment tracing migration of BrdU labelled cells over the period between three and four days PI detected a similar reduction in cell migration in Brg1 deficient epithelium. Although complete Brg1 loss might not have been achieved over this time period, this observation provided some support in favour of the hypothesis that impaired migration was a primary effect of Brg1 deletion. Interestingly, a significant decrease in villus length was detected in Brg1 deficient epithelium at day four PI. Considering the lack of changes in cell proliferation at this stage, decreased villus length could be attributed to impaired migration due to the lack of positive upward force generated by epithelial cells migration along the underlying stroma (Heath, 1996).

In addition to decreased villus length and elevated levels of both apoptosis and BrdU incorporation, Brg1 deficient epithelium at day four PI displayed mild alterations in differentiation of certain cell types. Remarkably, the two cell types whose differentiation was affected by Brg1 loss belonged to different lineages, namely enteroendocrine cells from the secretory and enterocytes from the absorptive lineages respectively. Wnt signalling has been previously reported to play a crucial role in differentiation of small intestinal secretory cell types in a dose-dependent manner. Conditional deletion of the Wnt pathway co-activator Tcf4 has been shown to abrogate cell proliferation and differentiation of Paneth and Enteroendocrine cells, but not enterocytes or Goblet cells in developing gut (Korinek *et al.*, 1998; van Es *et al.*, 2005a). Overexpression of the Wnt pathway inhibitor Dkk1 has been found to result in a more severe phenotype as it not only inhibited cell proliferation, but also completely abrogated differentiation of all secretory cell lineages without affect-

ing enterocyte differentiation (Pinto *et al.*, 2003). In the current study short-term Brg1 loss was found to suppress enteroendocrine cell differentiation without affecting other secretory cell lineages or cell proliferation. It can be hypothesised, therefore, that Brg1 loss attenuates Wnt signalling to a level sufficient to impair enteroendocrine cell differentiation, but not cell proliferation or Goblet and Paneth cell differentiation. Notably, loss of the tumour suppressor Lkb1 in the murine small intestine has been reported to perturb normal Goblet and Paneth cell maturation via increased expression of the Notch pathway target gene *Hes5* (Shorning *et al.*, 2009). Resultant Lkb1 deficient Goblet and Paneth cells have been found to display an appearance characteristic of immature Intermediate cells, considered to represent a transitional step between undifferentiated and mature secretory cells (Troughton and Trier, 1969). Despite the observed interaction between Brg1 and Lkb1 (Marignani *et al.*, 2001), no changes (neither quantitative nor morphological) were registered in these cell types upon Brg1 deletion. This observation thus suggests a lack of functional interaction between Lkb1 and Brg1 in the small intestinal epithelium.

Although Brg1 loss did not block differentiation along the absorptive lineage completely, enterocytes in the Brg1 deficient epithelium displayed a very thin brush border compared to control epithelium. Notably, enterocyte differentiation has been found to be driven by Notch signalling, as constitutive activation of the Notch pathway suppressed differentiation of secretory cell lineages and induced differentiation of post-mitotic cells into enterocytes (Fre *et al.*, 2005). Conversely, treatment with Notch inhibitors has been shown to result in expansion of secretory lineages at the expense of enterocytes (Milano *et al.*, 2004). The fact that Brg1 loss perturbed the development of the brush border without increasing differentiation along secretory lineages, suggests that Brg1 loss does not block enterocyte differentiation, but rather decreases expression of the brush border components. Expression analysis of other enterocyte markers, such as Villin might be required to ascertain whether Brg1 loss impairs enterocyte differentiation. Since enterocyte differentiation relies on Notch signalling, expression analysis of Notch pathway target genes could provide an insight into the effects of Brg1 deficiency on Notch signalling in the small intestinal epithelium. Notably, β-catenin deletion in the small intestinal epithelium has been found to rapidly induce loss of the crypt progenitor cell marker CD44 and activation of alkaline phosphatase expression in the intervillus region indicating an early terminal differentiation of the intestinal progenitor cells (Fevr *et al.*, 2007). Contrary to this observation, no alkaline phosphatase expression was detected in the crypt region of Brg1 deficient intestine, suggesting that Brg1 deficient transit amplifying cells retained the progenitor phenotype at least for some time.

3.3.3 Brg1 loss compromises the function of the small intestinal stem cell

In drastic contrast to the mild immediate effects of Brg1 loss observed at four days PI, Brg1 deficient epithelium displayed a marked disruption of intestinal architecture and homeostasis as early as five days PI. Simple visual inspection of the tissue sections from Brg1 deficient epithelium at this stage revealed loss of normal architecture characterised by shortened villi and the disappearance of clear crypt villus junctions. Disruption of the intestinal architecture was accompanied by reduced cell proliferation as determined by quantification of Ki67 positive cells. Interestingly, Wnt signalling suppression in the small intestinal epithelium via conditional loss of β-catenin or Dickkopf-1 expression has been found to result in immediate and complete abrogation of cell proliferation and terminal differentiation of crypt progenitor cells (Fevr *et al.*, 2007; Kuhnert *et al.*, 2004). In contrast to these findings, loss of Brg1 resulted in gradual contraction of the intestinal proliferative compartment. This observation suggested that the proliferative compartment in Brg1 deficient epithelium was exhausted eventually with cells at the top of the crypt losing their proliferative capacity first.

The further attempt to age mice with Brg1 deficient intestinal epithelium resulted in rapidly deteriorating health and animal morbidity at around 7-8 days PI. Histological analysis of the small intestinal epithelium from sick animals revealed severe disruption of intestinal architecture with complete loss of normal crypt-villus organisation. At the same time, immunohistochemical analysis of Brg1 expression detected rare crypts that retained Brg1 expression. These crypts had an enlarged appearance and a number of these crypts were found to be undergoing the process of crypt fission. Crypt fission is a powerful mechanism of intestinal regeneration following damage caused, for instance, by ionising radiation (Cairnie and Millen, 1975). Interestingly, a similar increase in crypt fission was observed upon the loss of the intestinal stem cell marker and regulator Ascl2 in murine intestine (van der Flier *et al.*, 2009).

Taken together, the very mild immediate consequences of Brg1 deficiency and the severe crypt loss shortly afterwards led me to hypothesise that Brg1 may affect intestinal stem cell function. In order to investigate the effect of Brg1 inactivation on the stem cell population I performed a series of experiments aimed to assess the state of the stem cell population. Quantitative RT-PCR analysis of stem cell markers *Lgr5* and *Ascl2* revealed a significant decrease in expression of these genes. Notably, both *Lgr5* and *Ascl2* have been found to be target genes of the Wnt pathway (Barker *et al.*, 2007; Jubb *et al.*, 2006). Decreased expression of Lgr5 and Ascl2 can therefore be attributed to attenuated Wnt signalling rather than depletion of the stem cell population. In order to overcome this shortcoming of Lgr5 and Ascl2 as stem cell markers, I used *in situ* hybridisation analysis of *Olfm4*, a Wnt-independent stem cell marker, to assess the state of the stem cell population (van der Flier *et al.*, 2009). Similar to the other two stem cell

markers, *Olfm4* expression was substantially decreased in the Brg1 deficient epithelium. Coincidentally depletion of the stem cell population induced by conditional deletion of Ascl2 has been reported to be accompanied by a similar loss of *Olfm4* expression (van der Flier *et al.*, 2009). It should be noted that reduced expression of the stem cell markers was detected at day 4 PI, i.e. prior to any changes in cell proliferation, suggesting strongly that depletion in the stem cell population is a direct effect of Brg1 deficiency. Stem cell loss and subsequent exhaustion of the proliferative pool could result in the cell cycle arrest of transit amplifying cells consistent with increase in BrdU labelling prior to any visible changes to cell proliferation. These observations further supported the notion that Brg1 is essential for the small intestinal stem cell maintenance. Coincidentally, Brg1 has been previously reported to be involved in maintenance and differentiation of several somatic stem cells including neural (Matsumoto *et al.*, 2006) and mesenchymal (Alessio *et al.*, 2010; Napolitano *et al.*, 2007) stem cells.

While providing strong evidence in favour of the notion that pan-epithelial Brg1 loss results in compromised stem cell function, the data presented so far do not show directly that intestinal stem cells require functional Brg1 to maintain their activity. Indeed, Brg1 may be essential for the function of some auxiliary cell type, which, in turn, is indispensable for the stem cell maintenance. An obvious candidate for such a cell type would be the Paneth cells (Sato *et al.*, 2010). Equally important is the question of stem cell fate upon Brg1 inactivation. A limited increase in apoptosis, which was not entirely confined to the crypt bottom favours the notion that Brg1 loss does not cause stem cell death, but rather impairs its function.

To answer these questions I attempted to specifically delete Brg1 in the small intestinal stem cell compartment using the *Lgr5-EGFP-CreER* transgene (Barker *et al.*, 2007). This experimental system uses the *Lgr5* promoter to drive stem cell specific expression of an inducible Cre recombinase. GFP expression from the same construct provides an additional benefit of permitting visualisation of stem cells within the crypt. Stem cell-specific Brg1 loss was induced by tamoxifen administration. Analysis of GFP expression in the small intestinal epithelium at day 5 PI detected positive GFP staining of narrow cells intercalated between Paneth cells, that correspond to CBC cells. Quantification of GFP expression revealed an extremely low frequency of crypts expressing the transgene in both, animals carrying wild type and loxP targeted *Brg1* alleles. The *Lgr5-EGFP-CreER* construct has been found to be expressed only in a fraction of small intestinal crypts. It has been suggested that low expression of the transgene is caused by epigenetic silencing of the transgene during gut development (Sansom, personal communication). However, the level observed in animals used in the present study appears to be exceptionally low, possibly due to different genetic backgrounds of the animals used. Quantitative analysis of GFP expression detected a significantly lower frequency of crypts with detectable GFP expression in mice harbouring targeted *Brg1* alleles compared to control animals. This parameter, however, is likely to be strongly influenced by any variation in epigenetic

silencing of the transgene. In an attempt to eliminate variability introduced by epigenetic silencing I calculated the average number of GFP positive cells present in GFP expressing crypts. The rationale behind this mode of analysis lies in the monoclonality of small intestinal crypts. Crypts in the small intestine of adult mice have been shown to undergo monoclonal conversion, so that all cells populating the same crypt represent progeny of a single 'ancestor' stem cell (Winton *et al.*, 1988). It can therefore be assumed with a certain degree of confidence that all stem cells in a GFP expressing crypt originate from the same GFP positive progenitor cell and also express GFP. Since the average number of stem cell per crypt is fairly consistent between comparable sections of the gut, any detrimental effects of Brg1 loss on stem cell maintenance are likely to be manifest in a reduced number of GFP positive cells per crypt. Indeed, GFP expressing crypts in mice with targeted *Brg1* alleles contained significantly lower number of GFP positive cells per crypt.

Although likely to be unreliable due to the low level of the transgene expression, these observations provide extra support in favour of the notion that stem cell depletion is likely to be a direct consequence of Brg1 deficiency, rather than a secondary effect of a compromised function of some auxiliary cell type.

Brg1 deficiency-mediated depletion of GFP positive cells still did not clarify the intestinal stem cell fate upon Brg1 inactivation. In order to trace the progeny of Brg1 deficient stem cells I performed immunohistochemical analysis of Brg1 expression. Crypts containing clusters of Brg1 deficient cells were detected in the small intestinal epithelium of $Lgr5CreER^+Brg^{fl/fl}$ mice at a frequency comparable to that of GFP positive crypts. Staining of serial sections with antibodies against GFP and Brg1 detected GFP expression in crypts containing Brg1 deficient cells. However, careful examination of the staining pattern failed to detect GFP expression in Brg1 deficient cells. The GFP positive cells present in these crypts were therefore likely to be represented by stem cells escaping Brg1 deletion or early progenitors de-differentiating into stem cells. The absence of Brg1 deficient cells expressing GFP further suggests that loss of Brg1 is incompatible with stem cell functionality, as assessed by GFP expression. On the other hand, the presence of Brg1 deficient cell clusters indicated that stem cells retain their proliferative ability at least for a limited period of time.

Taken together, these data suggest that Brg1 loss induces stem cell commitment to terminal differentiation rather than cell death. This notion is consistent with the very small increase in apoptosis levels seen upon Brg1 deletion in $VillinCre^+Brg^{fl/fl}$ mice. Instead, stem cells appear to lose expression of stem cell markers and their ability to self-renew and turn into committed progenitor cells, retaining a limited ability to proliferate and differentiate. Coincidentally, conditional deletion of β-catenin has been found to result in terminal stem cell differentiation and loss of putative stem cell markers Sox4 and Diap3 suggesting that Brg1 loss might exert its phenotype by suppressing Wnt signalling within the stem cell population (Fevr *et al.*, 2007). It should be noted, however, that

unlike Brg1 deficiency, β-catenin loss induced a more severe phenotype causing terminal differentiation not only in the stem cell, but also in the progenitor cell compartment.

Considering delayed loss of cell proliferation and virtually no effect on differentiation of the secretory lineages upon Brg1 deletion, it appears that Brg1 deficiency has a very mild effect on Wnt signalling in the crypt progenitor cells. The drastic effect of Brg1 loss on the stem cell homeostasis could, therefore, be explained by two mechanisms. The first mechanism implies that the small intestinal stem cell require higher levels of Wnt signalling compared to progenitor cells. In this case, subtle attenuation of Wnt signalling by Brg1 loss would compromise functionality of the stem cell population, but leave progenitor cells unaffected. This mechanism is consistent with existence of the Wnt ligands gradient, which peaks around the crypt base (Gregorieff et al., 2005). Additionally, expression levels of the Wnt target genes, such as EphB2, have been found to display positive correlation with stem cell properties (Merlos-Suárez et al., 2011). An alternative mechanism proposes that other signalling pathways essential for the small intestinal stem cell maintenance (for example Notch) may rely on Brg1 for their proper function. The intestinal stem cell population has been found to exist in a steady state of symmetric divisions giving either two new stem cells (self-renewal) or two committed progenitor cells (differentiation) (Lopez-Garcia et al., 2010; Snippert et al., 2010). Given the Paneth cell role in creating the stem cell niche (Sato et al., 2010) the choice between self-renewal and differentiation appears to be determined by the proximity of the stem cell to the Paneth cell. It is plausible, therefore, that Brg1 is involved in mediation of the signalling pathways activated within stem cells by proximity to Paneth cells. Notably, Brg1 has been reported to regulate expression of genes involved in self-renewal and pluripotency in ES cells (Ho et al., 2009; Kidder et al., 2009). These include, but are not limited to Oct4, Sox2, Nanog, Stat3, Sall4 and others. It would be insightful, therefore, to ascertain whether Brg1 loss compromises the intestinal stem cell self-renewal by disrupting expression of these genes.

The marked difference between phenotypes seen upon partial versus complete loss of Brg1 could be explained in the context of the stem cell niche provided by Paneth cells (Figure 3.21). In both cases loss of Brg1 within the intestinal stem cell compartment induces stem cell commitment to terminal differentiation. Due to the expression pattern of AhCreER recombinase, this transgene only drives Brg1 loss in a limited populations of stem and early progenitor cells (Kemp et al., 2004). As a result, crypts that undergo Brg1 loss under control of AhCreER recombinase retain a substantial number of wild type cells (Figure 3.21a). In accordance with the steady state dynamics of crypt homeostasis, any stem cells that escaped Brg1 inactivation would be able to expand and repopulate the whole crypt (Snippert et al., 2010). Alternatively, in crypts, where AhCreER recombinase was successful in driving Brg1 loss in every stem cell, commitment to terminal differentiation and subsequent migration out of the crypt base would create points of access around existing Paneth cells. Undifferentiated progenitor cells retaining Brg1 expression could then gain access to the stem cell niche, undergo de-differentiation, assume the role of

stem cells and drive epithelial repopulation with Brg1 positive cells (Figure 3.21a). A similar situation is observed upon post-irradiation damage repair. The small intestinal epithelium has been found to contain a tiered system of stem and progenitor cells with gradually increasing resistance to ionising radiation. In this system low dose irradiation causes stem cells and lower tiers of progenitor cells to undergo apoptosis, while higher tiers of progenitor cells are capable of driving regeneration of the epithelium by assuming the role of stem cells (Potten, 1998). Intriguingly, a recent report by Montgomery *et al.* (2011) has provided convincing evidence of a predominantly quiescent stem cell population resistant to ionising radiation. It is plausible that the proposed system of progenitor cells may instead be comprised of such cells capable of driving epithelial regeneration upon radiation damage. Notably, the pattern of AhCreER recombinase expression in regard of the proposed quiescent stem cells remains to be established. A possibility, therefore, exists that lack of AhCreER expression in the quiescent stem cells could result in Brg1 retention and such sells could then contribute to repopulation of the intestinal epithelium with wild type cells.

Conversely, induction of Brg1 loss using VillinCre recombinase leads to ubiquitous Brg1 loss creating a dearth of wild type progenitor and/or reserve stem cells that would be capable of functionally replacing active stem cells (Figure 3.21b). Upon pan-epithelial loss of Brg1, epithelial homeostasis is maintained for a limited period of time due to the activity of transit amplifying cells. However, eventual depletion of the proliferative pool due to the lack of replenishment from the stem cell compartment sequentially results in cell cycle arrest and disruption of epithelial architecture.

3.3.4 Brg1 haploinsufficiency does not induce intestinal tumourigenesis, but impairs the stem cell clonogenic capacity

Biallelic loss of Brg1 has been widely reported in cancer cell lines and primary tumours (Becker *et al.*, 2009; Reisman *et al.*, 2003; Wong *et al.*, 2000). In contrast, a number of animal studies showed no increase in tumour incidence upon complete Brg1 loss (Glaros *et al.*, 2008; Wang *et al.*, 2009). Conversely, animals with heterozygous Brg1 loss have been found to be prone to tumourigenesis in a range of tissues (Bultman *et al.*, 2007; Glaros *et al.*, 2008). Importantly, tumours developing in Brg1 heterozygous animals have been found to retain a functional copy of Brg1. This observation suggested that at least in some tissues, Brg1 haploinsufficiency rather than loss of heterozygousity contributed to tumourigenesis. In this study I induced heterozygous loss of Brg1 in the small intestinal epithelium using AhCre recombinase. Survival analysis of Brg1 haploinsufficient mice revealed no significant decrease in survival compared to wild type controls. Furthermore, macroscopic and histological analysis of the small intestinal epithelium of animals aged for as long as 643 days PI revealed no signs of intestinal neoplasia. It appears, therefore, that Brg1 haploinsufficiency has no oncogenic effect in the context of the small intestinal
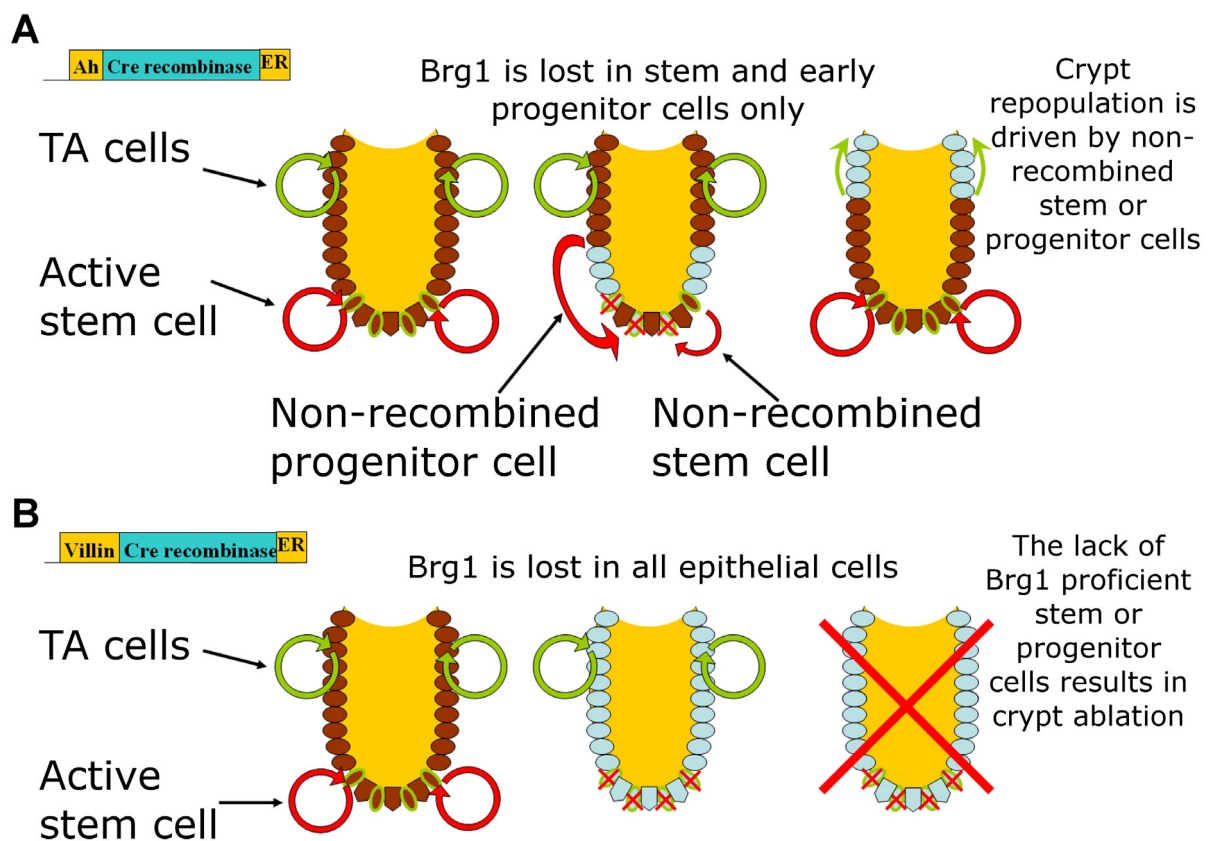
Figure 3.21: Scenarios of Brg1 loss in the small intestinal epithelium. **(a)** Depletion of the stem cell compartment upon partial loss of Brg1 can be rescued by non-recombined stem or progenitor cells that are able to repopulate the intestinal epithelium with wild type cells. **(b)** The lack of Brg1 proficient stem/progenitor cells upon complete Brg1 deletion results in gradual depletion of the proliferative pool and crypt ablation.

epithelium. This conclusion is consistent with the observation that tumourigenesis in mice constitutively heterozygous for Brg1 is limited to mammary epithelium (Bultman *et al.*, 2007).

Rapid repopulation of Brg1 deficient cells with wild type counterparts suggested a strong selective pressure against Brg1 deficient cells in the small intestinal epithelium. In order to investigate whether heterozygous loss of Brg1 confers a similar selective disadvantage I analysed retention of the recombined Brg1 allele. DNA samples were extracted from the small intestinal epithelium of $AhCre^+Brg^{+/fl}$ mice as late as 643 days PI and subjected to recombined PCR analysis. The signal corresponding to the recombined allele was detected in all $AhCre^+Brg^{+/fl}$ animals analysed. This observation demonstrated that Brg1 haploinsufficient cells were successfully retained in the small intestinal epithelium over an extensive period of time. Long-term retention of cells heterozygous for Brg1 suggests that under normal conditions Brg1 haploinsufficiency is unlikely to have any detrimental effect on the stem cell long-term maintenance. In order to assess the effect of Brg1 haploinsufficiency on small intestinal stem cell function under stress conditions, I carried out an analysis of clonogenic repopulation upon exposure to ionising radiation. The small intestinal epithelium of $VillinCre^+Brg^{+/fl}$ mice demonstrated a significantly reduced number of clonogenic units compared to control animals. Since the number of clonogenic units reflects the abundance of stem cells within the crypt, one could hypothesise that Brg1 haploinsufficient crypts contained a lower number of stem cells. This would imply, however, that heterozygous Brg1 loss somehow negatively affected stem cell homeostasis, which is unlikely in view of the long-term retention of Brg1 haploinsufficient cells in the small intestine. It is more likely, therefore, that the detrimental effect of Brg1 haploinsufficiency on stem cell physiology only manifests under stress conditions of ionising radiation, potentially due to higher susceptibility to the DNA damage.

To conclude, the findings presented here suggest that Brg1 heterozygousity has no detrimental effect on the normal small intestinal homeostasis under physiological conditions, but impairs regeneration upon radiation damage.

3.3.5   Future directions

Requirement of functional Brg1 for maintenance of the small intestinal stem cells provides a potentially useful tool to further our understanding of intestinal homeostasis. Analysis of the alterations to expression patterns upon Brg1 loss could unveil transcriptional networks involved in the regulation of intestinal stem cell physiology. To this end we are planning to carry out genome-wide expression analysis of Brg1 deficient small intestinal epithelium. This type of analysis, however, is likely to register transcriptional effects of Brg1 loss in the whole of the intestinal epithelium, which might obscure stem cell specific changes. The *Lgr5-EGFP-Cre* transgene could prove useful in enriching for the stem cell population in order to increase signal to noise ratio. However, rapid loss of GFP expression upon

Brg1 deletion creates a substantial obstacle in the isolation of Brg1 deficient stem cells. In order to overcome this limitation we are planning to use wild type mice harbouring *Lgr5-EGFP-Cre* transgene for Brg1 chromatin immunoprecipitation (ChIP) analysis of the stem cell enriched population of epithelial cells, in order to investigate locus-specific recruitment of Brg1. This could be followed by genome-wide analysis (ChIP-on-Chip) to determine stem cell-specific targets of Brg1-mediated expression.

Finally, in order to confirm that Brg1 loss directly targets stem cells, we are planning to conduct an *in vitro* experiment making use of organoid culture system published previously by Sato *et al.* (2009). Single cell suspension from $Lgr5CreER^+BrgHom^{fl/fl}$ small intestine will be enriched for GFP expressing cells and grown in media with or without tamoxifen supplementation. Preliminary results, however, demonstrated remarkably low yield of organoids from animals carrying *Lgr5-EGFP-Cre* transgene regardless of their Brg1 status.

Chapter 4

Investigating the multiple tissue phenotypes of Brg1 loss

4.1   Introduction

The data presented in the previous chapter described a range of responses observed in the small intestinal epithelium as a result of Brg1 loss, which I interpret to be due to compromised function of the small intestinal stem cell. A number of previous reports have implicated Brg1 in the development and maintenance of a wide range of tissues (Bultman *et al,*. 2005; Chi *et al.*, 2003; De *et al.*, 2011; Griffin *et al.*, 2008; Hang *et al.*, 2010; Inayoshi *et al.*, 2006; Indra *et al.*, 2005; Matsumoto *et al.*, 2006; Ohkawa *et al,*. 2006; Stankunas *et al.*, 2008; Xu *et al.*, 2006). In particular, adult mesenchymal stem cells have been reported to require tightly regulated Brg1 levels for their maintenance (Alessio *et al.*, 2010; Napolitano *et al.*, 2007). Furthermore, in a subset of tissues, heterozygous Brg1 loss has been demonstrated to induce or facilitate tumourigenesis (Bultman *et al.*, 2007; Glaros *et al.*, 2008), suggesting that in these tissues Brg1 acts as a *bona fide* tumour suppressor. Because of the off-target-tissue expression profile of the AhCreER recombinase I was able to analyse Brg1 loss in a range of tissues outside of the small intestine. Additionally, pan-intestinal expression of VillinCre recombinase enabled me to investigate the consequences of Brg1 deletion in the large intestinal epithelium. This chapter describes the effects of Brg1 deficiency in forestomach, glandular stomach, large intestine and bladder epithelial tissues[1].

---

[1]Some of the animals involved in the long-term ageing experiments using AhCreER recombinase were induced and dissected by Dr Boris Shorning. The subsequent analysis of the tissue sections was carried out by me.

4.2   Results

4.2.1   Brg1 haploinsufficiency does not induce tumourigenesis in multiple tissues expressing AhCre recombinase

Brg1 mutations have been detected in cancer cell lines and primary tumours from a range of tissues (Becker *et al.*, 2009; Reisman *et al.*, 2003; Wong *et al.*, 2000). More specifically, Brg1 haploinsufficiency has been reported to contribute to tumourigenesis in the mammary gland and lung epithelium Bultman *et al.*, 2007, Glaros *et al.*, 2008). In order to further explore the role of Brg1 as a tumour suppressor, I aimed to assess the tumourigenic effect of Brg1 haploinsufficiency in multiple tissues expressing AhCre recombinase, including large intestine, forestomach and glandular stomach epithelium, bladder urothelium and liver. To this end $AhCre^+Brg^{+/fl}$ mice were induced by four intraperitoneal injections of 80 mg/kg β-naphthoflavone and aged along with $AhCre^+Brg^{+/+}$ controls (for survival analysis see section 3.2.3). The organs reported to express AhCre recombinase were harvested at the end of the ageing experiment or earlier, if the animal developed signs of ill health. Tissue samples were fixed and processed for histology and genomic DNA was extracted from the paraffin embedded sections. Recombined PCR analysis detected a strong signal for the recombined *Brg1* allele in the liver, the glandular and forestomach, the small and large intestine of $AhCre^+Brg^{+/fl}$ animals (Figure 3.3) indicating successful retention of cells with heterozygous Brg1 loss. The signal for recombinant allele in the bladder urothelium was not detected. This, however, could be attributed to a smaller amount of tissue available for the analysis.

As described in section 3.2.3, analysis of survival probability revealed no significant difference between $AhCre^+Brg^{+/fl}$ and $AhCre^+Brg^{+/+}$ mice (Figure 3.2). Macroscopic analysis of internal organs from $AhCre^+Brg^{+/fl}$ mice at the time of dissection revealed no consistent causes of ill health. Among the most commonly observed symptoms of ill health were uterus and sebaceous gland inflammation in female and male animals respectively. Additionally, tumour-like formations in the liver were occasionally observed, which were identified as lymphomas and were encountered in both experimental and control animals. Histological analysis of the tissues with known AhCre expression revealed no signs of neoplastic transformation. As an example, H&E stained sections of the glandular and forestomach epithelium from $AhCre^+Brg^{+/fl}$ and control animals are presented in Figure 4.1.

4.2.2   Brg1 loss drives benign hyperplasia in the forestomach epithelium

Unlike the human stomach, the murine stomach is divided into two compartments: non-glandular forestomach and glandular stomach separated by the limiting ridge (Figure 4.2).
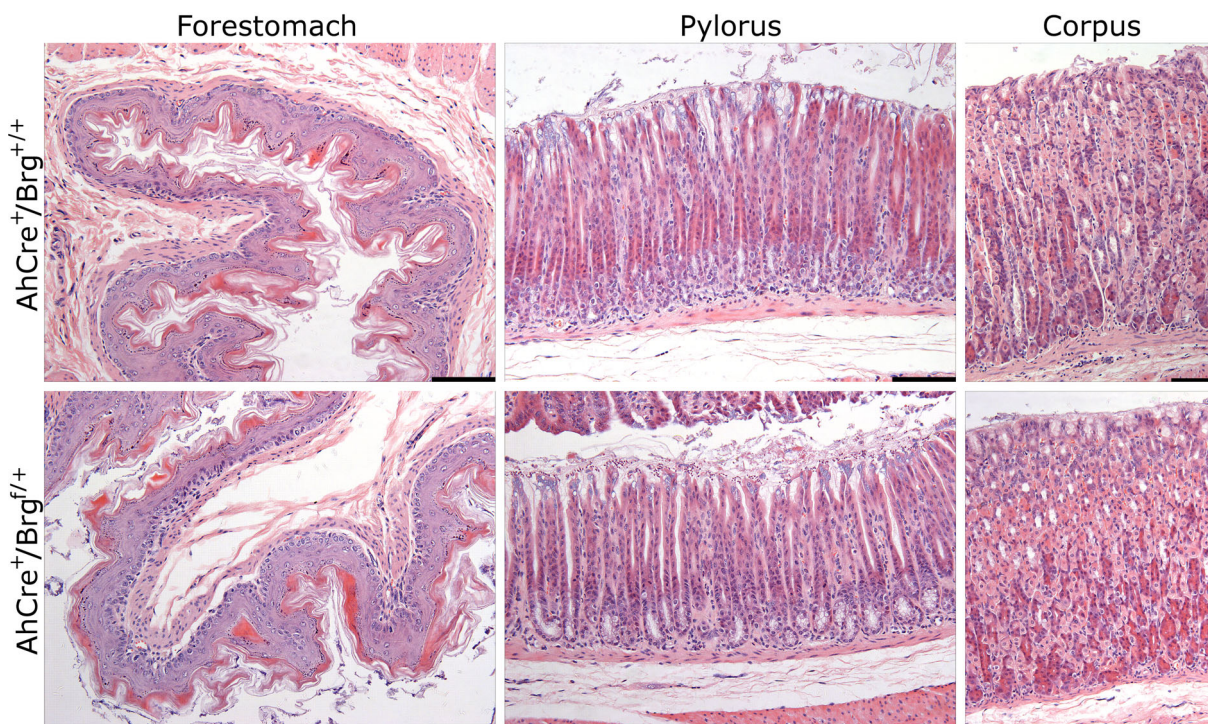
Figure 4.1: Brg1 haploinsufficiency does not induce oncogenic transformation in the tissues of the murine stomach. Histological analysis of H&E stained sections of the murine stomach from $AhCre^{+}$-$Brg^{+/fl}$ mice and $AhCre^{+}Brg^{+/+}$ controls revealed no signs of tumourigenesis in any of the stomach tissues over an observation period of 600 days. Scale bars represent 100 μm.

The forestomach is lined with soft keratinised stratified squamous epithelium, which it shares with oesophageal mucosa (Figure 4.2b). Proliferation in the forestomach epithelium is limited to the basal layer of cells, which differentiate and undergo keratinisation as they migrate towards the lumen (Karam, 1999).

4.2.2.1 Brg1 deficient cells are retained in the forestomach epithelium

Having established that no obvious oncogenic effect of Brg1 haploinsufficiency was observed in the murine forestomach epithelium, I aimed to examine the consequence of Brg1 deficiency in this tissue. To this end, $AhCreER^{+}Brg^{fl/fl}$ mice as well as $AhCreER^{-}$ controls were induced with five intraperitoneal injections of 80 mg/kg β-naphthoflavone and tamoxifen. Animals were dissected at day 35 PI and whole stomachs were harvested, processed and subjected to histological analysis. Immunohistochemical analysis of Brg1 expression in the forestomach epithelium of $AhCreER^{+}Brg^{fl/fl}$ mice at day 35 PI detected occasional Brg1 deficient cells intermingled with Brg1 positive cells (Figure 4.3). In contrast, all epithelial cells of wild type forestomach displayed high levels of Brg1 expression. Analysis of H&E stained sections, however, detected no marked differences in the histology of $AhCreER^{+}Brg^{fl/fl}$ and control forestomach (Figure 4.3).
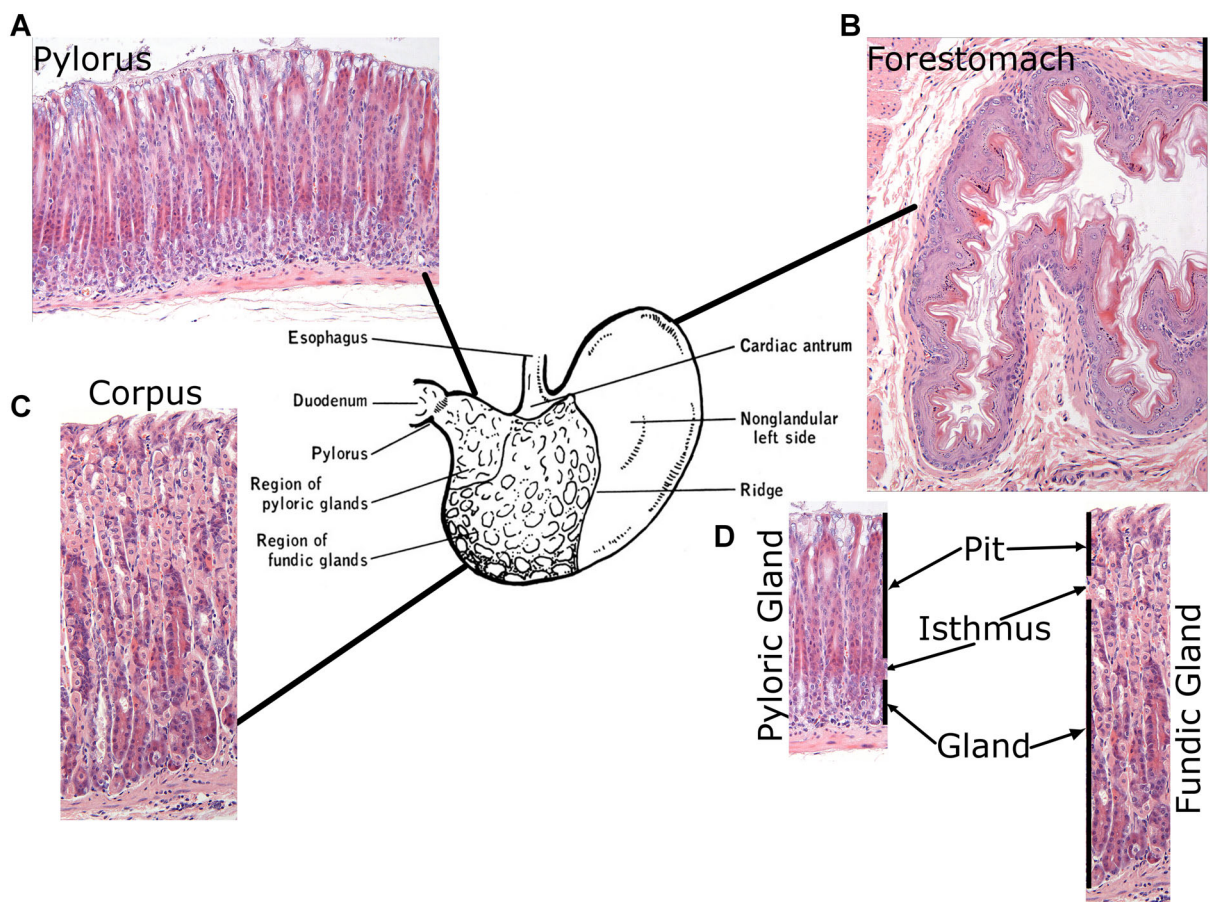
Figure 4.2: General anatomical structure of the murine stomach with representative H&E stained sections of the respective regions (a-c) and histological organisation of gastric glands **(d)**. See main text for detailed description. Adapted from (Green, 1966).
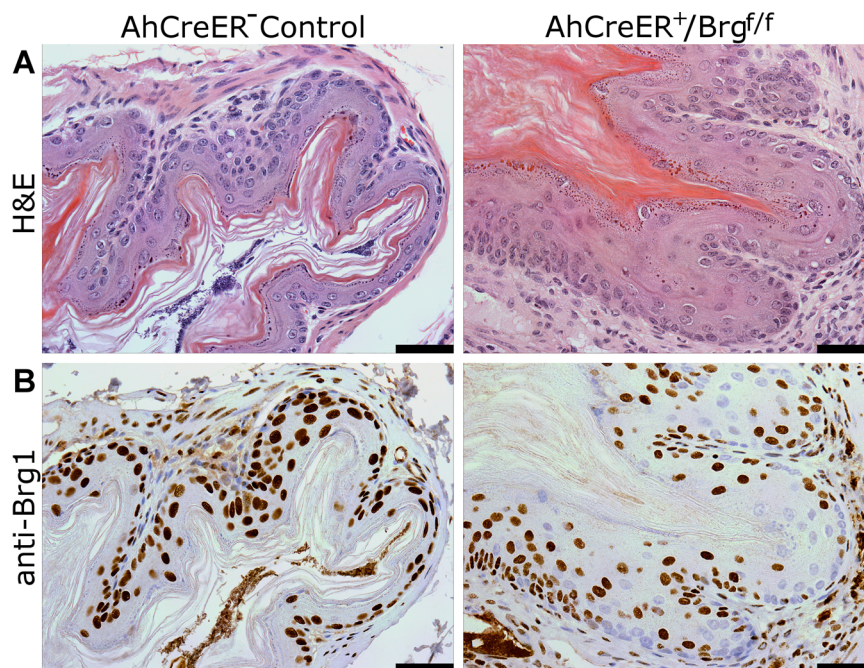
Figure 4.3: Brg1 deficient cells are retained in the forestomach epithelium of $AhCreER^+Brg^{fl/fl}$ mice. **(a)** Histological analysis of H&E stained sections of the forestomach epithelium from $AhCreER^+$-$Brg^{fl/fl}$ mice and Cre^- controls at day 35 PI revealed no gross differences in tissue morphology between the groups. **(b)** Immunohistochemical analysis of Brg1 expression in the forestomach epithelium of $AhCreER^+Brg^{fl/fl}$ mice at day 35 PI detected occasional Brg1 deficient cells distributed throughout the epithelium. No Brg1 deficient cells were detected in the forestomach epithelium of $AhCreER^-$ mice. Scale bars represent 50 μm.

4.2.2.2   Brg1 loss in the forestomach epithelium induces formation of squamous cell papillomas

In order to examine the long-term consequences of Brg1 loss in the forestomach epithelium, $AhCreER^+Brg^{fl/fl}$ mice were induced along with $AhCre^-$ controls as described above, aged and dissected at 80, 490 and 700 days PI (a minimum of 3 animals per time point). Histological analysis of H&E stained sections detected multiple lesions in the forestomach epithelium of $AhCreER^+Brg^{fl/fl}$ mice as early as day 80 PI (Figure 4.4a). Histopathological examination of the lesions identified them as squamous cell papillomas[2]. Histopathological analysis of the lesions at later time points revealed a substantial increase in the size of papillomas. However all lesions observed retained benign, highly differentiated histology with well defined borders and displayed no sign of dysplasia or invasive disease even at the latest time point (Figure 4.4). No lesions of any pathological nature were detected in the forestomach epithelium of $AhCre^-$ mice at any time point (n≥3 for all time points).

Immunohistochemical analysis of Brg1 expression in the forestomach epithelium of $AhCreER^+Brg^{fl/fl}$ mice revealed that papillomas were composed of Brg1 deficient cells (Figure 4.4a, bottom panels). Interestingly, Brg1 positive tissue that surrounded Brg1

---

[2]Histopathological description of forestomach lesions was provided by Prof Geraint T. Williams, Department of Pathology, University Hospital of Wales, Cardiff University, UK
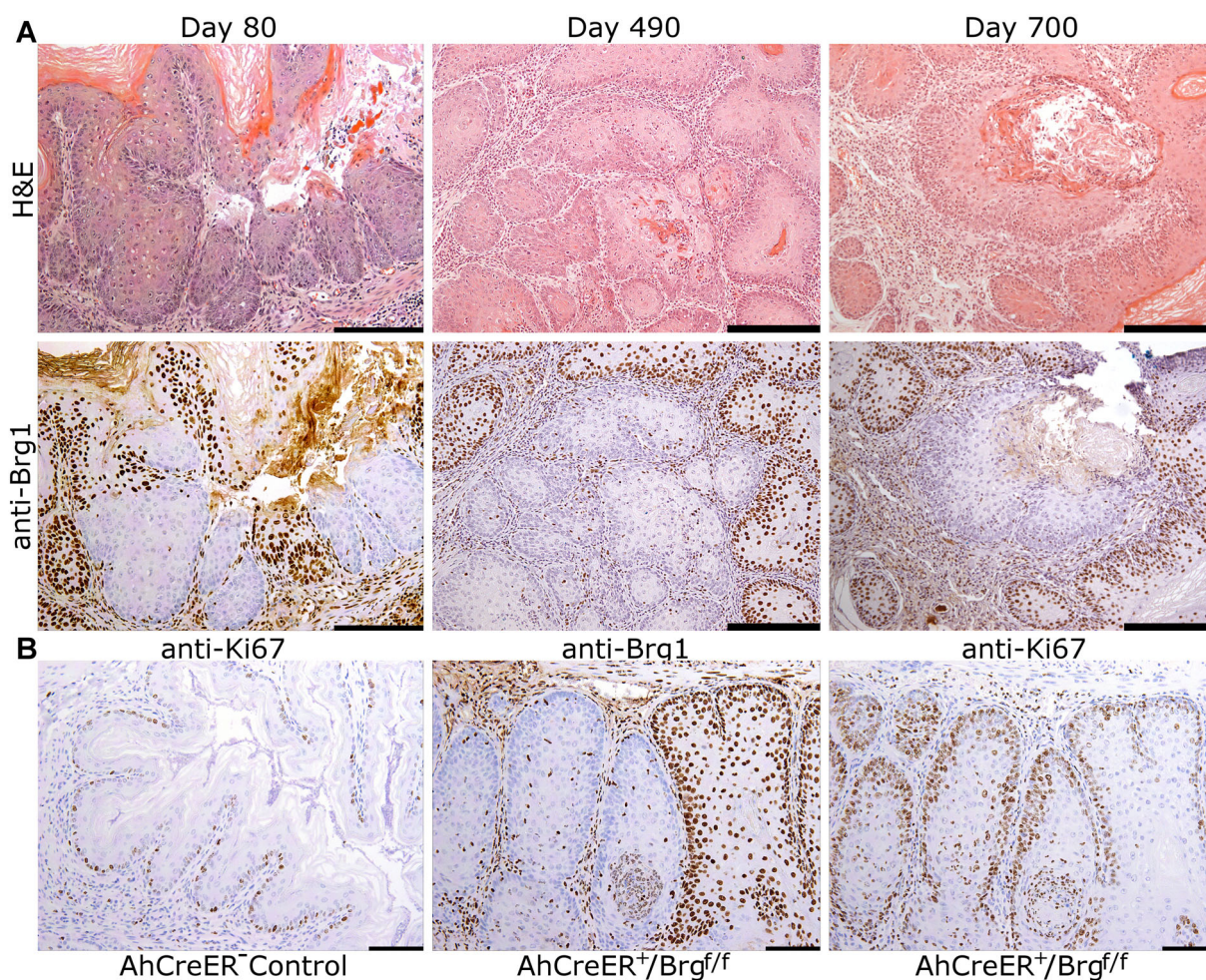
Figure 4.4: Brg1 loss in the forestomach epithelium induces formation of squamous cell papillomas. **(a)** Histological analysis of H&E stained sections of the forestomach epithelium from $AhCreER^{+}Brg^{fl/fl}$ mice at day 80, 490 and 700 PI revealed squamous cell papillomas. Although papillomas varied in size, no signs of invasive disease were detected. Immunohistochemical analysis of Brg1 expression in forestomach papillomas revealed that they were predominantly composed of Brg1 deficient cells with Brg1 expression status marking a clear border between hyperplastic and normal epithelium. **(b)** Immunohistochemical analysis of control Cre^{-} control mice revealed Ki67 staining in the basal layer of squamous epithelium. Immunostaining of serial sections of $AhCreER^{+}Brg^{fl/fl}$ forestomach at day 80 PI with antibodies against Brg1 and Ki67 revealed an expansion of Ki67 positive cells beyond the basal layer in Brg1 deficient epithelium. Note that despite aberrant appearance of some sections of Brg1 positive epithelium, Ki67 expression in these sections remained confined to the basal layer of cells. Scale bars represent 200 μm.

deficient papillomas occasionally had abnormal appearance (Figure 4.4a, bottom panels). This phenomenon could potentially be attributed to distortion of the architecture of the surrounding tissue by growing papilloma, which could result in abnormal appearance of tissue sections. Alternatively, Brg1 deficient cells could be secreting growth stimulating factors that would induce a proliferative response in the surrounding wild type tissue. In order to distinguish between these two possibilities I stained the forestomach sections with the proliferation marker Ki67 (Figure 4.4b). Immunohistochemical analysis of Ki67 expression revealed that proliferation in the forestomach epithelium of the control animal was largely limited to a single layer of basal cells (Figure 4.4b). Expression analysis of serial sections of Brg1 deficient forestomach epithelium stained with Brg1 and Ki67 revealed a substantially expanded proliferative compartment within Brg1 deficient lesions (Figure 4.4b). However, adjacent lesion-like Brg1 positive structures displayed the expression pattern of Ki67 comparable to that observed in control animals. This observation suggested that lesion-like appearance of Brg1 positive epithelium of $AhCreER^+Brg^{fl/fl}$ forestomach was most likely caused by a disturbed tissue architecture.

4.2.2.3 Brg1 deficient papillomas in the forestomach are not driven by activation of PI3K/AKT pathway, but by attenuated p21/pRb signalling

In order to investigate potential mechanisms leading to the formation of squamous cell papillomas in Brg1 deficient forestomach epithelium I assessed the status of a number of signalling pathways potentially involved in forestomach neoplasia.

Coordinated activation of the MEK/ERK and the PI3K/AKT pathways via simultaneous expression of activated form of Kras and loss of Pten has been reported to drive development of diffuse papillomatous hyperplasia of the forestomach epithelium (Marsh, in preparation). In order to investigate whether Brg1 loss induced papillomas in the murine forestomach epithelium by activating PI3K/AKT signalling, I analysed phosphorylation status of the PI3K/AKT pathway effector ribosome subunit S6. Immunohistochemical analysis of S6 phosphorylation in the forestomach epithelium of $AhCreER^+Brg^{fl/fl}$ and control mice revealed no difference in the levels of S6 phosphorylation between Brg1 deficient and wild type epithelium (Figure 4.5a). This suggests that activation of the PI3K/AKT pathway is unlikely to drive development of Brg1 deficient papillomas in the forestomach epithelium.

Brg1 has been reported to facilitate pRB-mediated cell cycle control via positive regulation of p21 expression, which in turn induces pRB hypophosphorylation and imposes cell growth arrest (Hendricks *et al.*, 2004; Kang *et al.*, 2004). In order to assess the effects of Brg1 loss on p21 expression I carried out immunohistochemical analysis of p21 expression in the forestomach epithelium of $AhCreER^+Brg^{fl/fl}$ and control mice. p21 expression analysis detected a substantially reduced staining levels in squamous cell papillomas compared to the epithelium of control mice (Figure 4.5b). Furthermore, regions
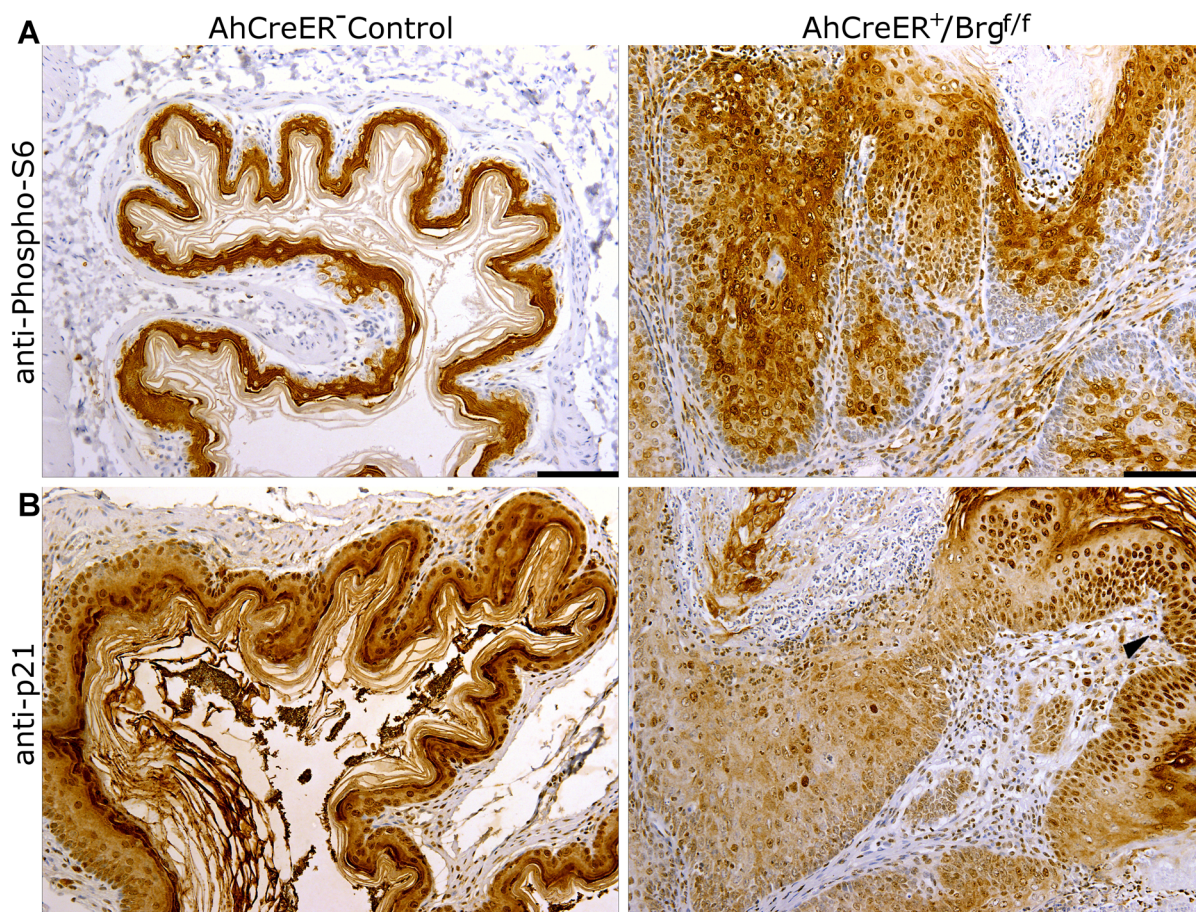
Figure 4.5: Brg1 deficient forestomach papillomas show no alterations in S6 phosphorylation, but exhibit p21 suppression. **(a)** Immunohistochemical analysis of expression of phosphorylated S6 ribosomal subunit in the forestomach epithelium of $AhCreER^+Brg^{fl/fl}$ and control mice at day 80 PI revealed no difference in S6 phosphorylation levels between hyperplastic and normal squamous epithelium. **(b)** Analysis of p21 expression in the forestomach epithelium of $AhCreER^+Brg^{fl/fl}$ and control mice at day 80 PI revealed a substantially reduced p21 expression in the forestomach papillomas compared to both adjacent normal epithelium and epithelium of control mice. Scale bars represent 100 μm.

of Brg1 proficient epithelium in the forestomach of $AhCreER^+Brg^{fl/fl}$ animals displayed levels of p21 expression compared to that observed in the forestomach of control mice (Figure 4.5, black arrowhead). These observations propose a model, where Brg1 loss induces the development of squamous cell papillomas in the forestomach epithelium via attenuation of p21 expression and inhibition of pRb-mediated control over the cell cycle.

4.2.3 The effects of Brg1 loss in the glandular stomach epithelium

The mucosa of the glandular stomach is composed of a simple columnar epithelium that forms tube-like invaginations into the lamina propria, structures termed gastric glands. Gastric gland morphology varies depending on their location within the stomach. Cardiac glands are the least abundant and are located in cardiac antrum, where the oesophagus enters the stomach. Pyloric glands are confined to the pylorus region of the stomach, just before it joins the small intestine (4.2a), while the most abundant fundic glands line the stomach body (corpus)(4.2c) (Seeley *et al.*, 2002). All glands share a common organisation in that they are divided in three structurally distinct parts: gastric pit, isthmus and proper gland. One or more proper glands enter the isthmus where they join with the gastric pit, which then opens into the stomach lumen. Fundic and pyloric glands differ from each other in the respective size of their compartments and cell composition (Lee, 1985). The pyloric gland is occupied by a relatively long gastric pit followed by short isthmus and gland, all of which are lined by mucous cells and infrequently scattered G cells that secrete gastrin (4.2d). Fundic glands are more structurally complex and consist of a short pit and isthmus followed by long gland. The gland itself is further subdivided into neck, body and base. The pit, isthmus and neck of fundic glands are lined with mucous producing Neck cells. The neck of the gland also contains eosinophilic Parietal (Oxyntic) cells secreting gastric acid and intrinsic factor. The body and the base of the fundic gland is mainly occupied by basophilic Chief (Zymogenic) cells secreting pepsinogen and a variety of Enteroendocrine cells producing hormones such as gastrin, its antagonist somatostatin, histamine, endorphins, serotonin, and cholecystokinin (Seeley *et al.*, 2002). All gastric cell lineages originate from the isthmal stem cell residing in the isthmus region of the gastric gland. Depending on the lineage some precursor cells retain a limited proliferative potential as they undergo terminal differentiation and migrate either towards the lumen of the gland base (Karam, 1999).

4.2.3.1 Brg1 deficient cells are retained in the glandular stomach epithelium

Having established that Brg1 haploinsufficiency has no obvious oncogenic effect in the glandular stomach epithelium, I set out to analyse the outcome of complete Brg1 loss in this tissue. To this end, $AhCreER^+Brg^{fl/fl}$ mice along with $AhCreER^-$ controls were induced by five intraperitoneal injections of 80 mg/kg β-naphthoflavone and tamoxifen.

The mice were then dissected 35 days PI, at which point whole stomachs were harvested and processed for histological analysis. Immunohistochemical analysis of Brg1 expression in the glandular stomach epithelium revealed occasional gastric glands composed of Brg1 deficient cells (Figure 4.6). Gastric glands containing Brg1 deficient cells were detected in the epithelium of both fundic (corpus) and pyloric regions of the glandular stomach (Figure 4.6). Analysis of H&E stained sections of the gastric epithelium revealed no abnormalities in the morphology of Brg1 deficient glands in either region of the gandular stomach (Figure 4.6)
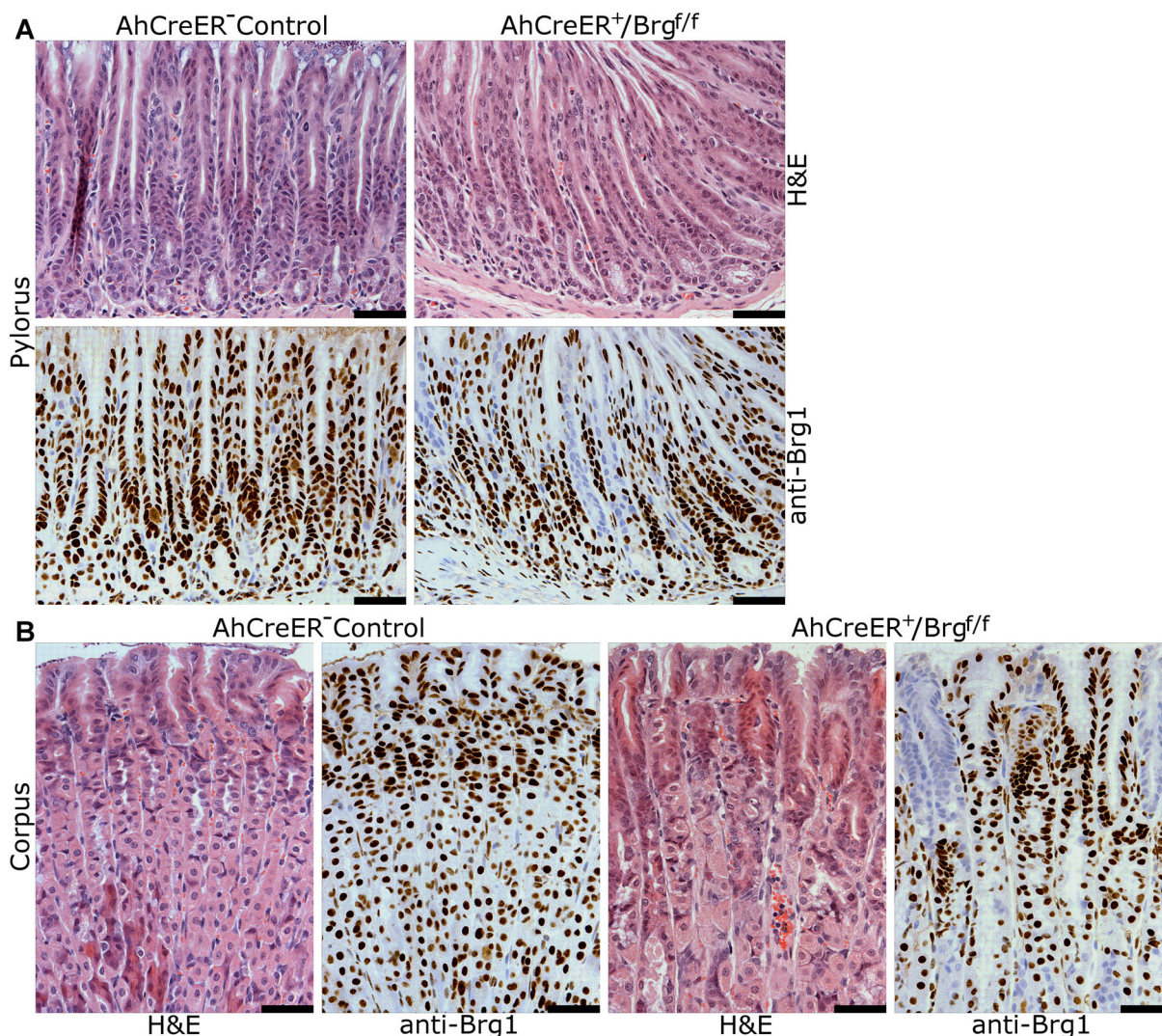
Figure 4.6: Brg1 deficient cells are retained in the pyloric and fundic epithelium of $AhCreER^{+}Brg^{fl/fl}$ mice. Immunohistochemical analysis of Brg1 expression in the pyloric **(a)** and fundic **(b)** epithelium of $AhCreER^{+}Brg^{fl/fl}$ mice at day 35 PI revealed occasional gastric glands largely populated by Brg1 deficient cells. While histological analysis of H&E stained sections of the pyloric stomach of $AhCreER^{+}$-$Brg^{fl/fl}$ mice revealed no morphological abnormalities **(a)**, Brg1 deficient fundic glands at day 35 PI displayed a moderate expansion of the mucinous neck cells in the gastric pit **(b)**. Scale bars represent 50 μm.

4.2.3.2   Brg1 loss in glandular stomach epithelium results in fundic gland polyposis

In order to assess the long-term effects of Brg1 loss in the gastric epithelium, $AhCreER^+$-$Brg^{fl/fl}$ mice were aged along with $AhCreER^-$ controls and whole stomachs were harvested at day 80, 490 and 700 PI (a minimum of 3 mice per time point). Histological analysis of the H&E stained sections of fundic stomach epithelium detected regions of hyperplastic growth in $AhCreER^+Brg^{fl/fl}$ mice as early as day 80 post induction (Figure 4.7a). Histopathological analysis of these hyperplastic malformations identified them as fundic gland polyps (FGPs) with characteristic superficial and deep cysts lined with mucous neck, parietal and chief cells[3]. Analysis of the glandular stomach epithelium at later time points (490 and 700 days PI) revealed that FGPs substantially increased in size and occasionally displayed low grade dysplasia. However, all the observed FGPs retained a high degree of differentiation and displayed no sign of invasive disease even at the latest time point analysed (Figure 4.7a). No signs of hyperplastic transformation was detected in the glandular stomach of $AhCreER^-$ mice at any time point.

Immunohistochemical analysis of Brg1 expression in $AhCreER^+Brg^{fl/fl}$ glandular stomach revealed that the polyps were largely composed of Brg1 deficient cells (Figure 4.6a, bottom panels). Histological analysis of the early Brg1 deficient lesions demonstrated that they were formed by expansion of mucous neck cells of the gastric pit and isthmus of the fundic gland (Figure 4.7a). This finding is consistent with the location of the gastric epithelium proliferative and stem cell compartments. In order to compare the proliferative activity of wild type and Brg1 deficient epithelium, sections of the glandular stomach were immunostained with an antibody against the proliferation marker Ki67 (Figure 4.7c). Analysis of Ki67 staining confirmed that proliferation in wild type fundic stomach was largely confined to a short region around the isthmus of the gastric gland. Conversely, in the fundic epithelium of $AhCreER^+Brg^{fl/fl}$ mice, Ki67 staining was found to be substantially expanded and distributed throughout the epithelium (Figure 4.7c).

Of note, all hyperplastic lesions observed in the glandular stomach epithelium were found to be located in the body of the stomach. Whilst Brg1 deficient pyloric glands were detected at all time points, they displayed no signs of hyperplasia (Figures 4.6a and 4.7b). Taken together, these observations suggest that long-term Brg1 loss is tolerated in the whole of the glandular stomach epithelium, but induces benign fundic gland polyposis. Brg1 thus appears to act as a tumour suppressor in the fundic, but not pyloric stomach epithelium.

---

[3]Histopathological description of glandular stomach hyperplasia was provided by Prof Geraint T. Williams, Department of Pathology, University Hospital of Wales, Cardiff University, UK
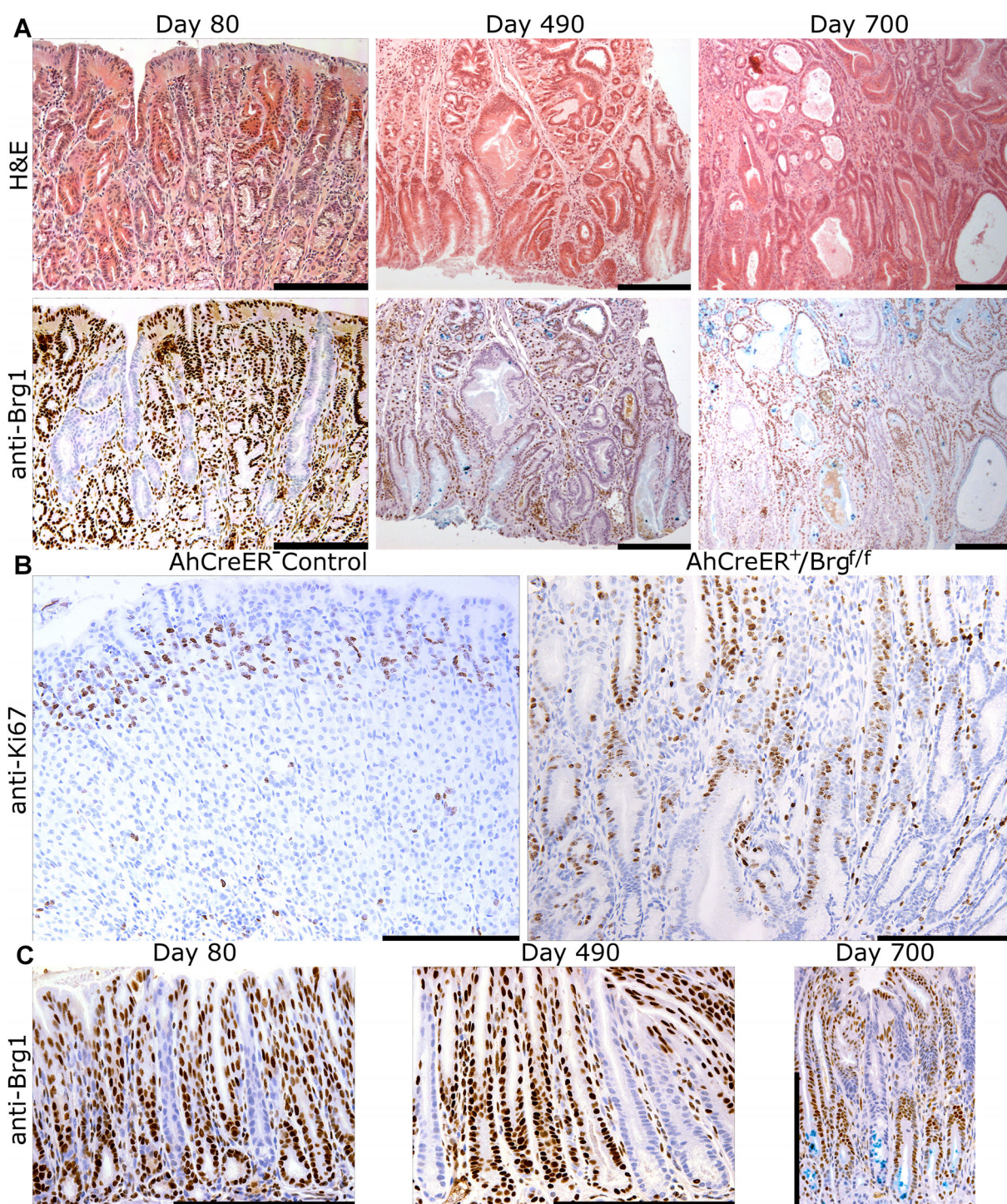
Figure 4.7: Brg1 loss induces gastric gland polyposis in the fundic, but not pyloric stomach. (a) Histological analysis of H&E stained sections of $AhCreER^+Brg^{fl/fl}$ fundic stomach epithelium revealed hyperplastic fundic gland polyps (FGPs) as early as day 80 PI. Analysis of the fundic stomach histology at later time points revealed an increase in polyp size, but no signs of invasive disease. Immunohistochemical analysis of Brg1 expression in $AhCreER^+Brg^{fl/fl}$ fundic stomach revealed a substantial Brg1 deficient component in FGPs. (b) Immunostaining with an antibody against Ki67 revealed an expansion of Ki67 positive cells in the fundic stomach of $AhCreER^+Brg^{fl/fl}$ mice compared to control fundic epithelium, where Ki67 expression was confined to the isthmus region of the gland. (c) Immunohistochemical analysis of Brg1 expression in the pyloric stomach of $AhCreER^+Brg^{fl/fl}$ mice revealed occasional Brg1 deficient glands at all inspected time points. No aberrations in morphology of Brg1 deficient pyloric glands were observed at any time point. Scale bars represent 200 μm.

4.2.3.3   Fundic gland polyposis in Brg1 deficient glandular stomach is not driven by the Wnt/β-catenin, PI3K/AKT, AMPK or p21/Rb pathways

In order to dissect the potential mechanisms leading to polyp formation in Brg1 deficient gastric epithelium, a number of signalling cascades implicated in gastrointestinal polyposis were analysed.

Tumours of a histopathological nature similar to that of Brg1 deficient fundic gland polyps are commonly detected in patients with Familial Adenomatous Polyposis (FAP) and attenuated FAP (AFAP), which are caused by a range of mutations in the *APC* gene (Abraham *et al.*, 2000). Furthermore, sporadic FGPs are frequently found to arise due to activating mutations in β-catenin (Abraham *et al.*, 2001). These observations strongly implicate activation of the Wnt pathway in fundic gland polyposis. Considering the previously reported requirement of functional BRG1 for trans-activation of Wnt pathway target genes (Barker *et al.*, 2001) and the fact that FGPs are commonly driven by activation of the Wnt pathway, makes the observation that Brg1 deficiency induces FGPs highly unexpected. I, therefore, aimed to investigate the state of Wnt signalling in Brg1 deficient FGPs. To this end, sections of glandular stomach from $AhCreER^{+}Brg^{fl/fl}$ mice containing Brg1 deficient FGPs were stained with an antibody against β-catenin (Figure 4.8a). Analysis of β-catenin intracellular distribution in Brg1 deficient FGPs revealed its strong cell membrane localisation in the majority of cells within the lesion (Figure 4.8a, white arrowhead), but with occasional cells exhibiting high levels of cytoplasmic β-catenin (Figure 4.8a, black arrowhead). No cells with distinct nuclear localisation of β-catenin were detected. This pattern of β-catenin distribution suggested that polyp formation was unlikely to be driven by Wnt pathway activation.

Having established that FGPs in the Brg1 deficient stomach epithelium did not display signs of Wnt pathway activation, I attempted to assess the state of other pathways involved in known intestinal polyposis conditions. Loss of the PTEN and LKB1 tumour suppressors have been found to be the genetic lesion underlying Cowden's and Peutz-Jeghers (PJS) syndromes respectively (Jenne *et al.*, 1998; Liaw *et al.*, 1997). Both syndromes have been linked to intestinal polyposis including polyps in gastric epithelium (reviewed in Bronner, 2003). These polyps, however, are histologically distinct from FGPs and are characterised by a more pronounced presence of stromal components. Loss of PTEN and LKB1 results in activation of the PI3K/AKT and AMPK pathways respectively and both pathways have been shown to converge on the mammalian target of rapamycin (mTOR) pathway that controls cell growth and is frequently deregulated in cancers (reviewed in Shackelford and Shaw, 2009). In order to investigate possible activation of the PI3K/AKT and AMPK pathways I assessed phosphorylation status of an mTOR downstream target, ribosomal subunit S6 (Figure 4.8b). Analysis of Brg1 deficient FGPs revealed strong phospho-S6 staining, indicating activation of the mTOR pathway
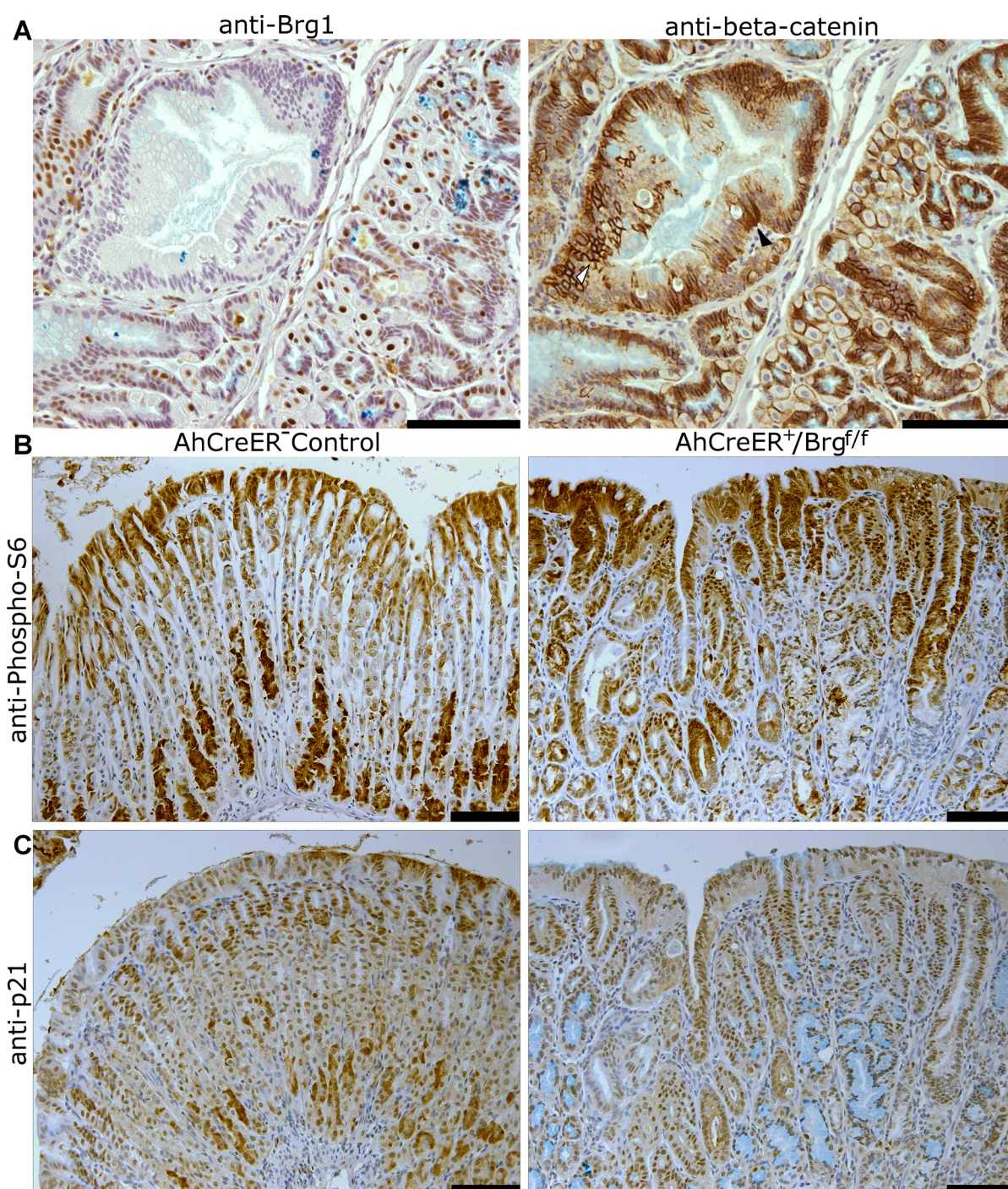
Figure 4.8: Brg1 deficient FGPs display no nuclear accumulation of β-catenin or changes in S6 phosphorylation and p21 expression. **(a)** Immunostaining of serial sections of Brg1 deficient FGPs at day 490 PI with antibodies against Brg1 and β-catenin revealed widespread membrane-associated β-catenin staining (white arrowhead) and occasional cells with elevated cytoplasmic β-catenin (black arrowhead). However, no distinct nuclear localisation of β-catenin was observed. (b,c) Immunohistochemical analysis of S6 phosphorylation **(b)** and p21 expression **(c)** in the fundic stomach at day 80 PI revealed no differences between control and $AhCreER^+Brg^{fl/fl}$ epithelium. Scale bars represent 100 μm.

in Brg1 deficient epithelium. However, a comparable intensity of phospho-S6 staining was observed in the proliferative compartment of wild type gastric glands (Figure 4.8b). It appears unlikely, therefore, that activation of PI3K/AKT or AMPK pathways is responsible for development of FGPs in the gastric epithelium of $AhCreER^{+}Brg^{fl/fl}$ mice.

Finally, Brg1 has been reported to participate in regulation of cell proliferation via control of p21 expression and subsequent Rb-mediated G1 checkpoint (Hendricks *et al.*, 2004; Kang *et al.*, 2004). In order to assess any potential role of the p21/Rb pathway in polyp formation, I analysed expression of p21 in wild type glandular stomach and Brg1 deficient FGPs. Immunohistochemical analysis of p21 expression demonstrated that both normal epithelium and FGPs displayed comparable levels of p21 expression (Figure 4.8c).

Together, these observations suggested that development of Brg1 deficient FGPs in the glandular stomach epithelium of $AhCreER^{+}Brg^{fl/fl}$ mice was unlikely to be mediated by aberrant activation of the Wnt/β-catenin, PI3K/AKT, AMPK or p21/Rb pathways.

4.2.4 Long-term Brg1 loss is tolerated in the large intestinal epithelium and has no oncogenic effect

Having detected no tumourigenic effect of Brg1 haploinsufficiency in the large intestinal epithelium, I aimed to analyse the outcome of complete Brg1 loss in this tissue. This was achieved by conditional deletion of Brg1 using either AhCreER or VillinCre recombinase and subsequent analysis of Brg1 deficient crypts[4]

4.2.4.1 Brg1 deficient cells are retained in the large intestine

In order to analyse the long-term consequences of Brg1 loss in the large intestinal epithelium, mice bearing loxP targeted *Brg1* alleles and *AhCreER* transgene were induced with 5 intraperitoneal injections of 80 mg/kg β-naphthoflavone and tamoxifen along with $AhCreER^{-}$ controls. Mice from both cohorts were then aged and harvested at 35, 80 and 490 days PI, at which point whole large intestines were harvested and processed for histological analysis.

Macroscopic analysis of the large intestinal epithelium at the time of dissection did not reveal any signs of large intestinal tumourigenesis at any of the time points. Immunohistochemical analysis of Brg1 expression in the large intestine of control animals revealed ubiquitous Brg1 expression throughout the epithelium (Figure 4.9). Conversely, analysis of Brg1 expression in the large intestinal epithelium of $AhCreER^{+}Brg^{fl/fl}$ mice at all time points revealed the presence of occasional crypts fully populated by Brg1 deficient cells (Figure 4.9). All Brg1 deficient crypts were indistinguishable from adjacent Brg1 proficient epithelium. They retained normal appearance and displayed no signs of

---

[4]The results presented in this section were obtained with the assistance of Joanna Krzystyniak. Breeding, induction and dissection of experimental animals were conducted by me. Histological and immunohistochemical analysis of tissue sections were conducted by Joanna under my direction and supervision.

AhCreER⁻Control   AhCreER⁺/Brgf/f

Day 35   Day 35   Day 80   Day 490
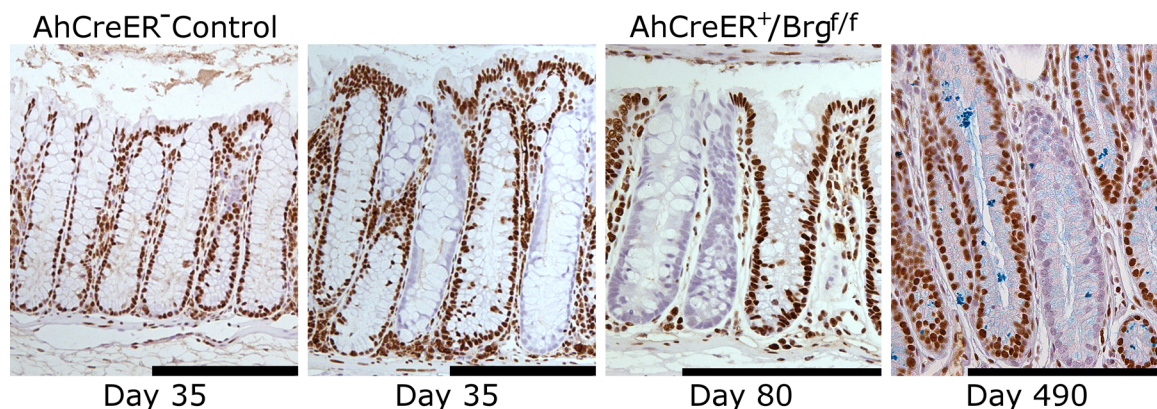
Figure 4.9: Brg1 deficient crypts are retained in the large intestinal epithelium. Immunohistochemical analysis of Brg1 expression in the large intestinal epithelium of $AhCreER^+Brg^{fl/fl}$ mice at day 35, 80 and 490 PI revealed occasional Brg1 deficient crypts. No gross morphological differences were observed between Brg1 deficient and adjacent Brg1 positive crypts. No Brg1 deficient crypts were detected in the large intestinal epithelium of control mice at any time point. Scale bars represent 200 μm.

tumourigenesis even at the latest time point. These observations suggested that Brg1 deficiency has no oncogenic effect in the context of the large intestinal epithelium, at least within the time period observed here.

4.2.4.2 Brg1 deficient large intestinal crypts retain normal levels of Wnt signalling

The long-term retention of Brg1 deficient crypts in the large intestinal epithelium suggested that Brg1 function is dispensable for large intestinal homeostasis. This observation is in apparent contradiction with the established role of Wnt signalling in large intestinal homeostasis (reviewed in Gregorieff and Clevers, 2005) and the proposed requirement of Brg1 for trans-activation of Wnt pathway target genes (Barker *et al.*, 2001). In order to investigate potential effects of Brg1 loss on Wnt signalling in the context of the large intestine, I aimed to analyse expression levels of Wnt target genes in Brg1 deficient crypts. Since AhCreER recombinase induced Brg1 loss with a limited efficiency, I used the VillinCre recombinase transgene to increase the frequency of Brg1 deficient crypts. Induction of $VillinCre^+Brg^{fl/fl}$ animals with a single intraperitoneal injection of 40 mg/kg tamoxifen was sufficient to generate large intestinal Brg1 deficient crypts at a frequency exceeding that observed in $AhCreER^+Brg^{fl/fl}$ mice.

Large intestinal samples from $VillinCre^+Brg^{fl/fl}$ mice were harvested at day 30 PI and subjected to immunohistochemical analysis of the Wnt target genes *c-Myc* and *CD44*. Analysis of serial sections stained with antibodies against Brg1, c-Myc and CD44 detected no discernible differences in Wnt target gene expression between Brg1 deficient and proficient crypts (Figure 4.10a, black and white arrowheads respectively).
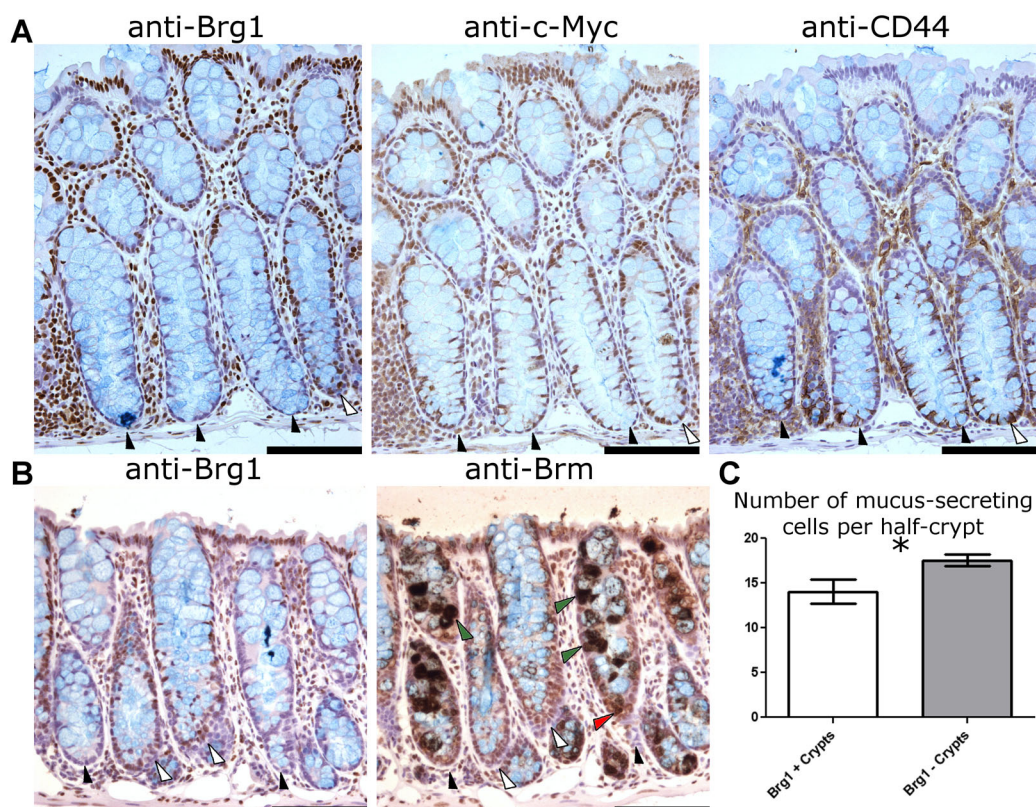
Figure 4.10: Brg1 loss in the large intestinal epithelium is compensated by Brm overexpression. **(a)** Immunohistochemical analysis of expression of the Wnt target genes *c-Myc* and *CD44* in the large intestinal epithelium of $VillinCre^+Brg^{fl/fl}$ mice at day 30 PI revealed no differences in the Wnt target genes expression between Brg1 deficient (black arrowheads) and adjacent Brg1 positive (white arrowhead) crypts. **(b)** Immunohistochemical analysis of Brm expression revealed a substantial increase in Brm levels in Brg1 deficient crypts (black arrowheads) compared to adjacent Brg1 positive tissue (white arrowheads). While occasional cells with prominent nuclear Brm localisation were detected (red arrow), Brm staining was predominantly confined to mucus containing compartment of Goblet cells (green arrows). **(c)** Quantitative analysis of Alcian blue stained sections of the large intestinal epithelium of $VillinCre^+Brg^{fl/fl}$ mice at day 30 PI revealed a significant increase in number of mucus secreting cells in Brg1 deficient crypts compared to adjacent Brg1 positive epithelium (One-Way ANOVA, p=0.017, n=3). Scale bars represent 100 μm. Error bars represent standard deviation.

4.2.4.3 Brg1 deficiency in large intestinal epithelium is compensated by Brm overexpression

The observation that Brg1 loss had no tangible effect on Wnt target gene expression in the large intestinal epithelium could be potentially attributed to a compensatory mechanism that ensured long-term retention of Brg1 deficient crypts. The Brg1 paralogue Brahma (Brm) represents a likely mechanism for such compensation. In order to investigate potential alterations to Brm expression in response to Brg1 deficiency, immunohistochemical analysis of Brm expression was carried out in the large intestinal epithelium of $VillinCre^{+}Brg^{fl/fl}$ mice. Moderate levels of Brm staining were detected throughout the large intestinal epithelium (Figure 4.10b). However, occasional crypts were found to display substantially elevated levels of Brm expression. Analysis of serial sections stained with antibodies against Brg1 and Brm revealed a consistent overlap between Brg1 deficient crypts and crypts with elevated Brm expression (Figure 4.10b, black and white arrowheads respectively). This observation suggested that loss of Brg1 function in the large intestine is likely to be compensated for by elevated levels of Brm expression, which in turn could explain the lack of any detrimental effects of Brg1 deficiency on large intestinal homeostasis and tumourigenesis. Curiously, whilst rare cells with prominent nuclear Brm staining were detected in the lower half of some Brg1 deficient crypts (Figure 4.10b, red arrowhead), elevated Brm staining was most prominent in what appeared to be mucus containing vacuoles of the Goblet cells (Figure 4.10b, green arrowheads). Although some goblet cells in the small intestine exhibited this staining pattern, no excessive Brm staining was detected in Brg1 positive large intestinal Goblet cells.

4.2.4.4 Brg1 loss in the large intestine promotes cell differentiation along mucus producing cells lineages

Having established that Brg1 loss does not compromise long-term crypt survival I set out to analyse more subtle parameters of epithelial homeostasis, namely cell differentiation. The large intestinal epithelium is comprised of three major cell lineages: vacuolated-columnar, Goblet and deep crypt secretory (DCS) cells (Karam, 1999). Of these, Goblet and DCS cells are characterised by mucus secretion and thus can be easily identified by staining with a mucus-affine dye, such as Alcian blue. In order to investigate cellular differentiation along these two lineages, large intestinal tissue sections were stained with Brg1 antibody and counter-stained with Alcian blue dye (Figure 4.10a, leftmost panel). The average number of Alcian blue positive cells per half-crypt was scored in Brg1 deficient and adjacent Brg1 positive crypt (10 pairs per mouse). This analysis was repeated in 3 mice and the overall average was calculated. The average number of Alcian positive cells ($\pm$ standard deviation) was found to be 14.07$\pm$1.39 and 17.53$\pm$0.651 in Brg1 positive and negative crypts respectively (Figure 4.10c). This difference was found to be statistically significant (One-way ANOVA, p=0.017, n=3). This observation suggested that Brg1

deficiency stimulated cell differentiation along the mucus secreting lineages of the large intestinal epithelium.

4.2.5 Long-term Brg1 loss is tolerated in the bladder urothelium and has no oncogenic effect

Bladder, as well as the rest of the genitourinary tract, including renal pelvis, ureter and prostatic urethra is lined with urothelium (traditionally also termed as transitional epithelium), a tissue unique for the urinary tract. Murine urothelium consists of three cellular levels: basal, intermediate and superficial (umbrella) of which only first two maintain direct contact with the basal membrane.The distinctive feature of the transitional epithelium is a substantial elasticity enabling it to accommodate significant changes in surface area (Wu *et al,*. 2009). Off-target-tissue expression of AhCreER recombinase in the bladder urothelium enabled me to investigate the effects of Brg1 loss in this tissue.

4.2.5.1 Brg1 deficient cells are retained in the bladder urothelium over a long period of time

In order to explore the potential consequences of Brg1 deficiency in the bladder urothelium, $AhCreER^{+}Brg^{fl/fl}$ mice along with $AhCreER^{-}$ controls were induced by intraperitoneal injection of 80 mg/kg β-naphthoflavone and tamoxifen. Mice from both cohorts were sacrificed at various time points and whole bladders were harvested and processed for histological analysis. Immunohistochemical analysis of Brg1 expression at day 10 PI revealed ubiquitous Brg1 expression in the bladder urothelium of control mice (Figure 4.11). Conversely, the bladder urothelium of $AhCreER^{+}Brg^{fl/fl}$ mice displayed a substantial loss of Brg1 expression (Figure 4.11). In order to investigate the long-term retention of Brg1 deficient cells in the bladder urothelium, bladder tissue was collected from $AhCreER^{+}Brg^{fl/fl}$ and control mice at day 100 and 490 PI. Immunohistochemical analysis of Brg1 expression revealed efficient retention of Brg1 deficient cells in the bladder urothelium of $AhCreER^{+}Brg^{fl/fl}$ mice even at the latest time point analysed (Figure 4.11). Histological analysis of H&E stained sections of the bladder urothelium revealed no discernible morphological differences between Brg1 deficient and wild type urothelium. No signs of tumourigenesis were detected in either Brg1 deficient or wild type urothelium at any of the time points analysed.
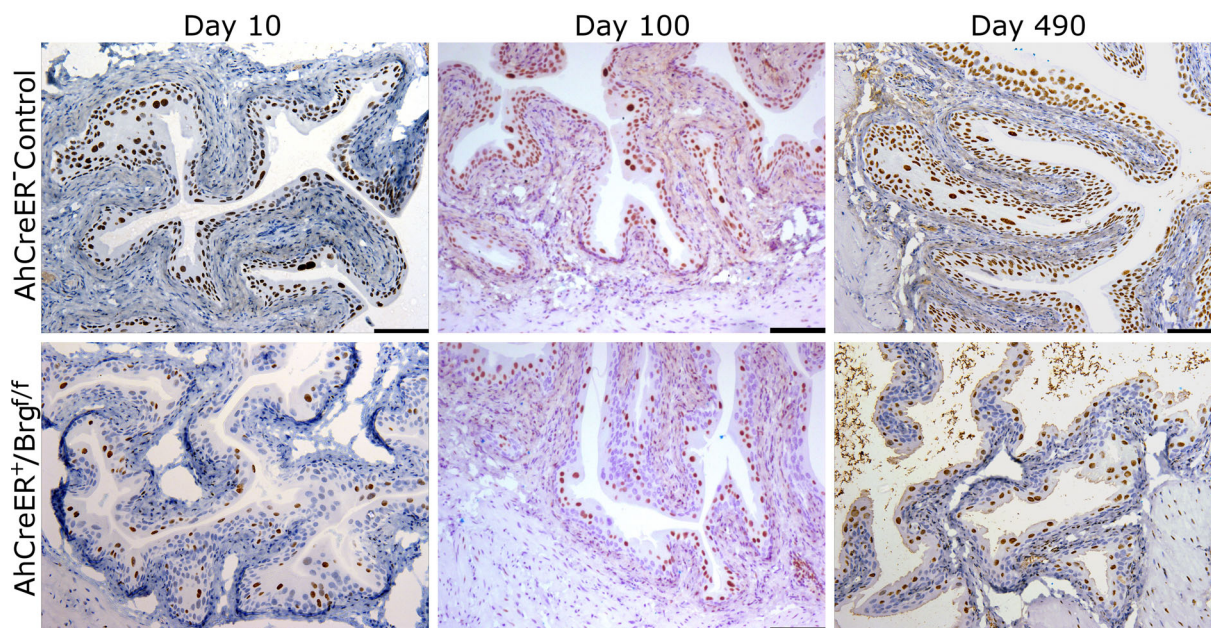
Figure 4.11: Brg1 deficient cells are retained in the bladder urothelium. Immunohistochemical analysis of Brg1 expression in the bladder urothelium of $AhCreER^{+}Brg^{fl/fl}$ mice at day 10, 100 and 490 PI detected a substantial number of Brg1 deficient cells distributed throughout the urothelium at all time points. Occasional Brg1 deficient cells were also detected in the urothelium of control mice albeit at a very low frequency. Scale bars represent 100 μm.

4.3   Discussion

4.3.1   Brg1 haploinsufficiency has no overt oncogenic effect in a subset of tissues expressing AhCre recombinase

A number of studies have suggested that Brg1 haploinsufficiency promotes tumourigenesis in mammary and lung epithelial tissue (Bultman *et al.*, 2007; Glaros *et al.*, 2007). Off-target-tissue expression of AhCre recombinase allowed me to investigate whether Brg1 loss induces tumourigenesis in a subset of epithelial tissues outside of the small intestinal epithelium. In contrast to the aforementioned findings, Brg1 haploinsufficiency failed to induce tumourigenesis in any of the analysed tissues, namely in the forestomach, glandular stomach, large intestine and bladder epithelia over a long period of observation. This observation is not entirely unexpected, since tumourigenesis induced by constitutive heterozygous loss of Brg1 has been found to be limited to the mammary gland epithelium (Bultman *et al.*, 2007). Together with the previously published data, findings presented in this chapter highlight the tissue-dependent ability of Brg1 haploinsufficiency to induce tumourigenesis.

4.3.2   Brg1 loss induces the development of benign tumours in epithelial tissues of the murine stomach

AhCreER recombinase expression in the epithelium of murine glandular and forestomach enabled me to investigate the effects of Brg1 loss in these tissues. The data presented in this chapter suggest that Brg1 loss results in early onset hyperplasia of murine stomach epithelium. Rather surprisingly, Brg1 loss induced formation of benign lesions in both parts of the stomach, despite their lining being represented by considerably distinct types of epithelium: simple columnar and keratinised stratified squamous epithelium in glandular and forestomach respectively (Karam, 1999). According to their respective tissues of origin, Brg1 deficient lesions were identified as squamous cell papillomas in the forestomach and fundic gland polyps in the glandular stomach epithelium. Interestingly, while Brg1 haploinsufficiency has been implicated in mammary tumourigenesis (Bultman *et al.*, 2007) and numerous studies have reported the presence of Brg1 mutations in cancer cell lines and primary tumours (Becker *et al.*, 2009; Reisman *et al.*, 2003; Wong *et al.*, 2000), no reports have demonstrated tumourigenesis as a direct consequence of Brg1 loss. Moreover, some reports have indicated that Brg1 loss in physiologically sound tissue may have an adverse effect on cancer initiation by inducing apoptosis (Glaros *et al.*, 2008, Wang *et al.*, 2009). Results presented in this chapter provide the first evidence that Brg1 loss directly induces tumourigenesis in the epithelial tissues of the murine stomach.

Despite the distinct tissues of origin and histopathological appearance of the tumours, Brg1 deficient lesions from both sections of the murine stomach shared a number of common characteristics. Brg1 deficient lesions appeared in both tissues within a similar time frame (between 35 and 80 days post induction) and tumours from both tissues remained benign for an extensive period of time (up to 700 days post induction). Although lesions from the two tissues shared a number of common features, it could not be conclusively demonstrated whether hyperplasia in both tissues was driven by a common signalling pathway. While some evidence suggested that the hyperproliferative response in either tissue was unlikely to rely on activation of Wnt, PI3K/AKT or AMPK signalling cascades, some data indicated that forestomach, but not glandular stomach hyperplasia was likely to be driven by reduced levels of p21, a negative cell cycle regulator.

It is worth noting that aberrant activation of a range of rather distinct signalling pathways have been implicated in similar hyperproliferative responses in glandular and forestomach epithelia. Simultaneous deletion of Pten and knock-in of an activated form of K-Ras (further referred to as Pten/K-Ras) oncogene results in development of squamous cell papillomas in the forestomach epithelium (Marsh *et al.*, in preparation). Notably, despite Pten loss and K-Ras activation having been widely implicated in the aberrant activation of PI3K/AKT and MEK/ERK pathways respectively (reviewed in McCubrey *et al.*, 2006), forestomach lesions from this model displayed no elevation in phosphorylated Akt and only a limited increase in MEK phosphorylation. Consistent with this, histo-

logically similar papillomas from Brg1 deficient forestomach epithelium failed to exhibit increased phosphorylation of S6 ribosomal subunit, which acts as a downstream target of PI3K/AKT pathway activation. However, an in depth analysis of MEK/ERK pathway activation status would be necessary to eliminate the possibility of MEK/ERK driven tumourigenesis in Brg1 deficient forestomach epithelium. In contrast to Brg1 deficient and Pten/K-Ras papillomas, the simultaneous inactivation of Pten and the TGFβ/BMP component Smad4 in murine forestomach has been reported to result in forestomach hyperplasia rapidly progressing to invasive squamous cell carcinoma (Teng *et al.*, 2006). In contrast to Pten/K-Ras deficient forestomach tumours, Pten/Smad4 double knock-out tumours displayed a drastic increase in the levels of phosphorylated Akt in line with their more aggressive nature. Interestingly, Pten/Smad4 double knock-out tumours displayed a substantial decrease in p21 expression levels, not dissimilar to the situation observed in Brg1 deficient tumours. Brg1 has been shown to mediate cell growth arrest via positive control of p21 expression and subsequent hypophosphorylation of RB protein (Hendricks *et al.*, 2004; Kang *et al.*, 2004). It appears, therefore, that Brg1 loss in the forestomach epithelium partially relaxes proliferative control over the tissue, most likely by compromising p21 expression. It should be noted, however, that expression analysis of pRb/E2F transcription targets, such as Cyclins A and E2, would be required to conclusively demonstrate that Brg1 loss induces such a relaxation of cell cycle control. The hyperproliferative response to Brg1 loss, however, is probably not sufficient to drive tumour progression to advanced stages over a substantial period of observation. Loss of another tumour suppressor, such as Pten or an oncogene activation, such as K-Ras might be required to advance Brg1-deficiency-induced tumourigenesis to aggressive disease.

Since non-keratinised squamous epithelium is shared by murine forestomach and oesophagus, the murine forestomach is a potentially attractive model tissue for human oesophageal neoplasia. However, some differences exist between the two tissues that need to be considered when developing mouse cancer models. Despite a lack of direct evidence, a number of observations indicate that Brg1 might play a differential tumour suppressor role in forestomach and oesophageal epithelia. Mouse models that induce tumourigenesis of the oesophagus are characterised by very short survival, due to early obstruction of alimentary tract and animal death from starvation (Teng *et al*,. 2006). An earlier observation has suggested that AhCreER recombinase is successfully induced in the oesophageal epithelium by an induction protocol similar to the one used in this work (Meniel, personal communication). Although no deliberate pathological analysis of oesophagus nor confirmation of Brg1 loss in oesophageal epithelium was conducted in this study, a number of observations indicate that Brg1 loss does not induce tumourigenesis in the oesophageal epithelium. Firstly, mice with Brg1 loss under control of AhCreER recombinase were able to survive for an extended period of time with no sign of weight loss. Secondly, no macroscopic abnormalities of oesophagus were detected at the time of dissection, while distinguishable overgrowth of epithelium was clearly visible in the forestomach of the same

mice. Together, these observations suggest that Brg1 loss specifically induces hyperplasia of the forestomach, but not in the oesophageal epithelium. This 'organ-specificity' of Brg1-loss-induced tumourigenesis is in apparent contrast with a number of previous reports that described tumour initiation in both organs upon tissue-specific loss of tumour suppressors or oncogene activation (Teng *et al.*, 2006; Vitale-Cross *et al.*, 2004). However, it may be a consequence of subtle differences in homeostasis and tumourigenesis between the two organs sharing the same type of epithelium. Apparent preference for Brg1 loss-driven tumourigenesis in forestomach, but not oesophagus, therefore, highlights potential differences in homeostasis of these tissues, which should be considered, when using murine stomach as a model tissue for oesophageal cancer.

Fundic gland polyps (FGPs) are hamartomatous lesions that develop in the mucosa of the body (fundus) of the stomach and are characterised by shortening of the gastric pits and cystic dilation of the gastric glands (Wu *et al.*, 1998). FGPs are composed of the cell types normally present in the normal fundic mucosa with cysts mainly lined with parietal and chief cells. While sporadic FGPs rarely undergo dysplastic transformation, FGPs in FAP patients frequently display neck cell and surface epithelial dysplasia (Wu *et al.*, 1998). The FGPs observed in the glandular stomach of $AhCreER^{+}Brg^{fl/fl}$ mice closely resembled this histopathological description, including dysplastic transformation of the surface epithelium being detected at late time points. These observations indicate that activation of Wnt signalling might be involved in the development of Brg1 deficient FGPs. This notion, however, is highly unexpected in the light of the proposed requirement of Brg1 for trans-activation of the Wnt target genes. Indeed, analysis of subcellular β-catenin localisation failed to detect nuclear β-catenin in Brg1 deficient FGPs. It is unlikely, therefore, that Wnt signalling activation is involved in the development of FGPs in the Brg1 deficient glandular stomach.

Whilst FGPs represent the most common gastric lesion type, a number of other inherited polyposis syndromes are also characterised by the development of gastric polyps. The most common of them are Peutz-Jeghers syndrome (PJS), Juvenile Polyposis Syndrome (JPS) and Cowden Syndrome (CS). It should be noted, however, that polyps arising in these conditions substantially differ from the FGPs observed in Brg1 deficient gastric epithelium. PJS polyps are characterised by frond-like overgrowth of otherwise normal epithelium and an abundance of smooth muscle tissue, which forms tree-like structures. Both JPS and CS share a common histological appearance and are characterised by the presence of inflamed stromal tissue (reviewed in Bronner *et al.*, 2003). The genetic aberrations underlying these syndromes were found to be inactivating mutations in LKB1, SMAD4 or BMPR1A and PTEN in PJS, JPS and CS respectively (Houlston *et al.*, 1998; Jenne *et al,.* 1998; Liaw *et al.*, 1997; Zhou *et al.*, 2001). Notably, loss of function of LKB1 and PTEN has been shown to result in activation of AMPK and PI3K/AKT pathways respectively. These two pathways have been found to converge on a common effector – mTOR pathway involved in control of protein synthesis, cell growth and sur-

vival (reviewed in Shackelford and Shaw, 2009). In order to explore potential activation of mTOR signalling as a mechanism responsible for the development of Brg1 deficient FGPs phosphorylation levels of mTOR downstream target ribosomal subunit S6 were analysed. However, no consistent difference in S6 phosphorylation was observed between proliferative isthmal region of wild type gastric epithelium and Brg1 deficient FGPs. Having said that, positive staining for phosphorylated S6 was more widespread in FGPs in line with the expanded proliferative compartment. This observation indicates that the mTOR pathway is active in proliferating cells of Brg1 deficient FGPs, but does not necessarily suggest that its hyperactivation acts as a driving force behind Brg1 deficiency-induced polyposis.

Finally, Brg1 has been reported to be involved in regulation of pRB-mediated cell cycle control by facilitating p21 expression. Loss of Brg1 in the gastric epithelium could, therefore, relax control over the cell cycle by attenuating p21 expression. This notion is particularly attractive in the light of the observed pattern of Ki67 expression in Brg1 deficient gastric epithelium. Ki67 staining was detected throughout enlarged fundic gland neck region. Notably, this region in wild type fundic glands is occupied by early progenitors of the cell lineages derived from the isthmal stem cell. It is, therefore, tempting to hypothesise that compromised exit from the cell cycle in this region would result in expansion of the proliferative compartment. Despite the attractiveness of this hypothesis, immunohistochemical analysis of p21 expression in Brg1 deficient FGPs found no evidence of reduced p21 expression compared to gastric epithelium of control mice. Interestingly, proliferating cells in Brg1 deficient FGPs were found to express p21 at levels comparable to that of differentiated cells of the wild type gastric epithelium. It appears, therefore, that hyper-proliferating Brg1 deficient cells were able to overcome the cell cycle control constraints imposed by the p21/pRb pathway. A similar overlap between expression of proliferative markers and p21 expression has been found to be characteristic of human FGPs displaying dysplasia of the gastric pit and surface epithelia (Wu *et al.*, 1998).

Taken together, the data presented in this chapter show that Brg1 loss drives benign hyperplasia in the glandular and forestomach epithelium. The oncogenic effect of Brg1 loss in these two tissues is, however, likely to be mediated by different mechanisms. While attenuated p21 expression in the hyperplastic forestomach epithelium implied alleviation of p21/pRb mediated cell cycle arrest as a potential driving force behind the squamous cell hyperplasia, no obvious candidate signalling cascade was found in case of the glandular stomach epithelium.

4.3.3 Long-term Brg1 loss is tolerated in the large intestinal and bladder epithelial tissue and has no tumourigenic effect

Having established that Brg1 loss induces benign hyperplasia in the epithelial tissues of the murine stomach I aimed to explore the impact of Brg1 deficiency on two more ep-

ithelial tissues expressing AhCreER recombinase, namely the large intestine and bladder. Immunohistochemical analysis of Brg1 expression detected retention of Brg1 deficient cells over a long period of observation.

Retention of Brg1 deficient cells in the bladder urothelium of $AhCreER^+Brg^{fl/fl}$ mice at 100 days PI could be attributed to the extremely slow turnover rate of this tissue (approximately 200 days) and associated low proliferation rate (Wu *et al.*, 2009). However, Brg1 deficient cells were still present in the bladder urothelium at day 490 PI, suggesting that Brg1 is likely to be dispensable for urothelium proliferation. Interestingly, a recent study have shown that activation of the Wnt pathway stimulates basal cell proliferation of the bladder epithelium in response to bacterial infection or chemical injury (Shin *et al.*, 2001). Although it is not clear whether the Wnt pathway drives physiological proliferation of the bladder epithelium, long-term retention of Brg1 deficient cells suggests that Brg1 is likely to be dispensable for Wnt signalling in the urothelium.

Retention of Brg1 deficient crypts in the large intestinal epithelium also highlights dispensability of Brg1 for large intestinal homeostasis. However, unlike in the urothelium, Wnt signalling has a long established role in maintaining the proliferative compartment of both the large intestinal epithelium and colorectal cancer (reviewed in de Santa Barbara *et al.*, 2003). It can therefore be extrapolated that the Wnt pathway in the large intestine does not require Brg1 for its physiological activity. Consistent with this notion, expression levels of the Wnt target genes *c-Myc* and *CD44* were found to be undistinguishable between Brg1 deficient and proficient crypts. This finding is in apparent contradiction with the proposed role of Brg1 in trans-activation of the Wnt target genes even more so considering that the original observation was made in CRC cells (Barker *et al.*, 2001). A number of factors could contribute to the discrepancy between the reliance of Wnt signalling of Brg1 function in cultured CRC cell and the lack of phenotype in Brg1 deficient large intestinal epithelium. The most likely explanation of such discrepancy is a dose-dependent reliance of Wnt signalling on Brg1 function. Whilst Brg1 is required to facilitate high levels of Wnt-driven transcription found in CRC cells, its requirement for physiological levels of Wnt signalling might be less stringent. In support of this hypothesis, Brm expression was found to be up-regulated in Brg1 deficient large intestinal crypts. It is plausible, therefore, that increased Brm expression is capable of maintaining physiological levels of Wnt signalling and thus compensate for Brg1 deficiency. Notably, the cell line used by Barker *et al.* (2001) to demonstrate Brg1 requirement for transcriptional activation of Wnt target genes also has been reported to express Brm at high levels (Watanabe *et al.*, 2010), suggesting that in the context of constitutively activated Wnt signalling Brm is unable to compensate for Brg1 loss. Interestingly, constitutive Brm knock-out mice are viable and fertile, which is thought to be due to compensation by up-regulated Brg1 (Reyes *et al.*, 1998). This compensation appears to be unidirectional as constitutive loss of Brg1 results in embryonic lethality (Bultman *et al.*, 2000). Data presented in this chapter suggest that Brm is capable of compensating for Brg1 loss at

the tissue level under physiological conditions. Concomitant deletion of Brm and Brg1 in the large intestinal epithelium would be insightful in establishing the overall role of SWI/SNF-mediated chromatin remodelling in large intestinal homeostasis.

While little evidence exists that would conclusively associate differentiation of particular large intestinal cell lineages with specific signalling cascades, extrapolation of the data available for the small intestinal epithelium would implicate active Wnt and Notch signalling in the differentiation of secretory and absorptive lineages respectively (reviewed in Crosnier *et al.*, 2006). Following this extrapolation, the increase in the number of secretory cells in Brg1 deficient crypts suggests either increased Wnt or suppressed Notch signalling. The first option, however, appears contradictory to the proposed relationship between Brg1 and Wnt signalling and the observation of normal expression levels of the Wnt target genes detected in Brg1 deficient crypts. Although a number of studies have implicated Brg1 containing complexes in the mediation of Notch signalling, such interaction has not been reported in the intestinal epithelium (Lamba *et al.*, 2008; Takeuchi *et al.*, 2007). Notably, an earlier study has reported preferential recruitment of Brm, but not Brg1 to the promoters of the Notch target genes *Hes1* and *Hes5* in mouse erythroleukemia cells (Kadam and Emerson, 2003). However the putative Notch pathway suppression in Brg1 deficient cells with substantially upregulated Brm expression makes such interaction in the large intestinal epithelium unlikely.

Curiously, one more tissue was found to tolerate long-term Brg1 loss without displaying any signs of tumourigenesis. Brg1 deficient glands were detected in the pyloric stomach of $AhCreER^{+}Brg^{fl/fl}$ mice at all the time points observed. These glands appeared indistinguishable from their Brg1 positive neighbours and pyloric crypts in the glandular stomach of control mice. Low frequency of Brg1 deficient pyloric glands, however prevented any detailed investigation of the effects of Brg1 deficiency on pyloric homeostasis.

Taken together, the findings presented in this and previous chapters highlight a remarkable tissue-specificity of Brg1 functions. These range from requirement for the stem cell maintenance in the small intestine to tumour suppression in glandular and forestomach, to potentially very subtle alterations of tissue homeostasis in the large intestine and bladder.

4.3.4   Future directions

Remarkably, Brg1 loss was found to induce hyperplasia of both the forestomach squamous and glandular stomach columnar epithelium. These were the only two tissues expressing AhCreER recombinase that displayed any signs of tumourigenesis induced by Brg1 deficiency. While observation of p21 suppression in Brg1 deficient forestomach papillomas suggested a putative mechanism for Brg1 loss-driven hyperplasia in this tissue, no such mechanism was evident in the fundic stomach epithelium. In view of these findings being the first evidence of direct oncogenic effect of Brg1 deficiency it would be insightful to

further investigate molecular events upon Brg1 loss in these tissues.

Chapter 5

Investigating the effects of small intestinal Brg1 loss in the context of activated Wnt signalling

5.1 Introduction

Despite the Wnt pathway being aberrantly activated in more than 90% of CRC cases, therapeutic approaches targeted against this pathway remain extremely limited (Goss and Kahn, 2011). A number of reasons are regarded to contribute to the scarcity of Wnt targeted therapies. Among them are the pathway complexity, redundancy between its components and its indispensability for maintenance of adult tissue homeostasis (Reviewed in Clevers, 2006). Despite the pathway complexity and diversity of its components, the vast majority of mutations leading to aberrant Wnt signalling activation in CRC involves either components of the destruction complex (e.g. APC and AXIN) or β-catenin (Paul and Dey, 2008). For this reason therapeutic targets downstream of β-catenin represent a particular interest. These include both pathway components, such as TCF1 and TCF4 (van de Wetering *et al.*, 2002), and Wnt target genes, such as c-Myc (Sansom *et al.*, 2007b). Targeting downstream components and target genes of the pathway may also impart an additional benefit of reducing toxicity to normal tissues.

The observation that BRG1 interacts with β-catenin and is required for trans-activation of Wnt target genes in CRC cells (Barker *et al.*, 2001) establishes BRG1 as a potential therapeutic target in Wnt driven tumourigenesis. The downstream position of Brg1 in relation to β-catenin makes it a particularly attractive target due to the reasons outlined above. In this chapter I aim to inspect the feasibility of Brg1 as an anti-Wnt therapeutic target by investigating the impact of Brg1 deficiency on Wnt driven carcinogenesis in the context of the murine small intestinal epithelium.

5.2 Results

5.2.1 Placing Brg1 loss in a context of aberrant Wnt signalling

In order to place Brg1 deficiency in the context of aberrant Wnt signalling, I aimed to simultaneously inactivate Apc and Brg1 in the small intestinal epithelium. To this end, I used the Cre/loxP conditional transgenesis system, employing a range of Cre recombinases to drive inactivation of the loxP targeted *Brg1* and *Apc* alleles. The effects of conditional inactivation of Brg1 have been described in Chapter 3. The targeted *Apc* allele I use here carries two loxP sites flanking exon 14 (Figure 2.1b). Cre recombinase-mediated recombination between these loxP sites introduces a frame-shift mutation and results in the expression of a truncated version of Apc effectively inducing loss of function (Shibata *et al.*, 1997).

5.2.2 Brg1 haploinsufficiency does not accelerate Wnt-driven tumourigenesis

A number of studies have demonstrated that tumours arising in animals with heterozygous loss of Brg1 retain functional copy of Brg1 (Bultman *et al,.* 2007; Glaros *et al.*, 2008). This observation indicates that Brg1 haploinsufficiency rather than loss of heterozygousity contributes to carcinogenesis in those animals. Heterozygous inactivation of Brg1 in the small intestinal epithelium described earlier in this work failed to induce tumourigenesis or indeed any adverse effects on tissue homeostasis. I, therefore, aimed to examine whether Brg1 haploinsufficiency would be able to accelerate Wnt-driven tumourigenesis. Heterozygous inactivation of Apc is a well established approach for induction of Wnt-driven tumourigenesis in the gastrointestinal tract. Spontaneous loss of the second copy of *Apc* results in the development of aberrant crypt foci, which then progress to adenomas. With this in mind, I generated two cohorts of mice expressing AhCre recombinase. Mice in the first cohort carried one targeted *Apc* allele, while mice from the second cohort carried loxP sites within one of the *Apc* and one of the *Brg1* alleles. Both $AhCre^+Apc^{+/fl}Brg^{+/+}$ and $AhCre^+Apc^{+/fl}Brg^{+/fl}$ mice were viable and fertile.

In order to examine the effects of Brg1 haploinsufficiency on the survival of mice with heterozygous inactivation of Apc, mice from both cohorts along with the $AhCre^+Apc^{+/+}$-$Brg^{+/+}$ controls (for all cohorts n≥9) were induced with four intraperitoneal injections of 80 mg/kg β-naphthoflavone at 8 hour intervals and regularly inspected for signs of intestinal tumourigenesis. Mice were then aged for a maximum of 600 days or until they developed signs of ill health due to extensive tumour burden and had to be sacrificed. While very few mice from the control cohort displayed signs of ill health within the time frame of the experiment, both $AhCre^+Apc^{+/fl}Brg^{+/+}$ and $AhCre^+Apc^{+/fl}Brg^{+/fl}$ mice started developing signs of intestinal neoplasia and becoming ill as early as 245 and 330 days post induction respectively. However, analysis of the overall survival probability re-

vealed no statistically significant difference between the two experimental cohorts (Figure 5.1, median survival 345 and 371 days for $AhCre^+Apc^{+/fl}Brg^{+/+}$ and $AhCre^+Apc^{+/fl}Brg^{+/fl}$ mice respectively, Log-Rank test p=0.22, n≥9).
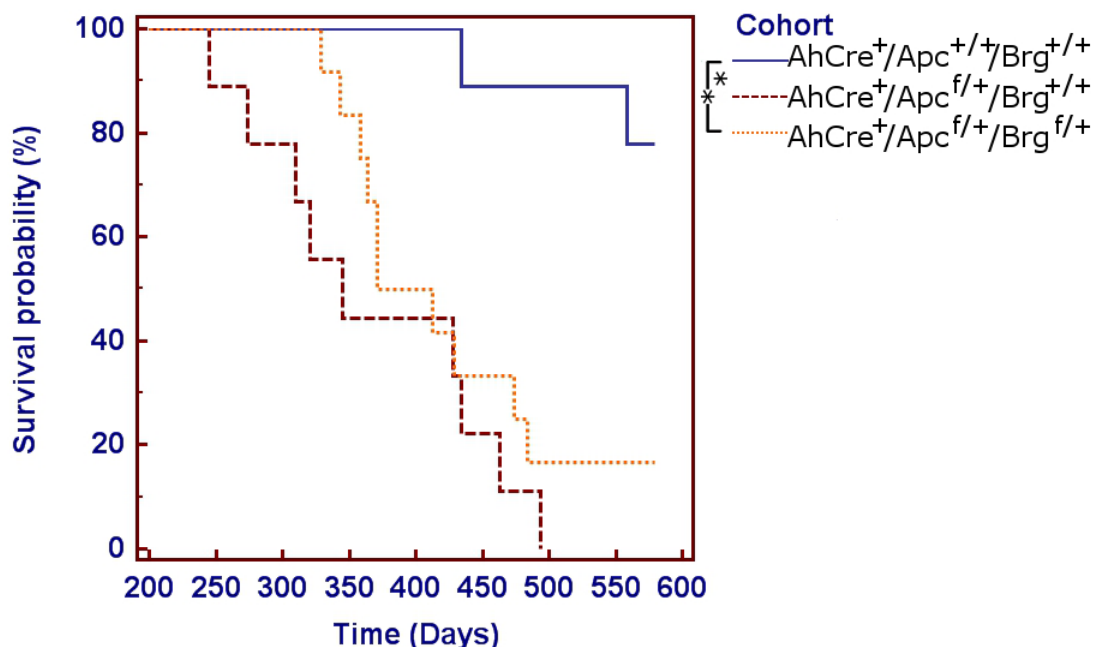
Figure 5.1: Brg1 haploinsufficiency does not impair survival of mice with heterozygous Apc loss. Cohorts of $AhCre^+Apc^{+/fl}Brg^{+/fl}$ and $AhCre^+Apc^{+/fl}Brg^{+/+}$ mice were induced with an appropriate protocol along with $AhCre^+Apc^{+/+}Brg^{+/+}$ control animals (n≥9). Mice were aged for 600 days PI or until have displayed signs of ill health. Survival data was presented as a Kaplan-Meier plot. Analysis of survival probability revealed a significantly reduced survival of $AhCre^+Apc^{+/fl}Brg^{+/fl}$ and $AhCre^+Apc^{+/fl}Brg^{+/fl}$ mice compared to control animals (for either cohort p<0.01, n≥9). No significant difference in survival probability was observed between two experimental cohorts (p=0.22, n≥9).

In order to analyse whether Brg1 haploinsufficiency affected Wnt-driven tumourigenesis in mice with heterozygous loss of Apc, the alimentary tract of $AhCre^+Apc^{+/fl}Brg^{+/+}$ and $AhCre^+Apc^{+/fl}Brg^{+/fl}$ animals was dissected at the time of sacrifice and analysed for parameters such as tumour number, size and position within the small and large intestines (Figure 5.2). Statistical analysis of these parameters revealed no significant difference between the two cohorts (Table 5.1).

Histological analysis of H&E stained sections of the tumours arising in the small and large intestinal epithelium of $AhCre^+Apc^{+/fl}Brg^{+/+}$ and $AhCre^+Apc^{+/fl}Brg^{+/fl}$ animals identified them as adenomas and detected no tangible differences in the tumour progression between the two cohorts (Figure 5.3, left panel). Immunohistochemical analysis of β-catenin expression showed that the tumours in both cohorts displayed nuclear localisation of β-catenin, indicating aberrant activation of Wnt signalling (Figure 5.3, middle panel). Staining with anti-Brg1 antibody revealed that all analysed tumours retained Brg1 expression (Figure 5.3, right panel) indicating that, at least at this stage in tumour development, there was no selective pressure favouring loss of the second Brg1 allele. At the same time, recombined PCR analysis of DNA extracted from tumour tissue detected retention of recombined allele in both small and large intestinal tumours (Fig-

Table 5.1: Analysis of small and large intestinal tumour burden observed in $AhCre^{+}$-$Apc^{+/fl}Brg^{+/+}$ and $AhCre^{+}Apc^{+/fl}Brg^{+/fl}$ mice

	Parameter	Cohort	Median	Mean	SD	p Value
Small intestine	Tumour Number	Apc Het	7.00	9.22	8.23	0.06
		Double	4.00	4.00	2.76	
	Tumour Size (mm2)	Apc Het	12.57	18.58	19.75	0.51
		Double	12.57	19.54	17.20	
	Tumour Position (cm from stomach)	Apc Het	26.90	24.83	14.41	0.10
		Double	12.00	17.64	15.17	
Large intestine	Tumour Number	Apc Het	4.00	4.67	3.61	0.29
		Double	2.00	3.55	4.50	
	Tumour Size (mm2)	Apc Het	12.57	22.67	20.72	0.61
		Double	12.57	14.61	10.00	
	Tumour Position (cm from rectum)	Apc Het	2.05	2.27	1.13	0.90
		Double	2.00	1.97	0.84	

$AhCre^{+}Apc^{+/fl}Brg^{+/+}$ (labelled here as **Apc Het**) and $AhCre^{+}Apc^{+/fl}Brg^{+/fl}$ (labelled here as **Double**) mice were aged for up to 600 days PI or until have dispalyed signs of ill health. The small and large intestines were dissected and inspected for macroscopic signs of tumourigenesis. Parameters of tumour burden, such as tumour number, size and position were recorded. p value was calculated by Mann-Whitney U test for Tumour Number and Mood's Median Test for Tumour Size and Position. Experimental units are represented by number of individual mice per group for Tumour Number and number of individual tumours per group for Tumour Size and Position
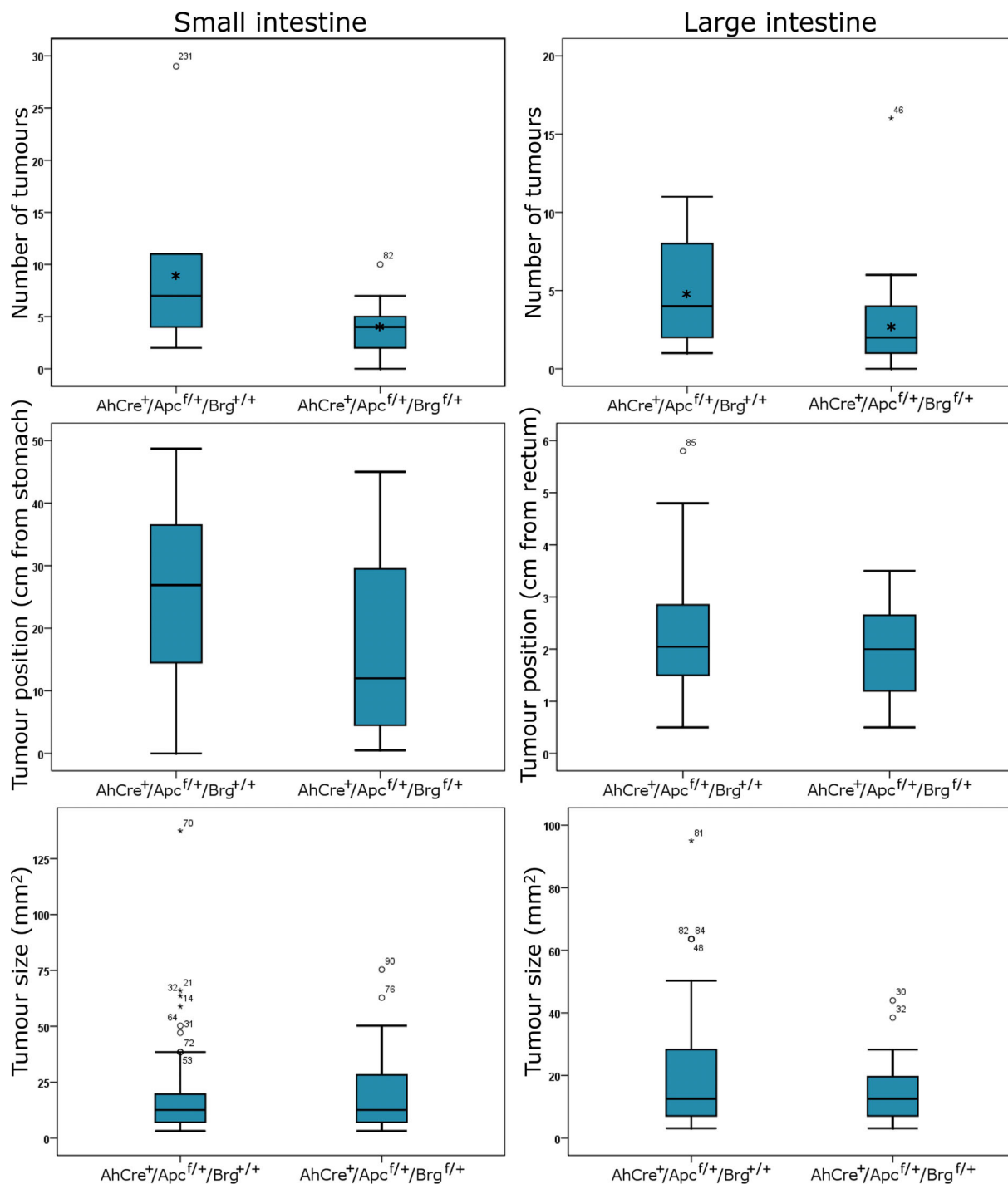
Figure 5.2: Brg1 haploinsufficiency does not affect intestinal tumourigenesis in mice with heterozygous Apc loss. Tumour burden was analysed in the small and large intestinal epithelium of $AhCre^+Apc^{+/fl}$-$Brg^{+/+}$ and $AhCre^+Apc^{+/fl}Brg^{+/fl}$ animals at the time of death. Statistical analysis of tumour burden parameters, such as tumour number, size and position, revealed no significant differences between the cohorts. Data is presented in the form of a Box Plot. Mean value for tumour number is marked with an asterisk. Outliers on the graphs with tumour number represent values for individual mice. Outliers on the graphs with tumour size and positions represent values for individual tumours. Exact values for each parameter's mean, median and standard deviation, along with p values (experimental units are represented by mice for tumour number and individual tumours for tumour size and position) are provided in Table 5.1.

ure 5.4). Together with the lack of difference in survival and tumour progression, these observations indicated that Brg1 haploinsufficiency neither attenuated nor accelerated Wnt-driven carcinogenesis in the small and large intestinal epithelium.
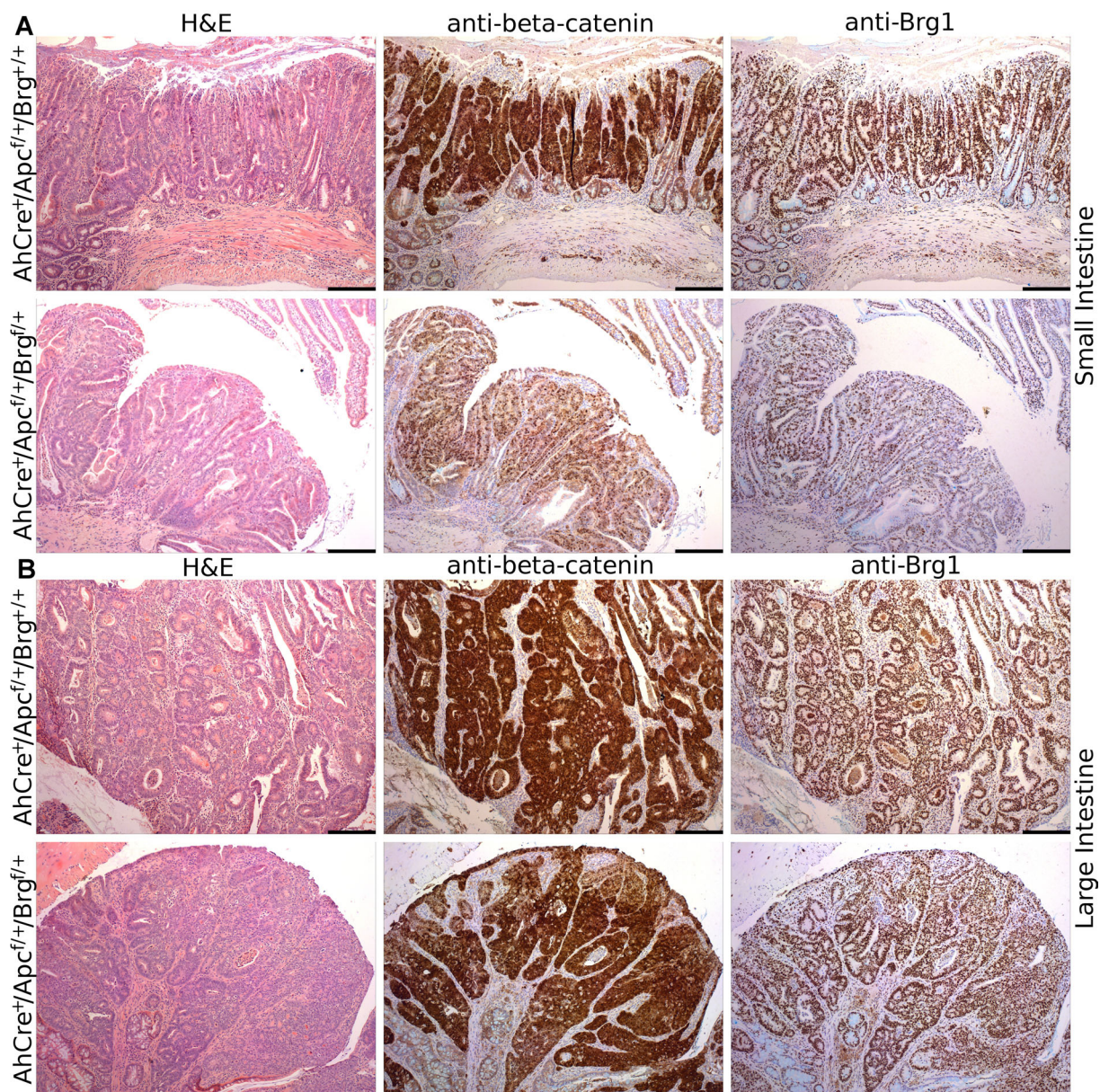
Figure 5.3: Brg1 haploinsufficiency does not affect tumour progression in mice with heterozygous loss of Apc. Histological analysis of H&E stained sections of small **(a)** and large **(b)** intestinal tumours from $AhCre^{+}Apc^{+/fl}Brg^{+/+}$ and $AhCre^{+}Apc^{+/fl}Brg^{+/fl}$ mice dissected at comparable time points revealed no differences in tumour progression between the groups. All macroscopic tumours from either group displayed nuclear localisation of β-catenin and retained Brg1 expression. Scale bars represent 100 μm.

5.2.3   Brg1 loss under the control of AhCreER recombinase is incompatible with Wnt activation

Since homozygous Brg1 loss under the control of AhCre recombinase caused embryonic lethality, I induced loss of Apc alone and in conjunction with Brg1 using the *AhCreER* transgene. To induce Cre recombinase expression and activation, mice were administered
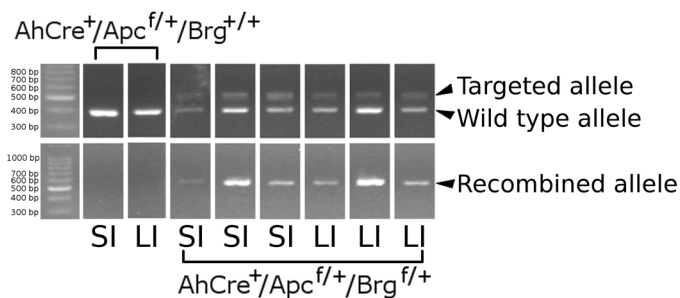
Figure 5.4: Brg1 heterozygous cells are retained in the intestinal tumours of $AhCre^+Apc^{+/fl}Brg^{+/fl}$ mice. A PCR reaction designed to detect the product of recombination of loxP sites in the targeted *Brg1* allele was carried out using DNA extracted from formalin fixed small and large intestinal tumours from $AhCre^+Apc^{+/fl}Brg^{+/+}$ and $AhCre^+Apc^{+/fl}Brg^{+/fl}$ mice dissected at various time points. Primers used for routine genotyping were used as a positive control to test for the presence of DNA in the sample and to confirm the genotype of the animal (407 bp and 500 bp products are amplified from the wild type and targeted *Brg1* alleles respectively, top section). Recombination-specific product (484 bp, bottom panel) was detected in all intestinal tumours from $AhCre^+Apc^{+/fl}Brg^{+/fl}$ mice. No recombination product was detected in the tumours from $AhCre^+Apc^{+/fl}Brg^{+/+}$.

five bi-daily doses of 80 mg/kg β-naphthoflavone and tamoxifen. Animals were sacrificed 10 days post induction and their small intestines were harvested for histological analysis.
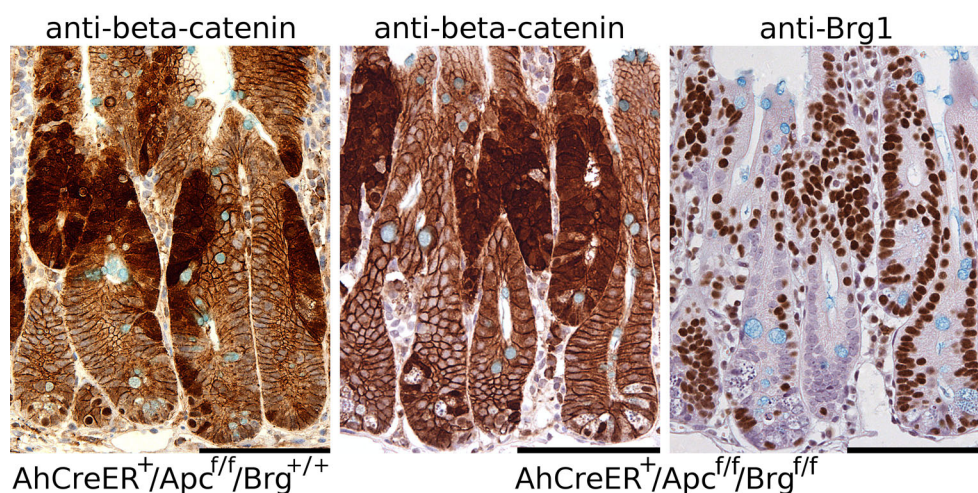
Figure 5.5: Brg1 loss is incompatible with Wnt signalling activation in the stem and early progenitor cells in small intestinal epithelium. Immunohistochemical analysis of β-catenin expression revealed numerous lesions with nuclear localisation of β-catenin in the small intestinal epithelium of $AhCreER^+$-$Apc^{fl/fl}Brg^{+/+}$ and $AhCreER^+Apc^{fl/fl}Brg^{fl/fl}$ mice at day 10 PI. Immunostaining of serial sections with antibodies against Brg1 and β-catenin revealed a non-overlapping pattern of Brg1 loss and lesions with nuclear accumulation of β-catenin. Scale bars represent 100 μm.

Immunohistochemical analysis of β-catenin expression revealed numerous aberrant crypt foci (ACF) with nuclear β-catenin in the small intestinal epithelium of $AhCreER^+$-$Apc^{fl/fl}Brg^{+/+}$ and $AhCreER^+Apc^{fl/fl}Brg^{fl/fl}$ mice (Figure 5.5, left and middle panels). Similarly, occasional crypts containing clusters of Brg1 deficient cells were detected upon staining with anti-Brg1 antibody (Figure 5.5, right panel). However, despite presence of both Wnt-activated ACFs and Brg1 deficient cell clusters, analysis of serial sections stained with anti-Brg1 and anti β-catenin antibodies failed to detect any overlap between these cell populations (Figure 5.5, middle and right panels). While Brg1 deficient Wnt-

activated cells could have been present at the level of single cells, they would be difficult to detect on serial sections. It appears therefore, that by the ACF stage all Brg1 deficient cells with activated Wnt signalling were eliminated and only cells that selectively lost Brg1 or Apc were able to survive for 10 days. This observation suggests that Wnt pathway activation in the small intestinal epithelium is somehow incompatible with Brg1 loss.

5.2.4   Brg1 loss improves survival in Apc deficient animals

In order to assess the long-term effects of Brg1 loss on Wnt-driven neoplasia in the small intestinal epithelium, cohorts of $AhCreER^+Apc^{fl/fl}Brg^{+/+}$ and $AhCreER^+Apc^{fl/fl}Brg^{fl/fl}$ mice were induced as above and aged for up to 100 days along with $AhCreER^-$ controls (for all cohorts n$\geq$8). Mice were aged until they developed signs of ill health, at which point they were humanely killed and intestinal tissues were harvested. Survival analysis of the aged cohorts showed that all $AhCreER^+Apc^{fl/fl}Brg^{+/+}$ animals became ill and had to be sacrificed within 3 weeks of induction (Figure 5.6, median survival 9 days). Conversely, $AhCreER^+Apc^{fl/fl}Brg^{fl/fl}$ mice survived significantly longer with some mice surviving past 100 days (Figure 5.6, median survival 58 days, Log-Rank test p<0.0001). None of the control mice developed signs of ill health within the time frame of the experiment (Figure 5.6).
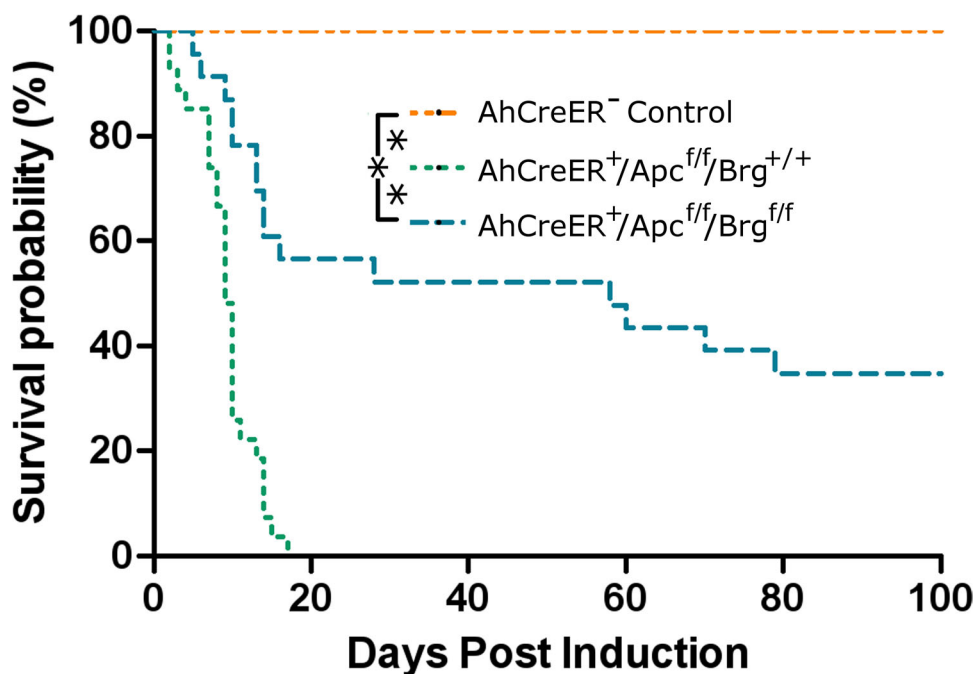
Figure 5.6: Concurrent Brg1 deletion improves survival of mice with intestinal Apc loss. $AhCreER^+$-$Apc^{fl/fl}Brg^{+/+}$ and $AhCreER^+Apc^{fl/fl}Brg^{fl/fl}$ mice were induced with an appropriate protocol along with Cre^- controls and aged for 100 days PI or until have developed signs of terminal ill health. Survival data was presented as Kaplan-Meier plot and revealed reduced survival probability of both experimental cohorts compared to control animals (for either comparison Log-Rank test p<0.0001, n$\geq$8). Comparison of survival probability between the experimental groups revealed a significantly improved survival of $AhCreER^+Apc^{fl/fl}Brg^{fl/fl}$ mice compared to $AhCreER^+Apc^{fl/fl}Brg^{+/+}$ animals (Log-Rank test p<0.0001, n$\geq$20).

5.2.5   Brg1 loss is incompatible with Wnt-driven adenoma formation

Immunohistochemical analysis of β-catenin expression in the small intestinal epithelium of $AhCreER^+Apc^{fl/fl}Brg^{fl/fl}$ mice 30 days post induction revealed numerous lesions with nuclear β-catenin localisation (Figure 5.7), indicating Wnt signalling activation. Notably, all lesions were found to express Brg1 as assessed by Brg1 immunostaining (Figure 5.7). Consistent with repopulation of Brg1 deficient cells seen in $AhCreER^+Brg^{fl/fl}$ mice (Section 3.2.5), no Brg1 deficient cells were detected in the normal epithelium of $AhCreER^+$-$Apc^{fl/fl}Brg^{fl/fl}$ either. A similar situation was observed in $AhCreER^+Apc^{fl/fl}Brg^{fl/fl}$ mice that survived up to 100 days post induction (not shown). Namely, all lesions with nuclear localisation of β-catenin were found to express Brg1. Surprisingly, large adenomas (Figure 5.7,b) were rarely detected in the small intestine of $AhCreER^+Apc^{fl/fl}Brg^{fl/fl}$ mice with the vast majority of Wnt-activated lesions being represented by small micro-adenomas confined within distended villi (Figure 5.7,a). The lack of large adenomas combined with Brg1 positive status of all Wnt-activated lesions in the small intestine indicated that Brg1 loss in conjunction with Wnt pathway activation somehow eliminated lesions with a potential to progress from adenoma to carcinoma.
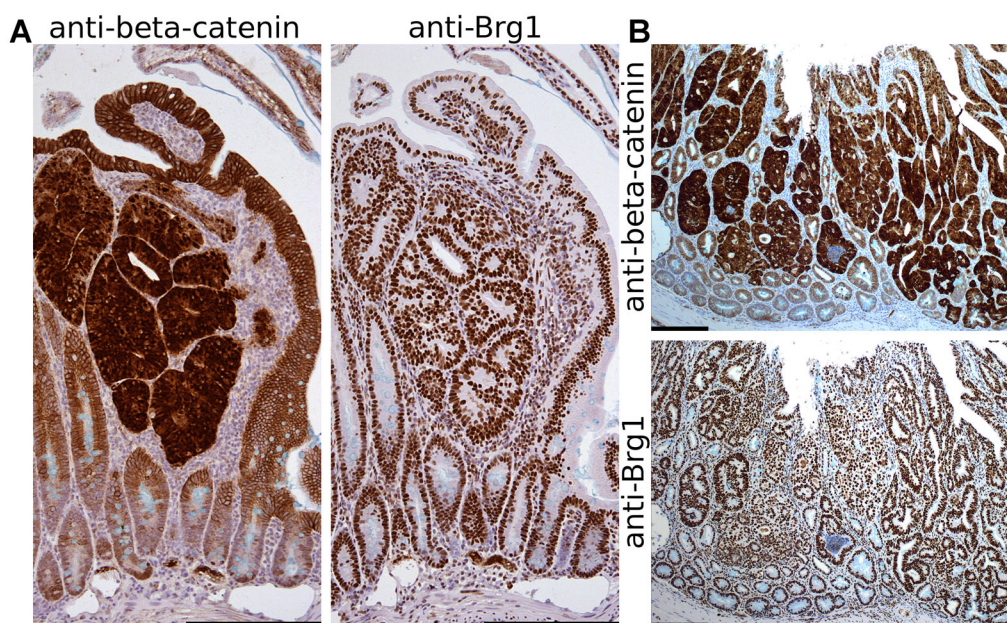
Figure 5.7: Concurrent Brg1 deletion prevents development of macroscopic adenomas in the small intestinal epithelium of $AhCreER^+Apc^{fl/fl}Brg^{fl/fl}$. Immunohistochemical analysis of β-catenin distribution in the small intestinal epithelium of $AhCreER^+Apc^{fl/fl}Brg^{fl/fl}$ at day 100 PI detected frequent microadenomas (a) and rare macroadenomas (b) with nuclear accumulation of β-catenin. Immunohistochemical analysis of Brg1 expression revealed that both types of adenomas retained Brg1 expression. Scale bars represent 200 μm.

5.2.6   VillinCre drives combined loss of Brg1 and Apc at high penetrance in the small intestine

In order to investigate the molecular mechanism behind the absence of Brg1 deficient Wnt activated lesions and the lack of advanced adenomas in the small intestinal epithelium of $AhCreER^+Apc^{fl/fl}Brg^{fl/fl}$ mice, I used VillinCre recombinase to induce high level recombination of Brg1 and Apc. $VillinCre^+Apc^{fl/fl}Brg^{+/+}$ and $VillinCre^+Apc^{fl/fl}$-$Brg^{fl/fl}$ mice were induced by four daily intraperitoneal injections of Tamoxifen at 80 mg/kg dose. Induced mice were then dissected at day 4 post induction and intestinal tissues were harvested for histological and gene expression analysis.
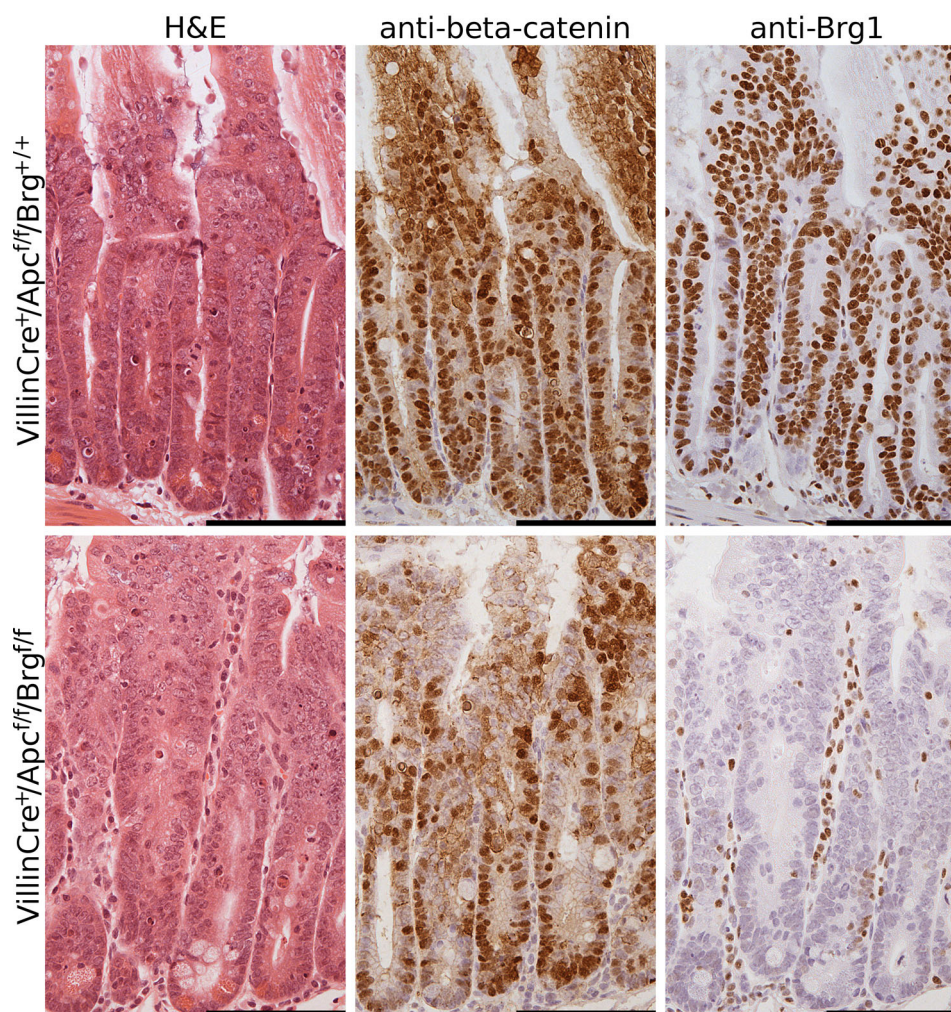
Figure 5.8: VillinCre recombinase drives simultaneous deletion of Brg1 and Apc in the small intestinal epithelium. Histological analysis of H&E stained sections of the small intestinal epithelium from $VillinCre^+Apc^{fl/fl}Brg^{+/+}$ and $VillinCre^+Apc^{fl/fl}Brg^{fl/fl}$ mice at day 4 PI revealed signs of aberrant Wnt signalling activation, such as elongated crypts and elevated apoptosis, in the small intestine of either group. Analysis of β-catenin distribution in these animals revealed nuclear accumulation of β-catenin in the small intestinal epithelium of animals from either group, although not as prominent in $VillinCre^+$-$Apc^{fl/fl}Brg^{fl/fl}$ intestine. Immunohistochemical analysis of Brg1 expression detected near complete loss of Brg1 in the epithelial cells of $VillinCre^+Apc^{fl/fl}Brg^{fl/fl}$ small intestine. Scale bars represent 100 μm.

Immunohistochemical analysis of Brg1 expression revealed nearly complete loss of

Brg1 in the small intestinal epithelium of $VillinCre^{+}Apc^{fl/fl}Brg^{fl/fl}$ mice (Figure 5.8). Similarly, analysis of β-catenin expression showed nuclear localisation of β-catenin in the majority of the epithelial cells (Figure 5.8) indicating efficient loss of Apc and Wnt signalling activation. Together, these observations suggested that VillinCre recombinase was successful in driving combined Brg1 and Apc inactivation with high penetrance. Most notably, short-term loss of Brg1 under the control of VillinCre recombinase was compatible with Wnt signalling activation. Unfortunately, both $VillinCre^{+}Apc^{fl/fl}Brg^{+/+}$ and $VillinCre^{+}Apc^{fl/fl}Brg^{fl/fl}$ animals became ill around day 5 PI and thus the long-term fate of double mutant cells could not be explored using this model.

5.2.7 Brg1 loss in the context of activated Wnt signalling attenuates some of the manifestations of Wnt pathway activation

Considering the proposed role of Brg1 as a mediator for trans-activation of Wnt target genes and the apparent incompatibility of Brg1 loss with Wnt signalling activation observed in the previous section, I investigated whether Brg1 loss attenuated the effects of aberrant Wnt pathway activation. Histological analysis of small intestinal tissue sections from $VillinCre^{+}Apc^{fl/fl}Brg^{+/+}$ and $VillinCre^{+}Apc^{fl/fl}Brg^{fl/fl}$ mice revealed that they shared histological features of Wnt activated intestinal epithelium, such as elongated crypts and high levels of mitosis and apoptosis (Figure 5.8, left panels), as has been previously reported (Sansom *et al.*, 2004). However, careful quantification of histological parameters (crypt and villus size, apoptosis and mitosis levels as well as BrdU incorporation) detected substantial differences between $VillinCre^{+}Apc^{fl/fl}Brg^{+/+}$ and double knock-out (DKO) animals (Figure 5.9, Table 5.2).

The length of crypts and villi were scored on H&E stained sections as the average number of cells ($\pm$ standard deviation) between the crypt base and the crypt-villus junction and between the crypt-villus junction and the tip of the villus respectively. Crypts in the intestinal epithelium of $VillinCre^{+}Apc^{fl/fl}Brg^{+/+}$ and DKO mice were found to be longer compared to control animals (for all comparisons p<0.001). Conversely, animals from both experimental groups displayed significantly longer villi compared to control mice (for all comparisons p=0.001). Comparison of crypt length between the experimental cohorts revealed significantly longer crypts in Apc deficient epithelium compared to DKO mice (46.36$\pm$4.97 and 41.21$\pm$1.85, p=0.049, n$\geq$4, Figure 5.9a). Quantification of the villus length, however, revealed no difference between the two groups (61.1$\pm$4.57 and 59.79$\pm$9.71, p=0.465, n$\geq$4, Figure 5.9b).

Apoptosis and mitosis levels were quantified on H&E stained sections as the average number ($\pm$ standard deviation) of apoptotic bodies and mitotic figures per half-crypt respectively. Quantification of apoptotic bodies within crypts revealed significantly elevated apoptosis in the intestine of the experimental animals compared to controls

Table 5.2: Quantitative analysis of the impact of Brg1 loss on the histology of Wnt activated small intestinal epithelium

Parameter	Cohort	Mean	SD	p Value		
				Control Vs Apc KO	Control Vs DKO	Apc KO Vs DKO
Crypt Length (cells)	Control	27.48	1.86	0.000	0.000	0.049
	Apc KO	46.36	4.97			
	DKO	41.21	1.85			
Villus Length (cells)	Control	76.11	3.26	0.001	0.001	0.465
	Apc KO	61.10	4.57			
	DKO	59.79	9.71			
Apoptosis per half-crypt	Control	0.14	0.09	0.001	0.008	0.002
	Apc KO	6.06	3.68			
	DKO	2.67	0.45			
Caspase positive cells per half-crypt	Control	0.11	0.04	0.000	0.011	0.006
	Apc KO	1.76	0.48			
	DKO	0.92	0.39			
Mitosis per half-crypt	Control	0.25	0.05	0.002	0.034	0.278
	Apc KO	0.75	0.29			
	DKO	0.61	0.15			
Ki67 positive cells per half-crypt	Control	17.28	4.28	0.000	0.001	0.000
	Apc KO	46.18	5.03			
	DKO	31.91	3.07			
BrdU positive cells per half-crypt	Control	8.41	0.90	0.000	0.001	0.010
	Apc KO	32.51	6.38			
	DKO	23.91	0.99			

Small intestinal tissue samples from $VillinCreER^{-}$ (marked here as **Control**), $VillinCreER^{+}Apc^{fl/fl}$-$Brg^{+/+}$ (marked here as **Apc KO**) and $VillinCreER^{+}Apc^{fl/fl}Brg^{fl/fl}$ (marked here as **DKO**) mice were collected at day 4 PI. Histological parameters, such as crypt and villus length, apoptosis, proliferation and BrdU incorporation were quiantified and compared between the three cohorts.
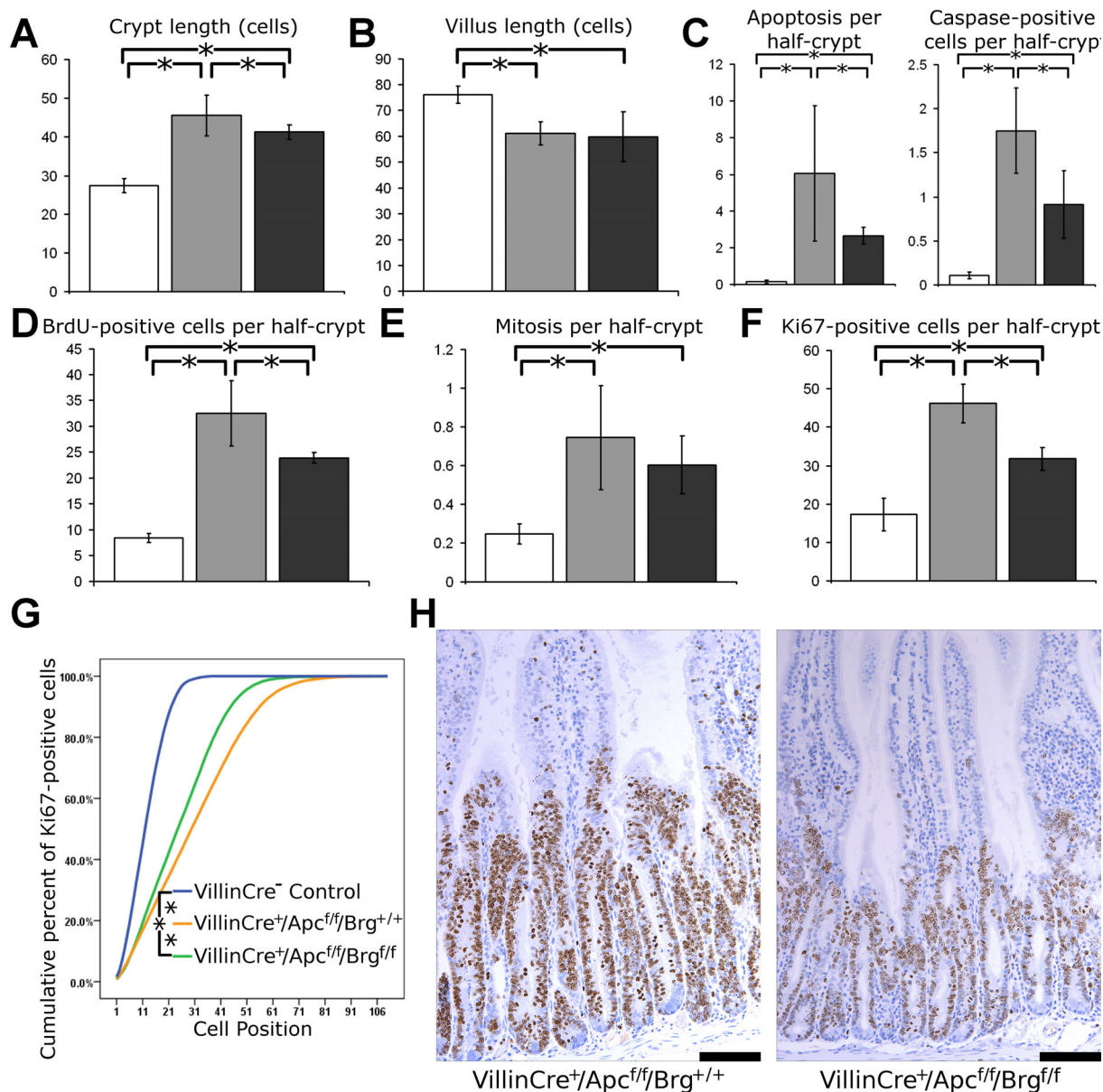
Figure 5.9: Histological analysis of the effects of short-term Brg1 deficiency in Wnt activated small intestinal epithelium. $VillinCre^+Apc^{fl/fl}Brg^{+/+}$ and $VillinCre^+Apc^{fl/fl}Brg^{fl/fl}$ mice were induced using the high-dose protocol along with Cre^- controls. Samples of the small intestinal epithelium were harvested at day 4 PI. (a-f) Histological parameters such as crypt length **(a)**, villus length **(b)**, apoptosis (c, left panel) and mitosis **(e)** were scored on H&E stained sections of the small intestinal epithelium from control (white bars), $VillinCre^+Apc^{fl/fl}Brg^{+/+}$ (grey bars) and $VillinCre^+Apc^{fl/fl}Brg^{fl/fl}$ (black bars) mice. The average numbers of BrdU **(d)**, cleaved Caspase3 (c, right panel) and Ki67 **(f)** positive cells were scored on respective immunostained sections. Error bars represent standard deviation. Asterisks mark histological parameters, which displayed a statistically significant difference (p value <0.05) between the groups. Exact values, standard deviations and respective p values are provided in Table 5.2; (g) Cumulative frequency analysis of Ki67 positive cells revealed an expansion of the proliferative compartment in $VillinCre^+Apc^{fl/fl}Brg^{+/+}$ and $VillinCre^+Apc^{fl/fl}Brg^{fl/fl}$ mice compared to control animals (for either comparison Kolmogorov-Smirnov Z test $p<0.0001$, $n\geq4$). Comparison of cumulative frequency of Ki67 positive cells between the experimental groups revealed a significantly shorter proliferative compartment in $VillinCre^+Apc^{fl/fl}Brg^{fl/fl}$ animals (Kolmogorov-Smirnov Z test $p<0.001$, $n\geq4$). (h) Immunohistochemical analysis of Ki67 expression confirmed a shorter proliferative zone in the small intestinal epithelium of $VillinCre^+Apc^{fl/fl}Brg^{fl/fl}$ mice. Scale bars represent 100 μm.

(for all comparisons p<0.01). Notably, significantly higher apoptosis levels were detected in $VillinCre^+Apc^{fl/fl}Brg^{+/+}$ mice compared to DKO animals (6.06±3.68 and 2.67±0.45, p=0.002, n≥4, Figure 5.9c). Quantification of cleaved Caspase-3 positive cells revealed a similar change in apoptosis levels. $VillinCre^+Apc^{fl/fl}Brg^{+/+}$ intestine displayed higher levels of Caspase-3 staining compared to DKO animals (1.76±0.48 and 0.92±0.39, p=0.006, n=5, Figure 5.9c).
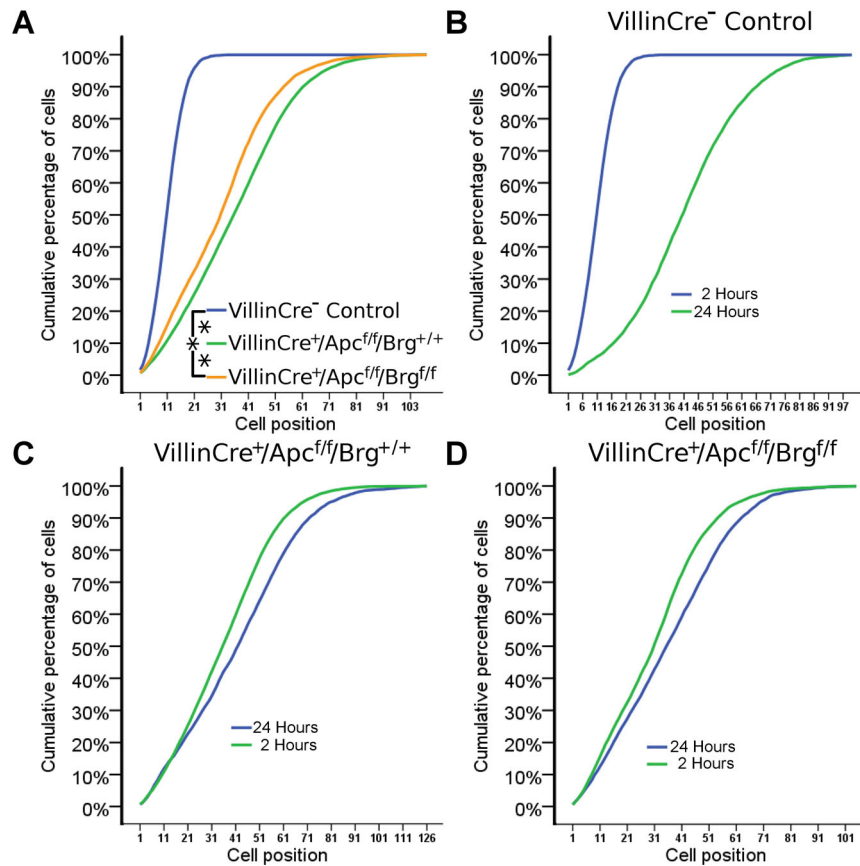
Figure 5.10: Brg1 loss attenuates BrdU incorporation and further impairs cell migration in Apc deficient small intestinal epithelium. **(a)** Cumulative frequency analysis of BrdU immunostaining 2 hours post labelling revealed a significant expansion of BrdU positive cells in the small intestine of $VillinCre^+$-$Apc^{fl/fl}Brg^{+/+}$ and $VillinCre^+Apc^{fl/fl}Brg^{fl/fl}$ mice at day 4 PI compared to control animals (for both comparisons Kolmogorov-Smirnov Z test p<0.0001, n≥4). Comparison of cumulative frequency of BrdU positive cells between the experimental groups also revealed a significantly shorter BrdU labelled zone in $VillinCre^+Apc^{fl/fl}Brg^{fl/fl}$ animals (Kolmogorov-Smirnov Z test p<0.0001, n≥4). **(b-d)** Cumulative frequency analysis of BrdU staining 24 hours post labelling between two experimental groups detected a marginally reduced cell migration in $VillinCre^+Apc^{fl/fl}Brg^{fl/fl}$ intestine (d, median migration distance 4.82 cells) compared to $VillinCre^+Apc^{fl/fl}Brg^{+/+}$ (c, median migration distance 6.54 cells) epithelium. Both groups exhibited a substantially reduced cell migration compared to control animals (b, median migration distance 30.39 cells).

Whilst both experimental cohorts displayed significantly elevated levels of mitosis compared to control animals (for all comparisons p<0.05), quantification of mitotic figures revealed no difference in their number between $VillinCre^+Apc^{fl/fl}Brg^{+/+}$ and DKO mice (0.75±0.29 and 0.61±0.15, p=0.278, n≥4, Figure 5.9e). Conversely, quantification of Ki67 positive cells detected significantly higher number of proliferating cells in $VillinCre^+$-$Apc^{fl/fl}Brg^{+/+}$ mice compared to DKO animals (46.18±5.03 and 31.91±3.07, p<0.001,

n≥4, Figure 5.9f,h). Additionally, the positions of Ki67 positive cells were scored in order to assess distribution of proliferating cells. Distributional analysis of Ki67 positive cell position revealed significant expansion of the proliferative compartment in Apc deficient epithelium compared to DKO mice (Figure 5.9g, Kolmogorov-Smirnov Z test p<0.001, n≥4). Finally, the number and position of BrdU positive cells 2 hours post labelling was scored to analyse quantity and distribution of cells in S-phase of the cell cycle. Quantification of BrdU positive cells per half-crypt ($\pm$ standard deviation) revealed significantly elevated BrdU incorporation in $VillinCre^+Apc^{fl/fl}Brg^{+/+}$ epithelium compared to DKO mice (32.51±6.38 and 23.91±0.99, p=0.01, n≥4, Figure 5.9d). In line with an expanded proliferative compartment as assessed by Ki67 staining, cumulative distribution analysis of BrdU positive cells detected a greater expansion of the proliferative compartment in Apc deficient intestine compared to DKO epithelium (Figure 5.10a, Kolmogorov-Smirnov Z test p<0.0001, n≥4).

Overall, histological analysis of the small intestinal epithelium from $VillinCre^+$-$Apc^{fl/fl}Brg^{+/+}$ and $VillinCre^+Apc^{fl/fl}Brg^{fl/fl}$ demonstrated that Brg1 loss in the context of Apc deletion was able to attenuate the effects of aberrant Wnt pathway activation, such as increased crypt length, apoptosis and the expansion of the proliferative compartment.

5.2.8   Brg1 loss in the context of Apc deficiency further inhibits cell migration

One of the effects of aberrantly activated Wnt signalling on intestinal homeostasis is impaired migration of the epithelial cells along the crypt-villus axis (Sansom *et al.*, 2004). In order to investigate the effects of Brg1 loss on cell migration in Wnt activated small intestinal epithelium, mice were treated with BrdU labelling agent 24 hours prior to dissection. The positions of BrdU labelled cells 24 hours post labelling were scored and compared to the positions of BrdU labelled cells at 2 hours post labelling. The average migration distance over a 22 hour period was determined as the distance between median positions of BrdU positive cells at 2 and 24 hours post labelling (Figure 5.10b-d). Cumulative distribution analysis of BrdU positive cells revealed that the average migration distance in Apc deficient epithelium (Figure 5.10c, median migration distance 6.54 cells) was marginally longer than in DKO animals (5.10d, median migration distance 4.82 cells). Notably, both experimental cohorts displayed markedly impaired epithelial migration compared to control animals (Figure 5.10b, median migration distance 30.39 cells). This observation suggested that Brg1 loss in the context of Apc deficiency further inhibited cell migration induced by aberrant Wnt pathway activation.

5.2.9   Brg1 loss modulates cell type-specific responses to aberrant Wnt signalling activation

Cell fate decisions governing differentiation of various mature cell types in the small intestinal epithelium are tightly regulated by the interplay between various signalling pathways, in particular the Wnt and Notch pathways (Fre *et al.*, 2009). Additionally, aberrant Wnt activation has been found to promote the proliferative program at the expense of cell differentiation (Sansom *et al.*, 2004). To investigate the effects of Brg1 loss on cell differentiation in the context of aberrant Wnt activation I quantified different mature cell types in the small intestinal epithelium of $VillinCre^+Apc^{fl/fl}Brg^{+/+}$ and $VillinCre^+Apc^{fl/fl}Brg^{fl/fl}$ mice (Figures 5.11 and 5.12). The results of quantitative analysis of differentiated cells in control, Apc deficient and DKO animals are collated in Table 5.3.

Table 5.3: Quantitative analysis of Brg1 deficiency impact on cell differentiation in the context of Wnt activated small intestinal epithelium

Parameter	Cohort	Mean	SD	p Value		
				Control Vs Apc KO	Control Vs DKO	Apc KO Vs DKO
Goblet cells per half-crypt	Control	4.85	0.85	0.037		
	Apc KO	3.26	1.08		0.219	
	DKO	3.73	1.81			0.408
Enteroendocrine cells per half-crypt	Control	0.76	0.09	0.467		
	Apc KO	0.71	0.21		0.418	
	DKO	0.68	0.24			0.474
Paneth cells per half-crypt	Control	1.13	0.31	0.003		
	Apc KO	2.12	0.45		0.500	
	DKO	1.14	0.49			0.004

Small intestinal tissue samples from $VillinCreER^-$ (marked here as **Control**), $VillinCreER^+Apc^{fl/fl}$-$Brg^{+/+}$ (marked here as **Apc KO**) and $VillinCreER^+Apc^{fl/fl}Brg^{fl/fl}$ (marked here as **DKO**) mice were collected at day 4 PI. Cell type-specific stains were used to detect major cell types of the small intestinal epithelium. Frequency of Goblet, Enteroendoctine and Paneth cells was quantified and compared between the three cohorts.

Specific staining for alkaline phosphatase located at the brush border formed by enterocytes revealed no difference between Apc deficient and normal intestinal epithelium (Figure 5.11a). However, the intestinal epithelium from DKO animals displayed consistently reduced staining for alkaline phosphatase (Figure 5.11a).

Consistent with impaired differentiation in Wnt activated small intestinal epithelium (Sansom *et al.*, 2004) staining with Alcian blue (Figure 5.11b) and scoring of positive cells revealed reduced numbers of Goblet cells per half-crypt-villus structure in the epithelium of $VillinCre^+Apc^{fl/fl}Brg^{+/+}$ mice compared to control animals (3.26±1.08 and
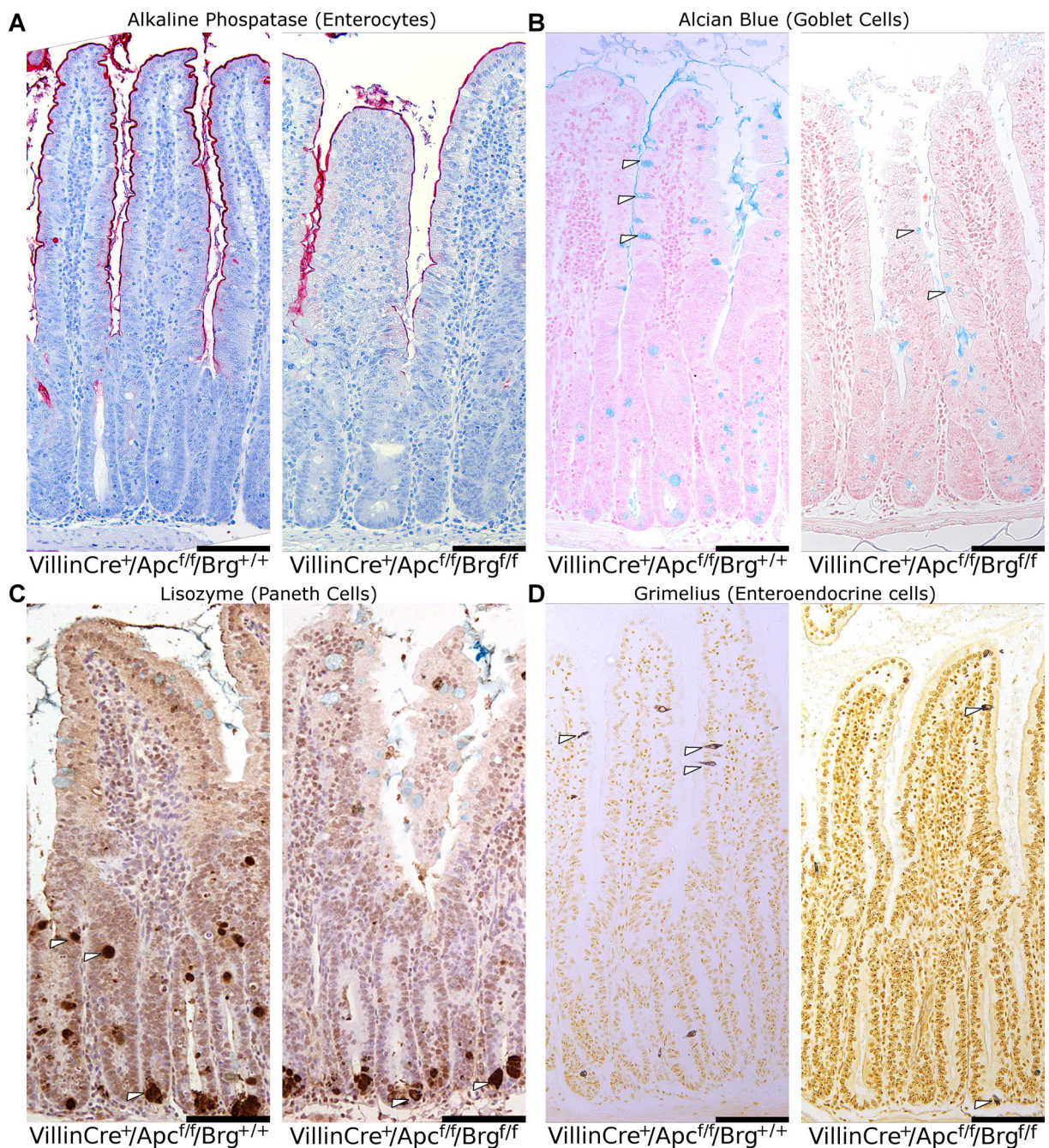
Figure 5.11: Qualitative analysis of cell differentiation upon Brg1 loss in Wnt activated small intestinal epithelium. Small intestinal sections of $VillinCre^{+}Apc^{fl/fl}Brg^{+/+}$ and $VillinCre^{+}Apc^{fl/fl}Brg^{fl/fl}$ mice at day 4 PI were subjected to cell type-specific stains to visualise Enterocytes **(a)**, Goblet cells **(b)**, Paneth cells **(c)** and Enteroendocrine cells **(d)**. Alkaline phosphatase staining revealed a slightly diminished brush border in the small intestine of $VillinCre^{+}Apc^{fl/fl}Brg^{fl/fl}$ mice **(a)**. No apparent differences were observed in differentiation of Goblet and Enteroendocrine cell lineages between the cohorts (b and d). While lysozyme staining revealed mislocalisation of Paneth cells in $VillinCre^{+}$-$Apc^{fl/fl}Brg^{+/+}$ mice, the small intestinal epithelium of $VillinCre^{+}Apc^{fl/fl}Brg^{fl/fl}$ animals displayed normal localisation of Paneth cells at the crypt base **(c)**. Arrows mark positive cells for each staining method. Scale bars represent 100 μm.
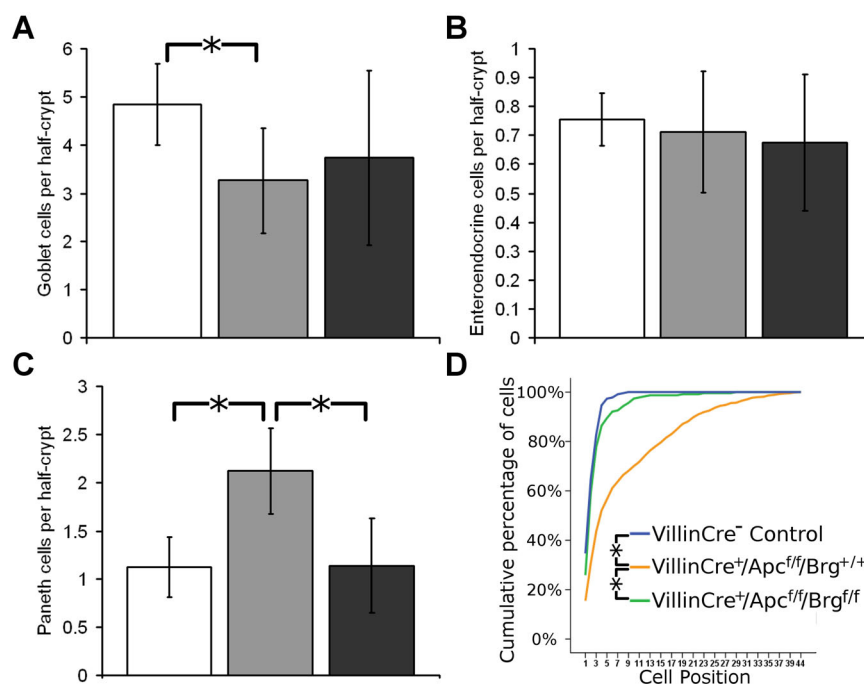
Figure 5.12: Quantitative analysis of cell differentiation upon Brg1 loss in Wnt activated small intestine. (a-c) The average number of Goblet **(a)**, Enteroendocrine **(b)** and Paneth **(c)** cells per half-crypt and associated villus was scored in the small intestine of control (white bars) $VillinCre^+Apc^{fl/fl}Brg^{+/+}$ (grey bars) and $VillinCre^+Apc^{fl/fl}Brg^{fl/fl}$ (black bars) mice at day 4 PI. While the number of Goblet cells was significantly reduced in $VillinCre^+Apc^{fl/fl}Brg^{+/+}$ mice compared to control animals (p=0.037, n≥4), no changes between the groups were detected in differentiation of Enteroendocrine cells. The number of Paneth cell was found to be significantly increased in $VillinCre^+Apc^{fl/fl}Brg^{+/+}$ mice compared to both $VillinCre^+Apc^{fl/fl}Brg^{fl/fl}$ and control animals (for both comparisons p<0.01, n≥4). Error bars represent standard deviation. Exact values, standard deviations and respective p values are provided in Table 5.3. **(d)** Cumulative frequency analysis of Paneth cell distribution revealed a significant expansion of Paneth cells throughout the crypt in $VillinCre^+Apc^{fl/fl}Brg^{+/+}$ small intestine compared to both $VillinCre^+Apc^{fl/fl}Brg^{fl/fl}$ and control animals (for either comparison Kolmogorov-Smirnov Z test p<0.001, n≥4).

4.85±0.85 respectively, p=0.037, n≥4, Figure 5.12a). Notably, scoring of Alcian blue stained sections of the small intestine of DKO animals detected an intermediate number of Goblet cells (3.73±1.81) which did not differ significantly from either Apc deficient or control epithelium (Figure 5.12a, for either comparison p>0.05, n≥4).

Grimelius staining was used to detect Enteroendocrine cells in the intestinal epithelium (Figure 5.11d). Quantification of positively stained cells revealed no difference in Enteroendocrine cell numbers per half-crypt-villus structure in control (0.76±0.09), $VillinCre^{+}Apc^{fl/fl}Brg^{+/+}$ (0.71±0.21) and DKO (0.68±0.24) animals (Figure 5.12b, for all comparisons p>0.05, n≥4).

Finally, immunohistochemical analysis of Lysozyme expression was used to detect Paneth cells in the small intestinal epithelium (Figure 5.11c). Quantification of Lysozyme positive cells (Figure 5.12c) revealed a significant increase in Paneth cell number per half-crypt in $VillinCre^{+}Apc^{fl/fl}Brg^{+/+}$ mice (2.12±0.45) compared to control animals (1.13±0.31, p=0.003, n≥4). Notably, scoring of Paneth cells in the intestinal epithelium of DKO mice detected full reversal to the normal level of Paneth cells, indistinguishable from control epithelium (1.14±0.49, p=0.500, n=4) and significantly lower compared to $VillinCre^{+}Apc^{fl/fl}Brg^{+/+}$ mice (p=0.004, n≥4). Since the Wnt pathway is involved in the regulation of Paneth cell positioning within the crypt, I also scored the positions of Lysozyme positive cells in control, $VillinCre^{+}Apc^{fl/fl}Brg^{+/+}$ and DKO epithelium. Cumulative distribution analysis revealed no difference in Paneth cell positions between epithelia of control and DKO animals (Figure 5.12d, Kolmogorov-Smirnov Z test p=0.17, n=4). Conversely, cumulative distribution analysis of Lysozyme positive cells in the epithelium of $VillinCre^{+}Apc^{fl/fl}Brg^{+/+}$ mice detected a significant expansion of the Paneth cell population compared to either control or DKO epithelium (Figure 5.12d, for either comparison Kolmogorov-Smirnov Z test p<0.001, n≥4). Visual inspection of Lysozyme stained sections confirmed confinement of Paneth cells to the crypt base in DKO small intestine, while epithelium of $VillinCre^{+}Apc^{fl/fl}Brg^{+/+}$ mice exhibited Paneth cell distribution throughout the crypt (Figure 5.11c).

5.2.10   Brg1 loss does not affect levels of activated β-catenin

Quantitative analysis of apoptosis, cell proliferation and differentiation in $VillinCre^{+}$-$Apc^{fl/fl}Brg^{+/+}$ and DKO mice suggested that Brg1 loss suppressed some components of the phenotype of aberrant Wnt signalling in the small intestinal epithelium. In order to dissect the mechanism of Brg1 loss-mediated suppression of aberrant Wnt signalling I analysed Wnt activation at the level of β-catenin stabilisation. One of the primary 'tumourigenic' effects of Apc loss is the disruption of the cytoplasmic destruction complex and stabilisation of β-catenin due to lack of phosphorylation at Ser37 and Thr41 residues. Stabilised β-catenin is therefore allowed to accumulate in the cytoplasm and nucleus resulting in activation of the Wnt transcriptional program (Waterman, 2002). Nuclear

accumulation of β-catenin is therefore one of the very first signs of activated Wnt signalling upon Apc inactivation. I therefore aimed to assess nuclear accumulation of β-catenin in the small intestinal epithelium of $VillinCre^+Apc^{fl/fl}Brg^{+/+}$ and DKO mice at day 4 post induction.

As previously mentioned, immunohistochemical analysis of β-catenin localisation in the intestinal epithelium demonstrated that both $VillinCre^+Apc^{fl/fl}Brg^{+/+}$ and DKO mice exhibited nuclear localisation of β-catenin (Figure 5.8). Closer inspection of the stained sections revealed substantial variation in β-catenin staining both, within and between samples of the same and different genotypes. Overall, nuclear localisation of β-catenin appeared to be more common in the intestinal epithelium of $VillinCre^+Apc^{fl/fl}$-$Brg^{+/+}$ mice (Figure 5.8). If Brg1 loss negatively affected accumulation of activated β-catenin, that would explain the attenuated phenotype of Apc inactivation in DKO mice.
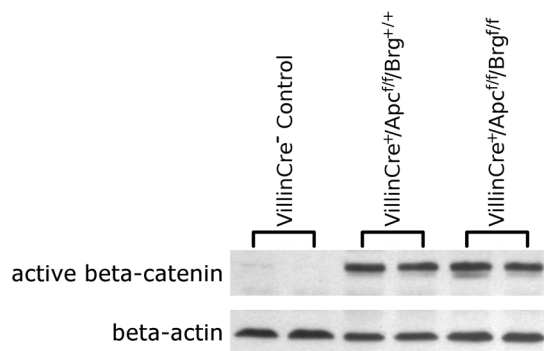
Figure 5.13: Brg1 loss in the context of Apc loss does not affect levels of activated β-catenin. Western blotting analysis of epithelial-enriched samples from $VillinCre^+Apc^{fl/fl}Brg^{+/+}$, $VillinCre^+Apc^{fl/fl}$-$Brg^{fl/fl}$ and Cre^- control animals revealed a substantial increase in the levels of activated β-catenin in the small intestine of experimental mice compared to control animals. However, no difference was detected in the levels of activated β-catenin between $VillinCre^+Apc^{fl/fl}Brg^{+/+}$ and $VillinCre^+Apc^{fl/fl}Brg^{fl/fl}$ small intestine. β-actin served as a loading control.

In order to investigate this hypothesis I aimed to quantitatively assess levels of activated β-catenin in the intestinal epithelium of $VillinCre^+Apc^{fl/fl}Brg^{+/+}$ and DKO animals. Since, immunohistochemistry is a non-quantifiable technique, Western blotting was used to assay the levels of activated β-catenin. Epithelial-enriched cell fractions were obtained from the small intestine of control, $VillinCre^+Apc^{fl/fl}Brg^{+/+}$ and DKO mice (n=3). These samples were further used for protein extraction and Western blotting analysis. Quantitative analysis of the protein samples detected substantially higher levels of activated β-catenin (de-phosphorylated at Ser37 and Thr41 residues) in both groups of experimental animals compared to controls (Figure 5.13). At the same time, no difference was detected in the levels of activated β-catenin between $VillinCre^+Apc^{fl/fl}Brg^{+/+}$ and DKO intestinal samples (Figure 5.13). This observation suggested that the attenuation of aberrant Wnt signalling caused by Brg1 loss is not mediated at the level of β-catenin stabilisation and accumulation and is more likely to occur downstream of β-catenin.

5.2.11   Brg1 deficiency attenuates the expression of Wnt target genes

In the original publication describing the interaction between β-catenin and Brg1, it has been proposed that Brg1 binds to the TCF/β-catenin complex and facilitates the trans-activation of Wnt target genes (Barker *et al.*, 2001). In order to investigate if Brg1 loss suppressed β-catenin mediated activation of the Wnt transcriptional program, quantitative analysis of Wnt target gene expression was performed on intestinal samples from control, $VillinCre^{+}Apc^{fl/fl}Brg^{+/+}$ and DKO animals (n$\geq$3). Total RNA was extracted from epithelial enriched samples of the small intestine and subjected to reverse transcription and quantitative real-time PCR (qRT-PCR) analysis of expression levels of a subset of Wnt target genes.
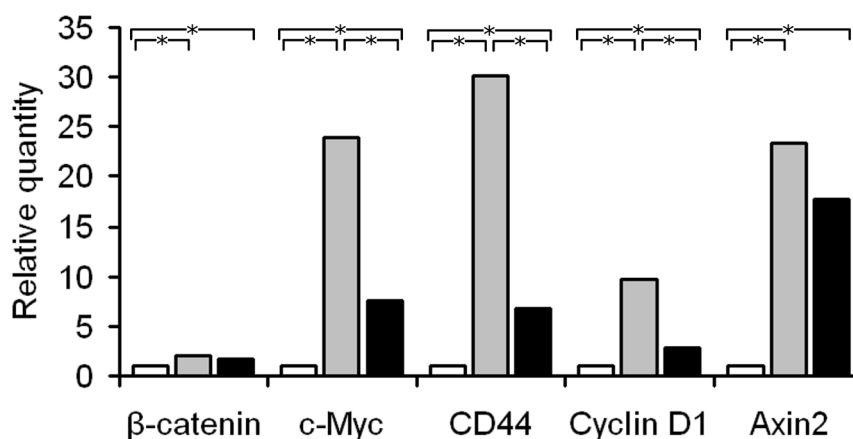
Figure 5.14: Brg1 loss attenuates expression of the Wnt target genes. Quantitative RT-PCR analysis revealed a significant up-regulation of a range of Wnt target genes in the small intestinal epithelium of $VillinCre^{+}Apc^{fl/fl}Brg^{+/+}$ (grey bars) and $VillinCre^{+}Apc^{fl/fl}Brg^{fl/fl}$ (black bars) mice compared to Cre^{-} controls (white bars) at day 4 PI. Expression levels of *c-Myc*, *CD44*, and *Cyclin D1*, but not *Axin2* or β-*catenin* were significantly reduced in $VillinCre^{+}Apc^{fl/fl}Brg^{fl/fl}$ mice compared to $VillinCre^{+}$-$Apc^{fl/fl}Brg^{+/+}$ animals. Asterisks mark the pair-wise comparisons that were found to be significantly different (p<0.05). For all comparisons n$\geq$3.

qRT-PCR analysis of *CD44*, *c-Myc* and *Cyclin D1* levels detected a significantly elevated expression of these genes in $VillinCre^{+}Apc^{fl/fl}Brg^{+/+}$ and DKO animals compared to control samples (Figure 5.14, for all comparisons p<0.05, n$\geq$3). Notably, however, up-regulation of these genes was less prominent in DKO mice compared to $VillinCre^{+}$-$Apc^{fl/fl}Brg^{+/+}$ samples (Figure 5.14, for all comparisons p=0.0285, n$\geq$3). Conversely, expression levels of *Axin2*, a commonly used readout of the Wnt pathway activation, were elevated in both $VillinCre^{+}Apc^{fl/fl}Brg^{+/+}$ and DKO mice compared to control animals (Figure 5.14, for both comparisons p<0.05, n$\geq$3), with no difference being detected in *Axin2* expression between the two experimental groups (Figure 5.14, p=0.2, n$\geq$3). Together these observations suggest that Brg1 deficiency is likely to suppress β-catenin mediated trans-activation of Wnt target genes, and indicate that this interaction is gene-specific.

5.2.12   Brg1 loss attenuates Wnt activation-mediated expansion of the stem cell population

The hyperproliferative response of Wnt pathway activation is associated with the expansion of the intestinal stem cell population (Jubb *et al.*, 2006; Merlos-Suárez *et al.*, 2011). Considering the devastating effect of Brg1 deficiency on the intestinal stem cell homeostasis in normal tissue, I aimed to examine if Brg1 loss suppressed the expansion of the stem cell population in Wnt activated intestinal epithelium. To this end, I analysed the expression levels of the intestinal stem cell markers *Ascl2* and *Lgr5* in RNA samples extracted from small intestinal epithelium of control, $VillinCre^+Apc^{fl/fl}Brg^{+/+}$ and DKO mice.
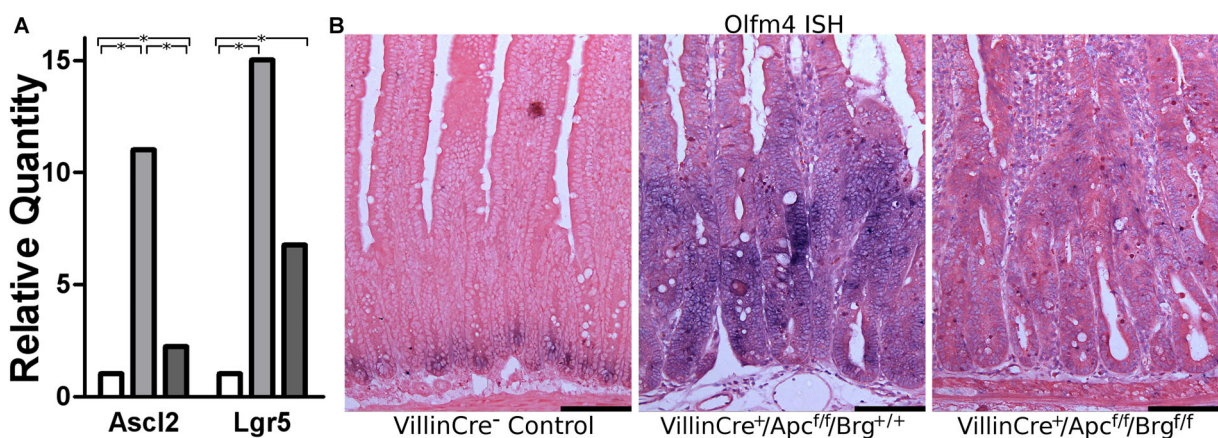
Figure 5.15: Brg 1 loss attenuates Wnt driven expansion of the small intestinal stem cell compartment. **(a)** Quantitative RT-PCR expression analysis revealed a significant up-regulation of the stem cell markers *Ascl2* and *Lgr5* in the small intestinal epithelium of $VillinCre^+Apc^{fl/fl}Brg^{+/+}$ (grey bars) and $VillinCre^+Apc^{fl/fl}Brg^{fl/fl}$ (black bars) mice compared to Cre^- controls (white bars) at day 4 PI (for all comparisons p<0.05, n≥3). Expression levels of *Ascl2*, but not Lgr5 were found to be significantly reduced in the small intestine of $VillinCre^+Apc^{fl/fl}Brg^{fl/fl}$ mice compared to $VillinCre^+Apc^{fl/fl}$-$Brg^{+/+}$ intestine. Asterisks mark the pair-wise comparisons that were found to be significantly different (p<0.05). For all comparisons n≥3. **(b)** *In situ* hybridisation analysis of *Olfm4* expression revealed a substantial expansion of the stem cell compartment in the small intestinal epithelium of $VillinCre^+$-$Apc^{fl/fl}Brg^{+/+}$ compared to control animals. While the signs of expanded stem cell population were detected in the small intestine of $VillinCre^+Apc^{fl/fl}Brg^{fl/fl}$ mice, the expression levels of *Olfm4*, appeared to be substantially lower compared to $VillinCre^+Apc^{fl/fl}Brg^{+/+}$ small intestine. Scale bars represent 100 μm.

Expression levels of *Ascl2* and *Lgr5* were significantly elevated in $VillinCre^+Apc^{fl/fl}$-$Brg^{+/+}$ and DKO mice compared to control animals (Figure 5.15a, for all comparisons p<0.05, n≥3), indicating an expanded stem cell population in both experimental groups. However, *Ascl2* expression levels were significantly lower in DKO mice compared to $VillinCre^+Apc^{fl/fl}Brg^{+/+}$ animals (Figure 5.15a, p=0.015, n≥3). Conversely, no significant difference was detected in *Lgr5* expression between $VillinCre^+Apc^{fl/fl}Brg^{+/+}$ and DKO mice, although DKO epithelium displayed a tendency to attenuated *Lgr5* expression (Figure 5.15a, p=0.115, n≥3).

Since both Ascl2 and Lgr5 have been shown to be Wnt target genes, their use as markers for the intestinal stem cell in this particular experimental system may be com-

promised. In order to assess the state of the stem cell population in a Wnt-independent manner, I resorted to *in situ* hybridisation analysis of *Olfm4* expression. Small intestinal samples from control, $VillinCre^+Apc^{fl/fl}Brg^{+/+}$ and DKO animals harvested at day 4 PI were stained using an anti-*Olfm4* riboprobe (Figure 5.15b)[1]. Analysis of *Olfm4* expression in control epithelium detected positive staining in the region of the crypt base (Figure 5.15b). Conversely, the small intestinal epithelium of $VillinCre^+Apc^{fl/fl}Brg^{+/+}$ mice displayed *Olfm4* staining throughout the crypt length, indicating an expansion of the stem cell compartment (Figure 5.15b). Meanwhile, *Olfm4* staining of the DKO epithelium failed to detect a similar expansion of the stem cell population (Figure 5.15b). Notably, loss of Brg1 in context of Apc deficiency did not restore normal stem cell localisation at the crypt bottom. Instead, *Olfm4* expression in DKO small intestine was found to be substantially lower compared to Apc deficient mice.

Taken together, these observations suggest that Brg1 deficiency in the context of activated Wnt signalling suppresses Wnt-driven expansion of the stem cell compartment.

5.3   Discussion

I have previously analysed the effects of Brg1 deficiency in the small intestinal epithelium. Despite numerous reports linking Brg1 loss to enhanced tumourigenesis in other tissues, neither heterozygous, nor homozygous Brg1 loss in the small intestinal epithelium was able to induce tumour formation over an extensive period of observation. Furthermore, induction of partial Brg1 loss resulted in the repopulation of Brg1 deficient cells with wild type counterparts, while induction of complete Brg1 loss led to rapid crypt abrogation due to compromised stem cell function. Taken together, these observations suggested that Brg1 deficiency or haploinsufficiency alone was not sufficient to induce carcinogenesis in the small intestinal epithelium. The reported interaction of Brg1 with β-catenin and the resulting requirement of Brg1 for trans-activation of Wnt target genes (Barker *et al.*, 2001) implicated Brg1 as a potential therapeutic target in Wnt-driven neoplasia. This contradicts with the recognised Brg1 role as a tumour suppressor in other tissues (Becker *et al.*, 2009; Reisman *et al.*, 2003; Wong *et al.*, 2000). Investigation of the Brg1 interaction with the Wnt pathway, and the effects of Brg1 deficiency and haploinsufficiency on aberrant Wnt signalling *in vivo* is therefore, of importance for the validation of Brg1 as a potential therapeutic target.

In this chapter I pursued two aims. First, to test whether Brg1 haploinsufficiency enhanced Wnt-driven intestinal tumourigenesis. Second, to study modulation of aberrant Wnt pathway activation by homozygous Brg1 loss. To this end, I exploited Cre recombinase constructs expressed in the intestinal epithelium to inactivate one or two *Brg1* alleles in the context of activated Wnt signalling. The latter was achieved by introducing an

---

[1] *Olfm4 in situ* hybridisation was carried out by Maddy Young on the small intestinal sections provided by me.

Apc allele targeted with loxP sites in transgenic mice also bearing a targeted *Brg1* allele and various Cre recombinase constructs. Data presented in this chapter show that Brg1 haploinsufficiency does not accelerate or in any other way enhance Wnt mediated carcinogenesis, while Brg1 deficiency inhibits Wnt-driven tumour formation via suppression of Wnt target genes and elimination of Wnt activated stem cells.

5.3.1   Brg1 haploinsufficiency does not accelerate Wnt driven intestinal tumourigenesis

Having established that heterozygous inactivation of *Brg1* does not induce tumourigenesis in normal intestinal tissue, I aimed to test whether Brg1 haploinsufficiency would enhance tumour formation in mice with heterozygous deletion of *Apc*. However, analysis of tumour burden and survival probability failed to detect differences in tumour incidence and progression between *Apc* heterozygous mice with or without Brg1 haploinsufficiency. The observation that Brg1 haploinsufficiency is unable to induce tumourigenesis alone or accelerate Wnt-driven tumour formation in the small intestine is in contrast to the findings that Brg1 haploinsufficiency promotes tumourigenesis in both the mammary and lung epithelium (Bultman *et al,.* 2007; Glaros *et al.*, 2008). This discrepancy indicates the tissue-specific nature of Brg1'1 role as a tumour suppressor and highlights the importance tissue-specific protein interactions in potential therapeutic target validation.

Loss of both *Brg1* alleles is a commonplace event in lung tumourigenesis (Fukoka *et al.*, 2004; Reisman *et al.*, 2003). I, however failed to observe any instances of *Brg1* loss of heterozygousity (LOH) in the tumours from $AhCre^{+}Apc^{+/fl}Brg^{+/fl}$ mice. Retention of the functional *Brg1* allele is all more remarkable considering the high chromosomal instability of Apc deficient tumours (Fodde *et al.*, 2001). Taken together, this finding indicates that Brg1 deficiency provides no selective advantage to Wnt driven intestinal tumours. On the other hand, the presence of the recombined *Brg1* allele in tumour tissue suggested retention of Brg1 haploinsufficient cells and thus the lack of selective pressure against Brg1 haploinsufficiency. It should be noted, however, that the recombined signal detected in tumours could be derived from normal Brg1 heterozygous tissue present within the tumour and genotyping of microdissected tumour tissue would be required to conclusively establish retention of recombined *Brg1* allele in tumour cells.

Combined with the data from Chapter 3, these results suggest that in the context of the normal small intestine, and Wnt-driven neoplasia, Brg1 haploinsufficiency is likely to act as a neutral factor, neither enhancing, nor impairing tumour formation or progression.

5.3.2   Brg1 deficiency attenuates the effects of aberrant Wnt activation by suppressing Wnt-driven gene expression

Given the proposed role of Brg1 as a Wnt signalling mediator (Barker *et al.*, 2001), I aimed to investigate the functional interaction between Brg1 and Wnt signalling in the murine small intestinal epithelium. To this end, I activated Wnt signalling by conditionally deleting Apc in the context of Brg1 deficiency using VillinCre recombinase.

The overall effect of Brg1 deficiency in Wnt activated small intestinal epithelium was the attenuation of responses driven by activated Wnt signalling. Quantitative measurements of histological parameters, such as crypt length, apoptosis and proliferation were all elevated in Wnt activated epithelium in both Brg1 deficient and proficient tissue compared to control mice, consistent with previous reports of conditional Apc deletion in the small intestine (Sansom *et al.*, 2004). However, the epithelium of double knock-out (DKO) mice displayed a significantly reduced degree of Wnt-mediated responses compared to Apc deficient mice with functional Brg1.

Consistent with an increase in crypt length and number of proliferating cells, positional analysis of Ki67 and BrdU positive cells at 2 hours post labelling detected spatial expansion of the proliferative compartment, which was nonetheless significantly less pronounced in DKO mice. Of note, the proliferative compartment's size or distribution was not affected upon Brg1 loss in otherwise normal epithelium at the comparable time point (Section 3.2.9), indicating that Brg1 might be specifically required for the Wnt activation-driven increase in proliferation. Expansion of the stem cell population in Wnt activated intestinal epithelium is postulated to contribute to the Wnt mediated proliferative response (Jubb *et al.*, 2006; Merlos-Suárez *et al.*, 2011). Interestingly, the attenuated increase in proliferation in DKO mice coincided with depletion of the stem cell compartment in the small intestine of these mice compared to Apc deficient animals. Notably, despite restoring normal localisation of Paneth cells, Brg1 loss in the context of activated Wnt signalling did not seem to restore stem cell localisation to the crypt bottom as assessed by *Olfm4* expression. Instead, DKO mice displayed attenuated expression of *Olfm4* throughout the crypt compartment.

One of the Wnt mediated responses not attenuated by Brg1 deficiency was abrogation of cellular migration. In contrast, migration of epithelial cells in the small intestine of DKO mice was marginally further impaired in comparison with Apc deficient epithelium. While this response seemed unexpected in the context of overall attenuated manifestations of activated Wnt signalling, it could be accounted for by the reduced proliferative activity of DKO intestinal epithelium. While Wnt pathway activation strongly impairs cell migration, active cell proliferation ensures some residual level of cell migration. It is possible therefore, that the attenuated cell proliferation seen in DKO mice would reduce this residual cell migration thus further impairing apparent migration. It should be noted however, that Brg1 deficiency in the otherwise normal small intestine impaired epithelial

cell migration at very early stages (Section 3.2.10). Further inhibition of cell migration in the context of aberrant Wnt signalling could thus indicate a cumulative effect of Brg1 deficiency and Wnt pathway activation on migration of the intestinal epithelium.

Brg1 loss was found to modulate a number of cell differentiation responses mediated by aberrant Wnt signalling. Most notable of these was the restoration of Paneth cell number and position to a state comparable with that of the normal intestine. Paneth cells are the only terminally differentiated intestinal cell type that exhibit high levels of Wnt signalling. The Paneth cell's transcriptional program governed by activated Wnt pathway drives EphB3 receptor expression, which combined with the Ephrin ligand gradient in normal intestine ensures the Paneth cell's strict confinement to the crypt base (Batlle *et al.*, 2002). Aberrant activation of the Wnt pathway has been found to disrupt control over Paneth cell differentiation and position. As a result, Wnt activated intestinal epithelium has been shown to exhibit an increased number of Paneth cells and their presence throughout the crypt as opposed to crypt-base confinement in normal epithelium (Sansom *et al,.* 2004). Brg1 deficiency in the context of aberrant Wnt signalling was found to reverse both Paneth cell number and positioning to the normal state. Notably, Brg1 loss was not sufficient to repress other Wnt mediated responses, such as apoptosis, cell proliferation and migration, to physiological levels. Taken together, these data suggest that Brg1 might be preferentially involved in trans-activation of particular Wnt target genes, rather than homogeneously regulating the entire Wnt transcriptional program. This notion is consistent with the observation that Brg1 knock-down in the HEK293T cancer cell line down-regulates less than 70% of the genes induced by Wnt pathway activation the same cells (Mahmoudi *et al.*, 2010). Although to a lesser extent, Brg1 was found to modulate differentiation of Goblet cells. While Goblet cells were significantly under-represented in Apc deficient mice compared to normal intestine, combined Brg1-Apc loss resulted in an intermediate phenotype, neither significantly different from Apc deficient mice, nor from wild type controls. Quantification of enteroendocrine cells found that their frequency was unaltered between control, Apc deficient and DKO mice. This observation is in contrast with the previous study of Apc deletion in the small intestine (Sansom *et al.*, 2004), which reported a decrease in enteroendocrine cell number in Wnt activated epithelium. Several differences in experimental design, however, could contribute to this discrepancy. Sansom *et al.*, studied the effects of Apc loss at day 5 post induction (as opposed to day 4 in this study), which allowed more time for Wnt mediated responses to develop. Additionally, the reported decrease in enteroendocrine cell number was observed within the transformed crypt compartment, whilst in this study enteroendocrine cells were scored throughout the crypt-villus axis. Similarly, while Apc deficient intestine was reported to display diminished expression of alkaline phosphatase (Sansom *et al.*, 2004), no apparent decrease in alkaline phosphatase expression was detected in Apc deficient mice in this study. This, again, could be attributed to an earlier time point used in the present experiment. Surprisingly, however, the small intestinal epithelium of DKO mice was

consistently found to exhibit reduced alkaline phosphatase staining. This observation is consistent with impaired alkaline phosphatase expression in Brg1 deficient mice (Section 3.2.11) and suggests that Brg1 might play a role in enterocyte maturation independent of Wnt signalling.

In summary, Brg1 deficiency attenuated a range of responses mediated by aberrant Wnt signalling, in particular apoptosis, proliferation and differentiation of Goblet and Paneth cells, while not affecting cell migration and enteroendocrine cell differentiation. At the same time, the impaired enterocyte maturation caused by Brg1 deficiency appears to be independent of Wnt activation.

In order to investigate the mechanism behind the attenuated phenotype of Apc loss in Brg1 deficient epithelium, I explored a number of possibilities. At least one study suggested that Brg1 may be involved in modulation of the Wnt pathway at two levels, expression of Wnt receptors and trans-activation of Wnt target genes (Griffin et $al.$, 2011). The former option implies that Brg1 deficiency might attenuate Wnt signalling by suppressing expression of Wnt receptors and thus causing a suboptimal level of Wnt activation. In this case, one can expect to observe a reduced level of β-catenin activation in response to Brg1 loss. β-catenin activation in the small intestinal epithelium can be assessed qualitatively by examining its nuclear accumulation or quantitatively by assessing levels of active β-catenin, which is not phosphorylated at residues Ser37 and Thr41. Immunohistochemical analysis of β-catenin localisation proved to be variable between and within samples, potentially due to fixation/staining artefacts. However, the overall trend suggested that cells with nuclear β-catenin were more common in Apc deficient epithelium than the epithelium of DKO mice, indicating a reduced level of β-catenin activation in DKO animals. However, quantitative Western-blotting analysis of active β-catenin levels revealed no differences between Apc deficient and DKO small intestinal epithelium, indicating that Brg1 loss did not affect the stabilisation and accumulation of active β-catenin. Interestingly, the reported physical interaction between Brg1 and β-catenin (Barker et $al.$, 2001) may facilitate nuclear retention of β-catenin and thus account for reduced nuclear β-catenin accumulation in the epithelium of DKO mice. Overall, these observations suggest that while Brg1 loss is unlikely to affect β-catenin stabilisation and accumulation, it might impair nuclear retention of β-catenin, which could contribute to the attenuation of Wnt mediated responses.

In order to examine the second possibility, namely Brg1 mediated modulation of Wnt signalling by trans-activation of Wnt target genes, I assessed the expression levels of a number of genes known to be a part of Wnt signalling transcriptional program. Indeed a subset of Wnt target genes (*CD44, c-Myc, Cyclin D1, Lgr5*) was found to be down-regulated in the small intestinal epithelium of DKO mice compared to Apc deficient epithelium. Notably, at least some Wnt target genes (*Axin2*) were found to escape this down-regulation. This observation raises two possibilities. The first is that there is differential Brg1 involvement in the trans-activation of different Wnt targets. The second is

consistent with reduced accumulation of nuclear β-catenin in the epithelial cells of DKO mice and implies a dose-dependent trans-activation of Wnt target genes. If the dose of Wnt signal (in the form of nuclear β-catenin) required for a gene to be expressed is different for different genes, partial inhibition of nuclear accumulation of β-catenin would result in impaired expression of 'high-dose' genes (*c-Myc*, etc), while 'low dose' genes (*Axin2*) would receive sufficient signal to be transcribed to a 'fully activated' state. An elegant study by Kielman *et al.* (2002) used ES cells expressing truncated versions of Apc protein of various severity to generate teratomas. Kielman *et al.* observed an increase in tissue differentiation defects along with increasing severity of Apc mutations and degree of nuclear accumulation of β-catenin. Expression profiling of teratomas with various doses of Wnt/β-catenin signal revealed a substantial number of differentially expressed genes. Although not stressed by authors, a subset of these genes displayed a substantial increase or decrease in expression when compared between teratomas with the highest and intermediate levels of Wnt activation. These genes require a high level of Wnt signal in order to be fully transcribed and thus represent the 'high-dose' group. Conversely, another subset of genes was found to be up- or down-regulated in Apc deficient teratomas compared to wild type conterparts, while their expression levels were indistinguishable between teratomas with the highest and intermediate degree of Wnt activation (Kielman *et al.*, 2002). Unfortunately, none of the genes examined in the present work was reported as differentially expressed in the study by Kielman *et al.*, which prevents direct comparison.

To summarise, the results presented in this chapter suggest that the immediate effect of Brg1 loss in the context of aberrant Wnt signalling activation is impaired expression of a number of Wnt target genes (notably those involved in proliferative response). This suppression is likely to be caused by either suboptimal ability of the β-catenin/TCF complex to trans-activate its target genes in the absence of Brg1 or by impaired nuclear retention of β-catenin and, as a result, reduced likelihood of the complex formation. Diminished levels of Wnt target gene expression then can lead to attenuated cellular responses to Wnt pathway activation, such as aberrant cell proliferation, differentiation and apoptosis.

5.3.3   Brg1 loss suppresses Wnt-driven tumourigenesis in the small intestinal epithelium

In order to test the long-term effects of Brg1 loss in the context of activated Wnt signalling, targeted *Brg1* and *Apc* alleles were deleted using the AhCreER recombinase. Experimental cohorts of DKO and $AhCreER^{+}Apc^{fl/fl}Brg^{+/+}$ mice were aged along with $AhCreER^{-}$ controls. A proportion of animals were sacrificed at early time-points (day 7–10 PI) to analyse early Brg1 deficient lesions with aberrant Wnt signalling. Surprisingly, no DKO lesions were detected despite presence of apparently normal Brg1 deficient cell clusters and Wnt activated lesions, which retained Brg1 expression. The lack

of DKO lesions was unexpected, when compared to DKO mice expressing VillinCre re-combinase, which displayed combined Brg1 and Apc loss in nearly 100% of epithelial cells. The difference in the expression pattern of AhCreER and VillinCre recombinases should, however, be considered, when comparing results from these two models (see Figure 3.1b,c). VillinCre recombinase is expressed in the entirety of the small intestinal epithelium and thus is able to induce simultaneous loss of the targeted alleles in all epithelial cells. AhCreER, in contrast, is expressed in a limited cell population, mainly confined to the intestinal stem cells and their early progenitors. In the latter model, for the cells with induced loss of the targeted alleles to become detectable it is necessary to undergo several rounds of cell division. In the case of Apc loss, although smaller lesions with nuclear β-catenin can be detected at early time points, it is at the aberrant crypt focus (ACF) stage that they can be reliably identified, before which an induced cell would have undergone numerous divisions. It appears, therefore, that even if DKO cells arise in the small intestine of $AhCreER^+Apc^{fl/fl}Brg^{f/f}$ mice, they are eliminated before they can reach the ACF stage and the only surviving mutant cells are those that incidentally underwent complete loss of only one of the two targeted genes. Of these, Brg1 deficient cells are gradually repopulated leaving Brg1 positive Wnt activated lesions as the only mutant cells. Together, these observations suggest that Brg1 loss is incompatible with long-term activation of the Wnt pathway, most likely due to attenuation of Wnt signalling, although this can be tolerated for a short period of time. A more intriguing explanation of the apparent lack of DKO lesions in the small intestine of $AhCreER^+Apc^{fl/fl}Brg^{f/f}$ mice can be derived from the differences in spatial expression pattern of VillinCre and AhCreER recombinases. As previously discussed, VillinCre recombinase drives deletion of the targeted alleles in all intestinal cell populations, including transit amplifying and differentiated cells. Conversely AhCreER activity is largely confined to the stem cell population. The lack of DKO lesions in $AhCreER^+Apc^{fl/fl}Brg^{f/f}$ mice may, therefore, signal the stem cell-specific incompatibility of Brg1 deficiency and aberrant Wnt activation. This notion is consistent with the attenuated expansion of the stem cell population observed in $VillinCre^+Apc^{fl/fl}Brg^{f/f}$ mice.

Survival analysis of the experimental cohorts revealed a significant survival advantage of DKO mice compared to Apc deficient animals. Whilst all $AhCreER^+Apc^{fl/fl}Brg^{+/+}$ mice became ill and had to be sacrificed within 3 weeks of Cre recombinbase induction, a substantial proportion of DKO mice survived significantly longer, with some DKO mice surviving past 100 days PI. This increase in survival is consistent with long-term incompatibility of Brg1 loss with aberrant Wnt activation. Due to limited efficiency of Cre recombinase, three distinct subpopulations of mutant cells in the intestinal epithelium of DKO mice would be represented by Apc deficient cells (Apc$^-$), Brg1 deficient cells (Brg1$^-$) and double mutant cells (Brg$^-$/Apc$^-$) (Figure 5.16a). Elimination of all the double mutant cells would result in an overall decrease in numbers of Apc deficient cells resulting in lower tumour burden and improved animal survival (Figure 5.16b). This
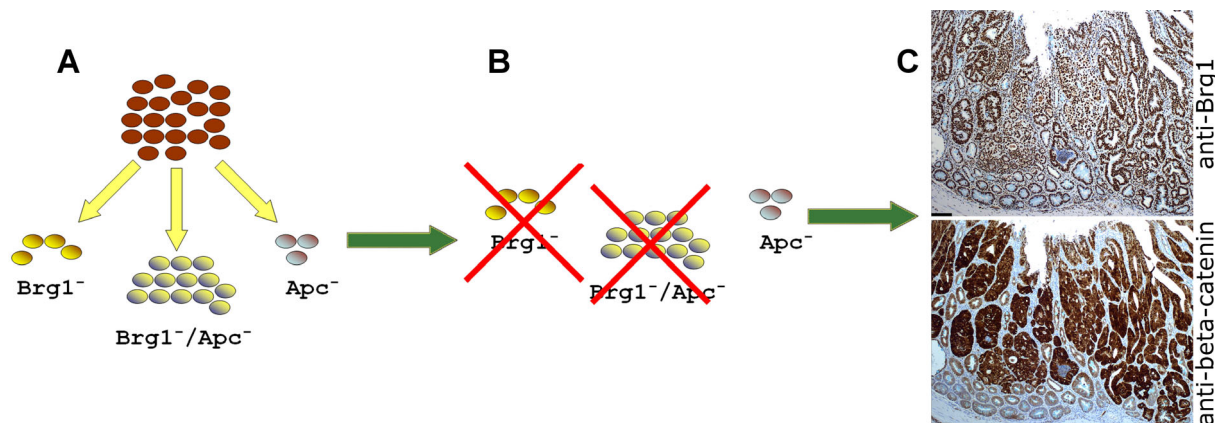
Figure 5.16: Brg1 deficiency in the context of small intestinal Wnt-driven tumourigenesis improves animal survival by reducing tumour burden. See the main text for detailed explanation.

model is supported by retention of Brg1 expression in all adenomas in the small intestine of $AhCreER^+Apc^{fl/fl}Brg^{fl/fl}$ mice (Figure 5.16c). Interestingly, a similar relationship between Brg1 loss and the tumour suppressor Snf5/Ini1 was observed in another mouse cancer model. Simultaneous deletion of Snf5 and Brg1 using T-cell lineage specific Lck-Cre recombinase resulted in reduced tumour incidence and slower onset of disease. Similar to our observations, all the tumours detected in that model retained Brg1 expression, indicating their origin from a sub-population of mutant cells that had lost only Snf5 (Wang et al., 2009). An additional mechanism that might have contributed to the improved animal survival derives from the notion that the intestinal stem cell acts as the cell of origin of cancer. It has been observed that aberrant activation of the Wnt pathway within the intestinal stem cell population leads to the development of rapidly growing adenomas, whilst transit-amplifying cells with activated Wnt signalling give rise to micro-adenomas with restricted growth (Barker et al., 2009, Figure 5.17). Notably, numerous micro-adenomas were detected in the small intestinal epithelium of long-surviving DKO mice, while large adenomas were infrequently observed in these mice. This mechanism is further supported by the notion that Brg1 loss is incompatible with long-term survival of the Wnt activated small intestinal stem cells discussed earlier in this section. Together, these observations suggest that small intestinal Brg1 loss in the context of aberrant Wnt signalling improves animal survival not only by reducing the tumour burden, but also by eliminating stem cell-derived Wnt-driven tumours with a higher potential to progress to advanced cancer.

5.3.4   Future directions

In summary, the findings presented in this chapter suggest that Brg1 is required for optimal activation of the Wnt transcriptional program and Wnt-driven tumourigenesis in the murine small intestinal epithelium.

It has been recently reported that in HEK293T cancer cell line BRG1 is involved in the
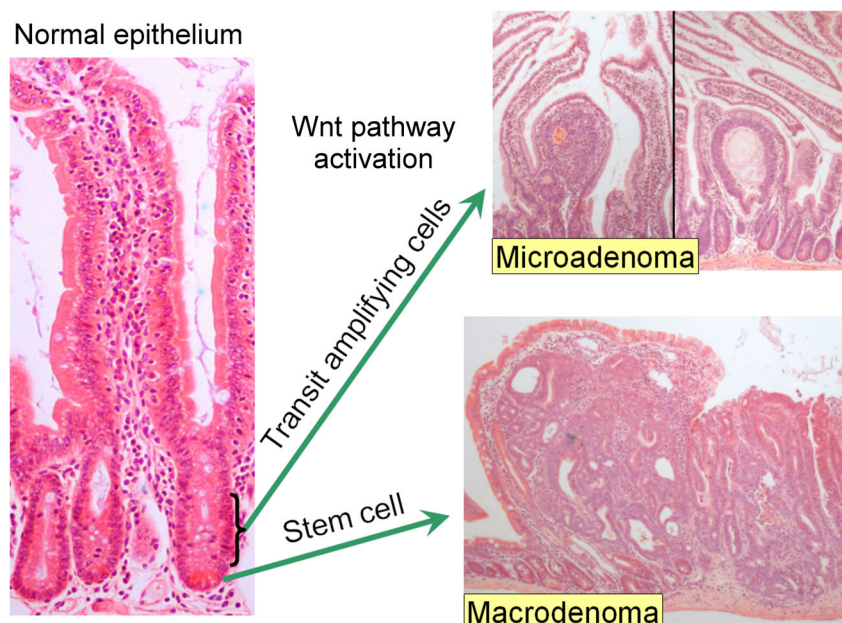
Figure 5.17: Brg1 deficiency in the context of small intestinal Wnt-driven tumourigenesis improves animal survival via specific elimination of stem cell-derived adenomas with high tumourigenic potential. See the main text for detailed explanation.

regulation of a diverse transcriptional program of which Wnt target genes constitute only 20% (Mahmoudi *et al.*, 2010). It therefore would be interesting to explore the genome-wide effects of Brg1 loss on the Wnt pathway activation *in vivo*. To this end, we are planning to carry out genome-wide expression analysis of the Wnt activated small intestinal epithelium with and without Brg1 loss using an Illumina microarray. Additionally, Brg1 chromatin immunoprecipitation (ChIP) analysis of the Wnt activated small intestinal epithelium will be carried out in order to verify whether Brg1 occupies promoters of Wnt target genes *in vivo*.

An intriguing concept stemming from the data presented in this chapter is that targeting intestinal stem cells with aberrant Wnt signalling may have therapeutic benefits, for instance in patients with FAP, where elimination of Wnt activated stem cells would prevent development of adenomas with the higher potential for malignant transformation. We are planning to explore the suitability of Brg1 as a therapeutic target using two types of mouse cancer models. The first aims to verify whether stem-cell specific loss of Brg1 in the context of the Wnt pathway activation is able to improve animal survival by preventing the development of advanced adenomas. To this end, targeted *Brg1* and/or *Apc* alleles are to be deleted in the intestinal stem cells using Lgr5CreER recombinase (Barker *et al.*, 2007). In this scenario mice carrying only the targeted *Apc* allele are expected to rapidly develop macro-adenomas, which would be absent in the small intestine of DKO mice. The second model will aim to assess the ability of Brg1 loss to act as a therapeutic factor in a pre-formed tumour. To this end animals harbouring targeted *Brg1* alleles and Lgr5CreER recombinase are to be interbred with mice carrying the Apc^{MIN} allele. As previously mentioned, Apc^{MIN} mice develop multiple intestinal tumours within 6 months

of age. These adenomas are to be treated by the induction of Lgr5CreER recombinase activity thus facilitating Brg1 deletion in normal and cancer stem cell populations. Tumour burden is then to be analysed in animals with and without induction of Brg1 loss.

Chapter 6

Investigating the multiple tissue phenotypes of combined Apc and Brg1 loss

6.1 Introduction

Mutations of the core components of the Wnt pathway that ultimately result in the pathway's aberrant activation have been found in cancers with diverse tissues of origin. These include, but are not limited to, cancers of the gastrointestinal tract, breast, liver, ovarian, endometrial and pancreatic cancers as well as melanoma (reviewed extensively in Giles *et al.*, 2003). Of these, colorectal cancer and the role of Wnt signalling in its pathogenesis are arguably the most studied, presumably due to its high clinical significance, the well defined mechanisms of tumour initiation and progression and the availability of established animal models (reviewed in Schneikert and Behrens, 2007). However, the involvement of aberrant Wnt signalling in the tumourigenesis of other organs implies that the development of therapies targeted against Wnt signalling could prove beneficial in various types of cancer (reviewed in Ewan and Dale, 2008).

With this in mind I set about to examine the consequences of Wnt activation via conditional deletion of a loxP targeted *Apc* allele in multiple tissues expressing AhCreER recombinase. Additionally, I aimed to investigate modulation of the Apc loss-induced phenotype in these tissues by concurrent loss of Brg1. Importantly, any attempt to study Apc deficiency using AhCreER recombinase is likely to be hampered by the severe intestinal phenotype of Wnt activation and limited animal survival (Ahmad *et al.*, 2011; Marsh *et al.*, 2008). To circumvent this difficulty I relied on the extended life span of Apc/Brg1 double knock-out animals described in the previous chapter, which enabled me to study relatively long-term consequences of AhCreER recombinase-induced Apc loss.

This chapter describes the consequences of Apc deficiency in forestomach, fundic, pyloric, large intestinal and bladder epithelia, as well as the impact of Brg1 loss on Wnt-

driven tumourigenesis in these tissues. Additionally, I investigated tumour initiation in non-intestinal AhCre recombinase expressing tissues via examination of the effects of heterozygous deletion of Apc and modulation of this phenotype by Brg1 haploinsufficiency.

6.2 Results

6.2.1 Combined Brg1 and Apc heterozygous loss has no apparent oncogenic effect in tissues outside of the intestinal epithelium

The results presented in Chapter 4 suggested that Brg1 haploinsufficiency alone does not induce tumour formation in tissues expressing AhCre recombinase within the observed time frame. At the same time, the data presented in the previous chapter demonstrated that Brg1 haploinsufficiency did not modulate Wnt driven tumourigenesis in the small or large intestinal epithelium of mice with heterozygous loss of Apc allele. To study the consequences of combined Apc and Brg1 loss in AhCre recombinase expressing tissues outside of the intestinal epithelium I analysed a range of tissues harvested from $AhCre^{+}$-$Apc^{+/fl}Brg^{+/fl}$ and $AhCre^{+}Apc^{+/fl}Brg^{+/+}$ mice. Mice in these cohorts were induced by 5 intraperitoneal injections of 80 mg/kg β-naphthoflavone. Mice from each cohort were then aged for up to 600 days post induction or until they developed signs of terminal ill health. Tissues from sacrificed animals were harvested and processed for histological analysis.

Histological analysis of H&E stained sections of forestomach, glandular stomach and bladder epithelium of either $AhCre^{+}Apc^{+/fl}Brg^{+/+}$ or $AhCre^{+}Apc^{+/fl}Brg^{+/fl}$ revealed no signs of tumourigenesis in any of the tissues analysed at any time point. Occasional mice displayed tumour-like formations in the liver, which were identified as lymphomas.

6.2.2 Brg1 loss is permissive of Wnt-driven tumourigenesis in the pyloric, but not fundic or forestomach epithelium

The extended survival of $AhCreER^{+}Apc^{fl/fl}Brg^{fl/fl}$ mice allowed me to analyse the long-term effects of Brg1 deficiency on Wnt driven tumourigenesis in tissues with delayed tumour development, such as the glandular and forestomach epithelium. $AhCreER^{+}$-$Apc^{fl/fl}Brg^{+/+}$ and $AhCreER^{+}Apc^{fl/fl}Brg^{fl/fl}$ mice were induced along with $AhCreER^{-}$ controls by five intraperitoneal injections of 80 mg/kg β-naphthoflavone and tamoxifen. Mice were sacrificed at defined time points or upon displaying signs of ill health, at which point they were dissected and whole stomachs were harvested and processed for histological analysis.

6.2.2.1 $AhCreER^+Apc^{fl/fl}Brg^{fl/fl}$ mice develop Wnt-driven adenomas in the pyloric stomach

Immunohistochemical analysis of β-catenin expression in the glandular stomach of $AhCreER^+$-$Apc^{fl/fl}Brg^{fl/fl}$ mice revealed small lesions in the pyloric stomach that exhibited nuclear localisation of β-catenin as early as day 19 PI (n=3, Figure 6.1a, leftmost panel). These lesions were characterised by an abnormal glandular architecture and increased nucleus-to-cytoplasm ratio and were identified as gastric adenomas. Analysis of Brg1 expression revealed positive Brg1 staining in the vast majority of these lesions (Figure 6.1a, middle panel). In fact, no Brg1 deficient lesions with nuclear β-catenin were observed in the pyloric stomach of $AhCreER^+Apc^{fl/fl}Brg^{fl/fl}$ mice at this time point. Rare $AhCreER^+$-$Apc^{fl/fl}Brg^{+/+}$ mice that survived until day 19 PI displayed Wnt activated pyloric lesions of comparable size (n=2, Figure 6.1a, rightmost panel). Immunohistochemical analysis of Brg1 and β-catenin expression in the pyloric epithelium of $AhCreER^+Apc^{fl/fl}Brg^{fl/fl}$ mice at 30 days PI revealed a similar pattern of Brg1 expression and nuclear accumulation of β-catenin (n=6, not shown). Analysis of Brg1 expression in pyloric stomach at day 60 PI, however, detected occasional lesions with nuclear β-catenin that displayed loss of Brg1 expression (n=6, Figure 6.1b). While most of the Wnt activated lesions in the pyloric stomach remained relatively small and sessile, a single macroscopic lesions was observed in the pyloric junction of an $AhCreER^+Apc^{fl/fl}Brg^{fl/fl}$ mouse that survived past 100 days PI (n=6, Figure 6.1c). This tumour exhibited nuclear localisation of β-catenin and was identified as a well differentiated gastric adenoma with low-grade dysplasia[1]. Immunohistochemical analysis of Brg1 expression in the gastric adenoma revealed occasional Brg1 deficient clusters within the predominantly Brg1 positive tumour (Figure 6.1c, rightmost panel).

Comparative analysis of β-catenin localisation in Brg1 positive and negative pyloric lesions revealed a reduction in the levels of nuclear β-catenin in Brg1 deficient lesions (Figure 6.1d). β-catenin staining of Brg1 deficient lesions was substantially stronger than that of surrounding normal tissue. However, nuclear localisation of β-catenin was found to be less prominent than that observed in Brg1 positive lesions. This pattern of β-catenin distribution in Brg1 deficient pyloric lesions was consistently observed at all the time points analysed irrespective of the lesion size.

6.2.2.2 Brg1 loss suppresses some Wnt targets in the Wnt-driven pyloric lesions

The presence of Brg1 deficient lesions with increased levels of β-catenin suggested that Brg1 may be dispensable for Wnt-driven tumourigenesis in the pyloric stomach epithelium. On the other hand, the late onset of Brg1 deficient lesions, their low number and the lack

---

[1]Histopathological description was provided by Prof Geraint T. Williams, Department of Pathology, University Hospital of Wales, Cardiff University, UK
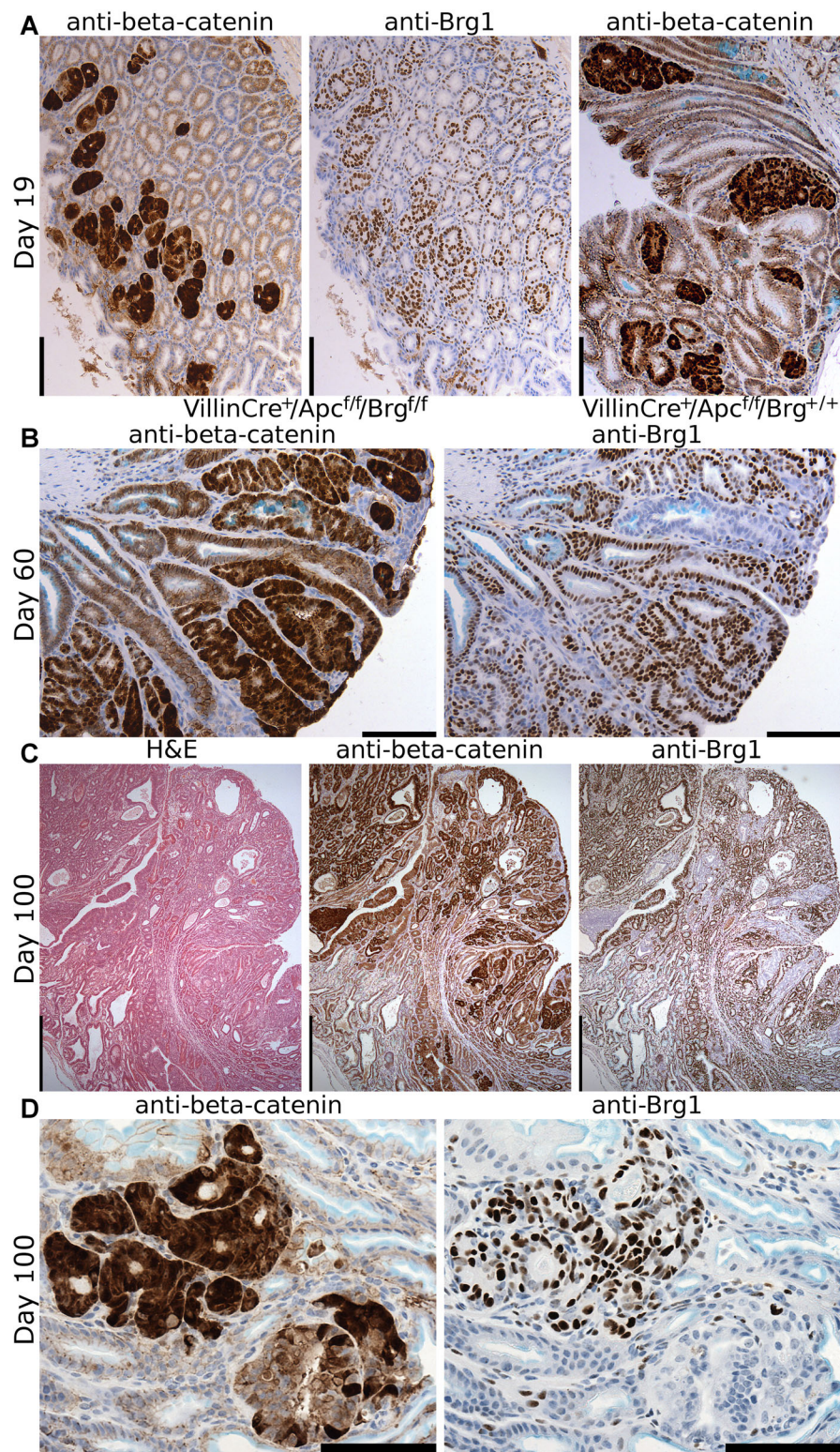
Figure 6.1: Brg1 loss in the pyloric stomach is permissive of Wnt-driven tumourigenesis. **(a)** Lesions with nuclear accumulation of β-catenin were revealed in the pyloric stomach of $AhCreER^{+}Apc^{fl/fl}$-$Brg^{+/+}$ and $AhCreER^{+}Apc^{fl/fl}Brg^{fl/fl}$ mice at day 19 PI. No loss of Brg1 expression was observed in pyloric lesions of $AhCreER^{+}Apc^{fl/fl}Brg^{fl/fl}$ mice at this time point. **(b)** Loss of Brg1 expression was revealed in occasional Wnt activated lesions in the pyloric stomach of $AhCreER^{+}Apc^{fl/fl}Brg^{fl/fl}$ mice as early as day 60 PI. **(c)** A single macroadenoma that developed in the pyloric epithelium of a $AhCreER^{+}Apc^{fl/fl}Brg^{fl/fl}$ mouse displayed nuclear accumulation of β-catenin and rare clusters of Brg1 deficient cells. **(d)** Analysis of β-catenin distribution revealed frequent attenuation of nuclear β-catenin accumulation in Brg1 deficient pyloric lesions. Scale bars represent 100 μm **(a,b)**, 500 μm **(c)** and 50 μm **(d)**.

of nuclear β-catenin staining all signalled that Brg1 loss in the context of Wnt activated pyloric epithelium could result in suboptimal levels of Wnt signalling. I, therefore, aimed to assess the effects of Brg1 loss on downstream Wnt target gene expression. To this end, immunohistochemical analysis of CD44 and c-Myc expression was performed on pyloric stomach sections containing both Brg1 positive and negative lesions. Comparative analysis of c-Myc expression revealed its frequent down-regulation in Brg1 deficient lesions compared to adjacent lesions retaining Brg1 expression (Figure 6.2). In contrast to this observation, no consistent correlation between the levels of CD44 expression and Brg1 status of the lesion was observed (Figure 6.2).
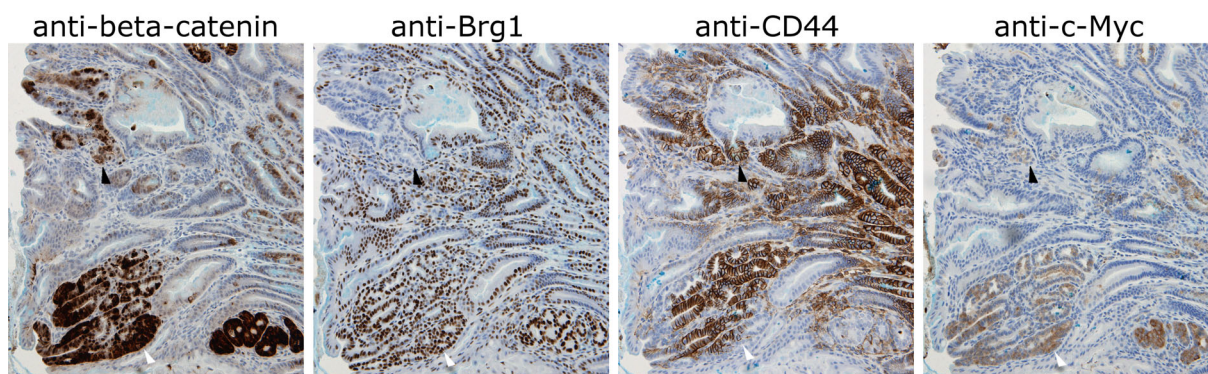
Figure 6.2: Brg1 loss in Wnt-driven pyloric adenomas suppressed c-Myc, but not CD44 expression. Immunohistochemical analysis of c-Myc and CD44 expression was carried out on serial sections of pyloric adenomas from $AhCreER^+Apc^{fl/fl}Brg^{fl/fl}$ mice at day 105 PI. Comparative analysis of Brg1 positive (white arrowhead) and negative (black arrowhead) adenomas revealed attenuation of c-Myc expression in Brg1 deficient adenomas. No changes in CD44 expression were detected between Brg1 positive and negative adenomas. Scale bars represent 200 μm.

6.2.2.3 Wnt pathway activation does not induce tumourigenesis in the fundic or forestomach epithelium

Immunohistochemical analysis of β-catenin expression detected no lesions with nuclear β-catenin in the fundic portion of the stomach epithelium neither in $AhCreER^+Apc^{fl/fl}$-$Brg^{+/+}$, nor in $AhCreER^+Apc^{fl/fl}Brg^{fl/fl}$ animals, indicating that activation of the Wnt pathway via Apc loss alone is not sufficient to drive tumourigenesis in this tissue.

Similarly, no signs of Wnt-driven tumourigenesis were observed in the forestomach epithelium of $AhCreER^+Apc^{fl/fl}Brg^{fl/fl}$ mice. While very small (4-6 cells in cross section) lesions with prominent nuclear localisation of β-catenin were detected in the basal layer of the forestomach epithelium of $AhCreER^+Apc^{fl/fl}Brg^{+/+}$ and $AhCreER^+Apc^{fl/fl}$-$Brg^{fl/fl}$ animals at day 10 PI (n=3, Figure 6.3a), no similar lesions were observed at later time points. Surprisingly, occasional regions of the forestomach epithelium from $AhCreER^+Apc^{fl/fl}Brg^{fl/fl}$ mice were found to display loss of Brg1 (Figure 6.3b, right-most panel). These regions appeared indistinguishable from adjacent Brg1 positive epithelium and showed no sign of nuclear accumulation of β-catenin (Figure 6.3b, left and middle panels). These regions, thus, were likely to be represented by cells that have un-

dergone Brg1 deletion, but escaped loss of Apc. Additionally, rare lesions that resembled Brg1 deficient squamous papillomas found in $AhCreER^+Brg^{fl/fl}$ mice were detected in the forestomach of $AhCreER^+Apc^{fl/fl}Brg^{fl/fl}$ animals (Figure 6.3c). In contrast to the papillomas from $AhCreER^+Brg^{fl/fl}$ forestomach epithelium, Brg1 deficient lesions in the forestomach of $AhCreER^+Apc^{fl/fl}Brg^{fl/fl}$ animals remained very small in size as late as 160 days PI. These lesions exhibited loss of Brg1 expression and a moderate increase in β-catenin staining (Figure 6.3c). However, a similar pattern of β-catenin staining (an overall increase in intracellular β-catenin levels without any marked increase in nuclear localisation) was occasionally observed in the wild type forestomach epithelium. It is, therefore, difficult to ascertain whether increased β-catenin levels in the Brg1 deficient forestomach lesions of $AhCreER^+Apc^{fl/fl}Brg^{fl/fl}$ epithelium were a consequence of activated Wnt signalling and if, indeed, Apc was lost in these lesions.

6.2.3 Brg1 deficiency is permissive for Wnt-driven tumourigenesis in the large intestinal epithelium

Having established that Brg1 loss has no detrimental effect on the long-term maintenance of the large intestinal epithelium (see section 4.2.4), I aimed to ascertain whether loss of Brg1 would manifest a phenotype in the context of aberrant Wnt signalling. To this end, $AhCreER^+Apc^{fl/fl}Brg^{+/+}$ and $AhCreER^+Apc^{fl/fl}Brg^{fl/fl}$ mice were induced along with $AhCreER^-$ controls by five intraperitoneal injections of 80 mg/kg β-naphthoflavone and tamoxifen. Mice were sacrificed at defined time points or upon displaying signs of ill health, at which point samples of the large intestine were collected and processed for histological analysis.

6.2.3.1 Brg1 deficiency is permissive of Wnt-driven adenoma formation in the large intestinal epithelium

Immunohistochemical analysis of β-catenin expression in the large intestinal epithelium of $AhCreER^+Apc^{fl/fl}Brg^{fl/fl}$ mice detected small lesions that displayed nuclear localisation of β-catenin as early as day 19 PI (n=3, Figure 6.4a, left panel). These lesions were represented by individual abnormal crypts that displayed signs of low-grade dysplasia. Analysis of Brg1 expression in the large intestine of $AhCreER^+Apc^{fl/fl}Brg^{fl/fl}$ mice revealed that the majority of the Wnt activated lesions retained Brg1 expression. However, occasional Brg1 deficient lesions with nuclear β-catenin were detected as early as day 19 PI (Figure 6.4a, middle panel). Interestingly, rare Brg1 deficient crypts were detected in the large intestinal epithelium of $AhCreER^+Apc^{fl/fl}Brg^{fl/fl}$ mice that displayed no signs of dysplasia or nuclear β-catenin accumulation (Figure 6.4b, black arrowheads). These crypts most likely originated from cells that had lost Brg1 but escaped Apc deletion. The large intestine of $AhCreER^+Apc^{fl/fl}Brg^{fl/fl}$ mice thus contained all three cellular populations resulting from suboptimal Cre recombinase activity, namely Brg1 deficient, Apc deficient
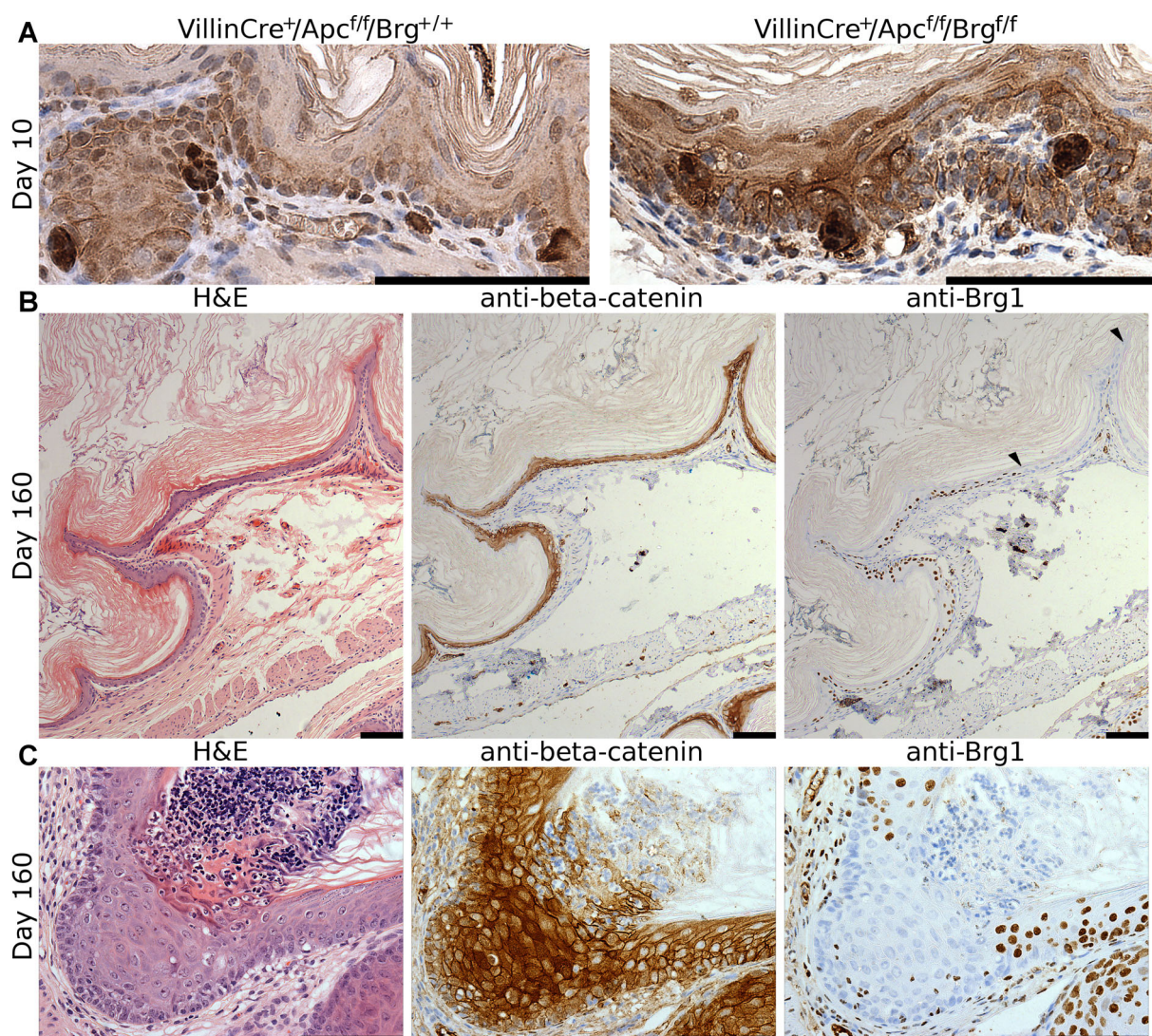
Figure 6.3: Activation of Wnt signalling in the forestomach epithelium fails to induce tumourigenesis. **(a)** Immunostaining with β-catenin antibody revealed small lesions with nuclear accumulation of β-catenin in the forestomach epithelium of $AhCreER^+Apc^{fl/fl}Brg^{+/+}$ and $AhCreER^+Apc^{fl/fl}Brg^{fl/fl}$ mice as early as day 10 PI. **(b)** No lesions with nuclear accumulation of β-catenin were detected in the forestomach epithelium of $AhCreER^+Apc^{fl/fl}Brg^{fl/fl}$ mice as late as day 160 PI. However, immunohistochemical analysis of Brg1 expression revealed occasional forestomach regions of Brg1 loss in these mice (marked by black arrowheads). These regions were indistinguishable from normal epithelium on H&E stained sections and displayed no sign of nuclear accumulation of β-catenin. **(c)** Rare Brg1 deficient malformations were detected in the forestomach epithelium of $AhCreER^+Apc^{fl/fl}Brg^{fl/fl}$ mice. Despite increased levels of β-catenin expression in these structures, no prominent nuclear accumulation of β-catenin was observed. Scale bars represent 100 μm

and double knock-out cells. The large intestine of occasional $AhCreER^+Apc^{fl/fl}Brg^{+/+}$ mice that survived until day 19 PI was found to contain Wnt activated lesions comparable in size to those observed in $AhCreER^+Apc^{fl/fl}Brg^{fl/fl}$ animals (Figure 6.4a, right panel).

Macroscopic analysis of the large intestinal epithelium from $AhCreER^+Apc^{fl/fl}Brg^{fl/fl}$ mice revealed occasional macroscopic tumours as early as day 60 PI (n=6, Figure 6.4d and e). Histological analysis of these tumours identified them as intestinal adenomas of characteristic pedunculated appearance. Adenomas were predominantly composed of epithelial cells, which displayed strong nuclear β-catenin staining and low-grade dysplasia (Figure 6.4d and e). Immunohistochemical analysis of Brg1 expression within the polyps revealed a mosaic pattern of Brg1 staining. The majority of the polyps contained both Brg1 positive and negative cells. These cells were organised into distinct substructures within the polyp, so that each substructure was completely composed of either Brg1 positive or negative cells rather that containing a mixture of both (Figure 6.4d). Notably, Brg1 deficient substructures displayed a pattern of β-catenin staining similar to that observed in Brg1 deficient fundic lesions. Whilst general level of β-catenin in these substructures was substantially higher compared to normal tissue, its nuclear accumulation was less prominent than in Brg1 positive substructures (Figure 6.4d). Additionally, adenomas containing only Brg1 positive substructures were also frequently observed (Figure 6.4e). Conversely, whilst individual Brg1 deficient lesions (similar to those present at day 19 PI) were occasionally observed (Figure 6.4c), no macroadenomas composed entirely of Brg1 deficient substructures were detected.

Macroscopic analysis of $AhCreER^+Apc^{fl/fl}Brg^{fl/fl}$ mice that survived past 100 days PI revealed multiple macroscopic tumours of adenoma appearance (n=6). Histological and immunohistochemical analysis of these tumours found them to be indistinguishable from the large adenomas observed at day 60 PI (Figure 6.4f). No signs of progression towards adenocarcinoma were detected in the large intestinal adenomas of $AhCreER^+$-$Apc^{fl/fl}Brg^{fl/fl}$ mice at any stage.

6.2.3.2 Large intestinal Brg1 loss does not alter the phenotype of aberrant Wnt signalling

[2] The presence of Brg1 deficient lesions with nuclear β-catenin in the large intestinal epithelium of $AhCreER^+Apc^{fl/fl}Brg^{fl/fl}$ mice suggested dispensability of functional Brg1 for Wnt driven tumourigenesis in this tissue. Conversely, the low frequency occurrence of Brg1 deficient Wnt activated substructures compared to Brg1 positive counterparts and the absence of Brg1 deficient large adenomas indicated suboptimal efficiency of Wnt-driven tumourigenesis in the context of Brg1 deficiency. In order to investigate whether Brg1 loss impaired Wnt-driven tumourigenesis in the large intestinal epithelium

---

[2]Quantitative analysis of cell proliferation and apoptosis in Brg1 positive and negative substructures was carried out by Joanna Krzystyniak under my direction and supervision.
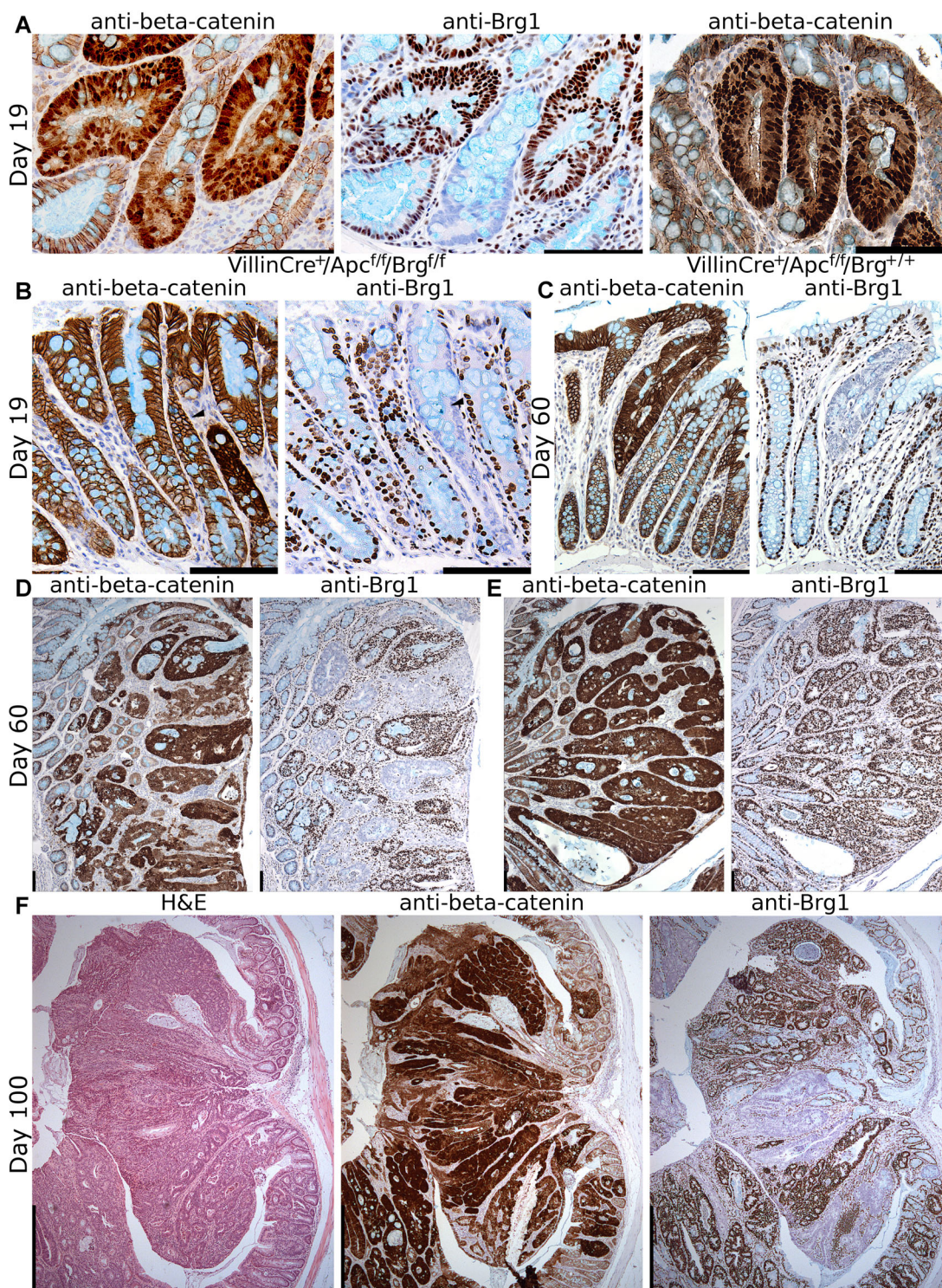
Figure 6.4: Brg1 deficiency is permissive of Wnt-driven tumourigenesis in the large intestinal epithelium. **(a)** Numerous lesions with nuclear accumulation of β-catenin were detected in the large intestinal epithelium of $AhCreER^+Apc^{fl/fl}Brg^{+/+}$ and $AhCreER^+Apc^{fl/fl}Brg^{fl/fl}$ mice as early as day 19 PI. Occasional large intestinal lesions of $AhCreER^+Apc^{fl/fl}Brg^{fl/fl}$ mice displayed Brg1 loss. **(b)** Rare Brg1 deficient crypts with normal appearance and no sign of nuclear β-catenin were detected in the large intestine of $AhCreER^+Apc^{fl/fl}Brg^{fl/fl}$ mice at various time points. **(c)** Individual Brg1 deficient lesions with nuclear β-catenin were detected at various time points. **(d, e)** Large intestines of $AhCreER^+Apc^{fl/fl}Brg^{fl/fl}$ mice were found to develop macroscopic adenomas as early as day 60 PI. These adenomas displayed nuclear accumulation of β-catenin and either mosaic loss of Brg1 **(d)** or no Brg1 loss at all **(e)**. **(f)** $AhCreER^+Apc^{fl/fl}Brg^{fl/fl}$ that survived past 100 days PI developed large benign adenomas with mosaic pattern of Brg1 loss and nuclear accumulation of β-catenin. Scale bars represent 100 μm **(a-e)** and 500 μm **(f)**.

of $AhCreER^+Apc^{fl/fl}Brg^{fl/fl}$ mice, I aimed to analyse certain phenotype manifestations of Wnt pathway activation in Brg1 deficient and proficient lesions.

To assess the impact of Brg1 deficiency on the expression levels of downstream Wnt target genes, large intestinal samples containing tumours with mosaic Brg1 loss were immunostained with antibodies against c-Myc and CD44 (Figure 6.5a). Comparative analysis of c-Myc and CD44 expression in Brg1 positive and negative portions of mosaic adenomas, however, failed to detect any consistent correlation between the expression levels and Brg1 status of the substructure (Figure 6.5a).
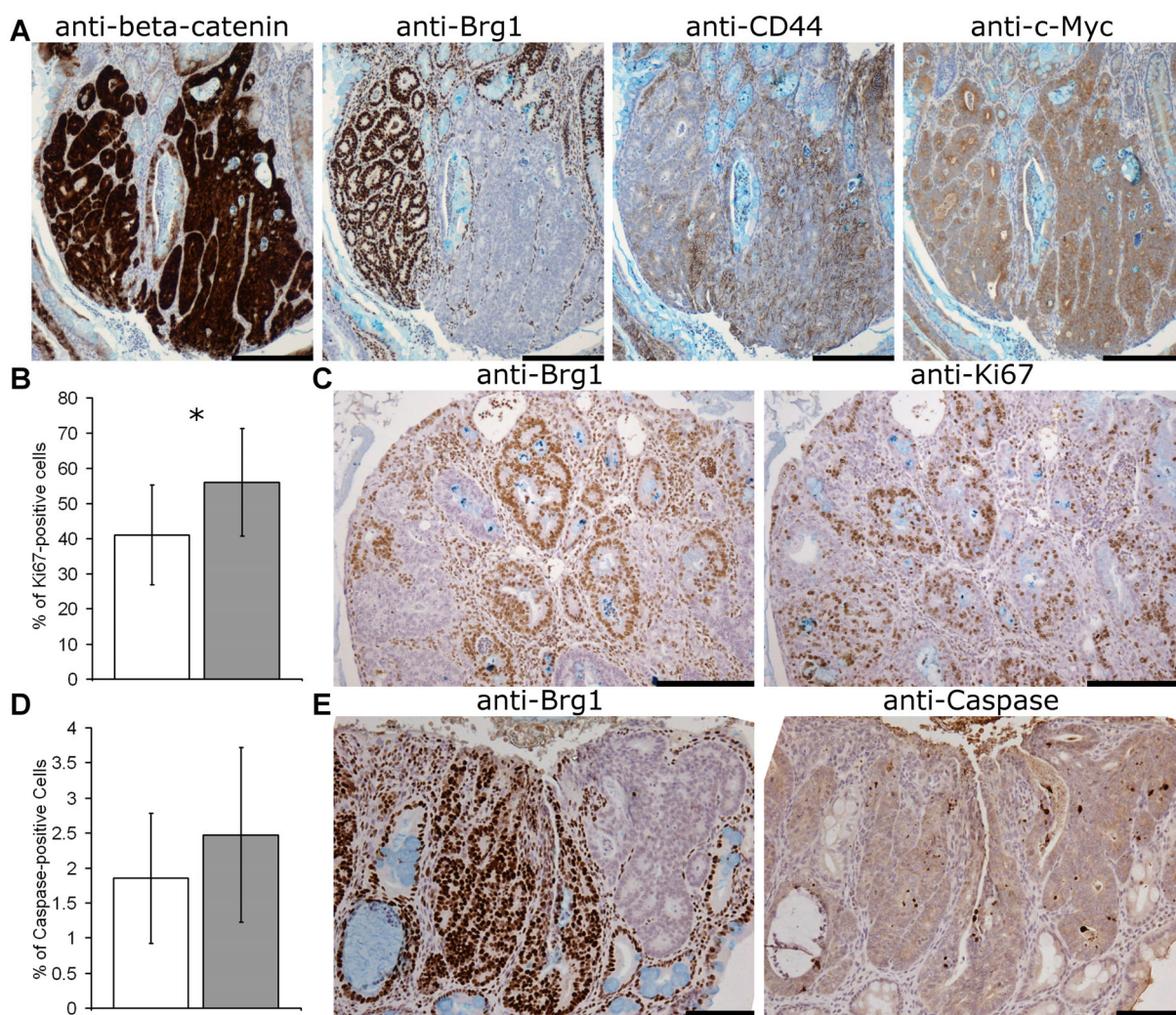
Figure 6.5: Brg1 loss in Wnt-driven large intestinal adenomas does not suppress Wnt target gene expression. **(a)** Immunohistochemical analysis of c-Myc and CD44 expression was carried out on serial sections of large intestinal mosaic adenomas from $AhCreER^+Apc^{fl/fl}Brg^{fl/fl}$ mice at day 105 PI. Comparative analysis of Brg1 positive and negative substructures revealed no consistent correlation between expression of Wnt target genes and Brg1 status of the lesion. (b,c) Quantitative analysis of Ki67 stained mosaic adenomas **(c)** revealed a significant increase in the number of proliferating cells in Brg1 deficient substructures (b, p=0.036, n≥9). **(d, e)** Quantitative analysis of Cleaved Caspase3 stained mosaic adenomas **(e)** revealed no significant difference in the number of apoptotic cells in between Brg1 negative (grey bars) and positive (white bars) substructures (d, p=0.135, n≥15). Error bars represent standard deviation. Scale bars represent 100 μm.

In order to investigate whether Brg1 loss in the context of activated Wnt signalling affected proliferative activity of the tumour cells, large intestinal sections from $AhCreER^+$-

$Apc^{fl/fl}Brg^{fl/fl}$ mice containing adenomas with mosaic Brg1 deletion were immunostained with nuclear proliferation marker Ki67 and the number of positively stained cells was scored as a percentage ($\pm$ standard deviation) of all cells in the substructure (Figure 6.5b and c). Rather counter intuitively, quantitative analysis of the Ki67 stained sections revealed a significantly lower number of Ki67 positive cells in Brg1 positive substructures compared to their Brg1 negative counterparts (41.05$\pm$14.19 and 56$\pm$15.28, p=0.036). A minimum of 9 substructures were scored per group (Figure 6.5b).

Finally, in order to assess the effects of Brg1 loss on cell death in the context of aberrant Wnt signalling, large intestinal sections containing adenomas with Brg1 positive and negative substructures were stained with an antibody against cleaved Caspase 3 and the number of positively stained cells was scored as a percentage ($\pm$ standard deviation) of all cells in the substructure (Figure 6.5d and e). Quantification of Caspase 3 positive cells did not reveal any significant difference in apoptosis levels between Brg1 proficient and deficient substructures (1.85$\pm$0.93 and 2.45$\pm$1.29, p=0.135). 15 substructures were scored per group (Figure 6.5d).

Taken together, these observations suggest that Brg1 deficiency is permissive for Wnt driven tumourigenesis in the context of the large intestinal epithelium. Brg1 deficiency in Wnt activated tissue has no effect on the expression levels of Wnt target genes or upon the levels of cell death. Brg1 loss, however, appears to increase cell proliferation in Wnt driven large intestinal tumours.

6.2.4 Brg1 deficiency weakly modifies the Wnt pathway activation in the context of the bladder urothelium

Having established that Brg1 haploinsufficiency does not induce urothelial carcinogenesis alone or in combination with heterozygous Apc loss, I aimed to investigate the consequences of urothelial Brg1 loss in the context of aberrant Wnt signalling. To achieve this, $AhCreER^+Apc^{fl/fl}Brg^{+/+}$ and $AhCreER^+Apc^{fl/fl}Brg^{fl/fl}$ mice along with $AhCreER^-$ controls were induced with five intraperitoneal injections of 80 mg/kg β-naphthoflavone and tamoxifen. The mice were dissected at defined time points, and whole bladders were harvested and processed for histological analysis.

6.2.4.1 Aberrant Wnt signalling in the bladder induces the development of short-lived lesions with nuclear β-catenin

Histological analysis of H&E stained sections of the bladder urothelium from $AhCreER^+$-$Apc^{fl/fl}Brg^{+/+}$ and $AhCreER^+Apc^{fl/fl}Brg^{fl/fl}$ mice at day 10 PI revealed numerous compact lesions (n=6, Figure 6.6, left panel). These lesions were characterised by a well defined border and an increased nucleus-to-cytoplasm ratio. Immunohistochemical analysis of β-catenin expression revealed nuclear localisation of β-catenin in both $AhCreER^+Apc^{fl/fl}Brg^{+/+}$ and $AhCreER^+Apc^{fl/fl}Brg^{fl/fl}$ lesions (Figure 6.6, middle

panel). Immunostaining with an antibody against Brg1 revealed strong Brg1 immunore-activity in $AhCreER^+Apc^{fl/fl}Brg^{+/+}$ lesions, while $AhCreER^+Apc^{fl/fl}Brg^{fl/fl}$ lesions displayed complete loss of Brg1 expression (Figure 6.6, right panel). No abnormalities in the urothelium morphology of AhCreER- control mice were observed at any time point.
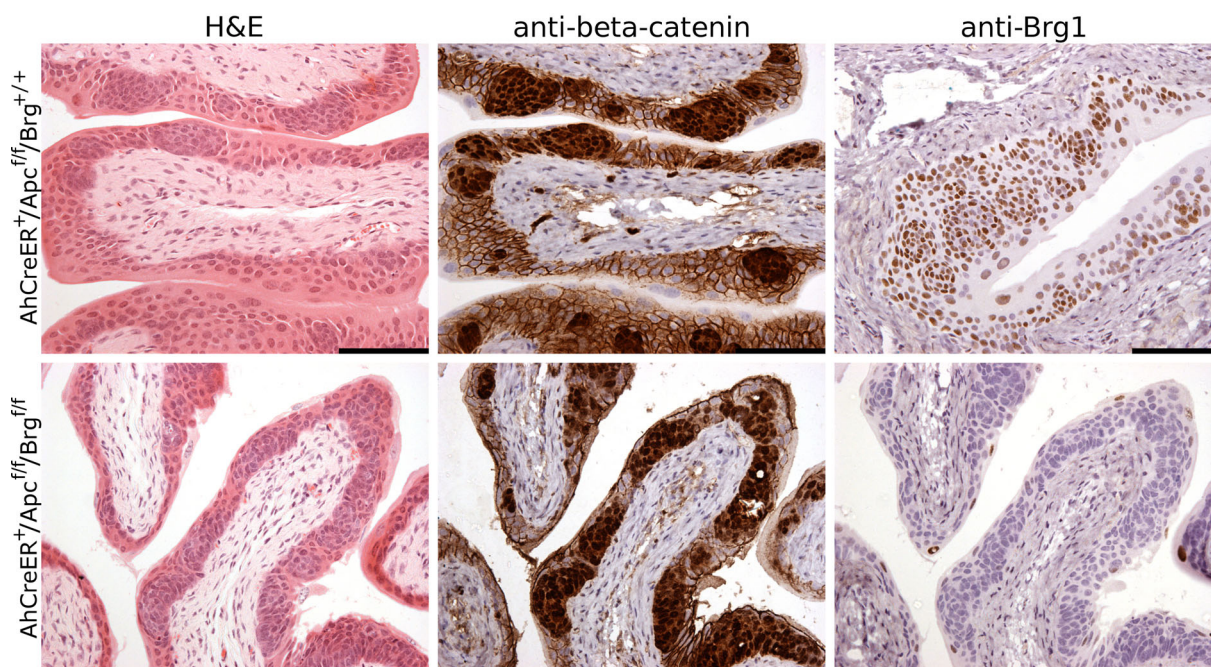
Figure 6.6: Brg1 deficiency is permissive of Wnt-driven tumourigenesis in the bladder urothelium. Histological analysis of H&E stained sections of the bladder urothelium from $AhCreER^+Apc^{fl/fl}Brg^{+/+}$ and $AhCreER^+Apc^{fl/fl}Brg^{fl/fl}$ mice at day 10 PI revealed numerous compact lesions. Analysis of β-catenin distribution revealed nuclear accumulation of β-catenin in these lesions. Immunohistochemical analysis of Brg1 expression revealed complete loss of Brg1 expression in $AhCreER^+Apc^{fl/fl}Brg^{fl/fl}$ bladder lesions. Scale bars represent 100 μm.

Despite their abundance in the bladder epithelium at day 10 PI, histological analysis of $AhCreER^+Apc^{fl/fl}Brg^{fl/fl}$ mice at day 30 PI failed to detect any urothelial lesions (not shown). This observation suggested that Wnt activated lesions in the bladder urothelium had a very short lifespan. In order to analyse the fate of the Wnt-driven urothelial lesions, mice were induced as described above and dissected at day 7, 10, 14 and 19 PI (n≥3 per time point). Immunostaining with an antibody against β-catenin allowed clear visualisation of the lesion size (Figure 6.7a). Visual analysis of the lesion size indicated initial growth, which stalled around day 14 PI. Analysis of $AhCreER^+Apc^{fl/fl}Brg^{+/+}$ and $AhCreER^+Apc^{fl/fl}Brg^{fl/fl}$ bladder urothelium at day 19 PI stained with a β-catenin antibody detected infrequent small lesions with nuclear β-catenin and large lacunae filled with dead cells, which appeared to be the remnants of the earlier resolved lesions (Figure 6.7a, black arrowheads).

In order to obtain a more quantitative measure of lesion fate I scored the number of cells per lesion in the $AhCreER^+Apc^{fl/fl}Brg^{+/+}$ and $AhCreER^+Apc^{fl/fl}Brg^{fl/fl}$ bladders at 7, 10 and 14 days PI (a minimum of 50 lesions was scored per cohort at each time point). Quantitative analysis of the lesion size revealed an initial increase in median
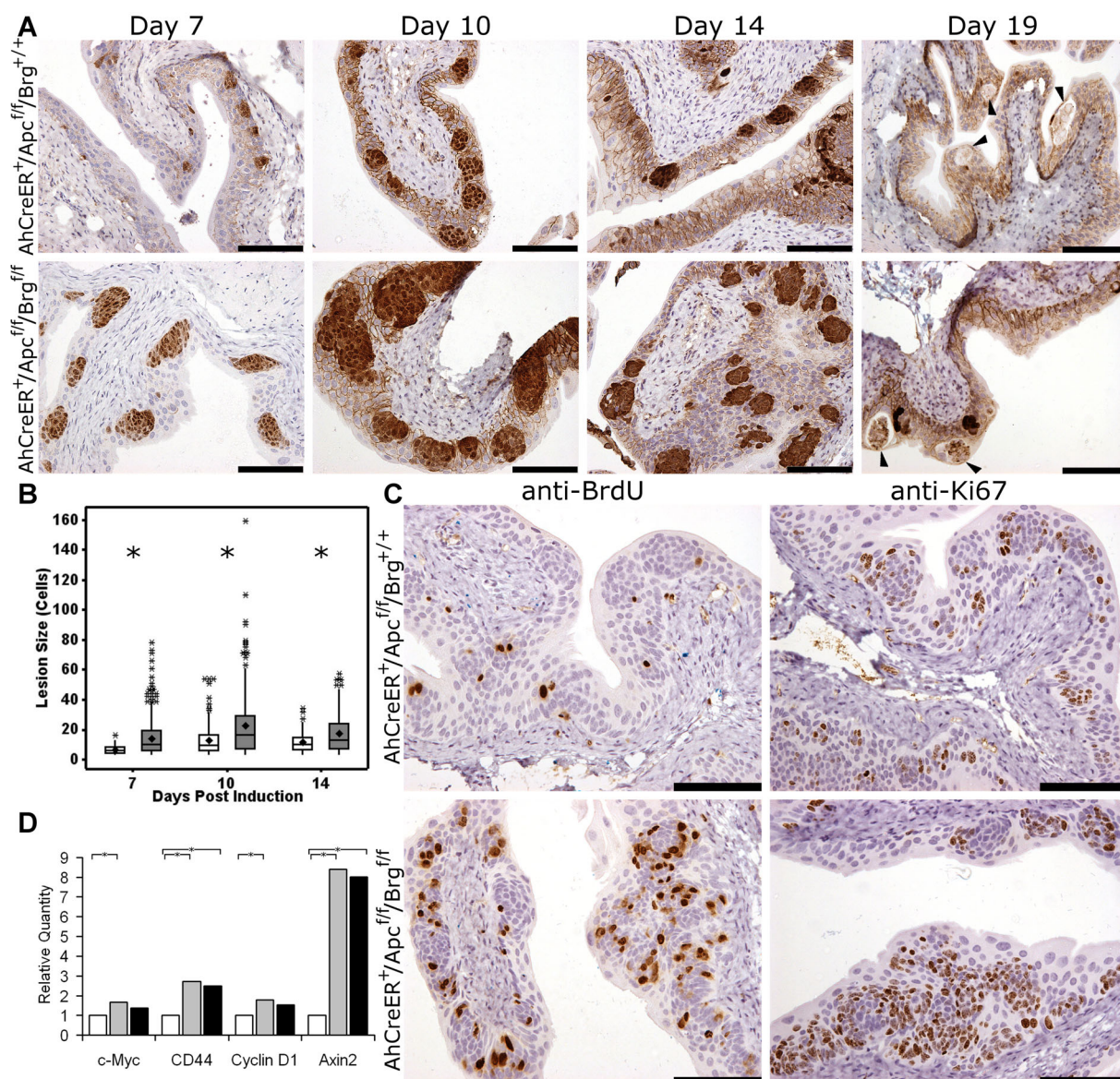
Figure 6.7: Brg1 facilitates Wnt-driven bladder tumourigenesis, but is unable to overcome lesions' regression. (a) Visual inspection of β-catenin stained urothelial lesions over the time course from day 7 to day 19 PI revealed an initial increase in the lesion size, which stalled around day 10 PI and regression of lesions around day 19. While lesions in the bladder of $AhCreER^+Apc^{fl/fl}Brg^{fl/fl}$ mice appeared larger than $AhCreER^+Apc^{fl/fl}Brg^{+/+}$ lesions at the same time point, they also were found to disappear around day 19. (b) Quantification of the lesion size confirmed that Brg1 deficient (grey bars) lesions were significantly larger than $AhCreER^+Apc^{fl/fl}Brg^{+/+}$ (white bars) lesions at the same time point (at each time point p<0.001, a minimum of 50 lesions was analysed per time point per genotype). The data were presented as a box plot. Filled dimond shape marks the mean value. (c) Immunohistochemical analysis of BrdU incorporation 3 hours post labelling and Ki67 expression, both revealed a substantial increase in the number of proliferating cells in Brg1 deficient lesions compared to bladder lesions from $AhCreER^+Apc^{fl/fl}Brg^{+/+}$ mice. Scale bars represent 100 μm. (d) Quantitative RT-PCR analysis of bladder urothelium at day 10 PI revealed no difference in expression levels of Wnt target genes between $AhCreER^+Apc^{fl/fl}Brg^{+/+}$ (grey bars) and $AhCreER^+Apc^{fl/fl}Brg^{fl/fl}$ (black bars) urothelium. While all Wnt target genes were up-regulated in $AhCreER^+Apc^{fl/fl}Brg^{+/+}$ epithelium compared to control Cre^- (white bars) mice, only $CD44$ and $Axin2$ were found to be up-regulated in $AhCreER^+$-$Apc^{fl/fl}Brg^{+/+}$ mice in comparison to control urothelium. Asterisks mark pairwise comparisons that showed a significant difference (p<0.05, n≥4).

lesion size between day 7 and 10 PI followed by the reduction in size between day 10 and 14 PI. This pattern was observed in both $AhCreER^+Apc^{fl/fl}Brg^{+/+}$ and $AhCreER^+$-$Apc^{fl/fl}Brg^{fl/fl}$ urothelium (Figure 6.7b). Although Brg1 deficient and proficient lesions displayed the same progression pattern and were largely eliminated by day 19 PI, at any time point Brg1 deficient lesions were larger in size based on the quantitative information (Figure 6.7a and b). Statistical comparison of the median lesion size between $AhCreER^+$-$Apc^{fl/fl}Brg^{+/+}$ and $AhCreER^+Apc^{fl/fl}Brg^{fl/fl}$ urothelium at each time point revealed a significant difference between the cohorts (Mood median test p<0.001 for each time point). Consistent with this observation, Brg1 deficient lesions from $AhCreER^+Apc^{fl/fl}$-$Brg^{fl/fl}$ urothelium displayed increased expression of the proliferation marker Ki67 and elevated levels of BrdU incorporation at 3 hours post labelling compared to $AhCreER^+$-$Apc^{fl/fl}Brg^{+/+}$ urothelium (Figure 6.7c).

Taken together, these observations demonstrate that aberrant activation of the Wnt pathway in the context of the bladder urothelium results in the development of short lived lesions. Both Brg1 positive and negative lesions are largely eliminated from Wnt activated bladder urothelium by day 19 PI. However, within the short life span of bladder Wnt-driven tumourigenesis, Brg1 deficient lesions display increased cell proliferation compared to Brg1 positive lesions. It appears therefore that Brg1 deficiency is favourable in a context of Wnt-driven bladder tumourigenesis, even though it is unable to avoid early regression of urothelial lesions.

6.2.4.2 Brg1 loss does not affect the expression levels of Wnt target genes in the Wnt activated bladder urothelium

In order to analyse the potential impact of Brg1 deficiency on Wnt signalling activation, I aimed to assess expression levels of the Wnt target genes in $AhCreER^+Apc^{fl/fl}Brg^{+/+}$ and $AhCreER^+Apc^{fl/fl}Brg^{fl/fl}$ bladder urothelium. To this end, $AhCreER^+Apc^{fl/fl}$-$Brg^{+/+}$ and $AhCreER^+Apc^{fl/fl}Brg^{fl/fl}$ mice were induced as described above along with AhCreER- controls. Mice were sacrificed at day 10 PI and the whole bladders were collected. The bladder urothelium was then separated from the muscular wall and subjected to RNA extraction and quantitative RT-PCR analysis.

Expression analysis of the Wnt target genes *c-Myc*, *CD44*, *Cyclin D1* and *Axin2* revealed a significant increase in their expression in the bladder urothelium of $AhCreER^+$-$Apc^{fl/fl}Brg^{+/+}$ mice compared to control animals (Figure 6.7d, for all genes p<0.05). However, no significant difference was detected in the Wnt target gene expression levels between $AhCreER^+Apc^{fl/fl}Brg^{+/+}$ and $AhCreER^+Apc^{fl/fl}Brg^{fl/fl}$ urothelium (Figure 6.7d, for all genes p>0.05). Furthermore, only a proportion of the Wnt target genes analysed were found to be significantly up-regulated in $AhCreER^+Apc^{fl/fl}Brg^{fl/fl}$ urothelium compared to control animals (Figure 6.7d, for *CD44* and *Axin2* p<0.05, for *Cyclin D1* and *c-Myc* p>0.05). It should be noted that, with the exception of *Axin2*, all the

Wnt target genes analysed displayed only a very moderate up-regulation in $AhCreER^+$-$Apc^{fl/fl}Brg^{+/+}$ and $AhCreER^+Apc^{fl/fl}Brg^{fl/fl}$ urothelium compared to control mice (Figure 6.7d).

6.3 Discussion

Despite numerous reports of Wnt pathway activating mutations in a diverse range of cancer types, these studies are often associative and do not provide clear evidence of the causative role of activated Wnt signalling in pathogenesis of these cancers (Giles *et al.*, 2003). In this chapter I investigated the ability of conditional Apc deletion to induce tumourigenesis in forestomach, fundic, pyloric, large intestinal and bladder epithelium. Additionally, I examined the ability of Brg1 loss to modulate Wnt-driven tumourigenesis in these tissues.

In summary, aberrant activation of Wnt signalling via Apc deletion failed to induce tumour formation in the forestomach and fundic epithelium and only produced short-lived lesions in the bladder urothelium. While Brg1 loss appeared to increase the proliferation rate of the Wnt-driven bladder lesions, it was unable to rescue the short life span of the lesions. Conversely, Apc loss was found to induce adenoma formation in the pyloric and large intestinal epithelium. While Brg1 loss appeared to impair the development of gastric adenomas, no detrimental effect of Brg1 deficiency on Wnt-driven large intestinal tumourigenesis was observed. Additionally, heterozygous loss of Apc failed to induce tumourigenesis in any of these tissues apart from the large intestine, as described in the previous chapter.

6.3.1 Heterozygous loss of Apc does not induce overt tumourigenesis in AhCre expressing non-intestinal tissues

Germline mutations in *Apc* gene have been linked to familial adenomatous polyposis (FAP), an inherited condition characterised by development of numerous gastrointestinal polyps (Groden *et al.*, 1991). In addition to numerous colonic polyps FAP patients are also prone to tumourigenesis of the upper gastrointestinal tract, including fundic gland polyps (Abraham *et al.*, 2000) and gastric adenocarcinoma (Park *et al.*, 2011). This observation was reproduced in animal models as mice with heterozygous truncation of Apc protein were found to develop gastric adenomas in addition to intestinal polyps (Pollard *et al.*, 2009; Tomita *et al.*, 2007). In the previous chapter I demonstrated that heterozygous loss of Apc under control of the AhCre recombinase was successful in driving tumourigenesis in the small and large intestines and was not affected by Brg1 haploinsufficiency. In this chapter I aimed to investigate Wnt-driven tumourigenesis and its modulation by Brg1 haploinsufficiency in the murine stomach tissues as well as the bladder urothelium. To this end, one copy of loxP targeted *Apc* allele was deleted under control of AhCre

recombinase with or without concurrent heterozygous loss of Brg1.

In contrast to previous murine models of heterozygous Apc loss (Pollard *et al.*, 2009; Tomita *et al.*, 2007) no malformations were observed in epithelial tissues of the stomach irrespective of Brg1 status. This discrepancy is even more remarkable considering substantially longer life span of $AhCre^+Apc^{+/fl}Brg^{+/+}$ and $AhCre^+Apc^{+/fl}Brg^{+/fl}$ mice compared to either Apc^{1322T} or Apc^{MIN} animals and, thus, a wider window of opportunity for tumour development. This discrepancy, however, may be attributed to a substantial variation of Apc deficiency phenotypes, depending on particular Apc mutations involved (Pollard *et al.*, 2009). As an example Apc^{1322T} mice display a substantially shortened life span and accelerated tumourigenesis compared to Apc^{MIN} animals (Pollard *et al.*, 2009). Notably, while no gastric adenomas were observed in the pylorus of $AhCre^+$-$Apc^{+/fl}Brg^{+/+}$ or $AhCre^+Apc^{+/fl}Brg^{+/fl}$, these lesions can be difficult to distinguish from duodenal adenomas in cases, where the tumour develops at the pyloric junction. Such adenomas were analysed as a part of the small intestinal phenotype of Apc loss (section 5.2.2).

Similarly, no bladder lesions were detected in mice with heterozygous loss of Apc at any time point irrespective of Brg1 status. This observation is consistent with a limited presence of Wnt activating mutations in urothelial carcinomas (Stoehr *et al.*, 2002) as well as a recent report indicating that Wnt activation alone has a restricted ability to induce tumourigenesis in the urothelium (Ahmad *et al.*, 2011).

The results presented in this chapter, therefore, indicate that among those tissues expressing AhCre recombinase, the ability of heterozygous Apc loss to induce tumour development is limited to the intestinal epithelium.

6.3.2 Brg1 loss partially attenuates aberrant Wnt signalling in the pyloric stomach, but is permissive for Wnt driven tumourigenesis

Gastric cancer is the fourth most common cancer and the second leading cause of cancer related death in the world (Hamilton and Meltzer, 2006). Although its role in gastric cancer is not as well established as in CRC, activation of the Wnt pathway has been implicated in the gastric neoplasia by numerous reports. Nuclear accumulation of β-catenin in gastric adenocarcinomas has been found to vary from 17% to 54% among different studies (Clements *et al.*, 2002; Oshima *et al.*, 2006; Woo *et al.*, 2001). The evidence for *APC* and *β-catenin* mutations in gastric cancer is as variable between different studies and has been reported to reach up to 60% for *APC* and 27% for *β-catenin* (Clements *et al.*, 2002; Ebert *et al.*, 2002; Lee *et al.*, 2002; Woo *et al.*, 2001). Furthermore, a number of transgenic mouse models with *Apc* gene truncations have been reported to develop gastric neoplasia (Pollard *et al.*, 2009; Tomita *et al.*, 2007).

Consistent with these observations, conditional deletion of Apc using AhCreER re-

combinase was found to induce adenomatous lesions in the pyloric stomach epithelium of $AhCreER^+Apc^{fl/fl}Brg^{+/+}$ mice as early as 19 days PI. These lesions displayed strong nuclear accumulation of β-catenin and were histologically similar to those reported in the stomach of Apc^{MIN} mice (Tomita *et al.*, 2007). Unfortunately, the short life span of $AhCreER^+Apc^{fl/fl}Brg^{+/+}$ mice due to small intestinal tumourigenesis prevented the long-term study of pyloric lesions in these mice. Conversely, the extended life span of $AhCreER^+Apc^{fl/fl}Brg^{fl/fl}$ enabled an investigation of the relatively long-term gastric adenoma progression. Due to suboptimal levels of Cre recombinase activity, the pyloric stomach of $AhCreER^+Apc^{fl/fl}Brg^{fl/fl}$ mice contained both Brg1 deficient and proficient lesions, all of which displayed nuclear localisation of β-catenin. In fact, whilst Brg1 positive pyloric adenomas were visible at day 19 PI, Brg1 deficient adenomas were not detected until approximately day 60 PI and were substantially under-represented compared to Brg1 positive lesions. The late onset and low frequency of Brg1 deficient pyloric adenomas suggested impaired Wnt-driven tumourigenesis in response to Brg1 loss. Consistent with this notion, Brg1 deficient adenomas were shown to display reduced expression levels of the Wnt target gene *c-Myc*, although the same pattern was not observed for another Wnt target, *CD44*. Additionally, Brg1 deficient adenomas displayed attenuated levels of nuclear β-catenin compared to Brg1 positive lesions. It is, therefore tempting to hypothesise that Brg1 deficiency attenuates expression of some Wnt target genes in the Wnt activated pyloric epithelium, thus delaying the development of the Brg1 deficient adenomas without blocking it completely.

The vast majority of gastric adenomas observed in the pylorus of $AhCreER^+Apc^{fl/fl}$-$Brg^{fl/fl}$ mice remained small and sessile over the whole period of observation (up to 160 days PI) irrespective of their Brg1 status. In fact, only one macroscopic polyp-like adenoma was detected amongst six mice that survived past 100 days PI. While predominantly Brg1 positive, this macroadenoma also contained small clusters of Brg1 deficient cells. All pyloric adenomas remained benign and displayed no signs of invasive disease. This observation is consistent with that made in Apc^{MIN} mice (Tomita *et al.*, 2007). Only Apc^{MIN} mice that were additionally treated with N-methyl-N-nitrosourea (MNU) were reported to progress to invasive adenocarcinomas, whilst adenomas in the stomach of untreated Apc^{MIN} mice remained benign (Tomita *et al.*, 2007). Together, these observations suggest that while activation of Wnt signalling via Apc loss in the pyloric epithelium is able to initiate adenoma formation, additional mutations are required to drive its progression towards advanced disease.

6.3.3   Aberrant Wnt signalling does not induce tumourigenesis in the fundic and forestomach epithelium

In contrast to the pyloric stomach, activation of the Wnt pathway failed to induce tumourigenesis in fundic and forestomach epithelium of either $AhCreER^+Apc^{fl/fl}Brg^{fl/fl}$

or $AhCreER^+Apc^{fl/fl}Brg^{+/+}$ mice. Whilst small lesions with nuclear β-catenin were observed in the basal cell layer of the forestomach epithelium of both cohorts at day 10 PI, no Wnt activated lesions were identified at later time points. Due to the short life span of $AhCreER^+Apc^{fl/fl}Brg^{+/+}$ animals it cannot be established with certainty whether long-term Wnt activation would be able to induce tumourigenesis in these tissues. It could therefore, be hypothesised that it was the loss of Brg1 that prevented the development of Wnt driven lesions in the fundus and forestomach of long surviving $AhCreER^+Apc^{fl/fl}$-$Brg^{fl/fl}$ mice. However, given the suboptimal efficiency of AhCreER recombinase in the analysed tissues, one could expect to find a residual subpopulation of Apc-only deficient cells. This was not, however, the case as the only mutant cells detected in these two tissues were occasional Brg1 deficient cells with no sign of nuclear β-catenin in the forestomach epithelium. Thus, the lack of Wnt-driven tumours in the fundic and forestomach epithelium of $AhCreER^+Apc^{fl/fl}Brg^{fl/fl}$ mice strongly suggests that Wnt signalling activation alone is insufficient to induce tumourigenesis in these tissues regardless of Brg1 status.

Interestingly, the inability of Wnt pathway activation to drive tumourigenesis in the forestomach and fundic epithelium coincides with the lack of Wnt signalling in the normal homeostasis of these tissues. Morphogenesis and patterning of the oesophagus and stomach epithelial compartments have been reported to rely on Wnt pathway suppression. Expression of the homeodomain transcription factor Barx1 in the mesenchymal tissue underlying prospective oesophagus and stomach has been found to be essential for developmental specification of the stomach (Kim *et al.*, 2005) and oesophageal (Woo *et al.*, 2011) epithelium by stimulating expression of Wnt antagonists, such as secreted frizzled-related proteins (sFRPs). Conversely, the lack of Barx1 expression in the intestinal mesenchyme is permissive of Wnt signalling and thus intestinal differentiation (Kim *et al.*, 2005).

In contrast to the fundic epithelium, pyloric stomach physiology appears to be closer to the small intestinal epithelium in terms of reliance on Wnt signalling. First of all, the pyloric but not fundic stem cells have been found to express the intestinal stem cell marker Lgr5 (Barker *et al.*, 2007). It should be noted, however, that Lgr5 expression in the pyloric epithelium has been found to be restricted to the base of the glands, which contrasts with the conventional position of the stomach stem cell at the gland isthmus (Karam, 1999). In spite of this controversy, Lgr5 positive cells have been reported to be able to drive long-term maintenance of the pyloric glands both *in vivo* and *in vitro*. Consistent with these findings, conditional deletion of the *Apc* gene in Lgr5 positive cells has been shown to induce gastric adenoma formation in the pyloric, but not fundic region of the murine stomach. Similarly, gastric adenomas in mice with constitutive heterozygous truncation of *Apc* were found to develop in pyloric, but not fundic epithelium (Pollard *et al.*, 2009; Tomita *et al.*, 2007). These observations are, however, inconsistent with common occurrence of genetic aberrations in *APC* and β-*Catenin* genes in FAP-related and sporadic cases of fundic gland polyps respectively (Abraham *et al.*, 2000, Abraham

et al., 2001). This discrepancy suggests potentially distinct mechanisms of Wnt-driven fundic gland polyposis in the human and murine stomach epithelium.

While Wnt pathway suppression is required for normal development and homeostasis of oesophageal epithelium, Wnt signalling activation have been shown to play a limited role in oesophageal neoplasia. Two major types of cancer can be distinguished in the oesophageal epithelium: oesophageal squamous cell carcinoma (ESCC) and oesophageal adenocarcinoma (EAC). Of these, ESCC accounts for nearly 95% of oesophageal cancer cases (Kuwano *et al.*, 2005). In contrast to ESCCs, which retain squamous epithelium identity, EACs undergo a metaplastic change and convert from squamous into columnar epithelium in response to chronic gastro-oesophageal reflux, a condition termed Barett's oesophagus (Flejou, 2005). Consistent with this intestine-like transformation of the epithelial identity, activation of the Wnt pathway has been associated with progression from Barett's oesophagus to EAC (Bian *et al.*, 2000). However, mutational analysis of primary components of the Wnt pathway, such as β-*Catenin*, *APC* and *AXIN* revealed that mutations in these genes are rarely detected (Bian *et al.*, 2000; Koppert *et al.*, 2004; Gonzalez *et al.*, 1997). Instead, *APC* and a Wnt signalling inhibitor *SFRP1* were found to be frequently silenced via promoter hypermethylation in Barett's oesophagus and EAC (Clement *et al.*, 2006). In the light of the notion that promoter hypermethylation tends to be a post-initiation event in cancer progression (Jones and Baylin, 2002), these reports suggest that aberrant activation of Wnt signalling in EAC is likely to occur at later stages and be involved in cancer progression rather than initiation.

In a similar manner to EAC, analysis of ESCC samples have suggested a limited role of the Wnt pathway in ESCC development. Expression analyses have detected nuclear β-catenin in a minority of ESCC samples as well as a more frequent increase in Cyclin D1 expression (Kudo *et al.*, 2007). Similarly, progression from basal cell hyperplasia to malignant ESCC has been found to correlate with a decrease in expression of APC and E-Cadherin as well as an increase in nuclear β-catenin and Cyclin D1 expression (Peng *et al.*, 2009). Additionally, a number of the Wnt pathway antagonists, such as WNT5A, SFRP1 and WIF1 have been frequently found to be epigenetically silenced in ESCC via promoter hypermethylation (Chan *et al.*, 2007; Li *et al.*, 2010; Meng *et al.*, 2011). However, despite these and other reports suggesting correlation of Wnt activation with ESCC progression, no study has yet implicated Wnt signalling activation in ESCC initiation.

Taken together, the observations presented in this chapter and earlier findings suggest that unlike the pyloric epithelium, which harbours Wnt-responsive stem cells, fundic and forestomach mucosa contain a Wnt-independent stem cell populations. Aberrant activation of Wnt signalling in these stem cell populations appears insufficient to drive neoplastic transformation in these tissues, although it might contribute to tumour progression.

6.3.4 Brg1 loss has no major detrimental effect on Wnt-driven large intestinal tumourigenesis

The role of aberrant Wnt signalling in colorectal cancer has been well established both *in vitro* using human CRC cell lines and *in vivo* (reviewed in Gregorieff and Clevers, 2005). Consistent with this role and previously reported mouse models of CRC (Sansom *et al.*, 2004; Shibata *et al.*, 1997; Su *et al.*, 1992), conditional deletion of *Apc* under the control of AhCreER recombinase induced rapid tumourigenesis in the large intestinal epithelium. Dysplastic aberrant crypt foci (ACF) with nuclear β-catenin were detected in the large intestine of both, $AhCreER^+Apc^{fl/fl}Brg^{+/+}$ and $AhCreER^+Apc^{fl/fl}Brg^{fl/fl}$ mice as early as day 19 PI. Although the majority of ACFs in the large intestine of double knock-out (DKO) $AhCreER^+Apc^{fl/fl}Brg^{fl/fl}$ animals retained Brg1 expression, a substantial number of lesions displayed Brg1 loss. The extended life span of DKO animals made it feasible to investigate the effects of Brg1 deficiency on long-term Wnt-driven tumourigenesis in the large intestinal epithelium. Although $AhCreER^+Apc^{fl/fl}$-$Brg^{+/+}$ mice became terminally ill by or around day 19 PI, Brg1 positive lesions in the large intestine of DKO mice could serve as a control for Wnt-driven tumours unaffected by Brg1 loss.

Analysis of the tumour burden in the large intestinal epithelium of DKO mice at day 60 PI and later revealed numerous macroscopic adenomas. Immunohistochemical analysis of Brg1 expression in these adenomas revealed two types of tumours. While some adenomas appeared to be fully composed of Brg1 positive cells, others displayed clear areas of Brg1 loss. Brg1 deficient cells in these tumours were organised in distinct substructures so that the whole substructure would be either fully Brg1 positive or negative, rather than comprised of a mixture of cells. The origin of such mosaic substructures implies two alternatives. The first suggests that each macroadenoma originated from a single Brg1 positive crypt that only lost one copy of Brg1 due to suboptimal efficiency of Cre recombinase. Some substructures of such Brg1 heterozygous adenoma could afterwards lose the second copy of Brg1 via loss of heterozygousity. This scenario is plausible in view of the high chromosomal instability of Apc deficient tumours (Alberici and Fodde, 2006). However, it implies that complete Brg1 loss confers a selective advantage over Brg1 positive substructures. In contrast to this notion, no macroadenomas were observed that would be fully populated by Brg1 deficient cells. Furthermore, such a mechanism would predict mosaic adenomas in the large intestine of Brg1 haploinsufficient $AhCre^+Apc^{+/fl}$-$Brg^{+/fl}$ mice (section 5.2.2). However, all adenomas observed in the large intestinal epithelium of these mice were found to retain Brg1 expression.

An alternative mechanism invokes a polyclonal origin for mosaic adenomas. In this scenario, outgrowth of several Brg1 positive and negative aberrant crypts generates a single macroadenoma. Notably, the polyclonal nature of large intestinal adenomas has been previously demonstrated both in FAP patients with XY/XO mosaicism (Novelli *et*

al., 1996; Thirlwell *et al.*, 2010), and in Apc^{MIN} mice (Merritt *et al.*, 1997). In support of this hypothesis, intermediate stages of polyp formation were detected in the large intestinal epithelium of $AhCreER^+Apc^{fl/fl}Brg^{fl/fl}$ mice. These mini-adenomas appeared as clusters of individual Brg1 negative and/or positive aberrant crypts that had not, or had only just started to, raise above the epithelial surface. Brg1 mosaicism was, therefore, detected at very early stages of adenoma formation, which supports a polyclonal origin for mosaic adenomas.

Interestingly, the mosaic nature of some adenomas enabled visualisation of individual clones within the adenoma, in a similar manner to the use of *ROSA26* marker driving expression of β-galactosidase in Apc^{MIN} mice (Merritt *et al.*, 1997). Brg1 mosaicism, however, holds an advantage over the use of X-Gal staining, which was found to have a limited penetration distance and which impaired the analysis of larger adenomas (Merritt *et al.*, 1997). The most prominent characteristic of the mosaic adenomas was a substantially increased size of the individual clones within the adenoma compared to individual aberrant crypts (both Brg1 positive and negative) elsewhere in the large intestinal mucosa. This finding suggests that clustering of several individual aberrant crypts may create a favourable environment for their growth. This notion is consistent with the observation that colorectal cancers express increased levels of Wnt ligands, such as Wnt2, compared to normal colonic mucosa (Holcombe *et al.*, 2002) and thus create a positive feedback loop creating a favourable environment for cancer progression.

Notably, while large adenomas fully comprised of Brg1 positive cells were almost as frequent as mosaic ones, no fully Brg1 deficient adenomas were detected. This observation could merely reflect a lower frequency of individual Brg1 deficient aberrant crypts compared to Brg1 positive lesions. A somewhat more interesting conclusion could be drawn from the observation that aberrant crypt foci (ACFs) grow via crypt fission of individual aberrant crypts (Fujimitsu *et al.*, 1996; Paulsen *et al.*, 1994). The lack of large Brg1 deficient adenomas could, therefore, imply a compromised ability of Brg1 deficient aberrant crypts to undergo fission. This notion, however, is undermined by the presence of a substantial number of individual Brg1 positive aberrant crypts in the large intestine of $AhCreER^+Apc^{fl/fl}Brg^{fl/fl}$ mice that survived past 100 days PI.

To investigate whether Brg1 loss impaired Wnt signalling in the large intestinal adenomas, I analysed expression levels of two Wnt target genes, *c-Myc* and *CD44*, in Brg1 positive and negative substructures within mosaic adenomas. However, comparative analysis revealed no consistent difference in *c-Myc* and *CD44* expression levels between the substructures. In order to obtain a more quantitative measure of Wnt signalling modulation by Brg1 deficiency, I quantified the levels of proliferation and cell death in Brg1 positive and negative substructures within mosaic adenomas. While no difference was detected in apoptosis levels, Brg1 deficient substructures were found to display increased levels of proliferation as assessed by expression of the proliferative marker Ki67. This result is unexpected considering the proposed role of Brg1 in mediation of the Wnt sig-

nalling in human CRC cell lines (Barker *et al.*, 2001). Additionally, this observation is in contrast to the situation observed in the murine small intestine, where Brg1 loss significantly suppressed proliferation in Wnt activated epithelium (section 5.2.7). On the other hand, increased proliferation in Brg1 deficient substructures is consistent with widely reported role of Brg1 as a tumour suppressor (Becker *et al.*, 2009; Reisman *et al.*, 2003; Wong *et al.*, 2000) and a mediator of the cell cycle control (Hendricks *et al.*, 2004).

6.3.5 Brg1 deficiency does not impair Wnt driven tumourigenesis in the bladder urothelium

Urothelial cell carcinoma (UCC) is the seventh most common cancer in the UK (excluding non-melanoma skin cancer) and is even more common worldwide (Cancer Research UK, 2011). Somatic mutations of the key components of the Wnt pathway have been reported in urothelial carcinomas (Miyamoto *et al.*, 1996, Shiina *et al.*, 2002), as well as frequent upregulation of β-catenin (Zhu *et al.*, 2000). A number of studies have also demonstrated correlation between Wnt signalling activation in bladder cancer and reduced survival (Kastritis *et al.*, 2009; Marsit *et al.*, 2005). Significantly, conditional activation of β-catenin and loss of Pten in murine urothelium have been reported to induce the development of urothelial papillary carcinoma (Ahmad *et al.*, 2011). Notably, while sole activation of Wnt signalling via expression of an activated form of β-catenin was sufficient to induce the development of hyperplastic lesions in the bladder urothelium, these lesions remained small and benign for as long an 18 months (Ahmad *et al.*, 2011).

Since activation of Wnt signalling has been shown to induce urothelial hyperplasia (Ahmad *et al.*, 2011), I aimed to investigate, whether Brg1 loss could modulate the effects of Wnt activation achieved by conditional loss of Apc. Both $AhCreER^{+}Apc^{fl/fl}Brg^{+/+}$ and $AhCreER^{+}Apc^{fl/fl}Brg^{fl/fl}$ mice were found to develop hyperplastic lesions by day 7 PI. These hyperplastic lesions displayed strong nuclear localisation of β-catenin. Notably, a similar time frame of hyperplasia development was reported by Ahmad *et al.* using the same transgenic system. Analysis of Brg1 expression in urothelial lesions of $AhCreER^{+}$-$Apc^{fl/fl}Brg^{fl/fl}$ mice revealed complete loss of Brg1, while $AhCreER^{+}Apc^{fl/fl}Brg^{+/+}$ animals displayed strong Brg1 staining. In contrast to large intestinal and pyloric Brg1 deficient adenomas, which displayed attenuated nuclear accumulation of β-catenin, no difference in nuclear β-catenin staining was detected between $AhCreER^{+}Apc^{fl/fl}Brg^{+/+}$ and $AhCreER^{+}Apc^{fl/fl}Brg^{fl/fl}$ lesions. Notably, responsiveness of the bladder urothelium to Wnt activation concurs with a physiological role for the Wnt pathway in this tissue. Thus, under normal conditions Wnt signalling in the urothelium is dormant in consonance with the near-quiescent state of the epithelial cells. However it has been found to be activated in response to epithelial injury and to drive post-injury epithelial repopulation (Shin *et al.*, 2011).

Analysis of the hyperplastic urothelial lesions at later time points revealed an initial

increase in the lesion size, which however stalled around day 14 PI. Analysis of the bladder urothelium from both experimental cohorts revealed the disappearance of lesions with nuclear β-catenin. Instead, apparently empty lacunae were detected, which appeared to be filled with the dead cells. These lacunae most likely represented the remnants of the lesions and signified a rapid death of the majority of hyperplastic cells. In contrast to this observation, urothelial lesions induced by β-catenin stabilisation via loss of both copies of glycogen synthase kinase 3 under the control of AhCreER recombinase, have been shown to persist in the bladder urothelium for as long as 4 months PI (Ahmad *et al.*, 2011). This discrepancy could be attributed to additional functionality of Apc outside of Wnt signalling suppression, such as regulation of mitotic spindle formation and chromosomal segregation (reviewed in Aoki and Taketo, 2007).

Ahmad *et al.* have demonstrated that the restricted growth pattern of Wnt activated hyperplastic lesions in the bladder urothelium was imposed by Pten overexpression. Accordingly, concurrent loss of Pten and Apc under the control of AhCreER recombinase resulted in significantly increased cell proliferation and enlarged lesions compared to the mice with sole loss of Apc (Ahmad *et al.*, 2011). In a similar fashion, Brg1 deficient lesions in the bladder urothelium of $AhCreER^+Apc^{fl/fl}Brg^{fl/fl}$ mice displayed significantly increased lesion size and elevated proliferation levels as assessed by BrdU incorporation and expression of the proliferation marker Ki67, when compared to $AhCreER^+Apc^{fl/fl}$-$Brg^{+/+}$ urothelium. Increased proliferation of Brg1 deficient lesions suggested a potential further increase in Wnt signalling activation in the absence of Brg1. To explore this possibility, I analysed the expression levels of known Wnt target genes in hyperplastic urothelium of $AhCreER^+Apc^{fl/fl}Brg^{+/+}$ and $AhCreER^+Apc^{fl/fl}Brg^{fl/fl}$ mice at day 10 PI using quantitative RT-PCR. Despite the increased cell proliferation in Brg1 deficient lesions, $AhCreER^+Apc^{fl/fl}Brg^{fl/fl}$ urothelium displayed no difference in the expression levels of Wnt targets compared to Brg1 proficient hyperplastic bladder epithelium. Moreover, when compared to wild type bladder urothelium, Brg1 deficient lesions showed no significant up-regulation of *c-Myc* or *Cyclin D1*, two Wnt targets directly involved in mediation of the proliferative response of activated Wnt signalling. These observations suggested that Brg1 deficiency accelerated proliferation in hyperplastic lesions via a mechanism independent of Wnt signalling. Notably, increased cell proliferation of Brg1 deficient hyperplastic bladder coincides with the reported role of Brg1 in p21/pRb pathway mediated cell cycle control (Kang *et al.*, 2004). Coincidentally, p21 was found to be substantially upregulated in hyperplastic lesions upon expression of activated β-catenin (Ahmad *et al.*, 2011). It would be insightful, therefore, to investigate expression levels of the tumour suppressors p21 and p16 in response to additional Brg1 loss in Wnt activated urothelial hyperplasia.

Despite accelerated proliferation of Brg1 deficient lesions, Brg1 loss was unable to rescue an early proliferation block and rapid loss of Wnt activated cells. Conversely, Pten loss combined with β-catenin activation has been shown to drive progression of

hyperplastic urothelial lesions towards urothelial cell carcinoma (Ahmad *et al.*, 2011). It appears, therefore, that activity of other tumour suppressors, most likely Pten and/or p53 (Wu, 2005), is able to impose cell cycle arrest and induce apoptosis in Wnt activated urothelial hyperplasia regardless of Brg1 status.

Chapter 7

General discussion

Colorectal cancer (CRC) is one of the most common cancers and the second leading cause of cancer-related mortality after lung cancer in the UK (Cancer Research UK). Although aberrant activation of the Wnt signalling is observed in more than 90% of CRC cases, therapies targeting the Wnt pathway are extremely limited (Goss and Kahn, 2011). One obstacle to the development of Wnt targeted therapies is a substantial toxicity of such compounds. Some therapies, which target upstream Wnt pathway components have shown promising results in certain cancers driven by paracrine expression of Wnt ligands. However, it is a common consensus that targeting downstream components and target genes of the Wnt pathway is preferable in order to minimise the potential toxicity of such therapies (reviewed in Ewan and Dale, 2008). The interaction of Brg1 with β-catenin and its requirement for trans-activation of Wnt target genes in CRC cells *in vitro* places Brg1 downstream of the majority of Wnt activating mutations (Barker *et al.*, 2001). Brg1, therefore, represents a potentially valuable therapeutic target in Wnt-driven neoplasia. However, the involvement of Brg1 in the mediation of various signalling cascades raises concerns of potential side effects induced by therapeutic inhibition of Brg1.

With a view to validating Brg1 as a potential therapeutic target in Wnt-driven tumourigenesis, I aimed to investigate the consequences of Brg1 loss in normal tissue homeostasis and in the context of aberrant Wnt signalling activation. While this investigation primarily focused on the small intestinal epithelium as a tissue of choice to model human colorectal cancer, these questions were also addressed in other epithelial tissues of the gastrointestinal tract as well as in the bladder urothelium.

The main findings described in this thesis are:

- Brg1 is essential for the maintenance of stem cell homeostasis in the small intestinal epithelium;

- Brg1 deficiency impedes Wnt-driven small intestinal neoplasia via attenuation of Wnt signalling and elimination of stem cell derived tumours, which have a higher tumourigenic potential;

- Epithelial tissues of the gastrointestinal tract and bladder display a remarkable diversity in their reliance on Brg1 for tissue homeostasis, tumour suppression and Wnt-driven tumourigenesis;

In this chapter I will discuss the latter two of these findings. The role of Brg1 in the maintenance of small intestinal stem cell homeostasis has been previously discussed in Chapter 3.

7.1 Brg1 loss highlights a remarkable tissue-specific diversity of Brg1 functions

Concordant with its role in the mediation of various signalling pathways (Trotter and Archer, 2008), Brg1 has been reported to participate in a plethora of developmental processes. These range from defining the very early stages of embryogenesis (Bultman *et al.*, 2006; Ho *et al.*, 2009; Kidder *et al.*, 2009; Wang *et al.*, 2010) to differentiation and homeostasis of particular tissues (Hang *et al.*, 2010; Indra *et al.*, 2005; Matsumoto *et al.*, 2006). Consistent with this diverse role, constitutive Brg1 loss was found to result in pre-implantation abortion of embryonic development (Bultman *et al.*, 2000). Tissue-specific loss of Brg1 has been reported to result in abnormal proliferation, differentiation and tissue morphogenesis (reviewed in de la Serna *et al.*, 2006). Notably, while the role of Brg1 in developing tissues is reasonably well described, its functions in adult tissues are less well-defined. The data presented in this thesis reveal a diversity of Brg1 roles in the homeostasis of adult tissues of the gastrointestinal tract and bladder under physiological conditions and in the context of activated Wnt signalling.

Analysis of the effects of Brg1 deficiency in epithelial tissues of the gastrointestinal tract and bladder revealed a gradient of tissue-specific reliance on Brg1 function (Figure 7.1a). If considered just through the impact of Brg1 on cell proliferation, a subset of tissues, namely the small intestinal epithelium, appear to require Brg1 for maintenance of the pluripotent and self-renewing stem cell population. This observation is consistent with an established role of Brg1 in the maintenance of neural (Matsumoto *et al.*, 2006) and mesenchymal stem cells (Alessio *et al.*, 2010; Napolitano *et al.*, 2007). The role of Brg1 in the normal small intestinal epithelium can, therefore, be viewed as largely pro-proliferative. Further down the gradient, another subset of tissues, namely the large intestinal, pyloric and bladder epithelia, are able to tolerate long-term Brg1 deficiency without displaying signs of perturbed homeostasis. Brg1 function, thus, appears dispensable for the maintenance of physiological proliferation in these tissues. Finally, at the other end of the spectrum tissues such as the forestomach and fundic epithelium require Brg1 in order to keep cellular proliferation in check, as loss of Brg1 in these tissues results in a hyperplastic response. Thus the role of Brg1 the forestomach and fundus appears to be that of an anti-proliferative tumour suppressor.

These observations reveal a full spectrum of Brg1 impact on cell proliferation, from maintenance of stem cell self-renewal to cell cycle suppression within a limited set of tissues. The diversity of roles for Brg1 is even more remarkable given that the majority of the analysed tissues belong to the same system of organs and share a similar histological organisation and, to some extent, signalling pathways involved in their homeostasis.
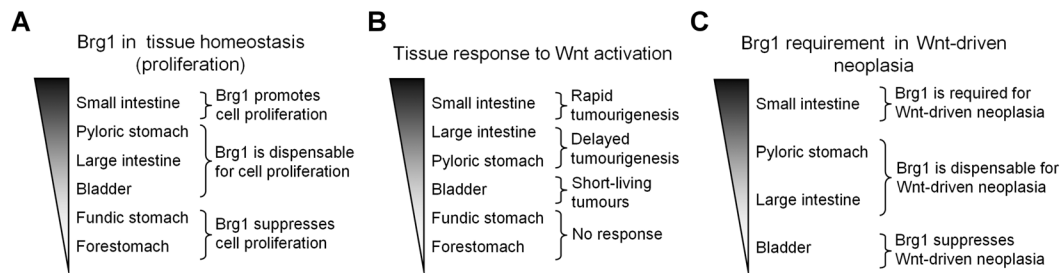
Figure 7.1: Epithelial tissues of the gastrointestinal tract and bladder exhibit a substantial diversity in Brg1 requirement for normal tissue homeostasis (**a**), which largely correlates with tissues' responsiveness to Wnt activation (**b**) and Brg1 requirement for the Wnt-driven tumourigenesis (**c**).

Consistent with the proposed interaction between Brg1 and the Wnt pathway, the gradient of requirement for functional Brg1 appears to reflect the gradient of these tissues' reliance upon active Wnt signalling for their development and homeostasis. Active Wnt signalling has been extensively reported to play a pivotal role in homeostasis of the small and large intestinal epithelium as well as the pyloric stomach (de Lau *et al.*, 2007; Mills and Shivdasani, 2011). Ablation of Wnt signalling in these gastrointestinal tissues by adenoviral expression of the Wnt inhibitor Dickkopf-1 has been found to result in a rapid crypt and villus loss in the small intestinal epithelium. The same phenotype, although delayed, was observed in the large intestine, while pyloric stomach was largely unaffected (Kuhnert *et al.*, 2004). This observation indicates that out of the three tissues, the small intestine is the most reliant on active Wnt signalling, followed by the large intestine and pylorus. Accordingly, Brg1 loss was found to cause severe crypt ablation in the small intestine, while the pylorus and large intestine were largely unaffected. Similarly, the bladder urothelium was found to tolerate Brg1 deficiency over an extensive period of time. This observation appears to coincide with the fact that the bladder epithelium is exposed to negligible levels of Wnt signal in steady-state homeostasis (Shin *et al.*, 2011). Finally, forestomach (oesophageal) and fundic epithelium rely on Wnt pathway suppression for their development and homeostasis (Kim *et al.*, 2005; Woo *et al.*, 2011). Curiously, dependence of these tissues on a lack of Wnt signalling coincides with a hyperplastic response to Brg1 loss. Taken together, these observations suggest a close correlation between a given tissues reliance on active Wnt signalling and its response to Brg1 deficiency.

Rather predictably, dependence of the analysed tissues on Wnt signalling for their normal homeostasis was found to correlate with responsiveness of these tissues to aberrant Wnt pathway activation (Figure 7.1b). While Wnt pathway activation fails to drive tumourigenesis in the forestomach and fundic stomach, all other tissues develop Wnt-

driven lesions consistent with previous reports (Ahmad *et al.*, 2011; Barker *et al.*, 2010; Sansom *et al.*, 2004; Shibata *et al.*, 1997). An apparent gradient in the tissue responses to Wnt activation was observed between the analysed tissues. Consistent with physiological levels of Wnt signalling in the respective tissues, the strongest response was observed in the small intestine followed by the large intestine and finally, pyloric epithelium. Interestingly, a similar pattern of tumourigenesis has been observed in Apc^{MIN} mice, which develop numerous small intestinal, less frequent large intestinal and rare pyloric adenomas (Su *et al.*, 1992; Tomita *et al.*, 2007). Bladder urothelium represents a peculiar case amongst the Wnt responsive tissues. While lesions with nuclear β-catenin appear soon after Apc deletion, they appear to undergo an early cell cycle arrest and regression. At least one report has provided strong evidence that this behaviour is likely to be mediated by up-regulation of tumour suppressors Pten and p21 (Ahmad *et al.*, 2011).

Notably, analysed tissues differed not only in the intensity of their response to Wnt activation, but also in the requirement for Brg1 in Wnt-driven tumourigenesis (Figure 7.1c). While small intestinal loss of Brg1 was utterly incompatible with Wnt signalling activation, other tissues were found to develop Brg1 deficient Wnt-driven tumours, albeit with altered penetrance. Intriguingly, while Brg1 appears to be dispensable for normal homeostasis of the pyloric, large intestinal and bladder epithelium, placing Brg1 deficiency in the context of aberrant Wnt signalling reveals slight differences between these tissues. Both the large intestinal and pyloric epithelium of the double knock-out (DKO) mice develop a mixture of Brg1 positive and negative Wnt-driven lesions, suggesting that Brg1 loss is permissive for Wnt-driven tumourigenesis in these tissues. Additionally, Brg1 deficient lesions appear to be under-represented in both tissues compared to Brg1 positive tumours. However, in contrast to pyloric epithelium, large intestinal Brg1 deficient lesions appear much earlier and go on to form a part of large mosaic adenomas. It is therefore tempting to speculate that Brg1 deficiency is less permissive for Wnt-driven tumourigenesis in the pylorus than it is in the large intestine. This speculation, however, is likely to be biased due to the fact that pyloric lesions generally develop slower than colonic tumours, regardless of Brg1 status. In contrast to both the pylorus and large intestine, all Wnt activated lesions in the bladder epithelium of DKO mice exhibit loss of Brg1 expression. Furthermore, within a short life span of urothelial hyperplasia, DKO lesions appear larger in size and display a higher rate of proliferation compared to Brg1 positive lesions. It therefore appears that Brg1 deficiency is not only permissive, but is favourable for Wnt-driven urothelial tumourigenesis. Taken together, the effects of Brg1 deficiency in the context of the Wnt-driven tumourigenesis highlight subtle differences between tissues that do not appear to require Brg1 for their normal homeostasis. The small intestine appears at the top of the gradient with absolute incompatibility of Brg1 loss and Wnt activation. It is followed by the pyloric and large intestinal epithelium with increasing degree of tolerance for Brg1 deficiency in Wnt activated lesions. Finally, in the bladder urothelium Brg1 deficiency appears favourable in the context of Wnt-driven

tumourigenesis.

Curiously, Wnt signalling activation in the forestomach and fundic epithelium appears to be able to negate the oncogenic effect of Brg1 loss in these tissues. While Brg1 loss alone results in a hyperplastic response in the forestomach and fundic epithelium, no lesions of similar histopathological nature are detected in the respective tissues of DKO mice. The lack of such lesions suggests that Wnt signalling activation is not only insufficient to drive tumourigenesis, but it is also likely to confer a survival disadvantage to Brg1 deficiency-induced hyperplasia of these tissues. This observation is particularly unusual considering that fundic gland polyps developing in Brg1 deficient stomach epithelium are histologically related to gastric polyps commonly linked to Wnt activating mutations in humans (Abraham *et al.*, 2000; Abraham *et al.*, 2001).

7.2   The tumour suppressor role of Brg1 is tissue- and dosage-dependent

Brg1 has been widely implicated as a tumour suppressor in a range of cancers due to the frequent incidence of Brg1 mutations in both cancer cell lines and primary cancers (Reviewed in de la Serna *et al.*, 2006). Previous attempts to explore the ability of Brg1 loss to induce or promote tumourigenesis *in vivo* have yielded some unexpected results. Mice with constitutive heterozygous deletion of Brg1 have been found to be prone to mammary tumourigenesis. Analysis of the mammary tumours arising in these mice, however, revealed retention of Brg1 expression, indicating that mammary tumourigenesis was driven by Brg1 haploinsufficiency rather than loss of heterozygousity (Bultman *et al.*, 2007). Similarly, analysis of chemically induced lung tumourigenesis has demonstrated that heterozygous, but not homozygous loss of Brg1 is able to facilitate tumour initiation (Glaros *et al.*, 2008). Similar to the mammary epithelium, lung tumours in Brg1 heterozygous mice were found to retain Brg1 expression, which again implicates Brg1 haploinsufficiency in tumour initiation. Conversely, biallelic Brg1 deletion in pre-formed lung tumours has been found to accelerate tumour progression (Glaros *et al.*, 2008). This observation is consistent with the correlation of Brg1 mutations in lung cancers with poor prognosis (Fukoka *et al.*, 2004; Reisman *et al.*, 2003). In this thesis I aimed to explore the tumour suppressor role of Brg1 in the tissues of the gastrointestinal tract and bladder. To this end, its hetero- and homozygous loss was analysed under physiologically normal conditions and in the context of activated Wnt signalling.

Although Brg1 haploinsufficiency has been reported to confer cancer susceptibility (Bultman *et al.*, 2007; Glaros *et al.*, 2008), no increase in gastric, intestinal or urothelial tumourigenesis was detected in mice with heterozygous Brg1 loss in these tissues. The lack of tumourigenesis in otherwise normal Brg1 deficient tissues is not entirely unexpected, as tumour formation in mice with constitutive heterozygous Brg1 loss was largely lim-

ited to the mammary gland epithelium (Bultman *et al.*, 2007), while lung carcinogenesis was facilitated by chemical mutagenesis to manifest Brg1-mediated tumour suppression (Glaros *et al.*, 2008).

Similarly, analysis of Brg1 haploinsufficiency in the context of heterozygous loss of Apc failed to reveal acceleration of Wnt-driven intestinal tumourigenesis as no significant difference in tumour size, number or distribution was observed between Apc heterozygous and double heterozygous animals. In addition to this finding, no significant difference in survival probability was observed between the cohorts. While these observations differ from the ones reported in the lung tumourigenesis (Glaros *et al.*, 2008), they underscore the tissue-specific nature of Brg1-mediated suppression of cancer progression. Consistent with this notion, Brg1 mutations appear to be exceptionally frequent in lung cancers, particularly in non-small cell lung carcinoma indicating a particularly important role for Brg1 in lung cancer pathogenetics (Medina *et al.*, 2008). Additionally, the lack of acceleration in tumour progression in the intestinal epithelium of double heterozygous mice could be related to the requirement of functional Brg1 for Wnt-driven tumourigenesis in the small intestinal epithelium, as discussed earlier.

While loss of Brg1 failed to induce tumourigenesis in the majority of epithelial tissues of the gastrointestinal tract and bladder urothelium, two tissues presented an exception to this rule. Brg1 deficiency in the forestomach and fundic epithelium resulted in relatively rapid development of hyperplastic lesions. The significance of this finding is that, while Brg1 mutations have been frequently observed in cancer cell lines and primary cancers (Medina and Sanchez-Cespedes, 2008), this is the first report to demonstrate tumourigenesis as a direct consequence of Brg1 deficiency. Importantly, no lesions of a similar histopathological nature were observed in the forestomach and fundic epithelium of mice with heterozygous loss of Brg1. This observation suggests that a single copy of *Brg1* is sufficient to suppress tumourigenesis in these tissues.

Taken together, previous findings and the data presented in this thesis suggest a dosage-dependent nature of Brg1-mediated tumour suppression across different tissues. Some tissues (the large intestinal, pyloric and bladder epithelium) do not seem to require Brg1 for tumour suppression. In others (forestomach and fundic epithelium) a single copy of *Brg1* gene appears sufficient to maintain effective tumour suppression as only loss of both copies results in hyperplastic response. Finally, a number of tissues (mammary and lung epithelium) require both copies of *Brg1* to suppress tumour initiation as Brg1 haploinsufficiency renders them prone to tumourigenesis (Bultman *et al.*, 2007; Glaros *et al.*, 2008).

7.3 Brg1 is a potential therapeutic target in the Wnt-driven neoplasia

In order to investigate the feasibility of Brg1 as a potential therapeutic target in Wnt-driven neoplasia *in vivo*, Brg1 was conditionally deleted in the context of activated Wnt signalling in the murine gastrointestinal tract. The data described in Chapter 5 of this thesis demonstrated that Brg1 loss in the context of aberrant activation of Wnt signalling had a profound therapeutic effect on animal survival by reducing the small intestinal tumour burden and specifically eliminating Wnt-driven tumours that arise from the stem cell population.

The specific requirement for Brg1 for the stem cell derived Wnt-driven tumours makes it a potentially attractive target in individuals with FAP syndrome. These individuals develop multiple benign adenomas in the colonic epithelium, some of which progress to carcinoma. In order to minimise the likelihood of adenoma-carcinoma transformation FAP patients have to undergo prophylactic colectomy in order to remove the affected regions or even the whole colon (Gryfe, 2009). Effective targeting of Wnt activated colonic stem cells in such patients could provide a valuable non-surgical alternative and substantially improve patients' quality of life. The data presented in this thesis serves as an *in vivo* proof of concept that such an approach of targeting the Wnt activated stem cell is feasible and may have a therapeutic advantage. It should be noted, however, that the diversity of Brg1 requirement for Wnt driven tumourigenesis even between Wnt responsive tissues suggests that Brg1 is unlikely to be a universal anti-Wnt signalling target and its utility may be limited to particular types of Wnt-driven neoplasia.

While targeting Brg1 was found to be effective in elimination of stem cell derived Wnt-driven tumours in the murine small intestine, it remains to be determined whether Brg1 could serve as a therapeutic target in human CRC. Notably, loss of Brg1 was unable to prevent Wnt-driven tumourigenesis in the murine large intestinal epithelium. This observation could undermine its significance as a therapeutic target in human CRC. However, a number of observations suggest that the murine small intestine might be a more representative tissue for modelling human CRC. A range of mouse models have been found to respond to heterozygous loss of Apc by developing predominantly small intestinal adenomas, while tumourigenesis driven by Apc loss in humans is largely confined to the colonic epithelium (Heyer *et al.*, 1999). In the particular case of Brg1, human CRC cell lines were found to suppress a range of Wnt target genes in response to inhibition of Brg1 function (Barker *et al.*, 2001). However, the data presented in this thesis show no evidence of Wnt target gene suppression in Brg1 deficient large intestinal lesions. In order to validate Brg1 as a potential therapeutic target in Wnt-driven neoplasia, the consequences of its loss must be studied in human colonic tissue. A research group led by Eduard Batlle at the Biomedical Research Institute in Barcelona has been successful in developing a method of culturing normal and malignant human colonic epithelium *in vitro* in the form

of spheroid culture (Jung *et al.*, 2011). A potential collaboration could therefore now be arranged to investigate the effects of BRG1 depletion (e.g. using shRNA against BRG1) in normal and neoplastic human colonic epithelium.

Extrapolation of the consequences of concurrent deletion of Brg1 and Apc into a clinical setting has a number of caveats. Simultaneous Brg1 and Apc loss prevents the development of stem cell derived Wnt-driven adenomas and thus represents a prophylactic treatment. It remains to be seen, whether Brg1 loss in pre-formed adenoma would be able to stop its further development and/or induce tumour regression. In the context of the intestinal stem cell niche provided by the Paneth cells (Sato *et al.*, 2010), a possibility remains that upon loss of Brg1 and subsequent ablation of Wnt activated stem cells within the adenoma, early cancer progenitor cells would be able to occupy the stem cell niche and acquire stem cell properties. A similar scenario is observed upon partial Brg1 loss in the murine small intestine, where either stem or progenitor cells retaining Brg1 expression are able to drive intestinal repopulation. While this process in Wnt-driven cancers could be prevented by sustained Brg1 inhibition, this is likely to result in substantial toxicity to normal intestinal mucosa, as seen upon high-penetrance Brg1 loss in the mouse small intestine. In order to partially address the ability of cancer progenitor cells to de-differentiate upon cancer stem cell ablation, we are currently generating Apc^{MIN} mice carrying the Lgr5-CreER transgene and loxP targeted Brg1 alleles. Induction of conditional Brg1 loss in normal and neoplastic mucosa of these mice should be able to create a situation more representative of therapeutic rather than prophylactic treatment. The use of a Brg1 inhibitor however, would be preferential for this type of study as alterations in expression patterns within tumour cells could result in suboptimal Cre recombinase expression. Furthermore, the question of the plasticity of cancer stem cells and their progenitors and trans-differentiation between these two populations has wider implications for the actively developing field of cancer stem cell targeted therapies (de Sousa *et al.*, 2011).

Another likely caveat of using Brg1 as a therapeutic target concerns the potential side effects due to the role of Brg1 as a transcriptional co-activator in various signalling pathways (Reviewed in Trotter and Archer, 2008). Analysis of the consequences of Brg1 loss in a limited number of epithelial tissues described in this work reveals a substantial diversity of responses to Brg1 deficiency between tissues. While the majority of analysed tissues tolerated long-term loss of Brg1 without perturbation of normal homeostasis, Brg1 deficiency induced benign cell hyperplasia in forestomach and fundic epithelium. Notably, the forestomach and fundic phenotype of Brg1 loss is likely to be unrelated to the interaction of Brg1 with the Wnt pathway, since Wnt signalling is suppressed in these tissues under physiological conditions (Kim *et al.*, 2005; Woo *et al.*, 2011). It should therefore be possible to avoid at least some of the potential side effects by specifically targeting Brg1/β-catenin interactions. Interestingly, a similar strategy targeting β-catenin/TCF interaction with small-molecule compounds has been shown to suppress Wnt signalling

and induce apoptosis in CRC cells (Leproucelet *et al.*, 2004). Specific targeting of the Brg1/β-catenin interaction, would mostly likely lead to tissue disruption if invoked at a high level in the small intestine. However, the small intestinal epithelium has demonstrated a sound capacity to regeneration upon partial Brg1 loss and might be successfully managed with an appropriate dosage and treatment plan.

Overall, although many aspects of targeting Wnt-driven cancers using Brg1-based therapies remain yet to be investigated, initial results presented in this thesis portray Brg1 as a promising potential therapeutic target.

Bibliography

Abraham, S. C., B. Nobukawa, F. M. Giardiello, S. R. Hamilton, and T. Wu (2000, September). Fundic gland polyps in familial adenomatous polyposis : Neoplasms with frequent somatic adenomatous polyposis coli gene alterations. *Am J Pathol 157*(3), 747–754.

Abraham, S. C., B. Nobukawa, F. M. Giardiello, S. R. Hamilton, and T. Wu (2001, March). Sporadic fundic gland polyps : Common gastric polyps arising through activating mutations in the beta-Catenin gene. *Am J Pathol 158*(3), 1005–1010.

Ahmad, I., J. P. Morton, L. B. Singh, S. M. Radulescu, R. A. Ridgway, S. Patel, J. Woodgett, D. J. Winton, M. M. Taketo, X. Wu, H. Y. Leung, and O. J. Sansom (2011, January). [beta]-Catenin activation synergizes with PTEN loss to cause bladder cancer formation. *Oncogene 30*(2), 178–189.

Alberici, P. and R. Fodde (2006). The role of the APC tumor suppressor in chromosomal instability. *Genome Dynamics 1*, 149–170. PMID: 18724059.

Alessio, N., T. Squillaro, M. Cipollaro, L. Bagella, A. Giordano, and U. Galderisi (2010, October). The BRG1 ATPase of chromatin remodeling complexes is involved in modulation of mesenchymal stem cell senescence through RB-P53 pathways. *Oncogene 29*(40), 5452–5463.

Amit, S., A. Hatzubai, Y. Birman, J. S. Andersen, E. Ben-Shushan, M. Mann, Y. Ben-Neriah, and I. Alkalay (2002, May). Axin-mediated CKI phosphorylation of beta-catenin at ser 45: a molecular switch for the wnt pathway. *Genes & Development 16*(9), 1066–76. PMID: 12000790.

Andrae, J., R. Gallini, and C. Betsholtz (2008, May). Role of platelet-derived growth factors in physiology and medicine. *Genes & Development 22*(10), 1276 –1312.

Andreu, P., S. Colnot, C. Godard, S. Gad, P. Chafey, M. Niwa-Kawakita, P. Laurent-Puig, A. Kahn, S. Robine, C. Perret, and B. Romagnolo (2005, March). Crypt-restricted proliferation and commitment to the paneth cell lineage following apc loss in the mouse intestine. *Development 132*(6), 1443 –1451.

Aoki, K. and M. M. Taketo (2007, October). Adenomatous polyposis coli (APC): a multi-functional tumor suppressor gene. *Journal of Cell Science 120*(19), 3327 –3335.

Arenas, R. B., A. Fichera, P. Mok, M. C. Blanco, and F. Michelassi (1996, October). Introduction of human adenomatous polyposis coli gene into min mice via cationic liposomes. *Surgery 120*(4), 712–717; discussion 717–718. PMID: 8862382.

Artavanis-Tsakonas, S., M. D. Rand, and R. J. Lake (1999, April). Notch signaling: Cell fate control and signal integration in development. *Science 284*(5415), 770 –776.

Bafico, A., G. Liu, L. Goldin, V. Harris, and S. A. Aaronson (2004, November). An autocrine mechanism for constitutive wnt pathway activation in human cancer cells. *Cancer Cell 6*(5), 497–506.

Barker, N., M. Huch, P. Kujala, M. van de Wetering, H. J. Snippert, J. H. van Es, T. Sato, D. E. Stange, H. Begthel, M. van den Born, E. Danenberg, S. van den Brink, J. Korving, A. Abo, P. J. Peters, N. Wright, R. Poulsom, and H. Clevers (2010, January). Lgr5(+ve) stem cells drive self-renewal in the stomach and build long-lived gastric units in vitro. *Cell Stem Cell 6*(1), 25–36. PMID: 20085740.

Barker, N., A. Hurlstone, H. Musisi, A. Miles, M. Bienz, and H. Clevers (2001, September). The chromatin remodelling factor brg-1 interacts with -catenin to promote target gene activation. *The EMBO Journal 20*(17), 49354943. PMC125268.

Barker, N., R. A. Ridgway, J. H. van Es, M. van de Wetering, H. Begthel, M. van den Born, E. Danenberg, A. R. Clarke, O. J. Sansom, and H. Clevers (2009, January). Crypt stem cells as the cells-of-origin of intestinal cancer. *Nature 457*(7229), 608–611.

Barker, N., J. H. van Es, J. Kuipers, P. Kujala, M. van den Born, M. Cozijnsen, A. Haegebarth, J. Korving, H. Begthel, P. J. Peters, and H. Clevers (2007, October). Identification of stem cells in small intestine and colon by marker gene lgr5. *Nature 449*(7165), 1003–1007.

Bartlett, C., T. J. Orvis, G. S. Rosson, and B. E. Weissman (2011, August). BRG1 mutations found in human cancer cell lines inactivate rb-mediated cell-cycle arrest. *Journal of Cellular Physiology 226*(8), 1989–1997. PMID: 21520050.

Batlle, E., J. T. Henderson, H. Beghtel, M. M. van den Born, E. Sancho, G. Huls, J. Meeldijk, J. Robertson, M. van de Wetering, T. Pawson, and H. Clevers (2002, October). beta-Catenin and TCF mediate cell positioning in the intestinal epithelium by controlling the expression of EphB/EphrinB. *Cell 111*(2), 251–263.

Becker, L., Q. Huang, and H. Mashimo (2008). Immunostaining of lgr5, an intestinal stem cell marker, in normal and premalignant human gastrointestinal tissue. *TheScientificWorldJournal 8*, 1168–1176. PMID: 19030762.

Becker, T. M., S. Haferkamp, M. K. Dijkstra, L. L. Scurr, M. Frausto, E. Diefenbach, R. A. Scolyer, D. N. Reisman, G. J. Mann, R. F. Kefford, and H. Rizos (2009). The chromatin remodelling factor BRG1 is a novel binding partner of the tumor suppressor p16INK4a. *Molecular Cancer 8*, 4. PMC2644676.

Belandia, B. and M. G. Parker (2003, August). Nuclear receptors: A rendezvous for chromatin remodeling factors. *Cell 114*(3), 277–280.

Bhanot, P., M. Brink, C. H. Samos, J. C. Hsieh, Y. Wang, J. P. Macke, D. Andrew, J. Nathans, and R. Nusse (1996, July). A new member of the frizzled family from drosophila functions as a wingless receptor. *Nature 382*(6588), 225–30. PMID: 8717036.

Bian, Y. S., M. C. Osterheld, F. T. Bosman, C. Fontolliet, and J. Benhattar (2000, October). Nuclear accumulation of beta-catenin is a common and early event during neoplastic progression of barrett esophagus. *American Journal of Clinical Pathology 114*(4), 583–590. PMID: 11026105.

Bjerknes, M. and H. Cheng (1981, January). The stem-cell zone of the small intestinal epithelium. III. evidence from columnar, enteroendocrine, and mucous cells in the adult mouse. *The American Journal of Anatomy 160*(1), 77–91. PMID: 7211718.

Bjerknes, M. and H. Cheng (2005, October). Re-examination of P-PTEN staining patterns in the intestinal crypt. *Nat Genet 37*(10), 1016–1017.

Bochar, D. A., L. Wang, H. Beniya, A. Kinev, Y. Xue, W. S. Lane, W. Wang, F. Kashanchi, and R. Shiekhattar (2000, July). BRCA1 is associated with a human SWI/SNF-Related complex: Linking chromatin remodeling to breast cancer. *Cell 102*(2), 257–265.

Boldrin, L., F. Muntoni, and J. E. Morgan (2010, November). Are human and mouse satellite cells really the same? *Journal of Histochemistry & Cytochemistry 58*(11), 941 –955.

Bonnet, D. and J. E. Dick (1997, July). Human acute myeloid leukemia is organized as a hierarchy that originates from a primitive hematopoietic cell. *Nat Med 3*(7), 730–737.

Bos, J. L., E. R. Fearon, S. R. Hamilton, M. V.-d. Vries, J. H. van Boom, A. J. van der Eb, and B. Vogelstein (1987, May). Prevalence of ras gene mutations in human colorectal cancers. *Nature 327*(6120), 293–297.

Bronner, M. P. (2003). Gastrointestinal inherited polyposis syndromes. *Mod Pathol 16*(4), 359–365.

BRUCE, W. R. and H. VAN DER GAAG (1963, July). A quantitative assay for the number of murine lymphoma cells capable of proliferation in vivo. *Nature 199*(4888), 79–80.

Buchholz, F., P. Angrand, and A. F. Stewart (1998, July). Improved properties of FLP recombinase evolved by cycling mutagenesis. *Nat Biotech 16*(7), 657–662.

Bultman, S., T. Gebuhr, D. Yee, C. La Mantia, J. Nicholson, A. Gilliam, F. Randazzo, D. Metzger, P. Chambon, G. Crabtree, and T. Magnuson (2000, December). A brg1 null mutation in the mouse reveals functional differences among mammalian SWI/SNF complexes. *Molecular Cell 6*(6), 1287–1295.

Bultman, S. J., T. C. Gebuhr, and T. Magnuson (2005, December). A brg1 mutation that uncouples ATPase activity from chromatin remodeling reveals an essential role for SWI/SNF-related complexes in -globin expression and erythroid development. *Genes & Development 19*(23), 2849 –2861.

Bultman, S. J., T. C. Gebuhr, H. Pan, P. Svoboda, R. M. Schultz, and T. Magnuson (2006, July). Maternal BRG1 regulates zygotic genome activation in the mouse. *Genes & Development 20*(13), 17441754. PMC1522071.

Bultman, S. J., J. I. Herschkowitz, V. Godfrey, T. C. Gebuhr, M. Yaniv, C. M. Perou, and T. Magnuson (2007, July). Characterization of mammary tumors from brg1 heterozygous mice. *Oncogene 27*(4), 460–468.

Cairnie, A. B., L. F. Lamerton, and G. G. Steel (1965, September). Cell proliferation studies in the intestinal epithelium of the rat : II. theoretical aspects. *Experimental Cell Research 39*(2-3), 539–553.

Cairnie, A. B. and B. H. Millen (1975, March). Fission of crypts in the small intestine of the irradiated mouse. *Cell and Tissue Kinetics 8*(2), 189–196. PMID: 1125969.

Cairns, J. (1975, May). Mutation selection and the natural history of cancer. *Nature 255*(5505), 197–200.

Chambers, I., D. Colby, M. Robertson, J. Nichols, S. Lee, S. Tweedie, and A. Smith (2003, May). Functional expression cloning of nanog, a pluripotency sustaining factor in embryonic stem cells. *Cell 113*(5), 643–655.

Chan, S. L., Y. Cui, A. van Hasselt, H. Li, G. Srivastava, H. Jin, K. M. Ng, Y. Wang, K. Y. Lee, G. S. W. Tsao, S. Zhong, K. D. Robertson, S. Y. Rha, A. T. C. Chan, and Q. Tao (2007, March). The tumor suppressor wnt inhibitory factor 1 is frequently methylated in nasopharyngeal and esophageal carcinomas. *Lab Invest 87*(7), 644–650.

Chan, T. A., Z. Wang, L. H. Dang, B. Vogelstein, and K. W. Kinzler (2002, June). Targeted inactivation of CTNNB1 reveals unexpected effects of -catenin mutation. *Proceedings of the National Academy of Sciences of the United States of America 99*(12), 8265–8270.

Chen, B., M. E. Dodge, W. Tang, J. Lu, Z. Ma, C. Fan, S. Wei, W. Hao, J. Kilgore, N. S. Williams, M. G. Roth, J. F. Amatruda, C. Chen, and L. Lum (2009, February). Small molecule-mediated disruption of wnt-dependent signaling in tissue regeneration and cancer. *Nat Chem Biol 5*(2), 100–107.

Cheng, H. (1974, December). Origin, differentiation and renewal of the four main epithelial cell types in the mouse small intestine. II. mucous cells. *The American Journal of Anatomy 141*(4), 481–501. PMID: 4440633.

Cheng, H. and C. P. Leblond (1974a, December). Origin, differentiation and renewal of the four main epithelial cell types in the mouse small intestine. i. columnar cell. *The American Journal of Anatomy 141*(4), 461–479. PMID: 4440632.

Cheng, H. and C. P. Leblond (1974b). Origin, differentiation and renewal of the four main epithelial cell types in the mouse small intestine v. unitarian theory of the origin of the four epithelial cell types. *American Journal of Anatomy 141*(4), 537–561.

Cheng, H., J. Merzel, and C. P. Leblond (1969, December). Renewal of paneth cells in the small intestine of the mouse. *The American Journal of Anatomy 126*(4), 507–525. PMID: 5369113.

Cheng, S. G., K. P. Davies, E. Yung, R. J. Beltran, J. Yu, and G. V. Kalpana (1999, May). c-MYC interacts with INI1/hSNF5 and requires the SWI/SNF complex for transactivation function. *Nat Genet 22*(1), 102–105.

Cheng, T., N. Rodrigues, H. Shen, Y.-g. Yang, D. Dombkowski, M. Sykes, and D. T. Scadden (2000, March). Hematopoietic stem cell quiescence maintained by p21cip1/waf1. *Science 287*(5459), 1804 –1808.

Chi, T. H., M. Wan, P. P. Lee, K. Akashi, D. Metzger, P. Chambon, C. B. Wilson, and G. R. Crabtree (2003, August). Sequential roles of brg, the ATPase subunit of BAF chromatin remodeling complexes, in thymocyte development. *Immunity 19*(2), 169–182.

Chiba, H., M. Muramatsu, A. Nomoto, and H. Kato (1994, May). Two human homologues of saccharomyces cerevisiae SWI2/SNF2 and drosophila brahma are transcriptional coactivators cooperating with the estrogen receptor and the retinoic acid receptor. *Nucleic Acids Research 22*(10), 1815–1820. PMID: 8208605 PMCID: 308079.

Choi, H., J. Gwak, M. Cho, M. Ryu, J. Lee, S. K. Kim, Y. H. Kim, G. W. Lee, M. Yun, N. M. Cuong, J. Shin, G. Song, and S. Oh (2010, January). Murrayafoline a attenuates the wnt/[beta]-catenin pathway by promoting the degradation of intracellular [beta]-catenin proteins. *Biochemical and Biophysical Research Communications 391*(1), 915–920.

Chow, E. and F. Macrae (2005, November). A review of juvenile polyposis syndrome. *Journal of Gastroenterology and Hepatology 20*(11), 1634–1640. PMID: 16246179.

Clement, G., R. Braunschweig, N. Pasquier, F. T. Bosman, and J. Benhattar (2006, January). Alterations of the wnt signaling pathway during the neoplastic progression of barrett's esophagus. *Oncogene 25*(21), 3084–3092.

Clements, W. M., J. Wang, A. Sarnaik, O. J. Kim, J. MacDonald, C. Fenoglio-Preiser, J. Groden, and A. M. Lowy (2002, June). -Catenin mutation is a frequent cause of wnt pathway activation in gastric cancer. *Cancer Research 62*(12), 3503 –3506.

Clevers, H. (2006, November). Wnt/[beta]-Catenin signaling in development and disease. *Cell 127*(3), 469–480.

Coopersmith, C. M., C. Chandrasekaran, M. S. McNevin, and J. I. Gordon (1997, July). Bi-transgenic mice reveal that K-rasVal12 augments a p53-independent apoptosis when small intestinal villus enterocytes reenter the cell cycle. *The Journal of Cell Biology 138*(1), 167 –179.

Cotsarelis, G., T. Sun, and R. M. Lavker (1990, June). Label-retaining cells reside in the bulge area of pilosebaceous unit: Implications for follicular stem cells, hair cycle, and skin carcinogenesis. *Cell 61*(7), 1329–1337.

Crosnier, C., D. Stamataki, and J. Lewis (2006, May). Organizing cell renewal in the intestine: stem cells, signals and combinatorial control. *Nat Rev Genet 7*(5), 349–359.

Crosnier, C., N. Vargesson, S. Gschmeissner, L. Ariza-McNaughton, A. Morrison, and J. Lewis (2005, March). Delta-Notch signalling controls commitment to a secretory fate in the zebrafish intestine. *Development 132*(5), 1093 –1104.

Dalerba, P., S. J. Dylla, I. Park, R. Liu, X. Wang, R. W. Cho, T. Hoey, A. Gurney, E. H. Huang, D. M. Simeone, A. A. Shelton, G. Parmiani, C. Castelli, and M. F. Clarke (2007, June). Phenotypic characterization of human colorectal cancer stem cells. *Proceedings of the National Academy of Sciences 104*(24), 10158 –10163.

Daniels, D. L. and W. I. Weis (2005, April). Beta-catenin directly displaces Groucho/TLE repressors from Tcf/Lef in wnt-mediated transcription activation. *Nature Structural & Molecular Biology 12*(4), 364–71. PMID: 15768032.

De, S., A. L. Wurster, P. Precht, W. H. Wood, K. G. Becker, and M. J. Pazin (2011, April). Dynamic BRG1 recruitment during t helper differentiation and activation reveals distal regulatory elements. *Mol. Cell. Biol. 31*(7), 1512–1527.

de la Chapelle, A. (2004, October). Genetic predisposition to colorectal cancer. *Nat Rev Cancer 4*(10), 769–780.

de la Serna, I. L., Y. Ohkawa, and A. N. Imbalzano (2006, June). Chromatin remodelling in mammalian differentiation: lessons from ATP-dependent remodellers. *Nat Rev Genet 7*(6), 461–473.

de Lau, W., N. Barker, and H. Clevers (2007). WNT signaling in the normal intestine and colorectal cancer. *Frontiers in Bioscience: A Journal and Virtual Library 12*, 471–491. PMID: 17127311.

De Santa Barbara, P., G. R. Van Den Brink, and D. J. Roberts (2003, July). Development and differentiation of the intestinal epithelium. *Cellular and Molecular Life Sciences 60*(7), 1322–1332. PMID: 12943221 PMCID: 2435618.

de Sousa, E. M. F., L. Vermeulen, D. Richel, and J. P. Medema (2011, February). Targeting wnt signaling in colon cancer stem cells. *Clinical Cancer Research 17*(4), 647 –653.

Debril, M., L. Gelman, E. Fayard, J. Annicotte, S. Rocchi, and J. Auwerx (2004, April). Transcription factors and nuclear receptors interact with the SWI/SNF complex through the BAF60c subunit. *The Journal of Biological Chemistry 279*(16), 16677–16686. PMID: 14701856.

Dilworth, F., C. Fromental-Ramain, K. Yamamoto, and P. Chambon (2000, November). ATP-Driven chromatin remodeling activity and histone acetyltransferases act sequentially during transactivation by RAR/RXR in vitro. *Molecular Cell 6*(5), 1049–1058.

Dnker, N. and K. Krieglstein (2000, December). Targeted mutations of transforming growth factor-beta genes reveal important roles in mouse development and adult homeostasis. *European Journal of Biochemistry / FEBS 267*(24), 6982–6988. PMID: 11106407.

Dymecki, S. M. (1996, June). Flp recombinase promotes site-specific DNA recombination in embryonic stem cells and transgenic mice. *Proceedings of the National Academy of Sciences 93*(12), 6191 –6196.

Ebert, M. P., G. Fei, S. Kahmann, O. Mller, J. Yu, J. J. Sung, and P. Malfertheiner (2002, January). Increased -catenin mRNA levels and mutational alterations of the APC and -catenin gene are present in intestinal-type gastric cancer. *Carcinogenesis 23*(1), 87 –91.

el Marjou, F., K. Janssen, B. H. Chang, M. Li, V. Hindie, L. Chan, D. Louvard, P. Chambon, D. Metzger, and S. Robine (2004, July). Tissue-specific and inducible cre-mediated recombination in the gut epithelium. *Genesis (New York, N.Y.: 2000) 39*(3), 186–93. PMID: 15282745.

Emami, K. H., C. Nguyen, H. Ma, D. H. Kim, K. W. Jeong, M. Eguchi, R. T. Moon, J. Teo, S. W. Oh, H. Y. Kim, S. H. Moon, J. R. Ha, and M. Kahn (2004, August). A small molecule inhibitor of beta-catenin/CREB-binding protein transcription [corrected]. *Proceedings of the National Academy of Sciences of the United States of America 101*(34), 12682–12687. PMID: 15314234.

Eng, C. and H. Ji (1998, May). Molecular classification of the inherited hamartoma polyposis syndromes: Clearing the muddied waters. *The American Journal of Human Genetics 62*(5), 1020–1022.

Engle, S. J., J. B. Hoying, G. P. Boivin, I. Ormsby, P. S. Gartside, and T. Doetschman (1999, July). Transforming growth factor 1 suppresses nonmetastatic colon cancer at an early stage of tumorigenesis. *Cancer Research 59*(14), 3379 –3386.

Eppert, K., S. W. Scherer, H. Ozcelik, R. Pirone, P. Hoodless, H. Kim, L. Tsui, B. Bapat, S. Gallinger, I. L. Andrulis, G. H. Thomsen, J. L. Wrana, and L. Attisano (1996,

August). MADR2 maps to 18q21 and encodes a TGF[beta]-Regulated MAD-Related protein that is functionally mutated in colorectal carcinoma. *Cell 86* (4), 543–552.

Escobar, M., P. Nicolas, F. Sangar, S. Laurent-Chabalier, P. Clair, D. Joubert, P. Jay, and C. Legraverend (2011, March). Intestinal epithelial stem cells do not protect their genome by asymmetric chromosome segregation. *Nat Commun 2*, 258.

Evans, M. J. and M. H. Kaufman (1981, July). Establishment in culture of pluripotential cells from mouse embryos. *Nature 292* (5819), 154–156.

Ewan, K. B. R. and T. C. Dale (2008, July). The potential for targeting oncogenic WNT/beta-catenin signaling in therapy. *Current Drug Targets 9* (7), 532–547. PMID: 18673239.

Fearon, E. R., K. R. Cho, J. M. Nigro, S. E. Kern, J. W. Simons, J. M. Ruppert, S. R. Hamilton, A. C. Preisinger, G. Thomas, and K. W. Kinzler (1990, January). Identification of a chromosome 18q gene that is altered in colorectal cancers. *Science (New York, N.Y.) 247* (4938), 49–56. PMID: 2294591.

Fearon, E. R. and B. Vogelstein (1990, June). A genetic model for colorectal tumorigenesis. *Cell 61* (5), 759–767.

Fedirko, V., I. Tramacere, V. Bagnardi, M. Rota, L. Scotti, F. Islami, E. Negri, K. Straif, I. Romieu, C. La Vecchia, P. Boffetta, and M. Jenab (2011, February). Alcohol drinking and colorectal cancer risk: an overall and dose-response meta-analysis of published studies. *Annals of Oncology: Official Journal of the European Society for Medical Oncology / ESMO*. PMID: 21307158.

Feil, R., J. Wagner, D. Metzger, and P. Chambon (1997, August). Regulation of cre recombinase activity by mutated estrogen receptor Ligand-Binding domains. *Biochemical and Biophysical Research Communications 237* (3), 752–757.

Fevr, T., S. Robine, D. Louvard, and J. Huelsken (2007, November). Wnt/beta-Catenin is essential for intestinal homeostasis and maintenance of intestinal stem cells. *Mol. Cell. Biol. 27* (21), 7551–7559.

Flejou, J. (2005, March). Barrett's oesophagus: from metaplasia to dysplasia and cancer. *Gut 54* (suppl_1), i6–i12.

Flowers, S., N. G. Nagl, G. R. Beck, and E. Moran (2009, April). Antagonistic roles for BRM and BRG1 SWI/SNF complexes in differentiation. *J. Biol. Chem. 284* (15), 10067–10075.

Fodde, R., W. Edelmann, K. Yang, C. van Leeuwen, C. Carlson, B. Renault, C. Breukel, E. Alt, M. Lipkin, and P. M. Khan (1994, September). A targeted chain-termination mutation in the mouse apc gene results in multiple intestinal tumors. *Proceedings of the National Academy of Sciences of the United States of America 91* (19), 8969–8973. PMID: 8090754.

Fodde, R., R. Smits, and H. Clevers (2001, October). APC, signal transduction and genetic instability in colorectal cancer. *Nat Rev Cancer 1* (1), 55–67.

Fre, S., M. Huyghe, P. Mourikis, S. Robine, D. Louvard, and S. Artavanis-Tsakonas (2005, June). Notch signals control the fate of immature progenitor cells in the intestine. *Nature 435* (7044), 964–968.

Fre, S., S. K. Pallavi, M. Huyghe, M. La, K. Janssen, S. Robine, S. Artavanis-Tsakonas, and D. Louvard (2009, April). Notch and wnt signals cooperatively control cell pro-

liferation and tumorigenesis in the intestine. *Proceedings of the National Academy of Sciences 106*(15), 6309 –6314.

Fujii, N., L. You, Z. Xu, K. Uematsu, J. Shan, B. He, I. Mikami, L. R. Edmondson, G. Neale, J. Zheng, R. K. Guy, and D. M. Jablons (2007, January). An antagonist of dishevelled Protein-Protein interaction suppresses beta-Catenin-Dependent tumor cell growth. *Cancer Res 67*(2), 573–579.

Fujimitsu, Y., H. Nakanishi, K. Inada, T. Yamachika, M. Ichinose, H. Fukami, and M. Tatematsu (1996, December). Development of aberrant crypt foci involves a fission mechanism as revealed by isolation of aberrant crypts. *Japanese Journal of Cancer Research: Gann 87*(12), 1199–1203. PMID: 9045953.

Fukuoka, J., T. Fujii, J. H. Shih, T. Dracheva, D. Meerzaman, A. Player, K. Hong, S. Settnek, A. Gupta, K. Buetow, S. Hewitt, W. D. Travis, and J. Jen (2004, July). Chromatin remodeling factors and BRM/BRG1 expression as prognostic indicators in Non-Small cell lung cancer. *Clinical Cancer Research 10*(13), 4314 –4324.

Gehrke, I., R. K. Gandhirajan, and K. Kreuzer (2009, November). Targeting the WNT/[beta]-catenin/TCF/LEF1 axis in solid and haematological cancers: Multiplicity of therapeutic options. *European Journal of Cancer 45*(16), 2759–2767.

Gerbe, F., B. Brulin, L. Makrini, C. Legraverend, and P. Jay (2009, December). DCAMKL-1 expression identifies tuft cells rather than stem cells in the adult mouse intestinal epithelium. *Gastroenterology 137*(6), 2179–2180.

Giles, R. H., J. H. van Es, and H. Clevers (2003, June). Caught up in a wnt storm: Wnt signaling in cancer. *Biochimica et Biophysica Acta (BBA) - Reviews on Cancer 1653*(1), 1–24.

Glaros, S., G. M. Cirrincione, A. Palanca, D. Metzger, and D. Reisman (2008, May). Targeted knockout of BRG1 potentiates lung cancer development. *Cancer Res 68*(10), 3689–3696.

Gonzlez, M. V., M. L. Artmez, L. Rodrigo, C. Lpez-Larrea, M. J. Menndez, V. Alvarez, R. Prez, M. F. Fresno, M. J. Prez, A. Sampedro, and E. Coto (1997, March). Mutation analysis of the p53, APC, and p16 genes in the barrett's oesophagus, dysplasia, and adenocarcinoma. *Journal of Clinical Pathology 50*(3), 212–217. PMID: 9155671.

Goss, K. H. and M. Kahn (Eds.) (2011). *Targeting the Wnt Pathway in Cancer*. New York, NY: Springer New York.

Gossen, M. and H. Bujard (1992, June). Tight control of gene expression in mammalian cells by tetracycline-responsive promoters. *Proceedings of the National Academy of Sciences of the United States of America 89*(12), 5547–5551. PMID: 1319065.

Gossen, M., S. Freundlieb, G. Bender, G. Mller, W. Hillen, and H. Bujard (1995, June). Transcriptional activation by tetracyclines in mammalian cells. *Science (New York, N.Y.) 268*(5218), 1766–1769. PMID: 7792603.

Grady, W. M., L. L. Myeroff, S. E. Swinler, A. Rajput, S. Thiagalingam, J. D. Lutterbaugh, A. Neumann, M. G. Brattain, J. Chang, S. Kim, K. W. Kinzler, B. Vogelstein, J. K. V. Willson, and S. Markowitz (1999, January). Mutational inactivation of transforming growth factor receptor type II in microsatellite stable colon cancers. *Cancer Research 59*(2), 320 –324.

Green, E. L. E. (1966). *Biology of the Laboratory Mouse*. McGraw-Hill.

Greenow, K. R., A. R. Clarke, and R. H. Jones (2009, January). Chk1 deficiency in the mouse small intestine results in p53-independent crypt death and subsequent intestinal compensation. *Oncogene 28*(11), 1443–1453.

Gregorieff, A. and H. Clevers (2005, April). Wnt signaling in the intestinal epithelium: from endoderm to cancer. *Genes & Development 19*(8), 877–90. PMID: 15833914.

Gregorieff, A., D. Pinto, H. Begthel, O. Destre, M. Kielman, and H. Clevers (2005, August). Expression pattern of wnt signaling components in the adult intestine. *Gastroenterology 129*(2), 626–638.

Griffin, C. T., J. Brennan, and T. Magnuson (2008, February). The chromatin-remodeling enzyme BRG1 plays an essential role in primitive erythropoiesis and vascular development. *Development 135*(3), 493 –500.

Griffin, C. T., C. D. Curtis, R. B. Davis, V. Muthukumar, and T. Magnuson (2011, February). The chromatin-remodeling enzyme BRG1 modulates vascular wnt signaling at two levels. *Proceedings of the National Academy of Sciences 108*(6), 2282 –2287.

Groden, J., A. Thliveris, W. Samowitz, M. Carlson, L. Gelbert, H. Albertsen, G. Joslyn, J. Stevens, L. Spirio, M. Robertson, L. Sargeant, K. Krapcho, E. Wolff, R. Burt, J. P. Hughes, J. Warrington, J. McPherson, J. Wasmuth, D. Le Paslier, H. Abderrahim, D. Cohen, M. Leppert, and R. White (1991, August). Identification and characterization of the familial adenomatous polyposis coli gene. *Cell 66*(3), 589–600.

Gryfe, R. (2009, November). Inherited colorectal cancer syndromes. *Clinics in Colon and Rectal Surgery 22*(4), 198–208. PMID: 21037810 PMCID: 2796102.

Guerra, C., N. Mijimolle, A. Dhawahir, P. Dubus, M. Barradas, M. Serrano, V. Campuzano, and M. Barbacid (2003, August). Tumor induction by an endogenous k-ras oncogene is highly dependent on cellular context. *Cancer Cell 4*(2), 111–120.

Hall, P., P. Coates, B. Ansari, and D. Hopwood (1994, December). Regulation of cell number in the mammalian gastrointestinal tract: the importance of apoptosis. *J Cell Sci 107*(12), 3569–3577.

Hamilton, J. P. and S. J. Meltzer (2006, April). A review of the genomics of gastric cancer. *Clinical Gastroenterology and Hepatology: The Official Clinical Practice Journal of the American Gastroenterological Association 4*(4), 416–425. PMID: 16616344.

Hampel, H., J. A. Stephens, E. Pukkala, R. Sankila, L. A. Aaltonen, J. Mecklin, and A. de la Chapelle (2005, August). Cancer risk in hereditary nonpolyposis colorectal cancer syndrome: Later age of onset. *Gastroenterology 129*(2), 415–421.

Hang, C. T., J. Yang, P. Han, H. Cheng, C. Shang, E. Ashley, B. Zhou, and C. Chang (2010, July). Chromatin regulation by brg1 underlies heart muscle development and disease. *Nature 466*(7302), 62–67.

Harada, N., Y. Tamai, T. Ishikawa, B. Sauer, K. Takaku, M. Oshima, and M. M. Taketo (1999, November). Intestinal polyposis in mice with a dominant stable mutation of the beta-catenin gene. *The EMBO Journal 18*(21), 5931–42. PMID: 10545105.

Haramis, A. G., H. Begthel, M. van den Born, J. van Es, S. Jonkheer, G. J. A. Offerhaus, and H. Clevers (2004, March). De novo crypt formation and juvenile polyposis on BMP inhibition in mouse intestine. *Science 303*(5664), 1684 –1686.

Hart, M., J. P. Concordet, I. Lassot, I. Albert, R. del los Santos, H. Durand, C. Perret, B. Rubinfeld, F. Margottin, R. Benarous, and P. Polakis (1999, February). The f-box protein beta-TrCP associates with phosphorylated beta-catenin and regulates its activity in the cell. *Current Biology: CB 9*(4), 207–10. PMID: 10074433.

Hay, T., T. Patrick, D. Winton, O. J. Sansom, and A. R. Clarke (2005, February). Brca2 deficiency in the murine small intestine sensitizes to p53-dependent apoptosis and leads to the spontaneous deletion of stem cells. *Oncogene 24*(23), 3842–3846.

Hcker, M. and B. Wiedenmann (1998, November). Molecular mechanisms of enteroendocrine differentiation. *Annals of the New York Academy of Sciences 859*, 160–174. PMID: 9928379.

He, B., L. You, K. Uematsu, Z. Xu, A. Y. Lee, M. Matsangou, F. McCormick, and D. M. Jablons (2004a, January). A monoclonal antibody against wnt-1 induces apoptosis in human cancer cells. *Neoplasia (New York, N.Y.) 6*(1), 7–14. PMID: 15068666 PMCID: 1508626.

He, X. C., J. Zhang, W. Tong, O. Tawfik, J. Ross, D. H. Scoville, Q. Tian, X. Zeng, X. He, L. M. Wiedemann, Y. Mishina, and L. Li (2004b, October). BMP signaling inhibits intestinal stem cell self-renewal through suppression of wnt-[beta]-catenin signaling. *Nat Genet 36*(10), 1117–1121.

Heath, J. P. (1996, February). Epithelial cell migration in the intestine. *Cell Biology International 20*(2), 139–146. PMID: 8935158.

Hecht, A., K. Vleminckx, M. P. Stemmler, F. van Roy, and R. Kemler (2000, April). The p300/CBP acetyltransferases function as transcriptional coactivators of [beta]-catenin in vertebrates. *EMBO J 19*(8), 1839–1850.

Hendricks, K. B., F. Shanahan, and E. Lees (2004, January). Role for BRG1 in cell cycle control and tumor suppression. *Mol. Cell. Biol. 24*(1), 362–376.

Heyer, J., K. Yang, M. Lipkin, W. Edelmann, and R. Kucherlapati (1999, September). Mouse models for colorectal cancer. *Oncogene 18*(38), 5325–5333. PMID: 10498885.

Hill, R. P. (2006, February). Identifying cancer stem cells in solid tumors: Case not proven. *Cancer Research 66*(4), 1891 –1896.

Hinoi, T., A. Akyol, B. K. Theisen, D. O. Ferguson, J. K. Greenson, B. O. Williams, K. R. Cho, and E. R. Fearon (2007, October). Mouse model of colonic Adenoma-Carcinoma progression based on somatic apc inactivation. *Cancer Res 67*(20), 9721–9730.

Ho, L., R. Jothi, J. L. Ronan, K. Cui, K. Zhao, and G. R. Crabtree (2009, March). An embryonic stem cell chromatin remodeling complex, esBAF, is an essential component of the core pluripotency transcriptional network. *Proceedings of the National Academy of Sciences 106*(13), 5187 –5191.

Holcombe, R. F., J. L. Marsh, M. L. Waterman, F. Lin, T. Milovanovic, and T. Truong (2002, August). Expression of wnt ligands and frizzled receptors in colonic mucosa and in colon carcinoma. *Molecular Pathology 55*(4), 220–226. PMID: 12147710 PMCID: 1187182.

Houlston, R., S. Bevan, A. Williams, J. Young, M. Dunlop, P. Rozen, C. Eng, D. Markie, K. Woodford-Richens, M. A. Rodriguez-Bigas, B. Leggett, K. Neale, R. Phillips, E. Sheridan, S. Hodgson, T. Iwama, D. Eccles, W. Bodmer, and

I. Tomlinson (1998, November). Mutations in DPC4 (SMAD4) cause juvenile polyposis syndrome, but only account for a minority of cases. *Human Molecular Genetics 7*(12), 1907 –1912.

Howe, J. R., J. L. Bair, M. G. Sayed, M. E. Anderson, F. A. Mitros, G. M. Petersen, V. E. Velculescu, G. Traverso, and B. Vogelstein (2001, June). Germline mutations of the gene encoding bone morphogenetic protein receptor 1A in juvenile polyposis. *Nat Genet 28*(2), 184–187.

Howe, J. R., S. Roth, J. C. Ringold, R. W. Summers, H. J. Jrvinen, P. Sistonen, I. P. M. Tomlinson, R. S. Houlston, S. Bevan, F. A. Mitros, E. M. Stone, and L. A. Aaltonen (1998, May). Mutations in the SMAD4/DPC4 gene in juvenile polyposis. *Science 280*(5366), 1086 –1088.

Huang, S. A., Y. M. Mishina, S. Liu, A. Cheung, F. Stegmeier, G. A. Michaud, O. Charlat, E. Wiellette, Y. Zhang, S. Wiessner, M. Hild, X. Shi, C. J. Wilson, C. Mickanin, V. Myer, A. Fazal, R. Tomlinson, F. Serluca, W. Shao, H. Cheng, M. Shultz, C. Rau, M. Schirle, J. Schlegl, S. Ghidelli, S. Fawell, C. Lu, D. Curtis, M. W. Kirschner, C. Lengauer, P. M. Finan, J. A. Tallarico, T. Bouwmeester, J. A. Porter, A. Bauer, and F. Cong (2009, October). Tankyrase inhibition stabilizes axin and antagonizes wnt signalling. *Nature 461*(7264), 614–620.

Iacopetta, B. (2003, March). TP53 mutation in colorectal cancer. *Human Mutation 21*(3), 271–276. PMID: 12619112.

Inayoshi, Y., K. Miyake, Y. Machida, H. Kaneoka, M. Terajima, T. Dohda, M. Takahashi, and S. Iijima (2006, February). Mammalian chromatin remodeling complex SWI/SNF is essential for enhanced expression of the albumin gene during liver development. *J Biochem 139*(2), 177–188.

Indra, A. K., V. Dupe, J. Bornert, N. Messaddeq, M. Yaniv, M. Mark, P. Chambon, and D. Metzger (2005, October). Temporally controlled targeted somatic mutagenesis in embryonic surface ectoderm and fetal epidermal keratinocytes unveils two distinct developmental functions of BRG1 in limb morphogenesis and skin barrier formation. *Development 132*(20), 4533–4544.

Ireland, H., C. Houghton, L. Howard, and D. J. Winton (2005, August). Cellular inheritance of a cre-activated reporter gene to determine paneth cell longevity in the murine small intestine. *Developmental Dynamics: An Official Publication of the American Association of Anatomists 233*(4), 1332–1336. PMID: 15937933.

Ireland, H., R. Kemp, C. Houghton, L. Howard, A. R. Clarke, O. J. Sansom, and D. J. Winton (2004, May). Inducible cre-mediated control of gene expression in the murine gastrointestinal tract: effect of loss of [beta]-catenin. *Gastroenterology 126*(5), 1236–1246.

Iversen, P. L., V. Arora, A. J. Acker, D. H. Mason, and G. R. Devi (2003, July). Efficacy of antisense morpholino oligomer targeted to c-myc in prostate cancer xenograft murine model and a phase i safety study in humans. *Clinical Cancer Research: An Official Journal of the American Association for Cancer Research 9*(7), 2510–2519. PMID: 12855625.

Janssen, K., F. E. Marjou, D. Pinto, X. Sastre, D. Rouillard, C. Fouquet, T. Soussi, D. Louvard, and S. Robine (2002, August). Targeted expression of oncogenic k-ras in intestinal epithelium causes spontaneous tumorigenesis in mice. *Gastroenterology 123*(2), 492–504.

Jass, J. R., J. Young, and B. A. Leggett (2002, January). Evolution of colorectal cancer: change of pace and change of direction. *Journal of Gastroenterology and Hepatology 17*(1), 17–26. PMID: 11987262.

Jenne, D. E., H. Reomann, J.-i. Nezu, W. Friedel, S. Loff., R. Jeschke, O. Muller, W. Back, and M. Zimmer (1998, January). Peutz-Jeghers syndrome is caused by mutations in a novel serine threoninekinase. *Nat Genet 18*(1), 38–43.

Jensen, J., E. E. Pedersen, P. Galante, J. Hald, R. S. Heller, M. Ishibashi, R. Kageyama, F. Guillemot, P. Serup, and O. D. Madsen (2000, January). Control of endodermal endocrine development by hes-1. *Nat Genet 24*(1), 36–44.

Jones, P. A. and S. B. Baylin (2002, June). The fundamental role of epigenetic events in cancer. *Nat Rev Genet 3*(6), 415–428.

Jubb, A. M., S. Chalasani, G. D. Frantz, R. Smits, H. I. Grabsch, V. Kavi, N. J. Maughan, K. J. Hillan, P. Quirke, and H. Koeppen (2006, March). Achaete-scute like 2 (ascl2) is a target of wnt signalling and is upregulated in intestinal neoplasia. *Oncogene 25*(24), 3445–3457.

Jung, P., T. Sato, A. Merlos-Suarez, F. M. Barriga, M. Iglesias, D. Rossell, M. M. Gallardo, M. A. Blasco, E. Sancho, H. Clevers, and E. Batlle (2011). Isolation and in vitro expansion of human colonic stem cells. *Nat Med advance online publication.*

Kadam, S. and B. M. Emerson (2003, February). Transcriptional specificity of human SWI/SNF BRG1 and BRM chromatin remodeling complexes. *Molecular Cell 11*(2), 377–389. PMID: 12620226.

Kang, H., K. Cui, and K. Zhao (2004, February). BRG1 controls the activity of the retinoblastoma protein via regulation of p21CIP1/WAF1/SDI. *Molecular and Cellular Biology 24*(3). PMC321457.

Karam, S. M. (1999, March). Lineage commitment and maturation of epithelial cells in the gut. *Frontiers in Bioscience: A Journal and Virtual Library 4*, D286–298. PMID: 10077541.

Karlsson, L., P. Lindahl, J. Heath, and C. Betsholtz (2000). Abnormal gastrointestinal development in PDGF-A and PDGFR-(alpha) deficient mice implicates a novel mesenchymal structure with putative instructive properties in villus morphogenesis. *Development 127*(16), 3457 –3466.

Karpowicz, P., C. Morshead, A. Kam, E. Jervis, J. Ramunas, V. Cheng, and D. van der Kooy (2005). Support for the immortal strand hypothesis. *The Journal of Cell Biology 170*(5), 721 –732.

Kastritis, E., S. Murray, F. Kyriakou, M. Horti, N. Tamvakis, N. Kavantzas, E. S. Patsouris, A. Noni, S. Legaki, M. A. Dimopoulos, and A. Bamias (2009, January). Somatic mutations of adenomatous polyposis coli gene and nuclear bcatenin accumulation have prognostic significance in invasive urothelial carcinomas: Evidence for wnt pathway implication. *International Journal of Cancer 124*(1), 103–108.

Katoh, Y. and M. Katoh (2006, December). Hedgehog signaling pathway and gastrointestinal stem cell signaling network (review). *International Journal of Molecular Medicine 18*(6), 1019–1023. PMID: 17089004.

Kedinger, M., P. M. Simon-Assmann, B. Lacroix, A. Marxer, H. P. Hauri, and K. Haffen (1986, February). Fetal gut mesenchyme induces differentiation of cultured intestinal endodermal and crypt cells. *Developmental Biology 113*(2), 474–483.

Kelly, P. N., A. Dakic, J. M. Adams, S. L. Nutt, and A. Strasser (2007, July). Tumor growth need not be driven by rare cancer stem cells. *Science 317*(5836), 337.

Kemp, R., H. Ireland, E. Clayton, C. Houghton, L. Howard, and D. J. Winton (2004). Elimination of background recombination: somatic induction of cre by combined transcriptional regulation and hormone binding affinity. *Nucleic Acids Research 32*(11), e92. PMC443557.

Khavari, P. A., C. L. Peterson, J. W. Tamkun, D. B. Mendel, and G. R. Crabtree (1993, November). BRG1 contains a conserved domain of the SWI2/SNF2 family necessary for normal mitotic growth and transcription. *Nature 366*(6451), 170–174.

Kidder, B. L., S. Palmer, and J. G. Knott (2009, February). SWI/SNF-Brg1 regulates Self-Renewal and occupies core Pluripotency-Related genes in embryonic stem cells. *Stem Cells 27*(2), 317–328.

Kielman, M. F., M. Rindapaa, C. Gaspar, N. van Poppel, C. Breukel, S. van Leeuwen, M. M. Taketo, S. Roberts, R. Smits, and R. Fodde (2002, December). Apc modulates embryonic stem-cell differentiation by controlling the dosage of [beta]-catenin signaling. *Nat Genet 32*(4), 594–605.

Kim, B., G. Buchner, I. Miletich, P. T. Sharpe, and R. A. Shivdasani (2005, April). The stomach mesenchymal transcription factor barx1 specifies gastric epithelial identity through inhibition of transient wnt signaling. *Developmental Cell 8*(4), 611–622. PMID: 15809042.

Kim, J., H. Crooks, A. Foxworth, and T. Waldman (2002, December). Proof-of-principle: oncogenic beta-catenin is a valid molecular target for the development of pharmacological inhibitors. *Molecular Cancer Therapeutics 1*(14), 1355–1359. PMID: 12516970.

Kim, S. H., K. A. Roth, A. R. Moser, and J. I. Gordon (1993, November). Transgenic mouse models that explore the multistep hypothesis of intestinal neoplasia. *The Journal of Cell Biology 123*(4), 877–893. PMID: 8227147.

Kinzler, K. W. and B. Vogelstein (1996, October). Lessons from hereditary colorectal cancer. *Cell 87*(2), 159–70. PMID: 8861899.

Kinzler, K. W. and B. Vogelstein (1998, May). Landscaping the cancer terrain. *Science 280*(5366), 1036 –1037.

Kitagawa, H., R. Fujiki, K. Yoshimura, Y. Mezaki, Y. Uematsu, D. Matsui, S. Ogawa, K. Unno, M. Okubo, A. Tokita, T. Nakagawa, T. Ito, Y. Ishimi, H. Nagasawa, T. Matsumoto, J. Yanagisawa, and S. Kato (2003, June). The Chromatin-Remodeling complex WINAC targets a nuclear receptor to promoters and is impaired in williams syndrome. *Cell 113*(7), 905–917.

Klose, R. J. and A. P. Bird (2006, February). Genomic DNA methylation: the mark and its mediators. *Trends in Biochemical Sciences 31*(2), 89–97.

Koppert, L. B., A. W. van der Velden, M. van de Wetering, M. Abbou, A. M. W. van den Ouweland, H. W. Tilanus, B. P. L. Wijnhoven, and W. N. M. Dinjens (2004). Frequent loss of the AXIN1 locus but absence of AXIN1 gene mutations in adenocarcinomas of the gastro-oesophageal junction with nuclear [beta]-catenin expression. *Br J Cancer 90*(4), 892–899.

Korinek, V., N. Barker, P. Moerer, E. van Donselaar, G. Huls, P. J. Peters, and H. Clevers (1998, August). Depletion of epithelial stem-cell compartments in the small intestine of mice lacking tcf-4. *Nature Genetics 19*(4), 379–83. PMID: 9697701.

Kosinski, C., V. S. W. Li, A. S. Y. Chan, J. Zhang, C. Ho, W. Y. Tsui, T. L. Chan, R. C. Mifflin, D. W. Powell, S. T. Yuen, S. Y. Leung, and X. Chen (2007). Gene expression patterns of human colon tops and basal crypts and BMP antagonists as intestinal stem cell niche factors. *Proceedings of the National Academy of Sciences 104*(39), 15418 –15423.

Kudo, J., T. Nishiwaki, N. Haruki, H. Ishiguro, Y. Shibata, Y. Terashita, H. Sugiura, N. Shinoda, M. Kimura, Y. Kuwabara, and Y. Fujii (2007). Aberrant nuclear localization of beta-catenin without genetic alterations in beta-catenin or axin genes in esophageal cancer. *World Journal of Surgical Oncology 5*, 21. PMID: 17309796.

Kuehn, M. R., A. Bradley, E. J. Robertson, and M. J. Evans (1987, March). A potential animal model for Lesch-Nyhan syndrome through introduction of HPRT mutations into mice. *Nature 326*(6110), 295–298.

Kuhnert, F., C. R. Davis, H. Wang, P. Chu, M. Lee, J. Yuan, R. Nusse, and C. J. Kuo (2004, January). Essential requirement for wnt signaling in proliferation of adult small intestine and colon revealed by adenoviral expression of dickkopf-1. *Proceedings of the National Academy of Sciences of the United States of America 101*(1), 266 –271.

Kuwano, H., H. Kato, T. Miyazaki, M. Fukuchi, N. Masuda, M. Nakajima, Y. Fukai, M. Sohda, H. Kimura, and A. Faried (2005). Genetic alterations in esophageal cancer. *Surgery Today 35*(1), 7–18. PMID: 15622457.

Kwon, C. S. and D. Wagner (2007, August). Unwinding chromatin for development and growth: a few genes at a time. *Trends in Genetics 23*(8), 403–412.

Lamba, D. A., S. Hayes, M. O. Karl, and T. Reh (2008, October). Baf60c is a component of the neural progenitor-specific BAF complex in developing retina. *Developmental Dynamics: An Official Publication of the American Association of Anatomists 237*(10), 3016–3023. PMID: 18816825.

Laurent-Puig, P., H. Blons, and P. H. Cugnenc (1999, December). Sequence of molecular genetic events in colorectal tumorigenesis. *European Journal of Cancer Prevention: The Official Journal of the European Cancer Prevention Organisation (ECP) 8 Suppl 1*, S39–47. PMID: 10772417.

Lee, D., J. W. Kim, T. Seo, S. G. Hwang, E. Choi, and J. Choe (2002, June). SWI/SNF complex interacts with tumor suppressor p53 and is necessary for the activation of p53-mediated transcription. *J. Biol. Chem. 277*(25), 22330–22337.

Lee, E. R. (1985, March). Dynamic histology of the antral epithelium in the mouse stomach: I. architecture of antral units. *The American Journal of Anatomy 172*(3), 187–204. PMID: 3887885.

Lee, J., S. C. Abraham, H. Kim, J. Nam, C. Choi, M. Lee, C. Park, S. Juhng, A. Rashid, S. R. Hamilton, and T. Wu (2002, August). Inverse relationship between APC gene mutation in gastric adenomas and development of adenocarcinoma. *The American Journal of Pathology 161*(2), 611–618. PMID: 12163385.

Lees, C., S. Howie, R. B. Sartor, and J. Satsangi (2005, November). The hedgehog signalling pathway in the gastrointestinal tract: Implications for development, homeostasis, and disease. *Gastroenterology 129*(5), 1696–1710.

Lepourcelet, M., Y. P. Chen, D. S. France, H. Wang, P. Crews, F. Petersen, C. Bruseo, A. W. Wood, and R. A. Shivdasani (2004, January). Small-molecule antagonists of the oncogenic tcf/[beta]-catenin protein complex. *Cancer Cell 5*(1), 91–102.

Li, A. F., P. Hsu, C. Tzao, Y. Wang, I. Hung, M. Huang, and H. Hsu (2009, September). Reduced axin protein expression is associated with a poor prognosis in patients with squamous cell carcinoma of esophagus. *Annals of Surgical Oncology 16*(9), 2486–2493. PMID: 19582507.

Li, L. and H. Clevers (2010, January). Coexistence of quiescent and active adult stem cells in mammals. *Science 327*(5965), 542–545.

Liang, J., M. Wan, Y. Zhang, P. Gu, H. Xin, S. Y. Jung, J. Qin, J. Wong, A. J. Cooney, D. Liu, and Z. Songyang (2008, June). Nanog and oct4 associate with unique transcriptional repression complexes in embryonic stem cells. *Nat Cell Biol 10*(6), 731–739.

Liang, P. S., T. Chen, and E. Giovannucci (2009, May). Cigarette smoking and colorectal cancer incidence and mortality: systematic review and meta-analysis. *International Journal of Cancer. Journal International Du Cancer 124*(10), 2406–2415. PMID: 19142968.

Liaw, D., D. J. Marsh, J. Li, P. L. M. Dahia, S. I. Wang, Z. Zheng, S. Bose, K. M. Call, H. C. Tsou, M. Peacoke, C. Eng, and R. Parsons (1997, May). Germline mutations of the PTEN gene in cowden disease, an inherited breast and thyroid cancer syndrome. *Nat Genet 16*(1), 64–67.

Lim, W., N. Hearle, B. Shah, V. Murday, S. V. Hodgson, A. Lucassen, D. Eccles, I. Talbot, K. Neale, A. G. Lim, J. O'Donohue, A. Donaldson, R. C. Macdonald, I. D. Young, M. H. Robinson, P. W. R. Lee, B. J. Stoodley, I. Tomlinson, D. Alderson, A. G. Holbrook, S. Vyas, E. T. Swarbrick, A. A. M. Lewis, R. K. S. Phillips, and R. S. Houlston (2003, July). Further observations on LKB1/STK11 status and cancer risk in Peutz-Jeghers syndrome. *British Journal of Cancer 89*(2), 308–313. PMID: 12865922.

Lin, H., R. Wong, M. Martinka, and G. Li (2010, August). BRG1 expression is increased in human cutaneous melanoma. *British Journal of Dermatology 163*(3), 502–510.

Link, K. A., C. J. Burd, E. Williams, T. Marshall, G. Rosson, E. Henry, B. Weissman, and K. E. Knudsen (2005, March). BAF57 governs androgen receptor action and Androgen-Dependent proliferation through SWI/SNF. *Mol. Cell. Biol. 25*(6), 2200–2215.

Liu, C., Y. Li, M. Semenov, C. Han, G. H. Baeg, Y. Tan, Z. Zhang, X. Lin, and X. He (2002, March). Control of beta-catenin phosphorylation/degradation by a dual-kinase mechanism. *Cell 108*(6), 837–47. PMID: 11955436.

Loeffler, M., T. Bratke, U. Paulus, Y. Q. Li, and C. S. Potten (1997, May). Clonality and life cycles of intestinal crypts explained by a state dependent stochastic model of epithelial stem cell organization. *Journal of Theoretical Biology 186*(1), 41–54.

Lopez-Garcia, C., A. M. Klein, B. D. Simons, and D. J. Winton (2010, November). Intestinal stem cell replacement follows a pattern of neutral drift. *Science 330*(6005), 822–825.

Lynch, H. T. and A. de la Chapelle (2003, March). Hereditary colorectal cancer. *The New England Journal of Medicine 348*(10), 919–932. PMID: 12621137.

Madison, B. B., K. Braunstein, E. Kuizon, K. Portman, X. T. Qiao, and D. L. Gumucio (2005, January). Epithelial hedgehog signals pattern the intestinal crypt-villus axis. *Development 132*(2), 279 –289.

Mahmoudi, T., S. F. Boj, P. Hatzis, V. S. W. Li, N. Taouatas, R. G. J. Vries, H. Teunissen, H. Begthel, J. Korving, S. Mohammed, A. J. R. Heck, and H. Clevers (2010, November). The Leukemia-Associated Mllt10/Af10-Dot1l are Tcf4/-Catenin coactivators essential for intestinal homeostasis. *PLoS Biol 8*(11), e1000539.

Malumbres, M. and M. Barbacid (2003, June). RAS oncogenes: the first 30 years. *Nat Rev Cancer 3*(6), 459–465.

Marignani, P. A., F. Kanai, and C. L. Carpenter (2001). LKB1 associates with brg1 and is necessary for brg1-induced growth arrest. *Journal of Biological Chemistry 276*(35), 32415 –32418.

Markowitz, S., J. Wang, L. Myeroff, R. Parsons, L. Sun, J. Lutterbaugh, R. Fan, E. Zborowska, K. Kinzler, B. Vogelstein, and a. et (1995, June). Inactivation of the type II TGF-beta receptor in colon cancer cells with microsatellite instability. *Science 268*(5215), 1336 –1338.

Marsh, V., D. J. Winton, G. T. Williams, N. Dubois, A. Trumpp, O. J. Sansom, and A. R. Clarke (2008, December). Epithelial pten is dispensable for intestinal homeostasis but suppresses adenoma development and progression after apc mutation. *Nat Genet 40*(12), 1436–1444.

Marshman, E., C. Booth, and C. S. Potten (2002). The intestinal epithelial stem cell. *BioEssays 24*(1), 91–98.

Marsit, C. J., M. R. Karagas, A. Andrew, M. Liu, H. Danaee, A. R. Schned, H. H. Nelson, and K. T. Kelsey (2005). Epigenetic inactivation of SFRP genes and TP53 alteration act jointly as markers of invasive bladder cancer. *Cancer Research 65*(16), 7081 –7085.

Matsukawa, Y., H. Nishino, Y. Okuyama, T. Matsui, T. Matsumoto, S. Matsumura, Y. Shimizu, Y. Sowa, and T. Sakai (1997, April). Effects of quercetin and/or restraint stress on formation of aberrant crypt foci induced by azoxymethane in rat colons. *Oncology 54*(2), 118–121. PMID: 9075782.

Matsumoto, S., F. Banine, J. Struve, R. Xing, C. Adams, Y. Liu, D. Metzger, P. Chambon, M. S. Rao, and L. S. Sherman (2006, January). Brg1 is required for murine neural stem cell maintenance and gliogenesis. *Developmental Biology 289*(2), 372–383.

May, R., T. E. Riehl, C. Hunt, S. M. Sureban, S. Anant, and C. W. Houchen (2008, March). Identification of a novel putative gastrointestinal stem cell and adenoma stem cell marker, doublecortin and CaM Kinase-Like-1, following radiation injury and in adenomatous polyposis Coli/Multiple intestinal neoplasia mice. *Stem Cells 26*(3), 630–637.

McCubrey, J. A., L. S. Steelman, S. L. Abrams, J. T. Lee, F. Chang, F. E. Bertrand, P. M. Navolanic, D. M. Terrian, R. A. Franklin, A. B. D'Assoro, J. L. Salisbury, M. C. Mazzarino, F. Stivala, and M. Libra (2006). Roles of the RAF/MEK/ERK and PI3K/PTEN/AKT pathways in malignant transformation and drug resistance. *Advances in Enzyme Regulation 46*, 249–279. PMID: 16854453.

Medina, P. P., J. Carretero, M. F. Fraga, M. Esteller, D. Sidransky, and M. Sanchez-Cespedes (2004). Genetic and epigenetic screening for gene alterations of the chromatin-remodeling factor, SMARCA4/BRG1, in lung tumors. *Genes, Chromosomes and Cancer 41*(2), 170–177.

Medina, P. P., O. A. Romero, T. Kohno, L. M. Montuenga, R. Pio, J. Yokota, and M. Sanchez-Cespedes (2008, April). Frequent BRG1/SMARCA4-inactivating mutations in human lung cancer cell lines. *Human Mutation 29*(5), 617–622.

Medina, P. P. and M. Sanchez-Cespedes (2008, March). Involvement of the chromatin-remodeling factor BRG1/SMARCA4 in human cancer. *Epigenetics 3*(2), 64–68.

Meng, Y., Q. Wang, J. Wang, S. Zhu, Y. Jiao, P. Li, and S. Zhang (2011, May). Epigenetic inactivation of the SFRP1 gene in esophageal squamous cell carcinoma. *Digestive Diseases and Sciences*. PMID: 21567192.

Merg, A. and J. R. Howe (2004, August). Genetic conditions associated with intestinal juvenile polyps. *American Journal of Medical Genetics. Part C, Seminars in Medical Genetics 129C*(1), 44–55. PMID: 15264272.

Merle, P., S. de la Monte, M. Kim, M. Herrmann, S. Tanaka, A. Von Dem Bussche, M. C. Kew, C. Trepo, and J. R. Wands (2004, October). Functional consequences of frizzled-7 receptor overexpression in human hepatocellular carcinoma. *Gastroenterology 127*(4), 1110–1122.

Merlos-Surez, A., F. M. Barriga, P. Jung, M. Iglesias, M. V. Cspedes, D. Rossell, M. Sevillano, X. Hernando-Momblona, V. da Silva-Diz, P. Muoz, H. Clevers, E. Sancho, R. Mangues, and E. Batlle (2011). The intestinal stem cell signature identifies colorectal cancer stem cells and predicts disease relapse. *Cell Stem Cell In Press, Corrected Proof.*

Merritt, A. J., K. A. Gould, and W. F. Dove (1997, December). Polyclonal structure of intestinal adenomas in ApcMin/+ mice with concomitant loss of apc+ from all tumorlineages. *Proceedings of the National Academy of Sciences 94*(25), 13927 – 13931.

Milano, J., J. McKay, C. Dagenais, L. Foster-Brown, F. Pognan, R. Gadient, R. T. Jacobs, A. Zacco, B. Greenberg, and P. J. Ciaccio (2004, November). Modulation of notch processing by -Secretase inhibitors causes intestinal goblet cell metaplasia and induction of genes known to specify gut secretory lineage differentiation. *Toxicological Sciences 82*(1), 341 –358.

Mills, J. C. and R. A. Shivdasani.

Miyamoto, H., T. Shuin, I. Ikeda, M. Hosaka, and Y. Kubota (1996, April). Loss of heterozygosity at the p53, RB, DCC and APC tumor suppressor gene loci in human bladder cancer. *The Journal of Urology 155*(4), 1444–1447. PMID: 8632608.

Moghaddam, A. A., M. Woodward, and R. Huxley (2007, December). Obesity and risk of colorectal cancer: a meta-analysis of 31 studies with 70,000 events. *Cancer Epidemiology, Biomarkers & Prevention: A Publication of the American Association for Cancer Research, Cosponsored by the American Society of Preventive Oncology 16*(12), 2533–2547. PMID: 18086756.

Montgomery, R. K., D. L. Carlone, C. A. Richmond, L. Farilla, M. E. G. Kranendonk, D. E. Henderson, N. Y. Baffour-Awuah, D. M. Ambruzs, L. K. Fogli, S. Algra, and D. T. Breault (2011, January). Mouse telomerase reverse transcriptase (mTert) expression marks slowly cycling intestinal stem cells. *Proceedings of the National Academy of Sciences 108*(1), 179 –184.

Morin, P. J., A. B. Sparks, V. Korinek, N. Barker, H. Clevers, B. Vogelstein, and K. W. Kinzler (1997, March). Activation of -Catenin-Tcf signaling in colon cancer by mutations in -Catenin or APC. *Science 275*(5307), 1787 –1790.

Muncan, V., O. J. Sansom, L. Tertoolen, T. J. Phesse, H. Begthel, E. Sancho, A. M. Cole, A. Gregorieff, I. M. de Alboran, H. Clevers, and A. R. Clarke (2006, November). Rapid loss of intestinal crypts upon conditional deletion of the Wnt/Tcf-4 target gene c-Myc. *Mol. Cell. Biol. 26*(22), 8418–8426.

Murphy, D. J., S. Hardy, and D. A. Engel (1999, April). Human SWI-SNF component BRG1 represses transcription of the c-fos gene. *Molecular and Cellular Biology 19*(4). PMC84065.

Nagase, H. and Y. Nakamura (1993). Mutations of the APC (adenomatous polyposis coli) gene. *Human Mutation 2*(6), 425–34. PMID: 8111410.

Nagayama, S., C. Fukukawa, T. Katagiri, T. Okamoto, T. Aoyama, N. Oyaizu, M. Imamura, J. Toguchida, and Y. Nakamura (2005, June). Therapeutic potential of antibodies against FZD10, a cell-surface protein, for synovial sarcomas. *Oncogene 24*(41), 6201–6212.

Naidu, S. R., I. M. Love, A. N. Imbalzano, S. R. Grossman, and E. J. Androphy (2009, May). The SWI/SNF chromatin remodeling subunit BRG1 is a critical regulator of p53 necessary for proliferation of malignant cells. *Oncogene 28*(27), 2492–2501.

Napolitano, M. A., M. Cipollaro, A. Cascino, M. A. B. Melone, A. Giordano, and U. Galderisi (2007, August). Brg1 chromatin remodeling factor is involved in cell growth arrest, apoptosis and senescence of rat mesenchymal stem cells. *J Cell Sci 120*(16), 2904–2911.

Neutra, M. R., A. Frey, and J. Kraehenbuhl (1996, August). Epithelial m cells: Gateways for mucosal infection and immunization. *Cell 86*(3), 345–348.

Nichols, J., B. Zevnik, K. Anastassiadis, H. Niwa, D. Klewe-Nebenius, I. Chambers, H. Schler, and A. Smith (1998, October). Formation of pluripotent stem cells in the mammalian embryo depends on the POU transcription factor oct4. *Cell 95*(3), 379–391.

Norat, T., S. Bingham, P. Ferrari, N. Slimani, M. Jenab, M. Mazuir, K. Overvad, A. Olsen, A. Tjnneland, F. Clavel, M. Boutron-Ruault, E. Kesse, H. Boeing, M. M. Bergmann, A. Nieters, J. Linseisen, A. Trichopoulou, D. Trichopoulos, Y. Tountas, F. Berrino, D. Palli, S. Panico, R. Tumino, P. Vineis, H. B. Bueno-de-Mesquita, P. H. M. Peeters, D. Engeset, E. Lund, G. Skeie, E. Ardanaz, C. Gonzlez, C. Navarro, J. R. Quirs, M. Sanchez, G. Berglund, I. Mattisson, G. Hallmans, R. Palmqvist, N. E. Day, K. Khaw, T. J. Key, M. San Joaquin, B. Hmon, R. Saracci, R. Kaaks, and E. Riboli (2005, June). Meat, fish, and colorectal cancer risk: the european prospective investigation into cancer and nutrition. *Journal of the National Cancer Institute 97*(12), 906–916. PMID: 15956652.

Novelli, M. R., J. A. Williamson, I. P. Tomlinson, G. Elia, S. V. Hodgson, I. C. Talbot, W. F. Bodmer, and N. A. Wright (1996, May). Polyclonal origin of colonic adenomas in an XO/XY patient with FAP. *Science (New York, N.Y.) 272*(5265), 1187–1190. PMID: 8638166.

O/'Brien, C. A., A. Pollett, S. Gallinger, and J. E. Dick (2007, January). A human colon cancer cell capable of initiating tumour growth in immunodeficient mice. *Nature 445*(7123), 106–110.

Ohkawa, Y., C. G. Marfella, and A. N. Imbalzano (2006, February). Skeletal muscle specification by myogenin and Mef2D via the SWI/SNF ATPase brg1. *EMBO J 25*(3), 490–501.

Olive, K. P., M. A. Jacobetz, C. J. Davidson, A. Gopinathan, D. McIntyre, D. Honess, B. Madhu, M. A. Goldgraben, M. E. Caldwell, D. Allard, K. K. Frese, G. DeNicola, C. Feig, C. Combs, S. P. Winter, H. Ireland-Zecchini, S. Reichelt, W. J. Howat, A. Chang, M. Dhara, L. Wang, F. Rckert, R. Grtzmann, C. Pilarsky, K. Izeradjene, S. R. Hingorani, P. Huang, S. E. Davies, W. Plunkett, M. Egorin, R. H. Hruban, N. Whitebread, K. McGovern, J. Adams, C. Iacobuzio-Donahue, J. Griffiths, and D. A. Tuveson (2009, June). Inhibition of hedgehog signaling enhances delivery of chemotherapy in a mouse model of pancreatic cancer. *Science 324*(5933), 1457 –1461.

Oshima, H., A. Matsunaga, T. Fujimura, T. Tsukamoto, M. M. Taketo, and M. Oshima (2006, October). Carcinogenesis in mouse stomach by simultaneous activation of the wnt signaling and prostaglandin e2 pathway. *Gastroenterology 131*(4), 1086–1095.

Oshima, M., H. Oshima, K. Kitagawa, M. Kobayashi, C. Itakura, and M. Taketo (1995, May). Loss of apc heterozygosity and abnormal tissue building in nascent intestinal polyps in mice carrying a truncated apc gene. *Proceedings of the National Academy of Sciences of the United States of America 92*(10), 4482–4486. PMID: 7753829.

Park, C. H., D. E. Bergsagel, and E. A. McCulloch (1971, February). Mouse myeloma tumor stem cells: a primary cell culture assay. *Journal of the National Cancer Institute 46*(2), 411–422. PMID: 5115909.

Park, H. S., R. A. Goodlad, and N. A. Wright (1995, November). Crypt fission in the small intestine and colon. a mechanism for the emergence of G6PD locus-mutated crypts after treatment with mutagens. *The American Journal of Pathology 147*(5), 1416–1427. PMID: 7485404.

Park, J., A. S. Venteicher, J. Y. Hong, J. Choi, S. Jun, M. Shkreli, W. Chang, Z. Meng, P. Cheung, H. Ji, M. McLaughlin, T. D. Veenstra, R. Nusse, P. D. McCrea, and S. E. Artandi (2009, July). Telomerase modulates wnt signalling by association with target gene chromatin. *Nature 460*(7251), 66–72.

Park, S., J. Gwak, M. Cho, T. Song, J. Won, D. Kim, J. Shin, and S. Oh (2006, September). Hexachlorophene inhibits wnt/beta-catenin pathway by promoting siah-mediated beta-catenin degradation. *Molecular Pharmacology 70*(3), 960–966. PMID: 16735606.

Park, S. Y., J. K. Ryu, J. H. Park, H. Yoon, J. Y. Kim, Y. B. Yoon, J. Park, S. H. Lee, S. Kang, J. W. Park, and J. H. Oh (2011, March). Prevalence of gastric and duodenal polyps and risk factors for duodenal neoplasm in korean patients with familial adenomatous polyposis. *Gut and Liver 5*(1), 46–51. PMID: 21461071.

Park, Y., D. J. Hunter, D. Spiegelman, L. Bergkvist, F. Berrino, P. A. van den Brandt, J. E. Buring, G. A. Colditz, J. L. Freudenheim, C. S. Fuchs, E. Giovannucci, R. A. Goldbohm, S. Graham, L. Harnack, A. M. Hartman, D. R. Jacobs, I. Kato, V. Krogh, M. F. Leitzmann, M. L. McCullough, A. B. Miller, P. Pietinen, T. E. Rohan, A. Schatzkin, W. C. Willett, A. Wolk, A. Zeleniuch-Jacquotte, S. M. Zhang, and S. A. Smith-Warner (2005, December). Dietary fiber intake and risk of colorectal cancer: a pooled analysis of prospective cohort studies. *JAMA: The Journal of the American Medical Association 294*(22), 2849–2857. PMID: 16352792.

Paul, S. and A. Dey (2008). Wnt signaling and cancer development: therapeutic implication. *Neoplasma 55*(3), 165–176. PMID: 18348648.

Paulsen, J. E., I. L. Steffensen, E. Namork, and J. Alexander (1994, October). Scanning electron microscopy of aberrant crypt foci in rat colon. *Carcinogenesis 15*(10), 2371–2373. PMID: 7955079.

Paulsson, M. (1992). Basement membrane proteins: structure, assembly, and cellular interactions. *Critical Reviews in Biochemistry and Molecular Biology 27*(1-2), 93–127. PMID: 1309319.

Peng, H., X. Zhong, K. Liu, and S. Li (2009, January). Expression and significance of adenomatous polyposis coli, beta-catenin, e-cadherin and cyclin d1 in esophageal squamous cell carcinoma assessed by tissue microarray. *Ai Zheng = Aizheng = Chinese Journal of Cancer 28*(1), 38–41. PMID: 19448414.

Phelan, M. L., S. Sif, G. J. Narlikar, and R. E. Kingston (1999, February). Reconstitution of a core chromatin remodeling complex from SWI/SNF subunits. *Molecular Cell 3*(2), 247–253.

Pinson, K. I., J. Brennan, S. Monkley, B. J. Avery, and W. C. Skarnes (2000, September). An LDL-receptor-related protein mediates wnt signalling in mice. *Nature 407*(6803), 535–8. PMID: 11029008.

Pinto, D., A. Gregorieff, H. Begthel, and H. Clevers (2003, July). Canonical wnt signals are essential for homeostasis of the intestinal epithelium. *Genes & Development 17*(14), 1709–13. PMID: 12865297.

Pollard, P., M. Deheragoda, S. Segditsas, A. Lewis, A. Rowan, K. Howarth, L. Willis, E. Nye, A. McCart, N. Mandir, A. Silver, R. Goodlad, G. Stamp, M. Cockman, P. East, B. Spencer-Dene, R. Poulsom, N. Wright, and I. Tomlinson (2009, June). The apc 1322T mouse develops severe polyposis associated with submaximal nuclear beta-catenin expression. *Gastroenterology 136*(7), 2204–2213.e1–13. PMID: 19248780.

Ponder, B. A. J., G. H. Schmidt, M. M. Wilkinson, M. J. Wood, M. Monk, and A. Reid (1985, February). Derivation of mouse intestinal crypts from single progenitor cells. *Nature 313*(6004), 689–691.

Porter, E. M., C. L. Bevins, D. Ghosh, and T. Ganz (2002, January). The multifaceted paneth cell. *Cellular and Molecular Life Sciences: CMLS 59*(1), 156–170. PMID: 11846026.

Potten, C., R. Gandara, Y. Mahida, M. Loeffler, and N. Wright (2009). The stem cells of small intestinal crypts: Where are they? *Cell Proliferation 42*(6), 731–750.

Potten, C. S. (1977, October). Extreme sensitivity of some intestinal crypt cells to x and gamma irradiation. *Nature 269*(5628), 518–521. PMID: 909602.

Potten, C. S. (1998, June). Stem cells in gastrointestinal epithelium: numbers, characteristics and death. *Philosophical Transactions of the Royal Society B: Biological Sciences 353*(1370), 821830. PMC1692280.

Potten, C. S., C. Booth, G. L. Tudor, D. Booth, G. Brady, P. Hurley, G. Ashton, R. Clarke, S.-i. Sakakibara, and H. Okano (2003, January). Identification of a putative intestinal stem cell and early lineage marker; musashi-1. *Differentiation; Research in Biological Diversity 71*(1), 28–41. PMID: 12558601.

Potten, C. S., W. J. Hume, P. Reid, and J. Cairns (1978, November). The segregation of DNA in epithelial stem cells. *Cell 15*(3), 899–906.

Potten, C. S., L. Kovacs, and E. Hamilton (1974, May). Continuous labelling studies on mouse skin and intestine. *Cell and Tissue Kinetics 7*(3), 271–283. PMID: 4837676.

Potten, C. S. and M. Loeffler (1990, December). Stem cells: attributes, cycles, spirals, pitfalls and uncertainties. lessons for and from the crypt. *Development (Cambridge, England) 110*(4), 1001–1020. PMID: 2100251.

Potten, C. S., G. Owen, and D. Booth (2002, June). Intestinal stem cells protect their genome by selective segregation of template DNA strands. *J Cell Sci 115*(11), 2381–2388.

Powell, S. M., N. Zilz, Y. Beazer-Barclay, T. M. Bryan, S. R. Hamilton, S. N. Thibodeau, B. Vogelstein, and K. W. Kinzler (1992). APC mutations occur early during colorectal tumorigenesis. *Nature 359*(6392), 235–237.

Prokhortchouk, A., O. Sansom, J. Selfridge, I. M. Caballero, S. Salozhin, D. Aithozhina, L. Cerchietti, F. G. Meng, L. H. Augenlicht, J. M. Mariadason, B. Hendrich, A. Melnick, E. Prokhortchouk, A. Clarke, and A. Bird (2006, January). Kaiso-Deficient mice show resistance to intestinal cancer. *Mol. Cell. Biol. 26*(1), 199–208.

Purdie, C. A., J. O'Grady, J. Piris, A. H. Wyllie, and C. C. Bird (1991, April). p53 expression in colorectal tumors. *The American Journal of Pathology 138*(4), 807–813. PMID: 1707233 PMCID: 1886110.

Rajagopalan, H., A. Bardelli, C. Lengauer, K. W. Kinzler, B. Vogelstein, and V. E. Velculescu (2002). Tumorigenesis: RAF/RAS oncogenes and mismatch-repair status. *Nature 418*(6901), 934.

Ramalho-Santos, M., D. A. Melton, and A. P. McMahon (2000, June). Hedgehog signals regulate multiple aspects of gastrointestinal development. *Development (Cambridge, England) 127*(12), 2763–2772. PMID: 10821773.

Rashid, ., P. S. Houlihan*, S. Booker+, . Petersen+, s. p. Giardiello+, and . Hamilton* (2000, August). Phenotypic and molecular characteristics of hyperplastic polyposis. *Gastroenterology 119*(2), 323–332.

Reisman, D. N., J. Sciarrotta, T. W. Bouldin, B. E. Weissman, and W. K. Funkhouser (2005, March). The expression of the SWI/SNF ATPase subunits BRG1 and BRM in normal human tissues. *Applied Immunohistochemistry & Molecular Morphology: AIMM / Official Publication of the Society for Applied Immunohistochemistry 13*(1), 66–74. PMID: 15722796.

Reisman, D. N., J. Sciarrotta, W. Wang, W. K. Funkhouser, and B. E. Weissman (2003, February). Loss of BRG1/BRM in human lung cancer cell lines and primary lung cancers: Correlation with poor prognosis. *Cancer Res 63*(3), 560–566.

Reya, T., S. J. Morrison, M. F. Clarke, and I. L. Weissman (2001, November). Stem cells, cancer, and cancer stem cells. *Nature 414*(6859), 105–111.

Reyes, J. C., J. Barra, C. Muchardt, A. Camus, C. Babinet, and M. Yaniv (1998, December). Altered control of cellular proliferation in the absence of mammalian brahma (SNF2alpha). *The EMBO Journal 17*(23). PMC1171046.

Ricci-Vitiani, L., D. G. Lombardi, E. Pilozzi, M. Biffoni, M. Todaro, C. Peschle, and R. De Maria (2007, January). Identification and expansion of human colon-cancer-initiating cells. *Nature 445*(7123), 111–115.

Roberts, A. B. and L. M. Wakefield (2003, July). The two faces of transforming growth factor in carcinogenesis. *Proceedings of the National Academy of Sciences of the United States of America 100*(15), 8621 –8623.

Roberts, C. W. M., S. A. Galusha, M. E. McMenamin, C. D. M. Fletcher, and S. H. Orkin (2000, December). Haploinsufficiency of snf5 (integrase interactor 1) predisposes to malignant rhabdoid tumors in mice. *Proceedings of the National Academy of Sciences of the United States of America 97*(25). PMC17655.

Roberts, C. W. M. and S. H. Orkin (2004, February). The SWI/SNF complex - chromatin and cancer. *Nat Rev Cancer 4*(2), 133–142.

Rodriguez-Nieto, S., A. Caada, E. Pros, A. I. Pinto, J. Torres-Lanzas, F. Lopez-Rios, L. Sanchez-Verde, D. G. Pisano, and M. Sanchez-Cespedes (2011, February). Massive parallel DNA pyrosequencing analysis of the tumor suppressor BRG1/SMARCA4 in lung primary tumors. *Human Mutation 32*(2), E1999–2017. PMID: 21280140.

Rodriguez-Nieto, S. and M. Sanchez-Cespedes (2009, April). BRG1 and LKB1: tales of two tumor suppressor genes on chromosome 19p and lung cancer. *Carcinogenesis 30*(4), 547–554.

Roose, J., M. Molenaar, J. Peterson, J. Hurenkamp, H. Brantjes, P. Moerer, M. van de Wetering, O. Destre, and H. Clevers (1998, October). The xenopus wnt effector XTcf-3 interacts with groucho-related transcriptional repressors. *Nature 395*(6702), 608–12. PMID: 9783587.

Rubinfeld, B., I. Albert, E. Porfiri, C. Fiol, S. Munemitsu, and P. Polakis (1996, May). Binding of GSK3beta to the APC-beta-catenin complex and regulation of complex assembly. *Science (New York, N.Y.) 272*(5264), 1023–6. PMID: 8638126.

Saladi, S. V., B. Keenen, H. G. Marathe, H. Qi, K. Chin, and I. L. de la Serna (2010, October). Modulation of extracellular matrix/adhesion molecule expression by BRG1 is associated with increased melanoma invasiveness. *Mol Cancer. 9*, 280–280. PMID: 20969766 PMCID: 3098014.

Samowitz, W. S., M. D. Powers, L. N. Spirio, F. Nollet, F. van Roy, and M. L. Slattery (1999, April). -Catenin mutations are more frequent in small colorectal adenomas than in larger adenomas and invasive carcinomas. *Cancer Research 59*(7), 1442 –1444.

Sancho, E., E. Batlle, and H. Clevers (2004). Signaling pathways in intestinal development and cancer. *Annual Review of Cell and Developmental Biology 20*, 695–723. PMID: 15473857.

Sangiorgi, E. and M. R. Capecchi (2008, July). Bmi1 is expressed in vivo in intestinal stem cells. *Nat Genet 40*(7), 915–920.

Sansom, O. J., J. Berger, S. M. Bishop, B. Hendrich, A. Bird, and A. R. Clarke (2003, June). Deficiency of mbd2 suppresses intestinal tumorigenesis. *Nat Genet 34*(2), 145–147.

Sansom, O. J., F. C. Mansergh, M. J. Evans, J. A. Wilkins, and A. R. Clarke (2007a, October). Deficiency of SPARC suppresses intestinal tumorigenesis in APCMin/+ mice. *Gut 56*(10), 1410–1414. PMID: 17299058.

Sansom, O. J., V. Meniel, J. A. Wilkins, A. M. Cole, K. A. Oien, V. Marsh, T. J. Jamieson, C. Guerra, G. H. Ashton, M. Barbacid, and A. R. Clarke (2006, September). Loss of apc allows phenotypic manifestation of the transforming properties

of an endogenous k-ras oncogene in vivo. *Proceedings of the National Academy of Sciences of the United States of America 103*(38), 1412214127. PMC1599922.

Sansom, O. J., V. S. Meniel, V. Muncan, T. J. Phesse, J. A. Wilkins, K. R. Reed, J. K. Vass, D. Athineos, H. Clevers, and A. R. Clarke (2007b, April). Myc deletion rescues apc deficiency in the small intestine. *Nature 446*(7136), 676–679.

Sansom, O. J., K. R. Reed, A. J. Hayes, H. Ireland, H. Brinkmann, I. P. Newton, E. Batlle, P. Simon-Assmann, H. Clevers, I. S. Nathke, A. R. Clarke, and D. J. Winton (2004, June). Loss of apc in vivo immediately perturbs wnt signaling, differentiation, and migration. *Genes & Development 18*(12), 1385–90. PMID: 15198980.

Sato, A. (2007, December). Tuft cells. *Anatomical Science International / Japanese Association of Anatomists 82*(4), 187–199. PMID: 18062147.

Sato, T., J. H. van Es, H. J. Snippert, D. E. Stange, R. G. Vries, M. van den Born, N. Barker, N. F. Shroyer, M. van de Wetering, and H. Clevers (2010, November). Paneth cells constitute the niche for lgr5 stem cells in intestinal crypts. *Nature advance online publication.*

Sato, T., R. G. Vries, H. J. Snippert, M. van de Wetering, N. Barker, D. E. Stange, J. H. van Es, A. Abo, P. Kujala, P. J. Peters, and H. Clevers (2009, March). Single lgr5 stem cells build cryptvillus structures in vitro without a mesenchymal niche. *Nature advanced online publication.*

Schepers, A. G., R. Vries, M. van den Born, M. van de Wetering, and H. Clevers (2011, March). Lgr5 intestinal stem cells have high telomerase activity and randomly segregate their chromosomes. *EMBO J 30*(6), 1104–1109.

Schmidt, G., D. Winton, and B. Ponder (1988). Development of the pattern of cell renewal in the crypt-villus unit of chimaeric mouse small intestine. *Development 103*(4), 785 –790.

Schneider, M. R., M. Dahlhoff, D. Horst, B. Hirschi, K. Trlzsch, J. Mller-Hcker, R. Vogelmann, M. Allguer, M. Gerhard, S. Steininger, E. Wolf, and F. T. Kolligs (2010). A key role for e-cadherin in intestinal homeostasis and paneth cell maturation. *PloS One 5*(12), e14325. PMID: 21179475.

Schneikert, J. and J. Behrens (2007, March). The canonical wnt signalling pathway and its APC partner in colon cancer development. *Gut 56*(3), 417 –425.

Schrder, N. and A. Gossler (2002, December). Expression of notch pathway components in fetal and adult mouse small intestine. *Gene Expression Patterns 2*(3-4), 247–250.

Scoville, D. H., T. Sato, X. C. He, and L. Li (2008, March). Current view: Intestinal stem cells and signaling. *Gastroenterology 134*(3), 849–864.

Seeley, R. R., T. D. Stephens, and P. Tate (2002, July). *Anatomy and Physiology 6/e* (7th Revised edition ed.). McGraw Hill Higher Education.

Sekhon, H. S., C. A. London, M. Sekhon, P. L. Iversen, and G. R. Devi (2008, June). c-MYC antisense phosphosphorodiamidate morpholino oligomer inhibits lung metastasis in a murine tumor model. *Lung Cancer 60*(3), 347–354.

Shackelford, D. B. and R. J. Shaw (2009). The LKB1-AMPK pathway: metabolism and growth control in tumour suppression. *Nat Rev Cancer 9*(8), 563–575.

Shaker, A. and D. C. Rubin (2010, September). Intestinal stem cells and epithelial-mesenchymal interactions in the crypt and stem cell niche. *Translational Research 156*(3), 180–187.

Shan, B., M. Wang, and R.-q. Li (2009, July). Quercetin inhibit human SW480 colon cancer growth in association with inhibition of cyclin d1 and survivin expression through wnt/beta-catenin signaling pathway. *Cancer Investigation 27*(6), 604–612. PMID: 19440933.

Sharma, S., T. K. Kelly, and P. A. Jones (2010, January). Epigenetics in cancer. *Carcinogenesis 31*(1), 27–36.

Shen, W., C. Xu, W. Huang, J. Zhang, J. E. Carlson, X. Tu, J. Wu, and Y. Shi (2007, February). Solution structure of human brg1 bromodomain and its specific binding to acetylated histone tails,. *Biochemistry 46*(8), 2100–2110.

Shi, Y. and J. Massagu (2003, June). Mechanisms of TGF-[beta] signaling from cell membrane to the nucleus. *Cell 113*(6), 685–700.

Shibata, H., K. Toyama, H. Shioya, M. Ito, M. Hirota, S. Hasegawa, H. Matsumoto, H. Takano, T. Akiyama, K. Toyoshima, R. Kanamaru, Y. Kanegae, I. Saito, Y. Nakamura, K. Shiba, and T. Noda (1997, October). Rapid colorectal adenoma formation initiated by conditional targeting of the apc gene. *Science 278*(5335), 120–123.

Shiina, H., M. Igawa, K. Shigeno, M. Terashima, M. Deguchi, M. Yamanaka, L. Ribeiro-Filho, C. J. Kane, and R. Dahiya (2002, November). Beta-catenin mutations correlate with over expression of c-myc and cyclin d1 genes in bladder cancer. *The Journal of Urology 168*(5), 2220–2226. PMID: 12394763.

Shin, K., J. Lee, N. Guo, J. Kim, A. Lim, L. Qu, I. U. Mysorekar, and P. A. Beachy (2011, April). Hedgehog/Wnt feedback supports regenerative proliferation of epithelial stem cells in bladder. *Nature 472*(7341), 110–114.

Shinin, V., B. Gayraud-Morel, D. Gomes, and S. Tajbakhsh (2006, July). Asymmetric division and cosegregation of template DNA strands in adult muscle satellite cells. *Nat Cell Biol 8*(7), 677–682.

Shmelkov, S. V., J. M. Butler, A. T. Hooper, A. Hormigo, J. Kushner, T. Milde, R. S. Clair, M. Baljevic, I. White, D. K. Jin, A. Chadburn, A. J. Murphy, D. M. Valenzuela, N. W. Gale, G. Thurston, G. D. Yancopoulos, M. DAngelica, N. Kemeny, D. Lyden, and S. Rafii (2008, June). CD133 expression is not restricted to stem cells, and both CD133+ and CD133 metastatic colon cancer cells initiate tumors. *The Journal of Clinical Investigation 118*(6). PMC2391278.

Shorning, B. Y., J. Zabkiewicz, A. McCarthy, H. B. Pearson, D. J. Winton, O. J. Sansom, A. Ashworth, and A. R. Clarke (2009, January). Lkb1 deficiency alters goblet and paneth cell differentiation in the small intestine. *PLoS ONE 4*(1), e4264.

Smith, G. H. (2005, February). Label-retaining epithelial cells in mouse mammary gland divide asymmetrically and retain their template DNA strands. *Development 132*(4), 681 –687.

Smith, M. W. (1985, October). Expression of digestive and absorptive function in differentiating enterocytes. *Annual Review of Physiology 47*(1), 247–260.

Smits, R., A. Kartheuser, S. Jagmohan-Changur, V. Leblanc, C. Breukel, A. de Vries, H. van Kranen, J. H. van Krieken, S. Williamson, W. Edelmann, R. Kucherlapati, KhanPM, and R. Fodde (1997, February). Loss of apc and the entire chromosome 18 but absence of mutations at the ras and tp53 genes in intestinal tumors from Apc1638N, a mouse model for apc-driven carcinogenesis. *Carcinogenesis 18*(2), 321 –327.

Snippert, H. J., L. G. van der Flier, T. Sato, J. H. van Es, M. van den Born, C. Kroon-Veenboer, N. Barker, A. M. Klein, J. van Rheenen, B. D. Simons, and H. Clevers (2010, October). Intestinal crypt homeostasis results from neutral competition between symmetrically dividing lgr5 stem cells. *Cell 143*(1), 134–144.

Snippert, H. J., J. H. van Es, M. van den Born, H. Begthel, D. E. Stange, N. Barker, and H. Clevers (2009, June). Prominin-1/CD133 marks stem cells and early progenitors in mouse small intestine. *Gastroenterology 136*(7), 2187–2194.e1.

Soriano, P. (1999, January). Generalized lacZ expression with the ROSA26 cre reporter strain. *Nat Genet 21*(1), 70–71.

Stankunas, K., C. T. Hang, Z. Tsun, H. Chen, N. V. Lee, J. I. Wu, C. Shang, J. H. Bayle, W. Shou, M. L. Iruela-Arispe, and C. Chang (2008, February). Endocardial brg1 represses ADAMTS1 to maintain the microenvironment for myocardial morphogenesis. *Developmental cell 14*(2), 298–311. PMID: 18267097 PMCID: 2274005.

Sternberg, N. and D. Hamilton (1981, August). Bacteriophage p1 site-specific recombination : I. recombination between loxP sites. *Journal of Molecular Biology 150*(4), 467–486.

Stoehr, R., R. C. Krieg, R. Knuechel, F. Hofstaedter, C. Pilarsky, D. Zaak, R. Schmitt, and A. Hartmann (2002, May). No evidence for involvement of beta-catenin and APC in urothelial carcinomas. *International Journal of Oncology 20*(5), 905–911. PMID: 11956582.

Strobeck, M. W., M. F. DeCristofaro, F. Banine, B. E. Weissman, L. S. Sherman, and E. S. Knudsen (2001, March). The BRG-1 subunit of the SWI/SNF complex regulates CD44 expression. *J. Biol. Chem. 276*(12), 9273–9278.

Strobeck, M. W., K. E. Knudsen, A. F. Fribourg, M. F. DeCristofaro, B. E. Weissman, A. N. Imbalzano, and E. S. Knudsen (2000, July). BRG-1 is required for RB-mediated cell cycle arrest. *Proceedings of the National Academy of Sciences 97*(14), 7748 –7753.

Strober, B. E., J. L. Dunaief, Guha, and S. P. Goff (1996, April). Functional interactions between the hBRM/hBRG1 transcriptional activators and the pRB family of proteins. *Molecular and Cellular Biology 16*(4), 1576–1583. PMID: 8657132.

Strumpf, D., C. Mao, Y. Yamanaka, A. Ralston, K. Chawengsaksophak, F. Beck, and J. Rossant (2005, May). Cdx2 is required for correct cell fate specification and differentiation of trophectoderm in the mouse blastocyst. *Development 132*(9), 2093 –2102.

Su, L. K., K. W. Kinzler, B. Vogelstein, A. C. Preisinger, A. R. Moser, C. Luongo, K. A. Gould, and W. F. Dove (1992, May). Multiple intestinal neoplasia caused by a mutation in the murine homolog of the APC gene. *Science (New York, N.Y.) 256*(5057), 668–70. PMID: 1350108.

Sumi-Ichinose, C., H. Ichinose, D. Metzger, and P. Chambon (1997, October). SNF2beta-BRG1 is essential for the viability of f9 murine embryonal carcinoma cells. *Molecular and Cellular Biology 17*(10), 59765986. PMC232446.

Suzuki, H., D. N. Watkins, K. Jair, K. E. Schuebel, S. D. Markowitz, W. Dong Chen, T. P. Pretlow, B. Yang, Y. Akiyama, M. van Engeland, M. Toyota, T. Tokino, Y. Hinoda, K. Imai, J. G. Herman, and S. B. Baylin (2004, April). Epigenetic inactivation of SFRP genes allows constitutive WNT signaling in colorectal cancer. *Nat Genet 36*(4), 417–422.

Takagi, Y., H. Kohmura, M. Futamura, H. Kida, H. Tanemura, K. Shimokawa, and S. Saji (1996, November). Somatic alterations of the DPC4 gene in human colorectal cancers in vivo. *Gastroenterology 111*(5), 1369–1372.

Takahashi-Yanaga, F. and T. Sasaguri (2009, February). Drug development targeting the glycogen synthase kinase-3beta (GSK-3beta)-mediated signal transduction pathway: inhibitors of the wnt/beta-catenin signaling pathway as novel anticancer drugs. *Journal of Pharmacological Sciences 109*(2), 179–183. PMID: 19179804.

Takaku, K., H. Miyoshi, A. Matsunaga, M. Oshima, N. Sasaki, and M. M. Taketo (1999, December). Gastric and duodenal polyps in smad4 (Dpc4) knockout mice. *Cancer Research 59*(24), 6113 –6117.

Takaku, K., M. Oshima, H. Miyoshi, M. Matsui, M. F. Seldin, and M. M. Taketo (1998, March). Intestinal tumorigenesis in compound mutant mice of both Dpc4(Smad4) and apc genes. *Cell 92*(5), 645–656.

Takeuchi, J. K., H. Lickert, B. W. Bisgrove, X. Sun, M. Yamamoto, K. Chawengsaksophak, H. Hamada, H. J. Yost, J. Rossant, and B. G. Bruneau (2007, January). Baf60c is a nuclear notch signaling component required for the establishment of left-right asymmetry. *Proceedings of the National Academy of Sciences of the United States of America 104*(3), 846–851. PMID: 17210915.

Tamai, K., M. Semenov, Y. Kato, R. Spokony, C. Liu, Y. Katsuyama, F. Hess, J. P. Saint-Jeannet, and X. He (2000, September). LDL-receptor-related proteins in wnt signal transduction. *Nature 407*(6803), 530–5. PMID: 11029007.

Tamai, K., X. Zeng, C. Liu, X. Zhang, Y. Harada, Z. Chang, and X. He (2004, January). A mechanism for wnt coreceptor activation. *Molecular Cell 13*(1), 149–56. PMID: 14731402.

Teng, Y., A. Sun, X. Pan, G. Yang, L. Yang, M. Wang, and X. Yang (2006, July). Synergistic function of smad4 and PTEN in suppressing forestomach squamous cell carcinoma in the mouse. *Cancer Research 66*(14), 6972 –6981.

Thiagalingam, S., C. Lengauer, F. S. Leach, M. Schutte, S. A. Hahn, J. Overhauser, J. K. Willson, S. Markowitz, S. R. Hamilton, S. E. Kern, K. W. Kinzler, and B. Vogelstein (1996, July). Evaluation of candidate tumour suppressor genes on chromosome 18 in colorectal cancers. *Nat Genet 13*(3), 343–346.

Thibodeau, S. N., G. Bren, and D. Schaid (1993, May). Microsatellite instability in cancer of the proximal colon. *Science (New York, N.Y.) 260*(5109), 816–819. PMID: 8484122.

Thirlwell, C., O. C. C. Will, E. Domingo, T. A. Graham, S. A. C. McDonald, D. Oukrif, R. Jeffrey, M. Gorman, M. Rodriguez-Justo, J. Chin-Aleong, S. K. Clark, M. R. Novelli, J. A. Jankowski, N. A. Wright, I. P. M. Tomlinson, and S. J. Leedham (2010, April). Clonality assessment and clonal ordering of individual neoplastic crypts shows polyclonality of colorectal adenomas. *Gastroenterology 138*(4), 1441–1454, 1454.e1–7. PMID: 20102718.

Tian, H., B. Biehs, S. Warming, K. G. Leong, L. Rangell, O. D. Klein, and F. J. de Sauvage (2011). A reserve stem cell population in small intestine renders lgr5-positive cells dispensable. *Nature advance online publication*.

Tomita, H., Y. Yamada, T. Oyama, K. Hata, Y. Hirose, A. Hara, T. Kunisada, Y. Sugiyama, Y. Adachi, H. Linhart, and H. Mori (2007, May). Development of

gastric tumors in ApcMin/+ mice by the activation of the -Catenin/Tcf signaling pathway. *Cancer Research 67*(9), 4079 –4087.

Tomlinson, I. P. and R. S. Houlston (1997, December). Peutz-Jeghers syndrome. *Journal of Medical Genetics 34*(12), 1007–1011. PMID: 9429144.

Trotter, K. W. and T. K. Archer (2008). The BRG1 transcriptional coregulator. *Nuclear Receptor Signaling 6*, e004. PMID: 18301784.

Trotter, K. W., H. Fan, M. L. Ivey, R. E. Kingston, and T. K. Archer (2008, February). The HSA domain of BRG1 mediates critical interactions required for glucocorticoid receptor-dependent transcriptional activation in vivo. *Molecular and Cellular Biology 28*(4), 1413–1426. PMID: 18086889.

Trouche, D., C. L. Chalony, C. Muchardt, M. Yaniv, and T. Kouzarides (1997, October). RB and hbrm cooperate to repress the activation functions ofE2F1. *Proceedings of the National Academy of Sciences of the United States of America 94*(21). PMC23436.

Troughton, W. D. and J. S. Trier (1969, April). Paneth and goblet cell renewal in mouse duodenal crypts. *The Journal of Cell Biology 41*(1), 251 –268.

Underhill, C., M. S. Qutob, S. Yee, and J. Torchia (2000, December). A novel nuclear receptor corepressor complex, N-CoR, contains components of the mammalian SWI/SNF complex and the corepressor KAP-1. *Journal of Biological Chemistry 275*(51), 40463 –40470.

van de Wetering, M., E. Sancho, C. Verweij, W. de Lau, I. Oving, A. Hurlstone, K. van der Horn, E. Batlle, D. Coudreuse, A. Haramis, M. Tjon-Pon-Fong, P. Moerer, M. van den Born, G. Soete, S. Pals, M. Eilers, R. Medema, and H. Clevers (2002, October). The beta-catenin/TCF-4 complex imposes a crypt progenitor phenotype on colorectal cancer cells. *Cell 111*(2), 241–250.

van den Brink, G. R. (2007, October). Hedgehog signaling in development and homeostasis of the gastrointestinal tract. *Physiological Reviews 87*(4), 1343 –1375.

van der Flier, L. G., M. E. van Gijn, P. Hatzis, P. Kujala, A. Haegebarth, D. E. Stange, H. Begthel, M. van den Born, V. Guryev, I. Oving, J. H. van Es, N. Barker, P. J. Peters, M. van de Wetering, and H. Clevers (2009, March). Transcription factor achaete Scute-Like 2 controls intestinal stem cell fate. *Cell 136*(5), 903–912.

van Es, J. H., P. Jay, A. Gregorieff, M. E. van Gijn, S. Jonkheer, P. Hatzis, A. Thiele, M. van den Born, H. Begthel, T. Brabletz, M. M. Taketo, and H. Clevers (2005a, April). Wnt signalling induces maturation of paneth cells in intestinal crypts. *Nat Cell Biol 7*(4), 381–386.

van Es, J. H., M. E. van Gijn, O. Riccio, M. van den Born, M. Vooijs, H. Begthel, M. Cozijnsen, S. Robine, D. J. Winton, F. Radtke, and H. Clevers (2005b, June). Notch/[gamma]-secretase inhibition turns proliferative cells in intestinal crypts and adenomas into goblet cells. *Nature 435*(7044), 959–963.

Vermeulen, L., M. Todaro, F. de Sousa Mello, M. R. Sprick, K. Kemper, M. Perez Alea, D. J. Richel, G. Stassi, and J. P. Medema (2008). Single-cell cloning of colon cancer stem cells reveals a multi-lineage differentiation capacity. *Proceedings of the National Academy of Sciences 105*(36), 13427 –13432.

Vitale-Cross, L., P. Amornphimoltham, G. Fisher, A. A. Molinolo, and J. S. Gutkind (2004, December). Conditional expression of k-ras in an epithelial compartment that

includes the stem cells is sufficient to promote squamous cell carcinogenesis. *Cancer Research 64*(24), 8804–8807.

Vogelstein, B., E. R. Fearon, S. R. Hamilton, S. E. Kern, A. C. Preisinger, M. Leppert, Y. Nakamura, R. White, A. M. Smits, and J. L. Bos (1988, September). Genetic alterations during colorectal-tumor development. *The New England Journal of Medicine 319*(9), 525–532. PMID: 2841597.

Waite, K. A. and C. Eng (2003, October). From developmental disorder to heritable cancer: it's all in the BMP/TGF-[beta] family. *Nat Rev Genet 4*(10), 763–773.

Wang, K., S. Sengupta, L. Magnani, C. A. Wilson, R. W. Henry, and J. G. Knott (2010, May). Brg1 is required for Cdx2-Mediated repression of oct4 expression in mouse blastocysts. *PLoS ONE 5*(5), e10622.

Wang, X., C. G. Sansam, C. S. Thom, D. Metzger, J. A. Evans, P. T. Nguyen, and C. W. Roberts (2009, October). Oncogenesis caused by loss of the SNF5 tumor suppressor is dependent on activity of BRG1, the ATPase of the SWI/SNF chromatin remodeling complex. *Cancer Res 69*(20), 8094–8101.

Watanabe, T., S. Semba, and H. Yokozaki (2010, November). Regulation of PTEN expression by the SWI/SNF chromatin-remodelling protein BRG1 in human colorectal carcinoma cells. *Br J Cancer*.

Waterman, M. L. (2002, January). Expression of lymphoid enhancer factor/T-cell factor proteins in colon cancer. *Current Opinion in Gastroenterology 18*(1), 53–9. PMID: 17031231.

Watt, F. M. and R. R. Driskell (2010, January). The therapeutic potential of stem cells. *Philosophical Transactions of the Royal Society B: Biological Sciences 365*(1537), 155 –163.

Wicha, M. S., S. Liu, and G. Dontu (2006, February). Cancer stem cells: An old Idea–A paradigm shift. *Cancer Res 66*(4), 1883–1890.

Willert, K., J. D. Brown, E. Danenberg, A. W. Duncan, I. L. Weissman, T. Reya, J. R. Yates, and R. Nusse (2003, May). Wnt proteins are lipid-modified and can act as stem cell growth factors. *Nature 423*(6938), 448–52. PMID: 12717451.

Williams, E. D., A. P. Lowes, D. Williams, and G. T. Williams (1992, October). A stem cell niche theory of intestinal crypt maintenance based on a study of somatic mutation in colonic mucosa. *The American Journal of Pathology 141*(4), 773–776. PMID: 1415475.

Wilson, A. and F. Radtke (2006, May). Multiple functions of notch signaling in self-renewing organs and cancer. *FEBS Letters 580*(12), 2860–2868.

Winton, D. J., M. A. Blount, and B. A. J. Ponder (1988, June). A clonal marker induced by mutation in mouse intestinal epithelium. *Nature 333*(6172), 463–466.

Wolin, K. Y., Y. Yan, and G. A. Colditz (2011, March). Physical activity and risk of colon adenoma: a meta-analysis. *British Journal of Cancer 104*(5), 882–885. PMID: 21304525.

Wong, A. K. C., F. Shanahan, Y. Chen, L. Lian, P. Ha, K. Hendricks, S. Ghaffari, D. Iliev, B. Penn, A. Woodland, R. Smith, G. Salada, A. Carillo, K. Laity, J. Gupte, B. Swedlund, S. V. Tavtigian, D. H. Teng, and E. Lees (2000, November). BRG1, a component of the SWI-SNF complex, is mutated in multiple human tumor cell lines. *Cancer Res 60*(21), 6171–6177.

Woo, D. K., H. S. Kim, H. S. Lee, Y. H. Kang, H. K. Yang, and W. H. Kim (2001, March). Altered expression and mutation of catenin gene in gastric carcinomas and cell lines. *International Journal of Cancer 95*(2), 108–113.

Woo, J., I. Miletich, B. Kim, P. T. Sharpe, and R. A. Shivdasani (2011, July). Barx1-Mediated inhibition of wnt signaling in the mouse thoracic foregut controls Tracheo-Esophageal septation and epithelial differentiation. *PLoS ONE 6*(7), e22493.

Workman, J. L. and R. E. Kingston (1998). Alteration of nucleosome structure as a mechanism of transcriptional regulation. *Annual Review of Biochemistry 67*, 545–579. PMID: 9759497.

Wu, T. T., S. Kornacki, A. Rashid, J. H. Yardley, and S. R. Hamilton (1998, March). Dysplasia and dysregulation of proliferation in foveolar and surface epithelia of fundic gland polyps from patients with familial adenomatous polyposis. *The American Journal of Surgical Pathology 22*(3), 293–298. PMID: 9500770.

Wu, X. (2005). Urothelial tumorigenesis: a tale of divergent pathways. *Nat Rev Cancer 5*(9), 713–725.

Wu, X., X. Kong, A. Pellicer, G. Kreibich, and T. Sun (2009, April). Uroplakins in urothelial biology, function, and disease. *Kidney Int 75*(11), 1153–1165.

Xu, Z., X. Meng, Y. Cai, M. Koury, and S. Brandt (2006, October). Recruitment of the SWI/SNF protein brg1 by a multiprotein complex effects transcriptional repression in murine erythroid progenitors. *Biochemical Journal 399*(2), 297.

Yang, Q., N. A. Bermingham, M. J. Finegold, and H. Y. Zoghbi (2001, December). Requirement of math1 for secretory cell lineage commitment in the mouse intestine. *Science 294*(5549), 2155 –2158.

Zhang, H., M. Gavin, A. Dahiya, A. A. Postigo, D. Ma, R. X. Luo, J. Harbour, and D. C. Dean (2000, March). Exit from g1 and s phase of the cell cycle is regulated by repressor complexes containing HDAC-Rb-hSWI/SNF and Rb-hSWI/SNF. *Cell 101*(1), 79–89.

Zhou, X. P., K. Woodford-Richens, R. Lehtonen, K. Kurose, M. Aldred, H. Hampel, V. Launonen, S. Virta, R. Pilarski, R. Salovaara, W. F. Bodmer, B. A. Conrad, M. Dunlop, S. V. Hodgson, T. Iwama, H. Jrvinen, I. Kellokumpu, J. C. Kim, B. Leggett, D. Markie, J. P. Mecklin, K. Neale, R. Phillips, J. Piris, P. Rozen, R. S. Houlston, L. A. Aaltonen, I. P. Tomlinson, and C. Eng (2001, October). Germline mutations in BMPR1A/ALK3 cause a subset of cases of juvenile polyposis syndrome and of cowden and Bannayan-Riley-Ruvalcaba syndromes. *American Journal of Human Genetics 69*(4), 704–711. PMID: 11536076.

Zhu, L., P. Gibson, D. S. Currle, Y. Tong, R. J. Richardson, I. T. Bayazitov, H. Poppleton, S. Zakharenko, D. W. Ellison, and R. J. Gilbertson (2009, January). Prominin 1 marks intestinal stem cells that are susceptible to neoplastic transformation. *Nature 457*(7229), 603–607.

Zhu, X., Y. Kanai, A. Saito, Y. Kondo, and S. Hirohashi (2000, December). Aberrant expression of catenin and mutation of exon 3 of the catenin gene in renal and urothelial carcinomas. *Pathology International 50*(12), 945–952.